Preparation and Properties of Natural, Demineralized, Pure, and Doped Carbons from Biomass; Model of the Chemical Structure of Carbonized Charcoal

THE UNIVERSITY OF
WAIKATO
Te Whare Wānanga o Waikato

A thesis
submitted in partial fulfillment
of the requirements for the degree
of
Master of Science in Chemistry
at
The University of Waikato

by

Jared Bourke

The University of Waikato
2006

Abstract

Pioneering work performed by Rosalind Franklin over half a century ago provided the first structural models of two distinct carbon types: those that become graphitic during carbonization at high temperatures, and those that do not. Moreover it is known that certain properties of carbonaceous materials including combustion, surface area, electrical resistivity, and catalytic properties are influenced by mineral impurities. The nature of this division in biocarbon structure and the known effects of minerals on carbon properties have led to this work; three principal topics were addressed; (1) the investigation of the solid state structure of biocarbons derived from various biomass feedstocks, (2) the removal of inorganic minerals from biomass, and (3) the investigation of biocarbon electronic structure subsequent to doping with select inorganic minerals.

Charcoals and carbonized charcoals (i.e. biocarbons) were prepared from a wide variety of biomass substrates, including pure sugars containing 5- and 6-membered rings with furanose and pyranose configurations, lignin, agricultural residues (corncob and nut shells) and a hard wood. These biocarbons were subject to proximate and elemental analysis, gas sorption analysis, and analysis by ICP-MS, SEM, XRD, ESR, ^{13}C CPMAS NMR, and MALDI-TOF MS. All the carbonized charcoals contained oxygen heteroatoms, had high surface areas, and were excellent conductors of electricity. Doping the biocarbon with boron or phosphorus resulted in a slight improvement in its electrical conductivity. The XRD analysis indicated that the carbonized charcoals possess an aromaticity of about 71% that results from graphite crystallites with an average size of about 20 Å. The NMR analysis confirmed the highly aromatic content of the carbonized charcoals. The ESR signals indicated two major types of carbon-centered organic radicals. A number of techniques employed highlighted differences between carbonized charcoals and synthetic graphite but none more so than MALDI-TOF spectrometry. The biocarbons contained readily desorbed discrete ions with *m/z* values of 701, 685, 465, 453, 429, and 317. All of the above findings were used to develop a model for the structure of carbonized charcoal that is consistent with the biocarbon's oxygen content,

microporosity and surface area, electrical conductivity, radical content, and its MALDI-TOF spectra.

The removal of inorganic mineral constituents from various biomass feedstocks was achieved via simple washing/soaking techniques using two different aqueous media; deionized water and citric acid. The most effective and consistent demineralization treatment for removing minerals from biomass involved a hot 0.1 $molL^{-1}$ citric acid percolation treatment, ca. 67% of inorganic mineral matter was removed. Mineral matter at the levels present in typical biomass derived charcoals and carbons had no significant influence upon the surface area or the electrical resistivity in carbonaceous materials after high heat treatment (950 °C).

Acknowledgements

I would like to thank my supervisors Dr Michael J Antal and Dr Merilyn Manley-Harris for presenting me this excellent opportunity and for the care with which they reviewed the original manuscript. Fellow colleagues associated with the Renewable Resources Research laboratory (R3) including Sam R. Wade, Teppei Nunoura, Lloyd S. Paredes, Chihiro Fushimi, and Kiyoshi Dowaki must also be thanked for their continuous support and friendship during and after my period of stay on the island of Oahu, Hawai'i.

Professor Brian Nicholson and Associate Professor Alan Langdon for help with XRD analyses and Jonathan Puddick for help with MALDI-TOF-MS.

I would also like to extend my gratitude towards Leiana who made my experience richer by introducing me to her lovely family and all things Hawaiian.

Finally my parents and family must be thanked for their support and encouragement. Without their backing I would not have been able to accept the opportunity extended towards me.

The work performed would not have been possible without the sponsorship and support of The Office of Naval Research (contract N00014-04-1-0682) and the Coral Industries Endowment of the University of Hawai'i.

Table of Contents

List of Tables

7.0 Mineral Matter in Biomass and Biomass Charcoals

List of Figures

1.0 Introduction

2.0 Literature Review

3.0 Selected Biomass Structures and Chemical Compositions

5.0 Structural Analysis of Biocarbons

6.0 New Biocarbon Model

7.0 Mineral Matter in Biomass and Biomass Charcoals

Nomenclature

AC	Activated Coconut Carbon
ASTM	American Society for Testing and Materials
BD	Boron-doped
BET	Brauner–Emmet–Teller
B&S	Barnebey and Sutcliffe
CC	Corncob
^{13}C CPMAS NMR	Cross Polarization Magic Angle Spinning Nuclear Magnetic Resonance
DFT	Density Functional Theory
DPPH	Diphenylpicrylhydrazyl
DTG	Derivative Thermogravimetric
ESR	Electron Spin Resonance
FC	Flash Carbonization™
FTIR	Fourier-Transform Infrared
HREM	High Resolution Electron Microscopy
HTT	Heat Treatment Temperature
KL	Kraft Lignin
MALDI-TOF-MS	Matrix Assisted Laser Desorption Ionization Time of Flight Mass Spectroscopy
MS/Macshell	Macadamia Nutshell
NA	Non-applicable
NM	Not Measured
OW	Oak Wood
PD	Phosphorus-doped
PSD	Post Source Decay
Py-GC-MS	Pyrolysis-Gas Chromatography-Mass Spectrometry
R3	Renewable Resources Research
SEM	Scanning Electron Microscopy
TEM	Transmission Electron Microscopy
TCNQ	7,7,8,8-tetracyanoquinodimethane

TG-MS	Thermogravimetric Mass Spectroscopy
VM	Volatile matter
XRD	X-ray Diffraction
Y_{char}	Charcoal Yield
Y_{fC}	Fixed Carbon Yield

1.0 Introduction

1.1 Charcoal Production and Applications

Charcoal is defined as the residue of solid non-agglomerated organic matter, of vegetable or animal origin, that results from carbonization by heat in the absence of air at a temperature above 300 °C[1].

Exquisite charcoal cave drawings dated as far back as 38 000 years ago illustrate the extensive history of charcoal manufacture and use[2]. The birth of the charcoal industry however is usually recognized around 1100 BC with the fuel playing a significant role in the recovery of iron and other metals from their ores. It is assumed that the early manufacture of charcoal involved poor yield, open pit methodology. Increased charcoal yields were obtained by employing closed charcoal pit and earthmound kiln techniques. Both techniques involved covering the biomass, in most cases wood, with earth. Earth was used to insulate the carbonizing chamber and to keep out oxygen. Although both these techniques were significantly better than the early open pit methods, they are still considered inefficient and were and still are major contributors to wood depletion and deforestation. Charcoal manufacture does not solely produce an energy dense solid, but also generates a variety of liquid and gaseous by-products. Raw materials such as acetic acid, produced from carbonization condensate (pyrolysis oil) caused growing interests from the chemical industry and ultimately brought about the development of new charcoal furnaces[1]. Industrial charcoal kilns in use today include the Missouri kiln and the Brazilian Beehive kiln. The Missouri kiln operating on a 7-12 day cycle produces charcoal at a 25% yield. Brazilian Beehive kilns operating on an 8 day cycle have achieved charcoal yields as high as 31-35%[3].

The charcoal industry today caters to numerous large markets including metallurgy, plastic fabrication, and activated carbon manufacture. Charcoal is utilized in a number of chemical processes and is prominent as a cooking fuel for both developed and undeveloped countries[1]. Charcoal is an excellent amendment for soil providing

superb conditions for plant growth. Heat treated charcoals develop a high degree of porosity and conduct electricity extremely well giving rise to applications in electrode manufacture[2].

Exact figures on world charcoal production are difficult to obtain. According to the Food and Agriculture Organization of the United Nations (FAO) 43 million tonnes of wood charcoal were produced in 2003 worldwide[4]. This is a substantial increase on the estimated production value offered 10 years ago, ~27 million tonnes. These statistics do not include charcoal manufactured from agricultural residues. Despite the growing uses of charcoal and the importance of the material to the world economy, the science of charcoal production is still in its infancy[3].

1.2 The General Process of Flash Carbonization™

Flash carbonization™ (FC) is described as the ignition and control of a flash fire at elevated pressure (~1 MPa) within a packed bed of biomass[5]. Below is the schematic diagram of the laboratory FC reactor employed to generate charcoal samples for the study described in this thesis. It should be noted that the catalytic afterburner present in the diagram below was absent during charcoal manufacture between June 2004 and June 2005.

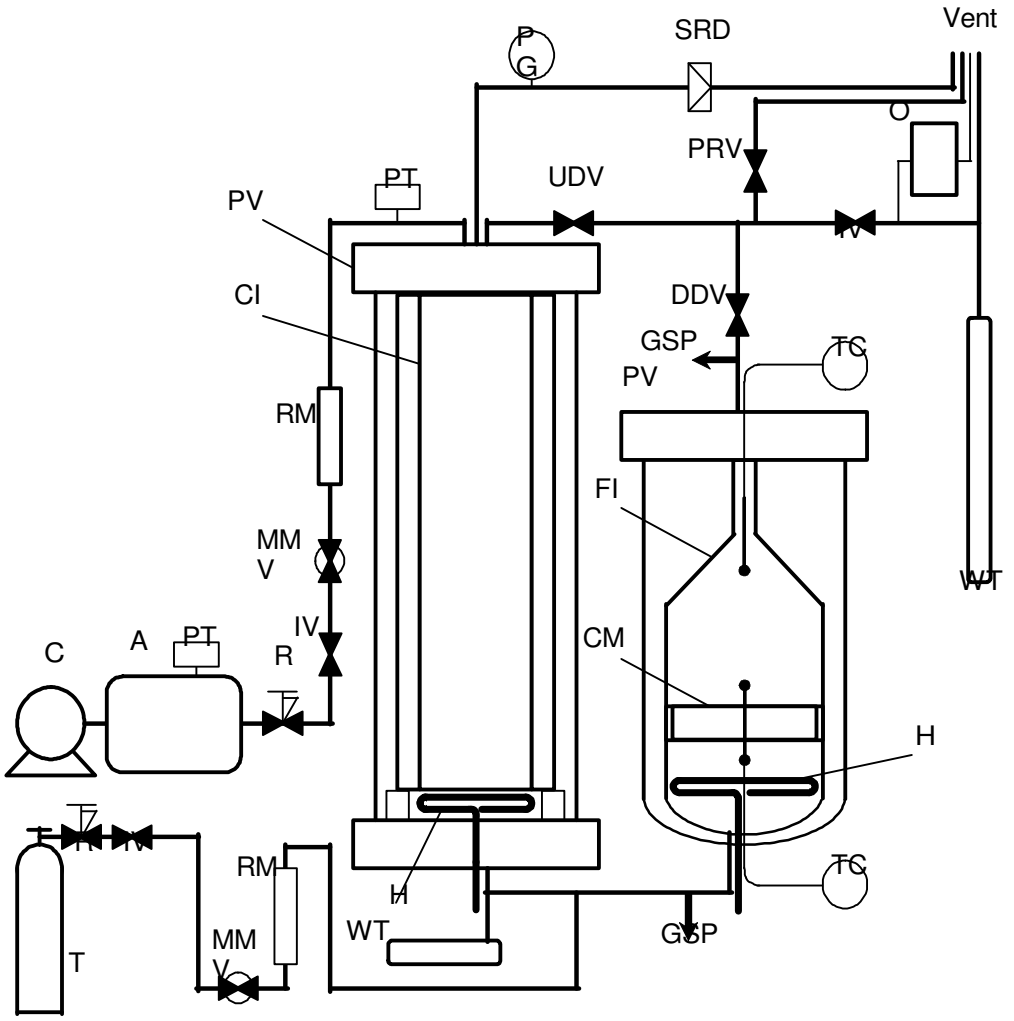

Figure 1.1: *Schematic Diagram of the Laboratory-Scale Flash Carbonization™ Reactor and the Catalytic Afterburner. A, air accumulator; C, compressor; CI, canister with insulation; CM, catalyst monolith; DDV, downdraft valve; FI, funnel with insulation; GSP, gas sampling port; H, electric heater; IV, isolation valve; MMV, micrometer valve; O, oxygen analyzer; PG, pressure gauge; PRV, pressure relief valve; PT, pressure transducer; PV, pressure vessel; R, regulator; RM, rotometer; SRD, safety rapture disk; T, air tank; TC, thermocouple; UDV, updraft valve; WT, water trap.*

In a typical carbonization experiment a measured amount of select biomass (typically 0.5-1.4 kg) is placed inside a cylindrical stainless steel canister. The canister is then lowered into the vertical pressure vessel (autoclave) and a robust pressure vessel lid is bolted in place. The autoclave is subsequently pressurized with air to a desired pressure (1.1-2.1 MPa). To begin the experiment, a desired amount of electric power

(1.9 kW-1.4 kW) is delivered to the electric heater positioned at the base of the autoclave. Ignition of raw biomass generally occurs within a couple of minutes whereat primary air is then delivered from the air accumulator system at a desired flow rate to the top of the reactor while combustion gas is vented from the bottom. The flash fire migrates up through the packed biomass bed, against the downward flow of primary air, converting raw biomass to charcoal. Power to the electric heaters is generally terminated after fourteen minutes. Primary air flow is stopped once sufficient air has been delivered to ensure complete bed carbonization. The estimated mass of air required to carbonize a full bed of given biomass is determined with the aid of an oxygen meter (Bacharach Oxor II), which monitors the oxygen content in combustion gas, and previously calculated air-to-biomass ratios. Once primary air delivery is terminated the autoclave is depressurized and allowed to cool (typically 24 hours). The canister is then removed from the autoclave and the carbonized contents are carefully separated into three sections, top, middle, and bottom. A representative charcoal sub-sample is taken from each section and subjected to proximate analysis according to ASTM D1762-84[5]. After each FC run the tarry organic liquid located in the liquid trap is also measured. It should be noted that with the catalytic afterburner in operation the tarry pyrolysis byproduct should be at a minimum.

It is important to recognize that some of the charcoals, which form the basis of this thesis, proceed through a distinct liquid phase during FC. These particular melt charcoals were prepared within a small metal beaker which was placed at the top of the biomass packed canister.

In theory the conversion of biomass to carbon should be quick and efficient. As indicated by thermochemical equilibrium calculations, carbon is a preferred product of biomass pyrolysis at moderate temperatures. Section 1.1 outlined both traditional and modern day charcoal production technologies offering insight into their respective efficiencies. The process of FC produces biocarbons with fixed carbon yields[1] that approach and in some cases obtain the thermochemical equilibrium

[1] Refer to section 4.2 for fixed carbon yield definition.

"limit"[2] in <30 minutes of reaction time. This production time is orders of magnitude faster than commercial technologies such as the Missouri Kiln[5].

Increases in fixed carbon yields using FC technology is explained via an increase in secondary carbon production. Secondary carbon is described as carbon formed from the decomposition of tarry organic vapors. At elevated pressures tarry vapors have an increased residence time in heat treatment zones resulting in increased volatile matter (VM) carbonization. In addition, secondary carbon formation is catalyzed by charcoal. VM produced from biomass carbonization is likely to be forced downwards through the hot charcoal bed by the primary air flow. This ensures a high conversion of tarry organic VM to solid carbon. Moreover, according to thermochemical equilibrium equations, oxygen preferentially attacks solid carbon as opposed to generated pyrolysis gases. However, it has been shown that the transport of oxygen to the carbons reactive surface is significantly slower than the fast intimate mixing of oxygen and combustion gases[5].

Feedstocks used to prepare the charcoals which were used in this study include: D-glucose, D-fructose, sucrose, inulin, Kraft lignin, corncob, macadamia nutshell, kukui nutshell, and oak wood. The term carbon or carbonized charcoal is used in reference to a charcoal which has been further heat treated to a temperature of ≥950 °C in the absence of air. Charcoals and carbons derived from D-glucose, D-fructose, sucrose, inulin, and Kraft lignin are herein referred to as melt charcoals or melt carbons due to their propensity to melt during carbonization. The oak wood was supplied by the Cowboy Charcoal Co., and the cob was obtained from the Waimanalo Research Farm both on the island of Oahu, Hawaii.

Pure chemicals (ca. 98 to 99 wt%) inulin, D-glucose, and D-fructose were obtained from Alfa Aesar; sucrose was bought off the shelf as C & H pure cane sugar. Kraft lignin (Indulin® AT) was obtained from MeadWestvaco and is described as a purified form of Kraft pine lignin having an ash content of about 3% (dry-basis, DB).

[2] Thermochemical equilibrium calculations set a limit on the maximum yield of carbon that can be obtained from any given type of biomass feedstock.

1.3 Objective

The research described in this thesis was performed at the Hawaii Natural Energy Institute based at the University of Hawaii at Manoa; three principal foci were addressed: (1) to investigate the solid state structure of biocarbons derived from various biomass feedstocks, (2) to explore the removal of inorganic minerals from biomass, and (3) to study the effects of doping charcoal substrates with select inorganic minerals.

The major focus addresses the possibility that charcoals and carbons derived from alternate biomass feedstocks have distinct physical and chemical properties. To investigate this supposition a number of biocarbons[3] were manufactured via FC (section 1.2). The previously listed biomass feedstocks represent possible alternate families of biocarbons. For example D-fructose is a simple monomeric ketose sugar which in its common crystalline form consists of pyranose rings, but when present in inulin or sucrose is in the furanose ring form. The aldose D-glucose is in the pyranose form in virtually all natural occurrences. It is also important to note that the oxonium ion of a ketose sugar differs from that derived from an aldose sugar and that pure sugars proceed through a distinct melt phase during pyrolysis. Evidence from literature involving the monitoring of sugar composition in water with respect to temperature[6, 7], indicated a preferred furanose conformation at higher temperatures. The thermodynamically favored isomoerization of pyranose units to furanose units is therefore anticipated to take place for the pure sugars during FC. We therefore envisage that charcoals derived from such feedstocks would consist primarily of condensed furanone rings and their fragments. Inulin was hence selected on the basis that it is a polyfuranose at room temperature and consequently offers alternative possibilities in terms of its pyrolysis chemistry from simple pyranose based feedstocks.

Biomass contains lignin; a complex three dimensional aromatic structure composed of phenyl propane units. It therefore seems plausible that a charcoal derived from this

[3] Biocarbons – term used to encapsulate both charcoals and carbonized charcoals.

particular feedstock would consist of condensed 6-membered rings analogous to graphite. A charcoal derived from corncob biomass was prepared as candidate to highlight the differences in pyrolysis chemistry associated with individual biomass substrate pyrolysis and combined substrate pyrolysis. Corncob is composed of 26.3% cellulose, 25.2% hemicelluloses, and 16.3% lignin[8]. It might be anticipated that a charcoal derived from corncob would consist of both condensed 6-membered rings in combination with pyrone[9] and furanone structures and their fragments. Biocarbons thus prepared were analyzed using techniques including: Scanning Electron Microscopy (SEM), X-ray Diffraction (XRD), Electron Spin Resonance (ESR), Thermogravimetry-Mass Spectroscopy (TG-MS), and ^{13}C Cross Polarization Magic-Angle Spinning Nuclear Magnetic Resonance (^{13}C CPMAS NMR). Electrical resistivity, density, and surface area measurements were also made for each biocarbon. Furthermore the relatively new application of Matrix Assisted Laser Desorption Ionization Time of Flight Mass Spectroscopy (MALDI-TOF-MS) was investigated as a possible new tool for obtaining information about charcoal and carbon structure. Results from such analyses were used to predict a model for such structures.

The secondary focus of this work investigates the removal of inorganic mineral constituents from various biomass feedstocks, with the aim of producing a low ash charcoal or carbon. Chemical and physical properties of subsequent low ash biocarbons were compared with regular biomass derived chars.

The last focus of this work evaluates the homogeneous introduction of an exotic mineral to a select charcoal substrate with the specific purpose of augmenting the carbons electrical properties. Two methods of exotic mineral incorporation in a carbon substrate were investigated; biomass loading via the interaction of a water soluble impurity with a desired carbohydrate-based feedstock and the direct solid phase interaction of an impurity salt with a pure carbohydrate source. Combinations of dopant impurity and feedstock investigated included boron and corncob, boron and sucrose, and phosphorus and sucrose.

1. Emrich, W., *Handbook of Charcoal Making - The Traditional and Industrial Methods*. D. Reidel Publishing Company: 1985.

2. M. J. Antal, J.; Grønli, M., The Art, Science, and Technology of Charcoal Production. *Ind. Eng. Chem. Res.* **2003,** 42, 1619-1640.

3. M. J. Antal, J.; Mok, W. S. L., Review of Methods for Improving the Yield of Charcoal from Biomass. *Energy & Fuels* **1990,** 4, (3), 221.

4. FAOSTAT data. In 2005.

5. M. J. Antal, J.; Mochidzuki, K.; Paredes, L. S., Flash Carbonization of Biomass. *Ind. Eng. Chem. Res.* **2003,** 42, 3690-3699.

6. Angyal, S. J., The Composition of Reducing Sugars in Solution. *Adv. Carbohydr. Chem. Biochem* **1984,** 42, 15-68.

7. Angyal, S. J., The Composition of Reducing Sugars in Solution: Current Aspects. *Adv. Carbohydr. Chem. Biochem* **1991,** 49, 19-36.

8. M. J. Antal, J.; Allen, S. G.; Dai, X.; Shimizu, B.; Tam, M. S.; Gronli, M., Attainment of the Theoretical Yield of Carbon from Biomass. *Ind. Eng. Chem. Res* **2000,** 39, (11), 4024-4031.

9. Montes-Morán, M. A.; Suárez, D.; Menéndez, J. A.; Fuente, E., On the Nature of Basic Sites on Carbon Surfaces: An Overview. *Carbon* **2004,** 42, 1219-1225.

2.0 Literature Review

2.1 Pyrolysis

Pyrolysis is defined as the transformation of a compound into one or more other substances by heat alone i.e. without oxidation[1]. The key difference between FC and pyrolysis of biomass is the presence of oxygen upon heating. Both processes involve the formation and release of low molecular weight gases and vapors as well as the formation of a solid char residue. Although the processes of pyrolysis and FC are distinct, it is generally accepted that char products formed from either are analogous.

Significant factors which affect biomass pyrolysis include biomass composition, heating conditions, ambient atmosphere, solid and volatile residence time, particle size, pressure, and the presence of inorganic minerals. These variables affect the sequence and kinetics of pyrolysis reactions[2].

Antal has compiled a comprehensive review on pyrolysis of carbohydrate and biomass[3, 4]. The following sections provide a detailed overview on the pyrolysis chemistry of major biomass constituents whilst paying particular attention to char formation and structure.

2.1.1 Cellulose Pyrolysis

Cellulose is the largest component of biomass and its pyrolysis chemistry has been extensively studied[3-13]. As early as 1964, cellulose pyrolysis both under vacuum and at atmospheric pressure was examined. It was proposed that the pyrolytic reactions, which produce a variety of products, occur through concurrent and consecutive reactions[5]. Such reactions include depolymerisation via glycosidic cleavage, dehydration, and elimination.

One of the earliest proposed kinetic models illustrating cellulose thermal decomposition was put forward by Shafizadeh and Broido[6]. The model is illustrated below:

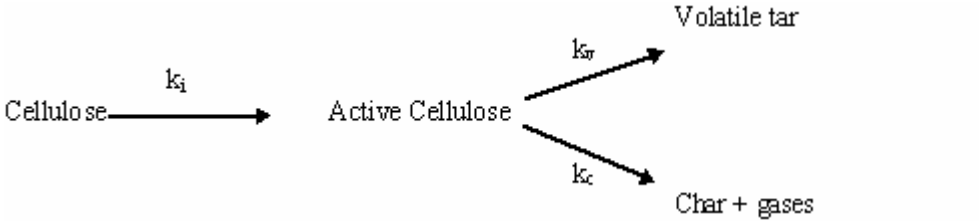

Char is thought to be derived from an active cellulose intermediate. In the majority of cellulose thermal degradation studies, minor structural alterations occur between temperatures 200-300 °C. Slightly modified cellulose, accompanied by significant weight loss is the result of such heating. This altered cellulosic structure is considered an active intermediate. The Shafizadeh-Broido model however, is considered inadequate as it fails to explain experimentally observed changes in the distribution of volatile products on increased temperature and heating rate[6].

One of the major products of cellulose pyrolysis was found to be the anhydrosugar 1,6-levoglucosan. A proposed mechanism for the formation of levoglucosan involves cleavage of the glycosidic bond (see Fig. 2.1). This cleavage may proceed through a homolytic or heterolytic process. Due to levoglucosan being found in high concentrations, char formation was therefore thought primarily to involve the anhydrosugar. Shafizadeh[5] performed cellulose pyrolysis in combination with 5% antimony trichloride (a Lewis acid catalyst). This caused cellulose degradation to occur at lower temperatures resulting in lower levoglucosan concentrations and increased char yields of more than 40%. Pyrolysis of cellulose under hard vacuum and at temperatures above 250 °C indicated that anhydrosugars are readily removed from the heated reaction zone[7]. This is seen by an increase of levoglucosan (80%) concentration found in the resulting tar fraction. At lower temperatures and at atmospheric pressure, levoglucosan is not readily removed from the pyrolysis process, and was therefore thought to continue playing a role in the many pyrolytic reactions.

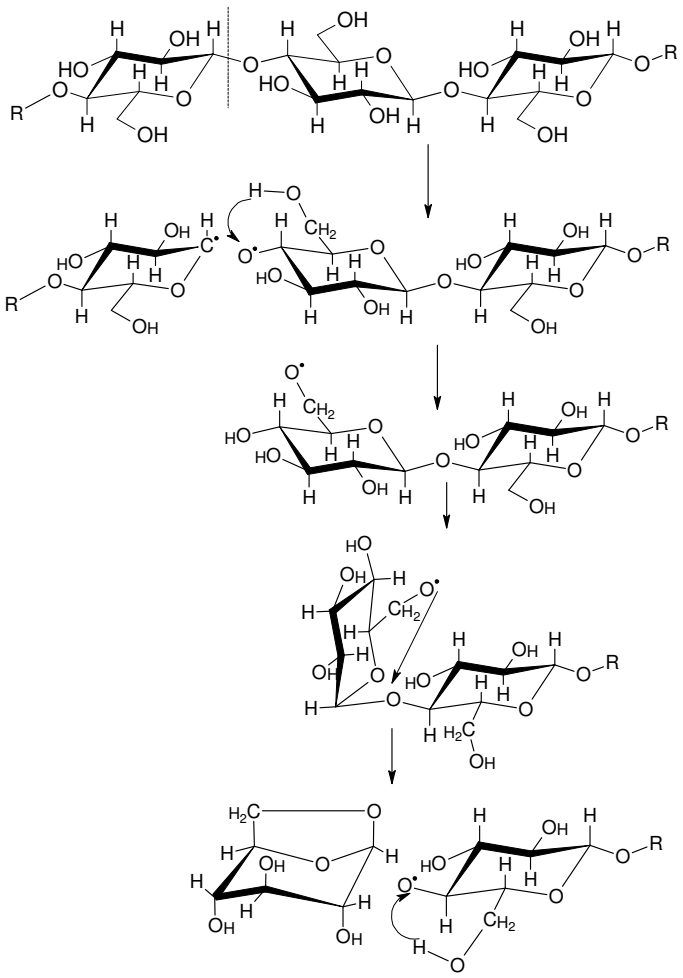

Figure 2.1: *Formation of Levoglucosan from Cellulose Pyrolysis by a Homolytic Mechanism – adapted from ref [3].*

Shafizadeh[7] continued to examine cellulose pyrolysis in great detail, paying particular attention to levoglucosan. He proposed that the thermal degradation of cellulose proceeded through two types of reactions; 1) a gradual degradation/ decomposition and charring at lower heating temperatures, and 2) rapid volatilization accompanied by the formation of levoglucosan at higher heating temperatures. The initial low temperature reactions were thought to involve depolymerisation, hydrolysis, oxidation, dehydration, and decarboxylation.

Research performed by Kawamoto[8, 9] attempted to confirm the key role of levoglucosan in char formation during cellulose pyrolysis. The conclusion from his studies was that, in sulfolane (a solvent for levoglucosan) levoglucosan upon

formation is dispersed throughout solution, preventing polymerization and therefore prohibiting the subsequent formation of solid char.

Glycoaldehyde is another major product obtained from both vacuum and fast pyrolysis of cellulose[10]. Under nitrogen in vacuum at 350 °C glycoaldehyde was found in yields up to 9.2%. A mechanism proposed for the formation of glycoaldehyde under the above conditions is illustrated in Figure 2.2.

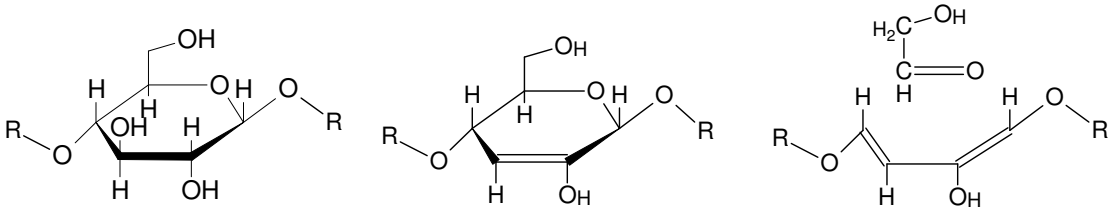

Figure 2.2: *Formation of Glycoaldehyde from Cellulose Pyrolysis – adapted from ref [10].*

More complex kinetic models have been put forward over the years including the Waterloo model proposed by Piskorz *et al*[6]. In this model two competing reactions utilize cellulose as the starting material. One reaction involves chain cleavage resulting in a low-degree polymerized cellulose, with the other reaction involving char formation through dehydration and elimination reactions. The low degree polymerized cellulose continues to react and degrade via two subsequent routes. The first route involves fragmentation reactions resulting in low molecular weight gases, whereas the second route involves depolymerisation to levoglucosan and other higher molecular weight derivatives. Due to the plethora of cellulose thermal decomposition products, this method also appears to be oversimplified. An even more complex model was put forward by Diebold[6] which involved an increased amount of steps and reaction routes. This was done in an attempt to take into account the great many pyrolytic products formed from cellulose pyrolysis. The latest pyrolysis model to be put forward was by Wooten *et al*[6]. ^{13}C Cross Polarization Magic-Angle Spinning (CPMAS) NMR was used to substantiate claims of both an intermediate cellulose and a final cellulose product being formed after heating cellulose at 300 °C for various time periods. The intermediate cellulose was degraded over time, forming final cellulose and various other low molecular weight volatiles, including some aromatics.

The final cellulose portion was further degraded to aromatic units, ultimately forming the basis of a large cross-linked aromatic structure proposed at increased temperatures.

Infrared spectroscopy has been used extensively as a method of examining cellulose degradation[7, 11, 12]. Under atmospheric conditions and at low temperatures, (25-250 °C) oxidative and dehydration reactions appear to be dominant. This was seen in the progressive development of C=O groups and the disappearance of carbohydrate hydroxyl groups. The decline in intensity of the CH_2 deformation band suggested that the primary hydroxyl group was preferentially oxidized. At temperatures above 250 °C (~40% weight loss) the crystalline structure of cellulose was grossly destroyed. This was observed through the disappearance of an infrared band at 900 cm^{-1} assigned to C-1 of D-glucose residues. A new band was also apparent and was assigned to carboxyl (C=O) stretches. The above changes are attributed to the cleavage of the oxygen ring and the subsequent formation of carboxylic functionalities. Oxygen at C-1 was thought to be next liberated as carbon monoxide, carbon dioxide, water, and as other volatiles. This process occurs between temperatures 240-370 °C, and results in the formation of aromatic units. At temperatures between 370-850 °C hydrogen was subsequently driven off, bringing the aromatic units closer together and ultimately leading to large cross-linked condensed aromatic structures[7].

The analytical technique of NMR spectroscopy has also been used extensively as a method of examining cellulose degradation[6, 13-15]. The technique CP/MAS ^{13}C-NMR was employed on cellulose chars produced under flowing nitrogen over the temperature range 325-500 °C[13]. Cellulose was exposed to successively higher temperatures over 5-minute time periods. ^{13}C-NMR spectra of cellulose samples prior to heating show several resonance peaks at 60-110 ppm. These peaks are associated with the unaltered carbon chain of glycosidic units. At a heat treatment temperature (HTT) of 325 °C a 37% weight loss was observed and attributed to the removal of water. Little difference was observed in the NMR spectra, apart from the appearance of broad peaks on both sides of the glycosyl carbon peaks. This was

interpreted as the formation of carbon-carbon double bonds and carbonyl functionalities. Additional heating at 350 °C produced more drastic changes. A 67% weight loss was observed and new resonance peaks appeared in the NMR spectrum. The new peaks were associated with more carbon-carbon double bonds, carboxyl groups, and carbonyl groups. Heating at 400 °C resulted in a 87% weight loss, producing a char which was relatively stable upon further heating. The 'stable' char corresponded to the complete loss of glycosyl carbon peaks previously observed at 60-110 ppm. Further heating to 500 °C had minor effects on the NMR spectrum, with increased condensation and cross-linking being the dominant process. Aromaticity increased as a function of temperature and was evaluated from the increase in intensity of the aromatic signals denoted by 110-150 ppm resonances. The increased aromaticity of the char between temperatures 400-500 °C, was attributed to the preferential loss of less stable parraffinic groups. Homolytic cleavage of these less stable groups is thought to promote further cyclization through the formation of free radicals.

Other novel techniques utilized in obtaining structural information of cellulosic chars include Pyrolysis-Gas Chromatography-Mass Spectrometry (Py-GC-MS)[12] and laser pyrolysis coupled with Molecular Beam Mass Spectroscopy [16]. Py-GC-MS analysis of low temperature chars (190 °C and 220 °C) identified mostly pyranones, furanones, and furans, besides the main product, levoglucosan. Chars produced at 310 °C gave rise to an increased amount of reduced aromatic units relative to the amount of oxygen-containing saturated compounds. Chars produced at higher temperatures still were composed of greatly condensed thermally stable aromatic compounds. Detectable compounds included benzofurans, dibenzofuran, fluorene, and naphthalene derivatives.

2.1.2 Noncellulosic Carbohydrate Pyrolysis.

The pyrolytic properties of hemicelluloses are not dissimilar to that of cellulose, however it is well-known that the hemicelluloses are thermally less stable than cellulose and lignin[2, 17, 18]. Thermogravimetric analysis (TGA) and Differential

Scanning Calorimetry (DSC) are two analytical techniques that have been employed to investigate the thermal degradation properties of extracted hemicelluloses[17]. It was observed that hemicelluloses degraded at a temperature of 180 °C, with a maximum rate of weight loss occurring between temperatures 240 °C and 320 °C. It was also noted that hemicelluloses degraded at a much faster rate than cellulose and lignin between temperatures 200 °C and 300 °C. The major products of hemicellulose pyrolysis include volatiles, levoglucosan, other anhydroglucoses, other anhydrohexoses, levoglucosenone, and various furans[19].

Below 200 °C, all noncellulosic carbohydrates undergo condensation reactions forming complex highly branched dextrins. Rapid decomposition of non-cellulosic carbohydrates occurs above 200 °C resulting in the production of a variety of anhydrosugars, light volatile organic compounds, H_2O, CO_2, CO, and char. Above 500 °C two competing global reactions in the vapor phase consume the reactive anhydrosugars and related solid phase pyrolysis products[3].

The polymerization of levoglucosan into branched dextrins was first described by Pictet in 1918[20]. Figure 2.3 illustrates the thermal polymerization of levoglucosan.

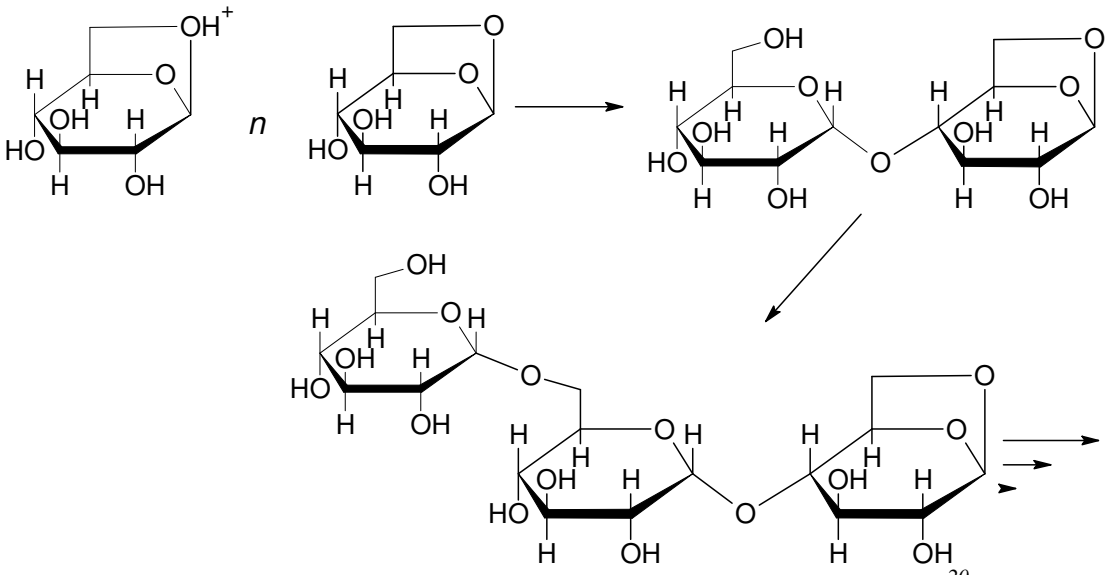

Figure 2.3: *Thermal Polymerization of Levoglucosan – adapted from ref [20].*

Pyrolysis of simple monomeric and dimeric sugars differs significantly from the pyrolysis of cellulose. Thermogravimetric analyses indicate that thermal decomposition of D-glucose occurs at significantly lower temperatures compared to cellulose. Pyrolysis of sugars D-glucose, D-fructose, and sucrose yield a greater percentage of furans, a lower percentage of anyhydrosugars, and a lower percentage of low molecular weight carbonyl compounds relative to pure cellulose. The larger yields of furans from simple monomeric and dimeric sugar pyrolysis are attributed to the presence of reducing sugar moieties. Cellulose contains only a single reducing sugar at one end of the polymer chain and cannot easily open up to acyclic forms. This property of cellulose results in the preferential formation of anhydrosugars. In addition, sugars that have intact furanose rings can directly form furans upon pyrolysis. Compounds furfural and 5-hydroxymethylfurfural are major pyrolysis products of D-glucose, D-fructose, and sucrose but only form in minor amounts from cellulose pyrolysis. Furans are also reasonably stable aromatic compounds, for example 90% of furfural is recovered unchanged when heated at 500 °C. There is also a kinetic preference to form five membered rings rather than six membered rings when both are possible[21]. Furfural resins formed from the polymerization of furan rings (Fig. 2.4) may be a significant relatively high temperature end product in pyrolyzed carbohydrates[22].

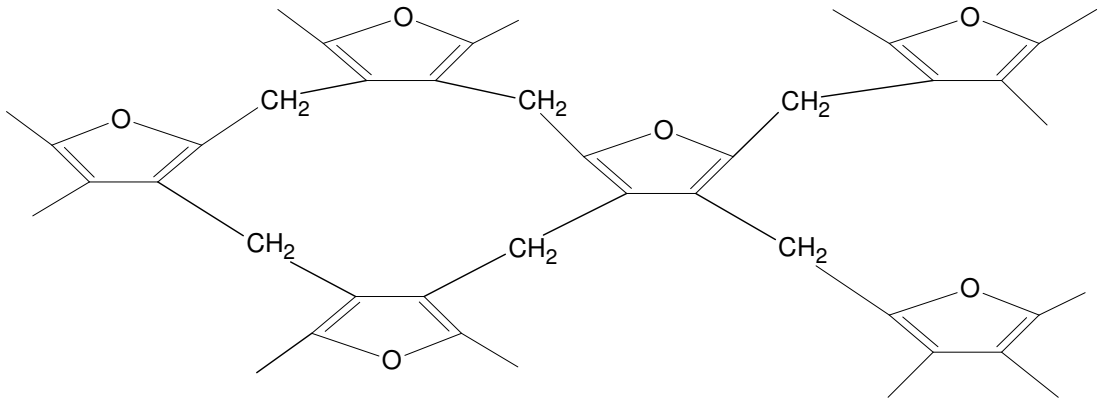

Figure 2.4: *Example of a Furfural Resin – adapted from ref [22].*

Ultimately the survivability of a substrate or a pyrolysis product depends upon its thermal stability and its vapor pressure under the reaction conditions[21].

2.1.3 Lignin Pyrolysis

Lignin is described as the most thermally stable component of biomass, with thermal degradation below 200 °C being very slow. It is important to note that the products of lignin pyrolysis reflect the source of the lignin. At more moderate temperatures lignin pyrolysis results in the formation of a solid char residue, an aqueous distillate, a viscous tar, and a mixture of permanent gases. Major components of the aqueous distillate include water, methanol, acetic acid, acetone, and acetaldehyde. Unlike carbohydrate pyrolysis products, tars resulting from lignin pyrolysis contain no single predominant compound. Lignin pyrolysis tars are composed of a wide variety of phenol related compounds. At high pyrolysis temperatures lignin chars decrease in yield whilst the production of condensable products and gases increase. Furthermore, the formation of unsaturated hydrocarbons is favored at higher temperatures[4]. Figure 2.5 illustrates the concurrent and consecutive pathways of lignin pyrolysis.

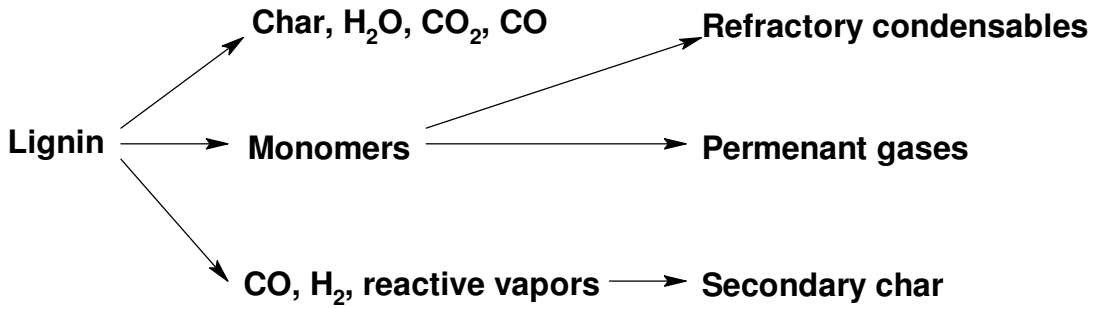

Figure 2.5: *Concurrent and Consecutive Pathways of Lignin Pyrolysis – adapted from ref [4].*

Sharma *et al*[23] studied the chemical characteristics of lignin char as they evolved with HTT. Lignin char aromaticity was observed to increase with temperature. Above 350 °C a large decrease in the char O/C ratio was observed and attributed to decarboxylation and dehydration. As the temperature was increased hydrogen and oxygen were preferentially lost. Above 450 °C the aromatic character of lignin char increased significantly, resulting in aromatic carbon contents of 70%. A speculative structure of a lignin char resulting from pyrolysis at 550 °C under nitrogen for 1 hour is offered by Gillet and Urlings (Fig. 2.6)[24].

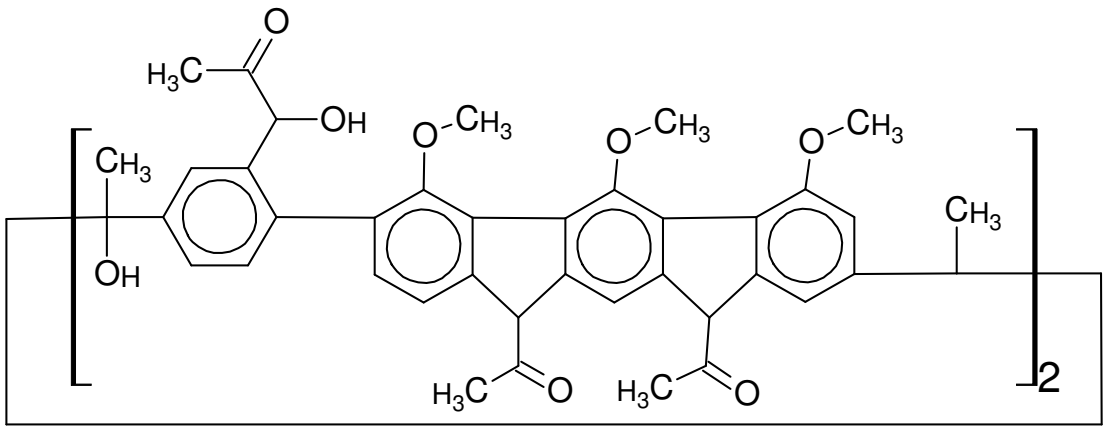

Figure 2.6: *Speculative Structure of a Braun's and Ethanolysis Lignin Char – adapted from ref [24].*

2.1.4 Lignocellulosic Pyrolysis

Pyrolysis chemistry of the major individual components of biomass has been studied extensively and reviewed above. The following section will address the pyrolysis chemistry associated with the thermal degradation of biomass as a whole. Evidence from the review offered by Antal[4] indicates that the pyrolytic behavior of wood is not a linear superposition of its components. It is known that lignin pyrolysis forms more char than wood pyrolysis, and wood pyrolysis forms more char than cellulose pyrolysis[13]. It should be noted however that carbon yield is strongly dependent on the vapor phase conditions present in the pyrolytic reactor, and cannot therefore be predicted by summing the yields of substrates cellulose, hemicelluloses, and lignin components[25]. The three known competing pathways (production of volatiles, production of tars, and production of char) noted to play a role in the pyrolysis of cellulose, hemicelluloses, and lignin are preserved in the pyrolysis of lignocellulosic materials. Condensation reactions at low temperatures give rise to the formation of a solid residue. At higher temperatures, transglycosylation and similar reactions result in the formation of syrups, tars and some gases. At temperatures above 500 °C reactive vapors evolved by solid phase pyrolysis reactions are converted into hydrocarbon rich synthesis gas, while competing vapor phase condensation reactions form refractory condensable materials[4].

Antal *et al*[26] used Fourier-Transform Infrared (FTIR) as a method for obtaining structural related information from heat treated flash carbonized charcoals. Macadamia nutshell biomass was flash carbonized producing a black char. Char samples were subsequently milled down to a desired particle size and carbonized at 650, 750, and 850 °C under an inert atmosphere. The untreated char was observed to have an alkyl aromatic structure with many oxygen containing functional groups, (C-OH, C=O, C-O-C). Upon carbonization these functionalities were almost completely destroyed. At 650 °C, the hydroxyl and aliphatic C-H stretches were greatly reduced and were almost non-existent. C=O stretching was also greatly reduced but was still apparent. Characteristic C-H out of plane bending modes intensified between 900 and 700 cm^{-1}, signaling an increase in aromatic development. At 750 °C, the C=O stretch was almost completely absent, as well as aromatic C-H groups. A weak C-H stretch still remained at 880 cm^{-1}, and was assigned to lone hydrogen atoms at the edges of condensed aromatic sheets. The use of Thermogravimetry-Mass Spectroscopy (TG-MS) confirms the decrease in aromatic C-H groups as a loss of hydrogen. Between 1700 and 1000 $cm^{-1}$of the IR spectrum a weak broad band was apparent and interpreted as skeletal stretching involving residual oxygen and or nitrogen atoms bound in aromatic units. At 850 °C the broad band became even weaker as did the aromatic C-H band. Important to note was the small observable differences in IR spectra between synthetically made graphite and high temperature carbonized charcoals. High temperature (~950 °C) carbonized charcoals produced from different biomass all had analogous IR spectra.

2.2 The Traditional View on the Structure of Charcoal

The physical properties of charcoal differ significantly from alternate highly carbonaceous materials. The three allotropic forms or carbon are graphite (Fig. 2.7 (a)), diamond (Fig. 2.7(b)), and fullerene (Fig. 2.7(c)). Graphite is a two-dimensional crystalline solid, composed of a series of stacked parallel layer planes, having trigonal sp^2 bonding. Within each layer, carbon atoms are bonded to three other carbon atoms forming a series of continuous hexagons. Graphite is black, opaque, metallic in luster, soft (hardness 1-2), and gives a black streak. Other

important properties of graphite include its lubricity and its ability to conduct electricity. Graphite has a density of 2.26 g/cm^3 and an extremely low specific surface area[27]. Diamond is a three dimensional transparent crystalline solid made up of covalently bound tetrahedral carbon units. Diamond is the hardest material known, a poor conductor of electricity, and converts to graphite at 1700 °C. Fullerenes can be made from either the combustion or pyrolysis of aromatic hydrocarbons. Carbon atoms in fullerene (C_{60}) are bonded in an icosahedral structure made up of 20 hexagons and 12 pentagons[28]. Fullerene carbon bonds deviate substantially from ideal sp^2-hybridised carbon bonds observed in graphite[29]. At room temperature fullerene has a density of 1.72 g/cm^3 and is readily soluble in solvents chloroform and toluene[30]. C_{60} is thermodynamically less stable than graphite and diamond, decomposing into graphite like materials when heated above 727 °C at atmospheric pressure. Decomposition is more rapid in the presence of oxygen[29].

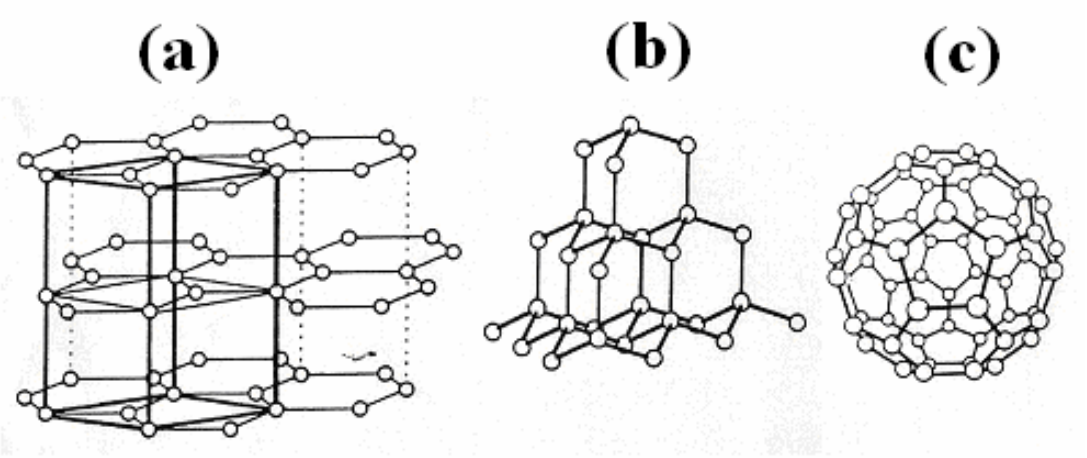

Figure 2.7: *Allotropic Forms of Carbon[28]. (a) graphite. (b) diamond. (c) fullerene. Reprinted from International Materials Reviews, Vol. 42, P. J. F. Harris, Structure of Non-graphitizing Carbons, 206-218, 1997, with permission from Elsevier.*

Carbon in the form of charcoal and coal is usually termed amorphous, that is, the crystals if any are too small to be detected by microscope[31]. Coal is divided up into three classes, lignites (72% carbon), bituminous (85% carbon), and anthracite (93% carbon)[32]. Lignin coals are described as being soft and dull with an earthy texture. Bituminous coal (see Fig. 2.8) is hard and black with shiny layers, while anthracite is bright and lustrous with a conchodial fracture[33]. Coal is not an electrical conductor[26].

A good quality charcoal was described by Chaturvedi as follows: "Charcoal of good quality retains the grain of the wood; it is jet black in color with a shining luster in a fresh cross-section. It is sonorous with a metallic ring, and does not crush, nor does it soil the fingers. It floats in water, is a bad conductor of heat and electricity, and burns without flame"[25].

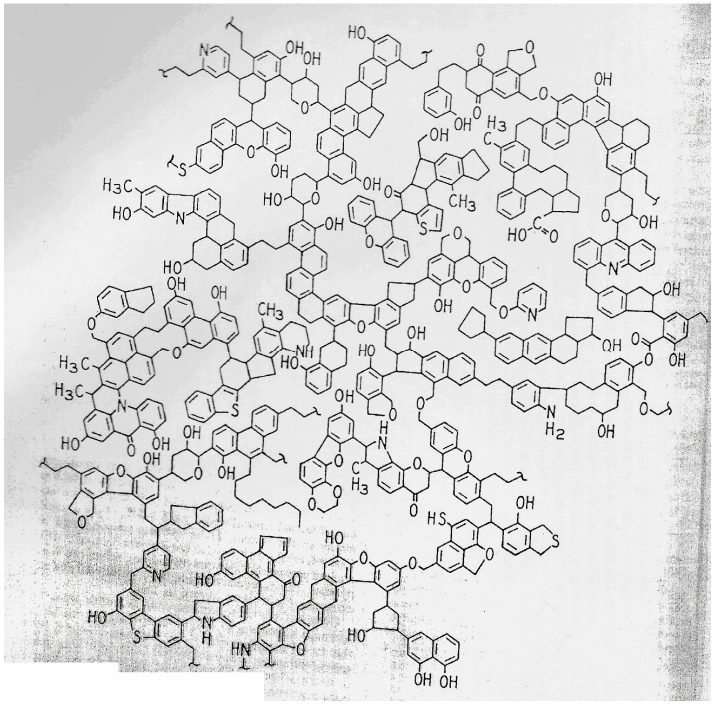

Figure 2.8: *Model of a Bituminous Coal Structure*[34]*. Reprinted from Fuel, Vol. 63, From Coal to Single-Stage and Two-Stage Products: A Reactive Model of Coal Structure, 1187-1196, 1984, with permission from Elsevier.*

It was proposed from early X-ray diffraction experiments that so-called amorphous carbon was in fact microcrystalline graphite[31]. An experiment performed by Walker and Seeley[35] examined the effect of fine grinding on a Ceylon natural graphite. The sharp intense (002) graphitic peak observed at 26.6 ° (2 θ) decreases rapidly upon fine grinding with the final XRD spectrum resembling a turbostratic[4,36] carbon. It should be noted however that the fine milling produced a pyrophoric material. The spontaneous ignition was attributed to severe oxidation, which may ultimately cause a

[4] A type of crystalline structure where elementary particles are arranged in a parallel fashion in groups and these groups are arranged in turbulent array[36].

change in the microcrystalline structure of the graphitic material. Numerous papers [37-39] have reported the presence of graphite and diamond like structures in non-graphitic carbons. The papers report using techniques such as Transmission Electron Microscopy (TEM) and High Resolution Electron Microscopy (HREM) to positively identify graphitic structures. Micrographs show both curved and flat carbon layers which are subsequently interpreted as imperfect graphene layers.

In 1951 Rosalind Franklin[40] demonstrated that two distinct classes of carbon are produced from the pyrolysis of organic materials, graphitizing carbons and non-graphitizing carbons. The structure of such carbons depends not only on the temperature of preparation, but also on the nature of the starting material. General physical properties associated with the two classes of carbon are outlined below:

Non-graphitizing carbon:	Hard
	Porous
	Low density
	No trace of homogeneous development of true graphitic structure, even after heating to 3000°C
Graphitizing carbon:	Soft
	Non-porous
	Relatively high densities
	Char structure readily transformed into crystalline graphite

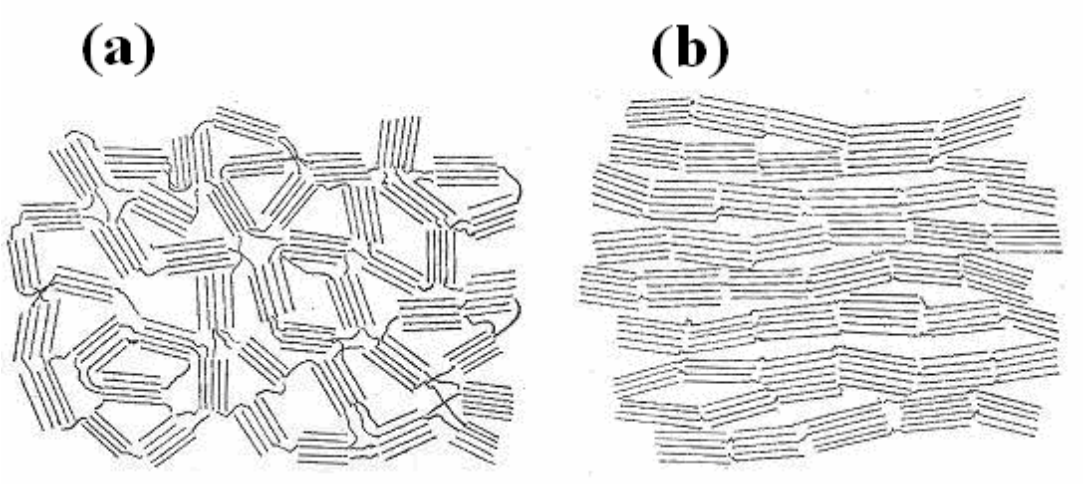

Figure 2.9: *Schematic Representations of (a) a Non-Graphitizing Carbon and (b) a Graphitizing Carbon*[40]*. Reprinted from Proc. R. Soc. London A, Vol. 209, Crystallite Growth in Graphitizing and Non-Graphitizing Carbons, 196-218, 1951, with permission from The Royal Society..*

Franklin's model (Fig. 2.9(a)) describing a non-graphitizing carbon involves randomly orientated individual units with extensive cross-linkages, which cause sufficient impediment so as to reduce parallel alignment of graphitic planes. Structural units in a graphitizing carbon (Fig. 2.9(b)) are very nearly parallel and are held together with a small number of weak cross-linkages. Formation of crystalline graphite from this model is expected to be relatively facile. It is known that high C/H ratios in the initial feedstock will enhance the formation of a three dimensional graphitic structure[41]. It is important to note that carbohydrate based carbons are classified as non-graphitizing carbons due to the initial feedstock containing significant amounts of oxygen[40].

Bryne and Marsh proposed a char model (Fig. 2.10(a)) comprised of sp^2 and sp^3 carbon atoms bonded in five, six, and seven membered rings[28]. An attempt was also made to illustrate the possible porosity of such a carbonaceous structure, (Fig. 2.10(b)).

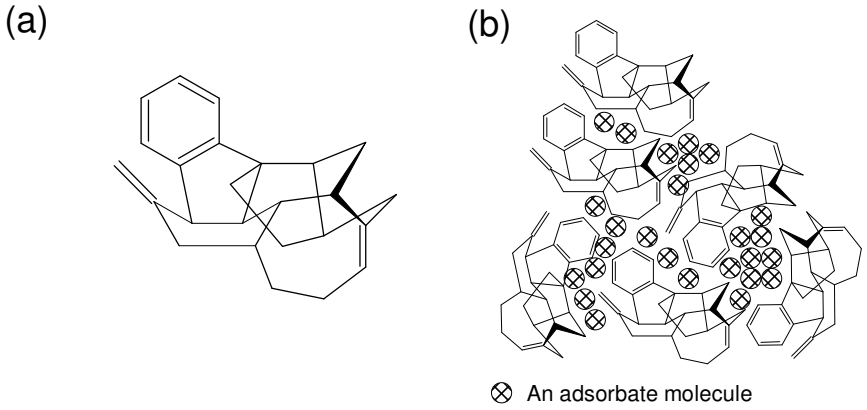

Figure 2.10: *(a) Possible Carbonaceous Structural Unit Produced by Pyrolysis of Cellulosic Precursor. (b) Model of Microporous Carbon – adapted from ref [28].*

In a review on the structure of non-graphitizing carbons, Harris[28] provides HREM evidence that non-graphitizing carbons may have a microstructure related to that of fullerenes. HREM analysis of heat treated sucrose indicated the presence of closed nanoparticles. The closed nanoparticles were interpreted as fullerene like elements and likened to particles which can be produced by arc evaporation in a fullerene generator. The model of a non-graphitizing carbon proposed by Harris (Fig. 2.11) consists of discrete fragments of randomly curved carbon sheets containing pentagons and heptagons.

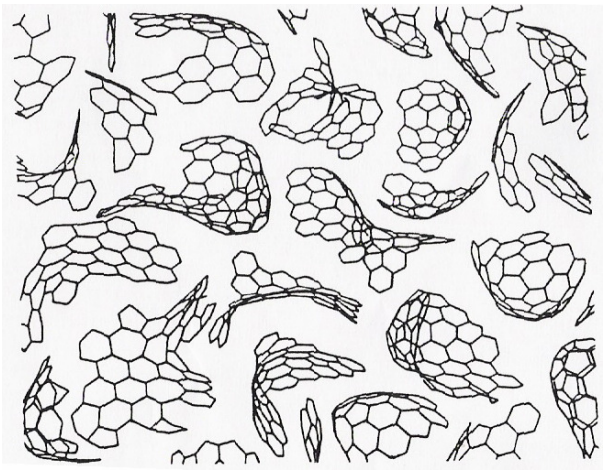

Figure 2.11: *Schematic Representation Proposed by Harris of a Non-Graphitizing Carbon[28]. Reprinted from International Materials Reviews, Vol. 42, P. J. F. Harris, Structure of Non-graphitizing Carbons, 206-218, 1997, with permission from Elsevier.*

2.2.1 Problems with Traditional Charcoal Models

In the case of Franklin's model, the cross-links between the graphitic fragments are not described. Such crosslink's would have to be extremely strong, to prevent graphitization at temperatures of 3000 °C and above. Some models incorporate sp^3 bonded carbon atoms, however the main problem with this is that sp^3 bonded carbon is unstable at high temperatures. Diamond is converted to graphite at 1700 °C. Non-graphitizing carbon models based on results obtained from electron micrographs also encounter some skepticism. In early micrographs of various carbons only the {0002} fringes were resolved, resulting in images having a ribbon like appearance. However, since only a part of the structure is being imaged, the appearance can be misleading. It should also be noted that attempts to extract C_{60} and other fullerene molecules from heat treated carbons has been unsuccessful[28]. Biocarbons are also found to contain significant amounts of oxygen; 4-6% for various charcoals carbonized at 950 °C[26]. Despite this analytical evidence or the additional supportive evidence summarized by Marsh *et al*[41] with respect to the possible oxygen functionalities associated with non-graphitizing biocarbons, no comprehensive biocarbon model to date incorporates the presence of the heteroatom. Present charcoal models also ignore the presence of free radicals, chemisorption, and the impact of porosity.

In general heat treated carbons derived from carbohydrate based materials are described as being largely condensed aromatic structures of graphitic nature.

2.3 Minerals in Biomass and Biomass Charcoal's

The process of demineralization involves washing the biomass material with a given solution. Carboxylic acid groups present in cellulose materials endow the material with ion exchange capacity, i.e. the ability to absorb metallic cations[42]. Washing biomass is aimed at removing inorganic minerals from such organic acid groups.

Biomass contains a range of inorganic minerals at different concentrations and in different forms. Common biomass macronutrients include nitrogen, phosphorus,

potassium, calcium, magnesium, and sulfur. Biomass minerals required in smaller quantities include iron, manganese, zinc, copper, boron, molybdenum, and chloride. These particular elements are also termed the micronutrients. Other minerals present in large quantities include aluminum, sodium and silicon[43].

The majority of minerals present in biomass have specific roles and functions:

Calcium is most notably associated with cell walls. The activity of calcium is related to its capacity for coordination, whereby it provides stable reversible intermolecular linkages[44]. Ca^{2+} is found in high concentrations in the middle lamella. The ion is bound to $R{\cdot}COO^-$ groups of polygalacturonic acids (pectin's) in a more or less readily exchangeable form. Calcium can also be found in plant cell vacuoles, present as precipitated calcium oxalate, calcium phosphate, and as water soluble Ca^{2+} [44].

The role of magnesium in plants is largely dependent on its capacity to interact with strongly nucleophilic ligands through ionic bonding. Magnesium also forms covalent bonds; the most notable example is magnesium bound to chlorophyll molecules. It is translocated readily in most plants taking part in a variety of enzymatic reactions[43]. If an abundant source of magnesium is available to biomass, the magnesium ion is often stored as inorganic salts in plant cell vacuoles[44]. Phosphorus when taken up into plants remains either as inorganic phosphate or is quickly esterified into simple organic phosphate esters. Exchange between the two forms occurs rapidly. Phosphorus is also involved in forming highly stable diesters, which connect organic units to more complex larger structures[44] for example in DNA. In general phosphorus is associated with metabolic processes carried out in plant cells for example energy manipulation via ATP.

In each component of a plant, within cells and plant tissues, the potassium ion is found to be highly mobile. Potassium is not metabolized and forms readily exchangeable complexes. Potassium is used in enzyme activation, protein synthesis, photosynthesis, and is one of the key inorganic solutes in osmoregulation[44].

The mobility of the chloride ion is very high in plants and it occurs usually as a free anion or is found loosely bound to readily exchangeable organic sites. Chlorine is also found structurally bound in chlorinated organic compounds. The role of chlorine in plants includes an involvement in the water splitting step of photosynthesis[43], stomatal regulation, and osmoregulation[44].

Silicon is initially taken up by plants as monosilicic acid. Monosilicic acid is known to interact with pectins and polyphenols located in plant cell walls. Plants can be distinguished into silicon accumulators and non-accumulators. The wetland Gramineae species rice is an example of a silicon accumulator. Long distance transport of soluble silicon is confined to the xylem with large amounts being deposited on the cell walls. Silica is deposited either as silica oxide or as opal phytoliths at the termini of the transpiration stream, the epidermal cells in plant leaves and intracellularly in 'silica cells'[44]. It appears that the role of silicon is largely associated with plant cell mechanical strength.

Sulfur is obtained by plants via the atmosphere as sulfur dioxide and via the root system as soluble sulfate ions. Before sulfur is utilized as a structural component of amino acids, proteins and coenzymes, it must be in its reduced form. Reduction of sulfate occurs predominantly in leaves as the reaction is enhanced by light[44].

As illustrated in section 3.4 the predominant cell type in softwoods is the vertically orientated longitudinal tracheid, more commonly termed fibers. This type of cell is what gives a tree its mechanical strength and support. The cells also serve as a pathway for translocation of water-soluble minerals. Arranged horizontally in softwoods are wood rays. The wood rays are largely composed of parenchyma cells, which serve as storage receptacles. Insoluble mineral compounds such as calcium oxalate and silica oxide can be found in such receptacles in relatively large concentrations[45]. Hardwoods are more complex than softwoods containing various cell types, however structural concepts are analogous. The parenchyma cell content in hardwoods is found to be on average much greater than in softwoods[45].

Biomass-fired, power boiler deposits are generally comprised of alkali and alkaline chlorides, sulfates, carbonates, and complex silicates. Reactions between potassium and silica with chlorine as a facilitator, leads to the formation of fused glassy deposits and slags at the usual boiler operating temperatures 800-900 °C[46]. The concentration of chlorine often dictates the amount of alkali minerals vaporized during combustion. Chlorine plays a shuttle role, aiding the transport of alkali minerals to biomass surfaces[47]. Potassium, silicon, and chlorine are found in high concentrations in straws. Wood however contains very little silicon and substantially lower amounts of potassium[47].

Numerous demineralization investigations have been carried out on select grass species [46, 48, 49]. Straw is seen as a fast growing renewable feedstock commonly used in biomass-fired, power boilers and as a result has received a growing amount of attention in terms of pretreatment prior to thermal degradation and combustion. In 1996, Jenkins *et al* [46] performed an extensive study on the properties of washed straw. Jenkins utilized various washing techniques combined with elemental analyses and scanning electron microscopy to evaluate the effect of washing biomass prior to thermal degradation. Rice straw and wheat straw, collected at three different times of the year, were used to form the basis of this study. Ash compositions of alternate herbaceous and wood materials were also examined but in less detail. It was noted that ash composition of the grasses, (gramineae) including rice and wheat straw, switch-grass, sugar cane trash (tops and leaves), and sugar cane bagasse had higher amounts of silica in comparison to the wood Douglas Fir, ~35.8-74.3% compared to 12.3% respectively. Potassium levels for all feedstock ash types also appear high compared to concentrations of other minerals present, ~4.2-18.4%. Also worth noting is that the Douglas Fir wood ash sample had a higher amount of calcium and magnesium compared to rice and wheat straw respectively, ~ 37.1 and 5.9% compared to 1.61-13.1% and 1.9-4.3%. Total ash analysis indicated that the grasses have significantly higher ash levels than the wood of Douglas Fir, ~2.44-19.60% compared to 0.45%.

A chemical fractionation test has been designed and implemented on numerous common biomass fuels in order to characterize the nature of the inorganic

components[50]. The test involves sequentially leaching the chosen fuel in water, ammonium acetate, and hydrochloric acid. The amount of mineral matter removed at each step is quantified. It has been found that the elements potassium, chlorine, and phosphorus present in biomass are largely removed via water leaching. Large fractions of alkali elements are also easily removed through leaching in hot (90 °C) water.

Jenkins *et al*[46] applied five leaching treatments to most samples of rice and wheat straw. All laboratory treatments were carried out using water at ambient temperature (20-25 °C).

Leaching methods included:

1. Spraying water over the top of a 30 mm thick straw bed supported on an expanded steel Mesh for a period of 1 minute.

2. Pouring tap or distilled water through the sample spread over a fine Mesh stainless steel screen. 20 L of water was poured over 100 g samples (particle size <19 mm) in 1 L increments. An additional smaller particle size (<0.85 mm) sample was leached in a similar fashion; vacuum filtered using 7 L of water in 0.5 L increments.

3. Submerging and soaking 100 g (whole straw) samples in 7 L of distilled water over a period of 24 hours.

In addition to the above samples, natural rain washed samples of rice straw were selected and analyzed in a similar fashion to the laboratory leached samples. Solid samples were analyzed for percentage ash content, percentage moisture, heating value and elemental composition. The ash content of the various straw samples was determined by igniting the sample in a muffle furnace set at 575 °C for a time period of 2 hours.

The average ash content of untreated rice straw is 19.6% (dry weight basis, DWB) compared to 13.0% obtained for that of wheat straw. All laboratory treatments were observed to reduce ash content compared to the untreated original value. Analysis of Variance (ANOVA) indicated that treated samples were significantly different from the untreated control sample for both rice and wheat straw. For rice straw there was insufficient evidence to show that any one treatment was better than another in terms of ash removal. Analysis of wheat straw however, indicated that sprayed samples were significantly different from the more effective flushing and soaking treatments but there was no significant difference between the latter two. The natural rain washed rice straw sample showed a slight reduction (8%) in ash content on comparison to the untreated sample. Elemental compositions of untreated, sprayed, soaked, and rain washed samples was examined with elements present expressed on an oxide basis. A significant reduction in potassium content is observed for both herbaceous samples, with the soaking treatment being the most effective in terms of removal. Chlorine also appears to be readily leached from wheat straw as a 96% reduction was observed after soaking in distilled water. For both herbaceous fuels, sodium and phosphorus also seem to be easily removed via water pretreatment; especially significant was the affect which soaking in distilled water has on these particular alkali minerals. Calcium, magnesium, silicon, and nitrogen levels appeared to be largely unaffected by any of the leaching treatments. Washing also reduced sulfur content with a greater impact being noted for wheat straw rather than rice straw. Jenkins ash results indicate that the percentage effectiveness of ash removal for rice straw was substantially lower than that of wheat straw, however this may be accounted for by comparing silica concentrations between the feedstocks, ~71.3% compared to 35.8% respectively.

Turn *et al*[48] also examined the removal of inorganic constituents from biomass. The idea of applying sugar-processing technology to a fast growing tropical grass (banagrass) was explored. 1.2 tones of banagrass was harvested and processed via two different industrial cutters, a forage chopper, and a jeffco cutter. The jeffco cutter yielded particle sizes ~1 mm, where as the forage chopper produced mean sized particles ~3.9 mm. The subsequent samples were then subjected to a total of four treatments:

1. Forage chopped – un-pressed
2. Forage chopped – pressed
3. Forage chopped – pressed, rinsed, pressed
4. Jeffco cut – pressed, rinsed, pressed.

Dewatering was performed with a 91-tonne press. Rinsing involved the feedstock sample being placed into a polyethylene barrel containing 52 L of tap water. The sample was then agitated by hand for approximately 3 minutes. Prior to ash analysis, the biomass was dried at 105 °C and then subsequently milled to a particle size of <1.68 mm.

Biomass ash analysis included the detection of Si, Al, Ti, Fe, Ca, Mg, Na, K, P, S, Cl, and CO_2. The five major constituents in decreasing order of concentration for untreated banagrass ash were identified as K, Si, Cl, Ca, and Mg. These results are similar to the untreated herbaceous grasses investigated by Jenkins *et al*[46]. Ash content was observed to decrease as treatment severity increased. A ~30% ash reduction was noted between treatments: Forage-un-pressed, ~3.9% and Forage/Jeffco-pressed, rinsed, pressed, ~2.7%. The decrease in ash content was attributed to the loss of inorganic minerals, K, Mg, S, and Cl. Si and Ca concentrations remained largely unaffected by all treatments with a reduction of less than 15% being observed. Leaching of alkali minerals was enhanced through a reduction in particle size.

Di Blasi *et al*[51] investigated the effectiveness of leaching inorganic minerals from Danish wheat straw chars in comparison to raw feedstock in order to take advantage of size reduction. A two-stage conversion process was proposed; low temperature devolatilization and combustion followed by demineralization. Devolatilization and combustion resulted in alkali metals being retained in the reduced (30-40% of original weight) solid phase char. It was stated that during heating and devolatilization Ca^{2+} and K^{+} ions precipitated out as inorganic salts or became ion exchanged to functional char matrix groups[52]. This may enable easier demineralization. Straw (cut in 2-3 cm lengths) and char particles (0.5-1 mm in diameter) were submerged and soaked in twice distilled water at approximately 90

°C. Soak times varied from 0-120 minutes. After each selected sample residence time, samples were filtered and dried at 115 °C for a period of four hours. The ash content of all samples was determined via calcination over the temperature range 417-517 °C for 135 minutes. Untreated straw char was found to contain roughly the same amount of ash as untreated straw biomass (5-5.5%). This indicates that low temperature conversion causes no appreciable loss in alkali metals. The ash content of straws and chars, as a factor of leaching time, showed that after being submerged for 10-20 minutes, a major portion of inorganic minerals was leached. It is apparent however, that straw char requires slightly longer leaching times than straw biomass, 20 minutes as opposed to 10 minutes for the majority of mineral loss. Leaching time was also seen to increase according to the degree of oxidative degradation. Additional leaching time (>20 mins) indicated a very slow extraction rate for both straw biomass and char. A minimum ash content of 2% was observed for straw after leaching for 120 minutes, whereas ash contents of between 3% and 4% were observed for straw chars of varying degradation. The reduced effectiveness of char water washing was attributed to possible physicochemical changes, which affect the char matrix. Another supposed reason included a change in inorganic compound composition upon oxidative degradation which may affect solubility's or physical retardation of minerals as they become locked in the organic structure resulting from lignin and hemicelluloses phase changes.

Straw is not the only feedstock material, which has been subjected to pretreatments designed to reduce ash content. Recently Varhegyi[53] *et al* investigated the effects of hot water washing on chestnut wood. Five chestnut wood samples were selected from different origins and pretreated separately with hot water and acetone prior to thermal degradation. Hot water leaching involved placing 1 g of wood into a stirred vessel containing 100 ml of 60 °C tempered distilled water for a time period of two hours. The mean percentage ash level obtained from the 5 untreated chestnut samples was 0.5%. After washing in hot water the mean percentage ash level was 0.4%. Ash reduction for this hard wood appears to be much less (20%) than results observed with herbaceous wheat straws (52-68%)[46].

Extraction of inorganic minerals from biomass has not only been investigated using water as the solvent. More aggressive pretreatments have been used including strong acids and bases. A study performed by Iniesta *et al*[54] involved the pretreatment of almond shells in ambient tempered sulfuric acid (10 wt.%) and sodium hydroxide (2 wt.%) solutions. Prior to treatment almond shells were washed, dried, crushed (1.5 – 2.0 mm) and sieved. Ash content of the untreated feedstock and subsequent treated samples was determined via calcination at 850 °C. The following treatments were investigated:

H_2SO_4 (10 wt.%) for 30 min, 1, 3, and 24 hours.
NaOH (2 wt.%) for 3 and 24 hours.
Combined treatment: acidic solution (3 h) + basic solution (3 h).
Combined treatment: basic solution (3 h) + acidic solution (3 h).

For each treatment approximately 300 g of almond shell was immersed in solution for the selected time period. The samples were then removed, washed to neutrality, and dried at 105 °C. For combined treatments, samples were washed and dried after the first step. Weight loss during chemical pretreatments was also obtained in order to take into account possible structural changes due to loss and degradation of cellulose, hemicelluloses, lignin, and extractable material. Ash analysis of the raw feedstock indicated that Ca, Mg, Na, and K were the major elements present. Almond shell samples treated with acid for time periods 3 hours and 24 hours achieved ash reductions of 62.9% and 71.0% respectively. The almond shell sample treated initially with base and then with acid achieved an ash reduction of 24.2%. All other treatments increased the ash content. High weight losses were observed for those samples treated under basic conditions. This is not an uncommon phenomenon as bases are known to attack the lignocellulosic portions of biomass. The Kraft process utilizing hot sodium hydroxide removes roughly 80-90%[55] of original lignin by nucleophilic cleavage and concomitant fragmentation and solubilization of the lignin polymer. Alkali also causes rapid degradation of hemicelluloses as well as of cellulose albeit more slowly.

Piskorz *et al*[56] pretreated samples of poplar wood with sulphuric acid and hydrochloric acid. Ash analysis was performed by slow combustion of biomass in a muffle furnace set at 650 °C. Poplar wood samples were submerged separately in hot (100 °C) 5% H_2SO_4 and 3.7% HCl solutions for a time period of 2 hours. Ash content was reduced from 0.46% to 0.04 and 0.05% respectively. This corresponds to a ~90% reduction in ash content.

The process of combustion and thermal degradation of biomass results in the loss of some inorganic minerals via volatilization. Knudsen *et al*[52] recently produced a very detailed study on the release of Cl, K, and S during the combustion of annual biomass. Six different herbaceous fuels were selected, cut, and homogenized. 4-g samples were taken and initially pyrolyzed with the resulting char being burned through the addition of oxygen. The remaining ash was then digested using $HF/HNO_3/H_2O_2$ and analyzed via ICP-OES. It was observed that below 700 °C very little potassium was released for any of the herbaceous samples. This phenomenon is in agreement with previous studies[57, 58]. K release in herbaceous fuels low in Si was observed to increase close to linearly between temperatures 700-1150 °C. Close to 90% of K was released at 1150 °C. K release in herbaceous fuels high in Si and Cl showed more variation. At 800 °C, 40-50% of K was released. The feedstock wheat which was high in K and Si but low in Cl showed only a 20% release of K at 800 °C. Between temperatures 900-1150 °C, silica rich fuels showed an abrupt increase in the release of K. Knudsen thus proposed that the Si and Cl content in herbaceous fuels has a large impact on potassium release. Cl release is in agreement with previous studies[57, 59]; occurring in two steps. For nearly all six annual fuels near complete release of Cl was observed at temperatures above 800 °C. The main form of Cl release was initially as HCl and at higher temperatures as KCl. Fuels high in Si showed increased release of S upon combustion. At 500 °C, 25-35% of S was released to the gas phase. Increasing temperatures to 800 °C showed additional release, ~40-50%. A steep increase in S release was observed at temperatures above 800 °C, with almost 100% being liberated at 1150 °C. Contrary to this were the feedstock fuels which contain low Si levels in which over the entire temperature range a near 50% of S was ultimately released. Evaporation of pure salts was also

analyzed. It was noted that K_3PO_4 is not evaporated in significant amounts within the experimental temperature range. Other K salts including KCl, K_2SO_4, and K_2CO_3 all showed significant volatile loss at increasing temperatures.

Notable variance in K and S release was observed between pyrolysis and combustion of herbaceous fuels. During pyrolysis only an insignificant amount of K was released at temperatures up to 900 °C compared to S. Alternately 20-50% of K was released during combustion at 900 °C. Above 900 °C however significant K release was observed under pyrolysis conditions. Initial release of S was attributed to the decomposition of thermally unstable organic S containing compounds. S liberation also appears to be affected by Si content at temperatures 700-800 °C. The increase in S release of Si rich fuels was attributed to the preferential combination of Ca and K into silicates over S. During pyrolysis and combustion some inorganic mineral loss was also a result of fly ash exiting the system.

2.4 Carbon Conduction and Carbon Doping

A large amount of the research described in this thesis included a detailed investigation into the electrical properties of heat treated carbohydrate-based carbon materials. It is therefore appropriate to have a good understanding of carbon conduction. The following describes the current literature with respect to carbon in its two main pure allotropic forms; graphite and diamond. In addition the effect of doping such materials with exotic minerals is described.

Graphite is a two-dimensional solid, composed of a series of stacked parallel layer planes, having trigonal sp^2 bonding[27]. Single crystal graphite (ideal) is stacked in an ABAB... type sequence. An alternate stacking sequence ABCABC... can occur for carbon, resulting in a rhombohedral unit cell. Rhombohedral graphite always occurs with hexagonal graphite, and can be induced by grinding single crystal graphite[60]. Within each layer, carbon atoms are bonded to three other carbon atoms forming a series of continuous hexagons. The bonding within the layers is of sigma covalent type, and has a short length, (0.141 nm), and a high strength, (524 kJ/mole). These

hexagonal layers are held loosely together by van der Waals forces[61]. The structure of the layered sheets is in effect, a massive collection of fused benzene rings[62]. Due to sp^2 hybridization, in the case of graphite, each carbon atom has one unhybridized free p orbital electron which is able to move freely within the pi conjugated planes providing a means of conducting electricity. However, between the layers, there is no electron movement, and as a result conduction in this direction is a minimized. This phenomenon is responsible for the high anisotropy which graphite exhibits[61]. It has been well established that graphite is classed as a semi metal, an excellent conductor in the basal plane ($2.5 – 5.0 \times 10^{-6}$ Ω·m), but a poor conductor normal to the basal plane (3000×10^{-6} Ω·m)[1].

The p orbitals of graphite's hexagonal structure lie perpendicular in space to the planar sp^2 bonding orbitals (refer to Fig. 2.12). Adjacent p orbitals overlap as in benzene, forming pi bonding and antibonding orbitals of intrinsically different energies. Due to the honey comb structure of graphite, many p orbitals are interacting in the basal plane producing different bonding and antibonding orbitals of mutually exclusive energies. As previously stated, due to hybridization there is one free electron located in the 2p orbital. The 2p orbital has the ability to hold a maximum of two electrons per atom. As a result of this property and the Pauli Exclusion principle (electrons cannot exist in identical energy states), there are many energy levels available for the free 2p electron to occupy which are only infinitesimal amounts of energy away. Therefore for basal graphite consisting of *n* amount of carbon atoms, there will be *n* amount of electrons and *n* amount of unoccupied energy states. When a potential difference is applied, the free 2p electrons are able to increase in energy, since there are plenty of unoccupied states of slightly higher energy available[63].

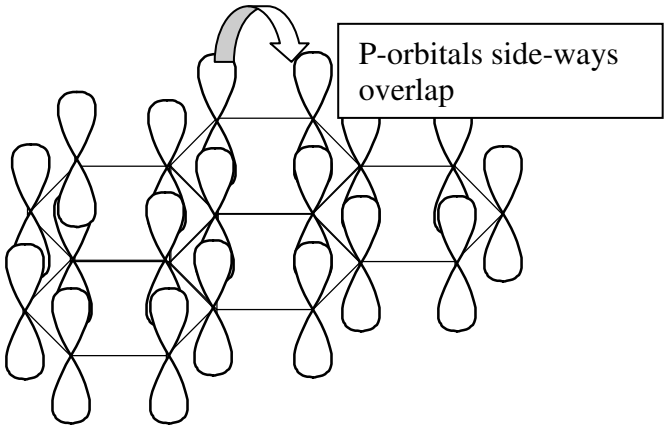

Figure 2.12: *Atomic Structure of Basal Graphite Showing Sideways P-Orbital Overlap.*

Perpendicular to the basal plane graphite exhibits insulator properties. The flow of electrons between the layered planes is extremely poor. The major reason for this effect can be attributed to the large physical gap (0.335 nm) present between graphitic planes. This spacing is more than twice the spacing between atoms within the basal plane and is approximately twice the van der Waals radius of carbon[27]. Electrons are unable to migrate from p orbitals in one plane to p orbitals in another plane due to the fact that there is no p orbital interaction between graphitic planes. It is also important to note that crystal imperfections of graphite including vacancies, stacking faults, disclination, and screw edge dislocations are a common physical property which may have considerable influence on the properties of the bulk material.

Diamond is a three dimensional solid made up of covalently bound tetrahedral carbon units. The sp^3 hybridization accounts for the tetrahedral nature of diamond. Four hybrid orbitals are formed by mixing the 2s orbital and the three 2p orbitals. The four equivalent hybrid orbitals are directed toward the four-corners of a normal tetrahedron[64]. All four sp^3 electrons take part in bonding leaving no free electrons. The nature of diamond's bonding gives rise to its well-known electrical and physical properties. Diamond is classed as an insulator having resistivities greater than 10^{18} $\Omega \cdot m$ and is extremely hard[27].

The electrical and physical properties of diamond and graphite can be altered through the inclusion of a small amount of impurity, the process of which is termed doping. In terms of a semiconductor two types can be manufactured depending on the type of impurity used. If the included impurity element has a greater number of valence electrons compared to the matrix valence electrons, an n-type semiconductor results. In the case of diamond if the included impurity arsenic were placed in the tetrahedral carbon lattice, one electron would remain largely excluded from bonding. Arsenic has five valence electrons compared with four for carbon, thus if arsenic is involved in tetrahedral covalent bonding one electron is left relatively free. Because of the small number of extra electrons, a doped semiconductor becomes slightly conducting[63]. However, if the included impurity element has less valence electrons compared to the number of matrix lattice valence electrons, a p-type semiconductor results. Again using the example of diamond, if the included impurity boron was placed in the tetrahedral carbon lattice, a hole would result. This occurs due to boron having only three valence electrons when involved in sp^3 hybridization. All three valence electrons are involved in the extensive tetrahedral covalent bonding structure creating a hole in the lattice. Electrons in nearby carbon atoms can jump into the lower energetic state hole therefore satisfying the stable tetrahedral unit cell. However this leaves a hole where that electron had previously been. The positive hole moves to a new location with each electron jump enabling the solid to carry an electric current[63]. It is important to note that doping is always accompanied by a more or less important distortion of the crystal lattice[65].

1. R. J. Lewis, S., *Hawley's Condensed Chemical Dictionary*. 12th ed.; Van Nostrand Reinhold: 1993.

2. Skille, J. Production of Activated Carbon from Biomass. The University of Trondheim, 1995.

3. *Biomass Pyrolysis: A Review of the Literature Part 1 - Carbohydrate Pyrolysis*. American Solar Energy Society Inc.: New York, 1982.

4. *Biomass Pyrolysis: A Review of the Literature Part 2 - Lignocellulose Pyrolysis*. American Solar Energy Society inc.: 1982.

5. Shafizadeh, F.; Fu, Y. L., Pyrolysis of Cellulose. *Carbohydrate Research* **1973,** 29, 113-122.

6. Wooten, J. B.; Seeman, J. I.; Hajaligol, M. R., Observation and Characterization of Cellulose Pyrolysis Intermediates by 13C CPMAS NMR. A New Mechanistic Model. *Energy and Fuels* **2004,** 18, (1).

7. Shafizadeh, F., Pyrolysis and Combustion of Cellulosic Materials. *Adv. Carbohydr. Chem. Biochem* **1968,** 23, 419-474.

8. Kawamoto, H.; Murayama, M.; Saka, S., Pyrolysis Behavior of Levoglucosan as an Intermediate in Cellulose Pyrolysis: Polymerization into Polysaccharide as a Key reaction to Carbonized Product Formation. *Journal of Wood Science* **2003,** 49, 469-473.

9. Kawamoto, H.; Hatanaka, W.; Saka, S. In *Thermochemical Conversion of Cellulose in Sulfoloane as a Solvent for Levoglucosan into Low Molecular-Weight Substances*, 5th International Biomass Conference of the Americas, Orland, FL, USA, 2001; Orland, FL, USA, 2001.

10. Richards, G. N., Glycoaldehyde from Pyrolysis of Cellulose. *Journal of Analytical and Applied Pyrolysis* **1987,** 10, 251-255.

11. Tang, M. M.; Bacon, R., Carbonization of Cellulose Fibers - I Low Temperature Pyrolysis. *Carbon* **1964,** 2, 211-220.

12. Pastrova, I.; Bottom, R. E.; Arisz, P. W.; Boon, J. J., Cellulose Char Structure: A Combined Analytical Py-GC-MS, FTIR, and NMR Study. *Carbohydrate Research* **1994,** 262, 27-47.

13. Sekiguchi, Y.; Frye, J. S.; Shafizadeh, F., Structure and Formation of Cellulosic Chars. *Journal of Applied Polymer Science* **1983,** 28, 3513-3525.

14. Wooten, J. B.; Crosby, B.; Hajaligol, M. R., Evolution of Cellulose Char Structure Monitored by 13C CPMAS NMR. *Fuel Chemistry Division Preprints* **2001,** 46, (1), 191.

15. McGrath, T. E.; Chan, W. G.; Hajaligol, M. R., Low Temperature Mechanism for the Formation of Polycyclic Aromatic Hydrocarbons from the Pyrolysis of Cellulose. *Journal of Analytical Applied Pyrolysis* **2003,** 66, 51-70.

16. Herring, A. M.; McKinnon, J. T.; Petrick, D. E.; Gneshin, K. W.; Filley, J.; McCloskey, B. D., Dectection of Reactive Intermediates During Laser Pyrolysis of Cellulose Char by Molecular Beam Mass Spectroscopy, Implications for the Formation of Polycyclic Aromatic Hydrocarbons. *Journal of Analytical Applied Pyrolysis* **2003,** 66, 165-182.

17. Sun, R.; Tomkinson, J.; Geng, Z. C.; Wang, N. J., Comparative Studies of Hemicelluloses Solubilized During the Treatments of Maize Stems with Peroxymonosulfuric Acid, Peroxyformic Acid, Peracetic Acid, and Hydrogen Peroxide. *Holzforschung* **2000,** 54, (5), 492.

18. Agriculture, U. S. D. o. *Thermal Degradation of Wood Components: a Review of the Literature*; 1970.

19. Alen, R.; Kuoppala, E.; Oesch, P., Formation Of The Main Degradation Compound Groups From Wood And Its Components During Pyrolysis. *Journal of Analytical and Applied Pyrolysis* **1996,** 36, 137-148.

20. Carvaliio, J. D. S.; Prins, W.; Schuerch, C., Addition Polymerization of Anhydrosugar Derivatives. I. A Polyanhydroglucose. *J. Am. Chem. Soc.* **1959,** 81, 4054-4058.

21. Sanders, E. B.; Goldsmith, A. I.; Seeman, J. I., A Model that Distinguishes the Pyrolysis of D-Glucose, D- Fructose, and Sucrose from that of Cellulose. Application to the Understanding of Cigarette Mmoke Formation. *Journal of Analytical Applied Pyrolysis* **2003,** 66, 29-50.

22. Tomasik, P.; Palasinski, M.; Wiejak, S., The Thermal Decomposition of Carbohydrates. Part I. The Decomposition of Mono-. Di, and Oligo-saccharides. *Adv. Carbohydr. Chem. Biochem* **1989,** 47, 203-270.

23. Sharma, R. K.; Wooten, J. B.; Baliga, V. L.; Lin, X.; Chan, W. G.; Hajaligol, M. R., Characterization of Chars from Pyrolysis of Lignin. *Fuel* **2004,** 83, 1469-1482.

24. Sarkanen, K. V.; Ludwig, C. H., *Lignins Occurrence, Formation, Structure and Reactions*. Wiley-Interscience: 1971.

25. M. J. Antal, J.; Grønli, M., The Art, Science, and Technology of Charcoal Production. *Ind. Eng. Chem. Res.* **2003,** 42, 1619-1640.

26. Mochidzuki, K.; Soutric, F.; Tadokoro, K.; M. J. Antal, J.; Tóth, M.; Zelei, B.; Várhegyi, G., Electrical and Physical Properties of Carbonized Charcoals. *Ind. Eng. Chem. Res.* **2003,** 42, 5140-5151.

27. Pierson, H. O., *Handbook of Carbon, Graphite, Diamond and Fullerenes - Properties, Processing and Applications*. William Andrew Publishing/Notes: 1994.

28. Harris, P. J. F., Structure of Non-Graphitizing Carbons. *International Materials Reviews* **1997,** 42, (5), 206-218.

29. Kadish, K. M.; Ruoff, R. S., *Fullerenes - Chemistry, Physics, and Technology*. A John Wiley and Sons, Inc.: 2000.

30. Taylor, R., *Lecture Notes on Fullerene Chemistry - A Handbook for Chemists*. Imperial College Press: 1999.

31. Randall, J. T., *The Diffraction of X-Rays and Electrons by Amorphous Solids, Liquids, and Gases*. John Wiley & Sons, Inc.: 1934.

32. Hamblin, W. K.; Christiansen, E. H., *Earth's Dynamic Systems*. Eighth ed.; Prentice-Hall, Inc.: 1998.

33. Roberts, J. L., *A Photographic Guide to Minerals, Rocks, and Fossils*. New Holland Publishers (UK) Ltd.: 2001.

34. Shinn, J. H., From Coal to Single-Stage and Two-Stage Products: a Reactive Model of Coal Structure. *Fuel* **1984,** 63, 1187.

35. P. L. Walker, J.; Seeley, S. B., Fine Grinding of Ceylon Natural Graphite. *Proceedings of the Third Biennial Carbon Conference* **1957**, 481-494.

36. Aylmore, L. A. G.; Quirk, J. P., Domain or Turbostratic Structure of Clays. *Nature* **1960,** 187, 1046 - 1048.

37. Ishimaru, K.; Vystavel, T.; Bronsveld, P.; Hata, T.; Imamura, Y.; Hosson, J. D., Diamond and Pore Structure Observed in Wood Charcoal. *Journal of Wood Science* **2001,** 47, 414-416.

38. Kurosaki, F.; Ishimaru, K.; Hata, T.; Bronsveld, P.; Kobayashi, E.; Imamura, Y., Microstructure of Wood Charcoal Prepared by Flash Heating. *Carbon* **2003,** 41, 3057-3062.

39. Hata, T.; Vystavel, T.; Bronsveld, P.; DeHosson, J.; Kiiuchi, H.; Nishimiya, K.; Imamura, Y., Catalytic Carbonization of Wood Charcoal: Graphite or Diamond? *Carbon* **2004,** 42, 961-964.

40. Franklin, R. E., Crystallite Growth in Graphitizing and Non-Graphitizing Carbons. *Proc. R. Soc. London A* **1951,** 209, 196.

41. Marsh, H.; Heintz, E. A.; Rodriguez-Reinoso, F., *Introduction to Carbon Technologies*. 1997.

42. Chai, X. S.; Hou, Q. X.; Zhu, J. Y.; Chen, S. L.; Wang, S. F.; Lucia, L., Carboxyl Groups in Wood Fibers. 1. Determination of Carboxyl Groups by Headspace Gas Chromatography. *Ind. Eng. Chem. Res* **2003,** 42, 5440-5444.

43. Kozlowski, T. T.; Pallardy, S. G., *Physiology of Woody Plants*. Second ed.; 1996.

44. Marschner, H., *Mineral Nutrition of Higher Plants*. 1995.

45. Rowell, R., *The Chemistry of Solid Wood*. 1983.

46. Jenkins, B. M.; Bakker, R. R.; Wei, J. B., On The Properties Of Washed Straw. *Biomass and Bioenergy* **1996,** 10, (4), 177-200.

47. Baxter, L. L.; Miles, T. R.; Jr, T. R. M.; Jenkins, B. M.; Milne, T.; Dayton, D.; Bryers, R. W.; Oden, L. L., The Behavior of Inorganic Material in Biomass-Fired Power Boilers: field and laboratory experiences. *Fuel Processing Technology* **1998,** 54, 47-78.

48. Turn, S. Q.; Kinoshita, C. M.; Ishimura, D. M., Removal of Inorganic Constituents of Biomass Feedstocks by Mechanical Dewatering and Leaching. *Biomass and Bioenergy* **1997,** 12, (4), 241-252.

49. Blasi, C. D.; Portoricco, G.; Borrelli, M.; Branca, C., Oxidative Degradation and Ignition of Loose-Packed Straw Beds. *Fuel* **1999,** 78, 1591-1598.

50. Baxter, L. L.; Miles, T. R.; T.R. Miles, J.; Jenkins, B. M.; Richards, G. H.; Oden, L. L., Transformations and Deposition of Inorganic Material in Biomass Boilers. *Second Int. Conf. on Combustion Technologies for a Clean Environment* **1993**, (1; Biomass II), 9-15.

51. Blasi, C. D.; Branca, C., The Effects of Water Leaching on the Isothermal Degradation Kinetics of Straw. *Ind. Eng. Chem. Res.* **2000,** 39, 2169-2174.

52. Knudsen, J. N.; Jensen, P. A.; Dam-Johansen, K., Transformation and Release to the Gas Phase of Cl, K, and S during Combustion of Annual Biomass. *Energy & Fuels* **2004,** 18, 1385-1399.

53. Varhegyi, G.; Gronli, M. G.; Blasi, C. D., Effects of Sample Origin, Extraction, and Hot-Water Washing on the Devolatilization Kinetics of Chestnut Wood. *Ind. Eng. Chem. Res.* **2004,** 43, 2356-2367.

54. Iniesta, E.; Sanchez, F.; Garcia, A. N.; Marcilla, A., Yields and CO_2 Reactivity of Chars from Almond Shells Obtained by a Two Heating Step Carbonization Process. Effect of Different Chemical Pre-treatments and Ash Content. *Journal of Analytical and Applied Pyrolysis* **2001,** 58-59, 983-994.

55. Weinstock, I. A.; Atalla, R. H.; Reiner, R. S.; Moen, M. A.; Hammel, K. E.; Houtman, C. J.; Hill, C. L.; Harrup, M. K., A New Environmentally Benign Technology for Transforming Wood Pulp into Paper, Engineering Polyoxometalates as Catalysts for Multiple Processes. *Journal of Molecular Catalysis A: Chemical* **1997,** 116, 89-84.

56. Piskorz, J.; Radlein, D.; Scott, D.; Czernik, S., Pretreatment of Wood and Cellulose for Production of Sugars by Fast Pyrolysis. *J. Anal. Appl. Pyrolysis* **1989,** 16, 127-142.

57. Jensen, P. A.; Frandsen, F. J.; Dam-Johansen, K.; Sander, B., Experimental Investigation of the Transformation and Release to Gas Phase of Potassium and Chlorine during Straw Pyrolysis. *Energy & Fuels* **2000,** 14, 1280-1285.

58. Dayton, D. C.; French, R. J.; Milne, T. A., Direct Observation of Alkali Vapor Release During Biomass Combustion and Gasification. 1. Application of Molecular Beam/Mass Spectrometry to Switchgrass Combustion. *Energy & Fuels* **1995,** 9, 855-865.

59. Bjorkman, E.; Stromberg, B., Release of Chlorine from Biomass at Pyrolysis and Gasification Conditions. *Energy & Fuels* **1997,** 11, 1026-1032.

60. Dresselhaus, M. S.; Dresselhaus, G.; Sugihara, K.; Spain, I. L.; Goldberg, H. A., *Graphite Fibers and Filaments*. Springer-Verlag: 1988.

61. Edwards, I. A. S.; Marsh, H.; Menendez, R.; Rand, B.; West, S.; Hosty, A. J.; Kuo, K.; McEnaney, B.; Mays, T.; Johnson, D. J.; Patrick, J. W.; Clarke, D. E.; Crelling, J. C.; Cray, R. J., *Introduction to Carbon Science*. Butterworths: 1989.

62. Swaddle, T. W., *Inorganic Chemistry an Industrial and Environmental Perspective*. 1997.

63. Giancoli, D. C., *Physics Principles with Applications*. Fifth ed.; 1998.

64. Chang, R., *Chemistry*. Fifth ed.; 1994.

65. Marchand, A., Electronic Properties of Doped Carbons. *Chemistry and Physics of Carbon* **1971**, 155.

3.0 Selected Biomass Structures and Chemical Compositions

Biomass is a broad term used to encompass a wide variety of materials including crop and forest residues, animal byproducts and some municipal wastes. Globally, biomass provides approximately eleven percent of the world's supply of primary energy[1]. The numerous advantages of using biomass as an energy source include sustainability, CO_2 neutrality, waste reduction, and reduced dependence on fossil fuels.

3.1 The Macroscopic Structure of Corncob

Corn (*Zea mays* L.) is a tall annual monocotyledon plant belonging to the grass family (Gramineae). The long stalk with a single leaf at each node is supported by a fibrous root system. The female (ear) and male (tassel) flowers are located separately on the same plant. The tassel is located at the top of the stalk while the ear is found at the end of short branches located near the bottom of the stalk. The ears develop to contain 300-1000 kernels in an often longitudinal or spiral pattern along a condensed inflorescence or rachis (cob)[2].

Corn is an extremely important cereal crop indigenous to the Americas. It is produced primarily for food and feed from the grain. Corn production is inherently focused on the uses of the fruit or kernel and as a result much of the corn plant remains unused or underused. The cob is a well-known agricultural residue with few profitable uses; for every 100 kg of corn grain, approximately 18 kg of corncob is produced. The annual worldwide production of corncob between 1982 and 1987 averaged around 70 million tones. Only a fraction (~1.1 million tonnes) of the corncob produced was utilized in industrial applications[2]. Corncob is therefore an abundant cheap renewable resource with the potential for use as an alternate energy source.

Corncob is a light yet surprisingly rigid material consisting of various types of tissue. Removal of the kernel gives rise to an indented topography marred with remaining chaff and glumes (Fig. 3.1a). Cross-sectional examination (Fig. 3.1b) of a mature corncob reveals soft-pith parenchyma cells at the cobs center. Surrounding the pith is a zone of hardened sclerenchyma cells. Interspersed between these two very different tissues is a branched vascular system[3].

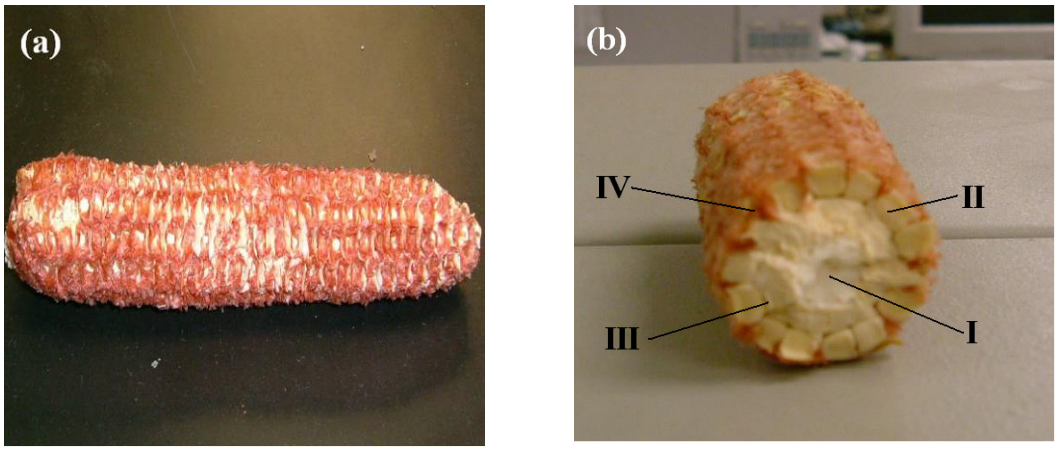

Figure 3.1: *Digital Photos of Corncob. (a) Outer surface of a mature corncob. (b) Cross-section of a mature corncob showing (I) pith, (II) sclerenchyma zone or woody ring, (III) chaff, and (IV) glumes.*

3.2 Chemical Composition of Corncob

Biomass is a complex heterogeneous material. The structure and composition of biomass varies for different plant parts, plant species, and even with plant locations. The major chemical components of biomass include cellulose, hemicelluloses, lignin, and extractives and ash. The chemical composition of corncob is summarized in Table 3.1.

Table 3.1: Chemical Composition of Corncob[a] (wt. %).

Cellulose [b]	Hemicellulose [b]	Lignin [c]	C	H	O	N	S	Ash
26.3	25.2	16.3	48.22	6.20	42.94	1.57	0.13	3.48

[a] Data obtained from ref. [4]. [b] Calculated using the following formulas: % cellulose = % glucose × 0.9 and % hemicellulose = (% galactose + % mannose) × 0.9 + (% xylose + % arabinose) × 0.88. [c] Measured acid-insoluble lignin.

Additional corncob chemical composition data and information can be found in references [3] and [5].

3.2.1 Cellulose.

Cellulose is a linear homopolysaccharide consisting of several thousand D-glucose units linked by β-(1→4)-glycosidic linkages[6], (Fig. 3.2). It is the most abundant organic compound on Earth, with plants producing up to 100 billion tons per year[7]. In plant cell walls many parallel cellulose molecules aggregate together forming microfibrils. The grouping of cellulose molecules in this way results in extensive intra- and intermolecular hydrogen bonding. The strong hydrogen bonding and fibrous structure of cellulose provides much of the mechanical strength for plants. Cellulose is insoluble in most solvents however certain chemical treatments and heating cause the native cellulose structure to be altered [8].

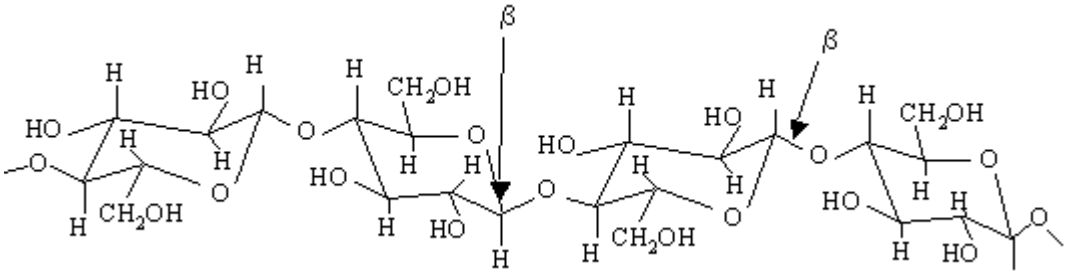

Figure 3.2: *Cellulose Polymer*[9].

3.2.2 Hemicelluloses

Hemicelluloses are a group of heteropolysaccharides located predominantly in plant cell walls. Most hemicelluloses have a degree of polymerization of only 200 and function in a structural supporting capacity. D-glucose, D-mannose, D-xylose, L-arabinose, and small amounts of L-rhaminose are the monomeric constituents formed by acid hydrolysis of hemicelluloses. Acid hydrolysis of hemicelluloses also yields D-glucuronic acid, 4-O-methyl-D-glucoronic acid, and D-galacturonic acid. The structure and composition of hemicelluloses differs between hard and soft woods. A substantial difference also exists between the different parts of a plant, i.e. the stem, branches, and bark. The major hemicelluloses found in softwoods include galactoglucomannans, arabinoglucuronoxylan, and arabinogalactan. The major hemicelluloses found in hardwoods include glucuronoxylan and glucomannan[8].

3.2.3 Lignin

Lignin is a complex three dimensional aromatic structure composed of phenyl propane units[10]. Lignins are located in all vascular plant cell walls and perform multiple functions. Lignins impart cell wall rigidity, they effect the internal transportation of water, nutrients, and metabolites, and lignified tissues help resist attacks by microorganisms[11]. There are two major classes of lignin, guaiacyl lignins and guaiacyl-syringyl lignins. Guaiacyl lignins are largely a polymerization product of coniferyl alcohol and are typically found in softwoods. Guaiacyl-syringyl lignins are a co-polymer of coniferyl and sinapyl alcohols and are found in both hardwoods and herbaceous species[8]. Isolation of lignins from wooded species produces a chemically different lignin correctly named after the chemical process, i.e. Kraft lignin (see Fig. 3.3).

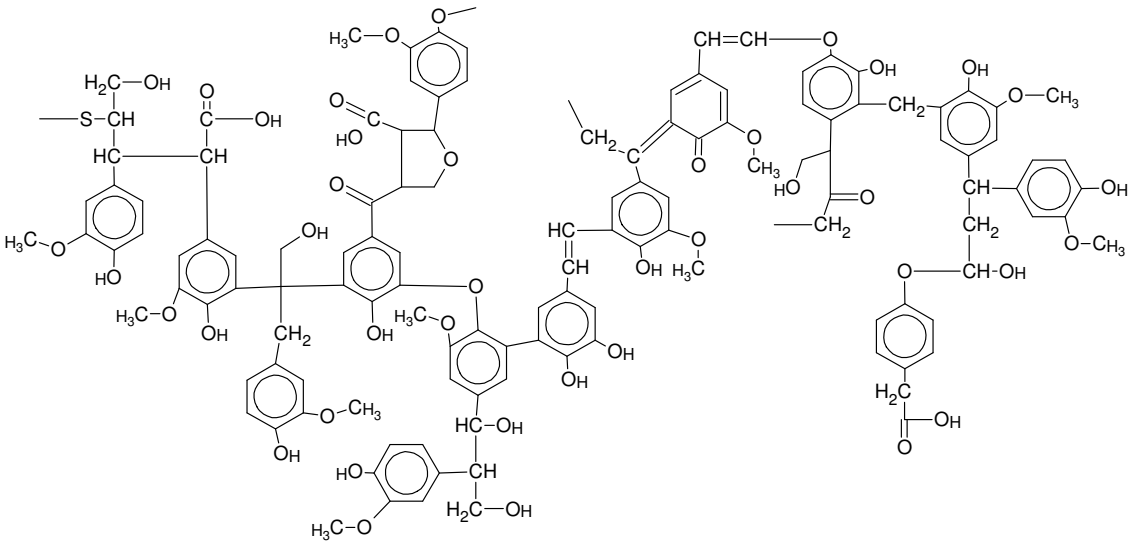

Figure 3.3: *Tentative Structural Features in a Segment of Pine Kraft Lignin Molecule – adapted from ref [11].*

3.2.4 Extractives and Ash

Extractives are compounds of diverse nature that are not an integral part of the cellular structure[9]. The compounds can be extracted from biomass by means of polar and non-polar solvents including water, ethanol, acetone and dichloromethane. ASTM 1690-95[12] is the standard method for the determination of biomass extractives. The types of extractives found in biomass samples are entirely dependent upon the sample itself. Extracted materials may contain resin, a variety of phenolic compounds, certain carbohydrates, tannins, and inorganic salts[8].

Ash in biomass is described by ASTM method E1755-95[13] as the residue remaining after dry oxidation (oxidation at 575 ± 25 ℃). The residue remaining after dry oxidation is nominally comprised of alkali and alkaline chlorides, sulfates, carbonates, and complex silicates[14].

3.3 The Macroscopic Structure of Wood

Wood is composed predominantly of longitudinal elongated cells, which are connected through openings referred to as pits. These cells vary in shape depending upon their function. Wood provides the necessary mechanical strength for a tree and

also performs the functions of storing and transporting water, carbohydrates, and minerals. Figure 3.4 represents the macroscopic structure of wood.

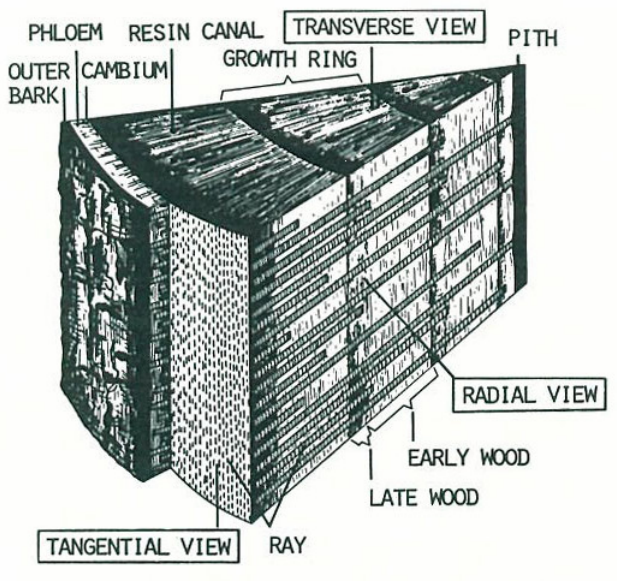

Figure 3.4: *Macroscopic Structure of Wood - Sections of a Four-Year Old Pine Stem*[8]. *Reprinted from Wood Chemistry - Fundamentals and Applications, E. Sjöström, 0-223, 1981, with permission from Elsevier.*

The pith represents the tissue formed during the first year of growth and is located at the stem or branch center[8]. Surrounding the pith are secondary growth elements formed from the meristematic cells of the vascular cambium. The vascular cambium produces secondary xylem (wood) to its interior and secondary phloem to its exterior. Interspersed between the longitudinal secondary tissues exists radial files of parenchyma cells termed xylem and phloem rays. These cells transport water and nutrients horizontally within a woody stem. As secondary growth continues over the years, layer upon layer of secondary xylem accumulates accounting for most of the increase in diameter of a woody plant[7].

3.4 Structure of Softwoods

Softwood longitudinal secondary xylem consists mainly of tracheids (~90%) and minor amounts of axial parenchyma and epithelial cells. The few horizontal elements in softwoods consist of ray tracheids, ray parenchyma cells and epithelial cells.

Longitudinal and horizontal resin ducts are also present and are scattered among the other major wood cells[15]. Figure 3.5 represents the structure of a softwood.

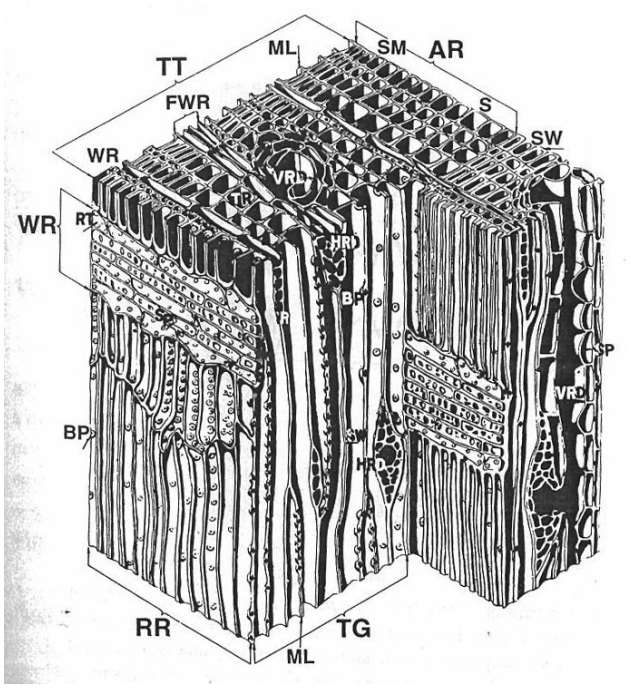

Figure 3.5: *Structure of a Softwood[15]. TT, Transection; RR, radial section; TG, tangential section; TR, tracheids; ML, middle lamella; S, earlywood; SM or SW, latewood; AR, annual ring; WR, wood ray; RT, ray tracheid; FWR, fusiform wood ray; SP, simple pit; BP, bordered pit; HRD, horizontal resin duct; VRD, vertical resin duct. Reprinted from Physiology of Woody Plants, T. T. Kozlowski and S. G. Pallardy, 1996, with permission from Elsevier.*

3.5 Structure of Hardwoods

There are more cell types in hardwoods compared to softwoods. The axial system of hardwoods consists of vessel elements, tracheids, fibers, and various parenchyma cells. The most notable difference in axial cell types between the two classes of wood is the presence of vessel members in hardwoods. Hardwoods also lack the orderly radial alignment of xylem elements, which are characteristic of softwoods. The radial system in hardwoods is made up of horizontal rays consisting exclusively of parenchyma cells[15]. Figure 3.6 represents the structure of a hardwood.

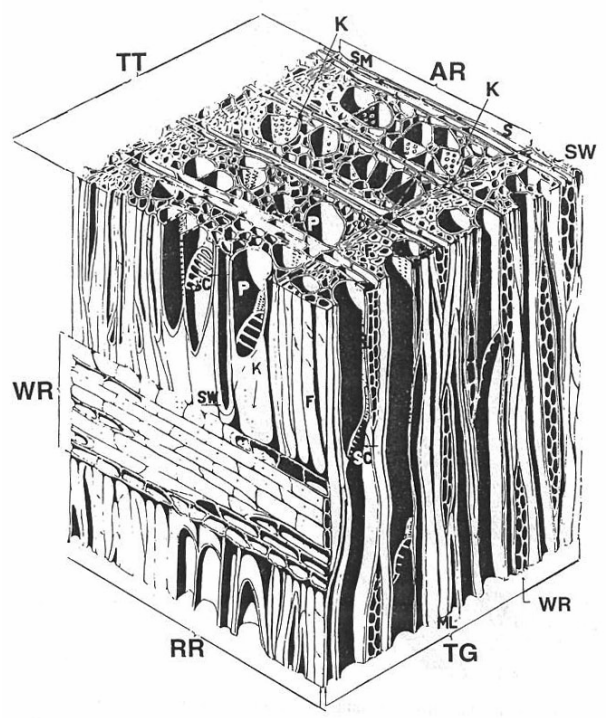

Figure 3.6: *Structure of a Hardwood*[15]*. TT, Transection;RR, radial section; TG, tangential section; P, vessel; SC, perforation plate at end of vessel; F, fibers; K, pit; WR, wood ray; AR, annual ring; S, earlywood; SM or SW, latewood; ML, middle lamella. Reprinted from Physiology of Woody Plants, T. T. Kozlowski and S. G. Pallardy, 1996, with permission from Elsevier.*

3.6 Chemical Composition of Wood

As mentioned previously in section 3.2, the structure and composition of biomass is extremely variable. Table 3.2 illustrates the general chemical composition of hardwoods and softwoods.

Table 3.2: Approximate Analysis of Hardwoods and Softwoods

Species	Cellulose (%)	Hemicelluloses (%)	Lignin (%)	Total Ash (%)
Softwood	41.0	24.0	27.8	0.4
Hardwood	39.0	35.0	19.5	0.3

Adapted from reference [16].

For more detailed chemical composition data on wood species refer to reference[17]. In general it appears that hardwoods contain more hemicelluloses and less lignin compared to softwoods.

3.7 Monosaccharides

Monosaccharides are carbohydrates that cannot be converted into smaller sugars by hydrolysis[6]. Examples of monosaccharides include glucose and fructose. Glucose and fructose can occur in both furanose and pyranose forms, however crystalline glucose and fructose occur only in the pyranose form[18, 19].

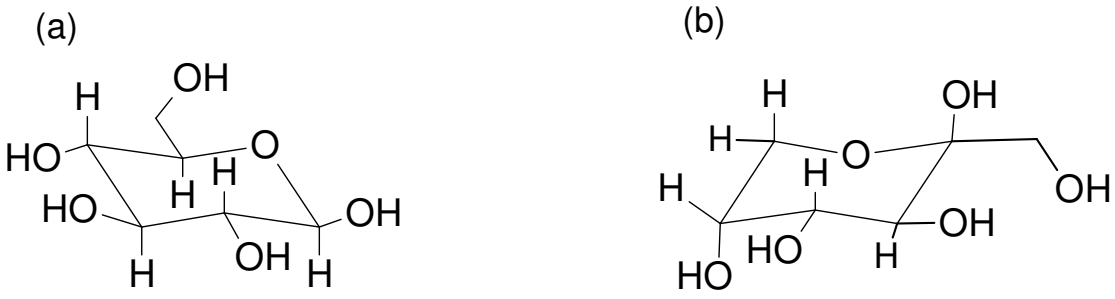

Figure 3.7: *(a) Crystalline Structure of β-D-Glucopyranose. (a) Crystalline Structure of β-D-Fructopyranose.*

3.8 Disaccharides

A disaccharide is a complex carbohydrate made up of two simple sugars. Disaccharides contain a glycosidic acetal bond between the anomeric carbon of one sugar and an –OH group at any position on the other sugar. Sucrose is an example of a disaccharide and in its crystalline form is made up of one fructofuranose monomer and one glucopyranose monomer. The two simple sugars are joined via a glycosidic link between the C1 of glucose and C2 of fructose. Sugar is one of the most abundant pure organic chemicals in the world[6].

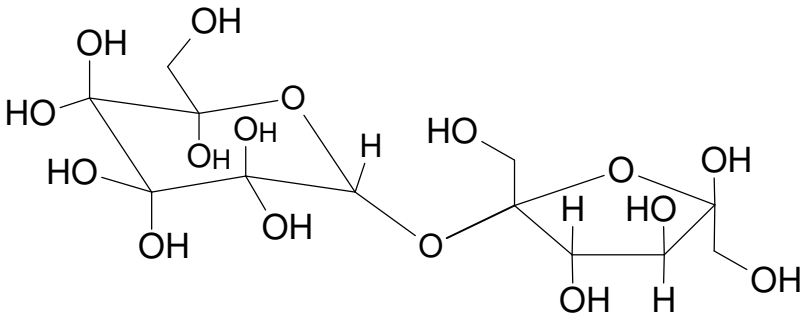

Figure 3.8: *Crystalline Structure of Sucrose [2-O-(β-D-Glucopyranosyl)-β-D-fructofuranoside].*

3.9 Polysaccharides

Polysaccharides are carbohydrates containing tens, hundreds, or even thousands of simple monomeric sugars linked together via glycosidic bonds. Polysaccharides are not reducing sugars and do not show noticeable mutarotation[6]. Examples of polysaccharides include cellulose (refer to Fig. 3.2) and inulin. Crystalline inulin is a small polysaccharide containing typically 35 fructofuranose monomers for every 1 glucopyranose monomer[20], (Fig. 3.9).

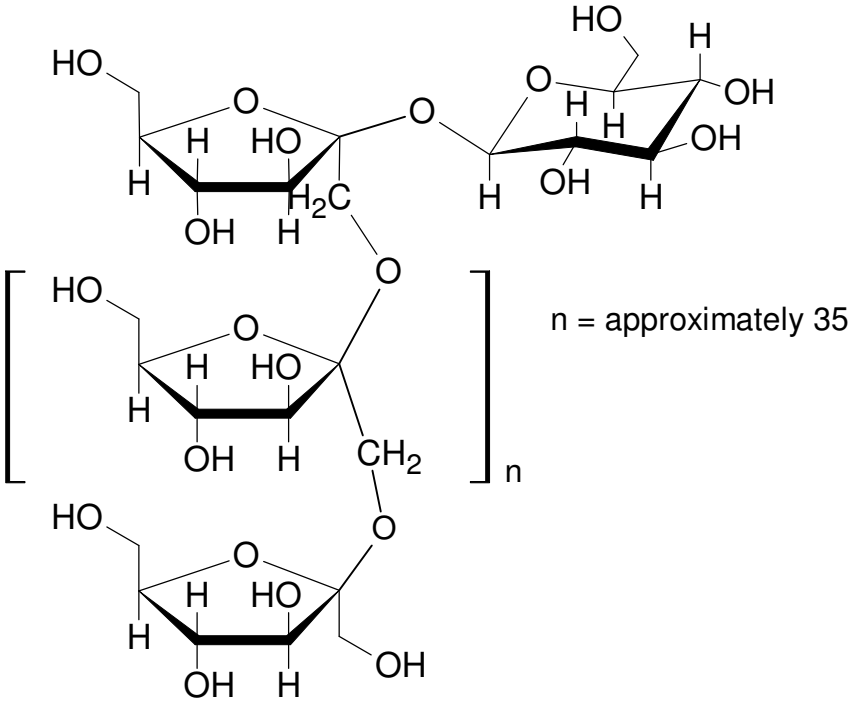

Figure 3.9: *Crystalline Structure of Inulin – adapted from ref [20].*

1. Sims., R. E. H., *Bioenergy Options for a Cleaner Environment*. Elsevier: 2003.

2. Watson, S. A.; Ramstad, P. E., *Corn: Chemistry and Technology*. American Association of Cereal Chemists, Inc.: 1987; p 605.

3. Lenz, L. W., Comparative Histology of the Female Inflorescence of Zea Mays L. *Annals of the Missouri Botanical Garden* **1948,** 35, 353-376.

4. M. J. Antal, J.; Allen, S. G.; Dai, X.; Shimizu, B.; Tam, M. S.; Gronli, M., Attainment of the Theoretical Yield of Carbon from Biomass. *Ind. Eng. Chem. Res* **2000,** 39, (11), 4024-4031.

5. Pomeranz, Y.; Munck, L., *Cereals: A Renewable Resource, Theory and Practice*. 1981; p 728.

6. McMurry, J., *Organic Chemistry*. Fifth ed.; Brooks/Cole: 2000.

7. Campbell, N. A.; Reece, J. B.; Mitchell, L. G., *Biology*. Fifth ed.; Addison-Wesley: 1999.

8. Sjöström, E., *Wood Chemistry - Fundamentals and Applications*. Academic Press: 1981; p 223.

9. U.S. Department of Energy - Energy Efficiency and Renewable Energy. http://www.eere.energy.gov/biomass/feedstock_glossary.html

10. M. J. Antal, J., Effects of Reactor Severity on the Gas-Phase Pyrolysis of Cellulose- and Kraft Lignin-Derived Volatile Matter. *Ind. Eng. Chem. Prod. Res. Dev.* **1983,** 22, 366.

11. Sarkanen, K. V.; Ludwig, C. H., *Lignins Occurrence, Formation, Structure and Reactions*. Wiley-Interscience: 1971.

12. ASTM E1690-01 Standard Test Method for Determination of Ethanol Extractives in Biomass. *Anual Book of ASTM Standards* **2005,** 11.05.

13. ASTM E 1755 - 95, Standard Test Method for Ash in Biomass. *Annual Book of ASTM Standards* **1995,** 11.05, 1243.

14. Jenkins, B. M.; Bakker, R. R.; Wei, J. B., On The Properties Of Washed Straw. *Biomass and Bioenergy* **1996,** 10, (4), 177-200.

15. Kozlowski, T. T.; Pallardy, S. G., *Physiology of Woody Plants*. Second ed.; 1996.

16. Shafizadeh, F., Introduction to Pyrolysis of Biomass. *Journal of Analytical and Applied Pyrolysis* **1982**, 283-305.

17. Rowell, R., *The Chemistry of Solid Wood*. 1983.

18. Pigman, W.; Horton, D., *The Carbohydrates - Chemistry and Biochemistry*. Academic Press: 1980; Vol. IB.

19. Herbert, K., Fructose. *Pharmaceutical Excipients* **2004**.

20. *The Merck Index - An Encyclopedia of Chemicals and Drugs*. Ninth ed.; Merck and Co., Inc.: 1976.

4.0 Biocarbon Preparation and Physical Properties

4.1 Flash Carbonization (FC) of Select Biomass Feedstocks

FC technology was employed to produce all biocarbons utilized in this investigation. A summary including run conditions and proximate analysis results for all biocarbons used to form the basis of this thesis is offered in appendix 9.1.

It is recognized that charcoal retains the form and structure of its biomass precursor to such an extent that the appearance of the charcoal can be used to identify its origin[1]. Figure 4.1(a) depicts a flash carbonized corncob; note the retention of form and structure. It was observed however that charcoals derived from precursors, D-glucose, D-fructose, sucrose, inulin, and Kraft lignin retain none of their original crystalline structure as they proceed through a distinct liquid phase during pyrolysis. The visual appearance of each melt charcoal differed to some extent from each other (refer to Fig. 4.1(b-f)).

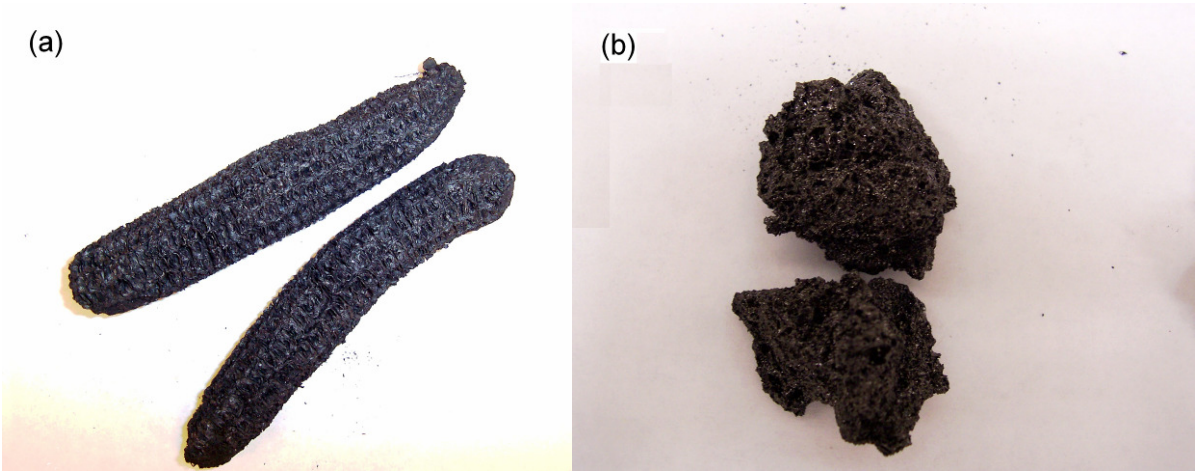

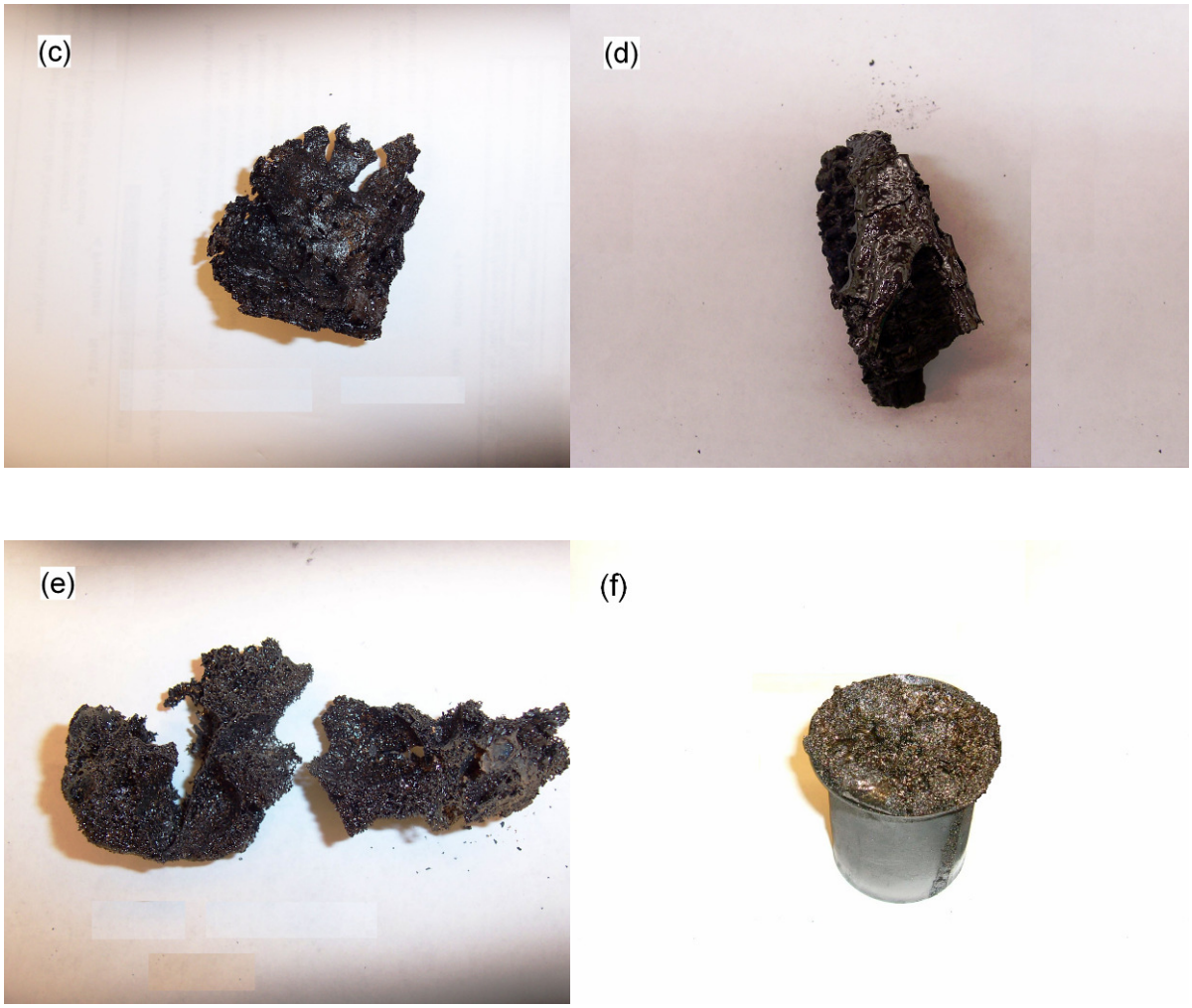

Figure 4.1: *Digital Photos of Select Flash Carbonized Feedstocks. (a) Corncob charcoal. (b) Sucrose charcoal. (c) α-D-Glucose charcoal. (d) β-D-Fructose Charcoal covering a piece of corncob charcoal. (e) Inulin charcoal. (f) Partially flash carbonized Kraft lignin charcoal.*

The charcoal resulting from sucrose pyrolysis was hard, sparkly, porous and, when mechanically broken apart, formed hard nuggets. Glucose charcoal was fragile, shiny and appeared less porous resembling a viscous tarry liquid. Fructose charcoal was extremely lustrous, fragile, metallic-looking, glassy, and fractured easily into thin films. The charcoal resulting from inulin pyrolysis, was again quite fragile, had a fine porosity, and had a sheen similar to the α-D-glucose charcoal. The inulin charcoal also appeared to be lightly covered with a pastel orange powder possibly indicating sample contamination. Kraft lignin clearly also underwent a liquid phase during pyrolysis. Visual inspection of the charcoal lead to the assessment that the feedstock

may have gone through a more viscous melt phase compared to the sugars. Fully carbonized Kraft lignin charcoal was quite similar in appearance to the α-D-glucose charcoal with a possible exception on the manner of which it fractured upon mechanical grinding, forming what appeared to be small discrete particles glued together. It is important to note that all melt carbons, once ground to a fine particulate size (<212 μm), had a similar physical appearance.

4.2 Proximate Analysis Results of Flash Carbonized Charcoals

Proximate analysis involved the determination of the percentage moisture content, the percentage VM content, and the percentage ash content in biocarbons. Proximate analysis was primarily designed to evaluate the quality of a charcoal. After FC, charcoal was split into three distinct portions according to the charcoal's original position within the lab-scale reactor canister. The split was also determined by means of a visual observation with regard to the overall homogeneity of the charcoal sample. After the sample split, the three distinct portions were placed into separate clean nalgene containers for a 24 h equilibration period. Representative samples were subsequently removed from each subsection and ground separately using a bench top Wiley mill. The ground charcoal was then divided into two principal particle sizes, 425 - 850 μm (20-40 Mesh) and <425 μm using a series of analytical sieves. Approximately 1 g (to the nearest 0.1mg) of 20-40 Mesh charcoal sample was added to an ambient temperature dry porcelain crucible. To determine the percentage moisture content, the crucible and charcoal sample was placed into an oven set at 105 °C for a time period of 2 hours. The dried sample was then placed into a desiccator to cool for 1 h and then weighed. The charcoal sample was considered oven-dry when the decrease in crucible weight of successive measurements (successive drying periods of no less than 1 h) was 0.0005 g or less. The percentage moisture content was determined by using equation (1). The percentage VM content was determined as the loss of weight at 950 °C. Once the muffle furnace had reached a temperature of 950 °C a dry charcoal sample with lid in place was initially placed on the open muffle furnace door for 2 minutes. The closed crucible was then moved to the inner ledge of the muffle furnace for 3 minutes, and then finally to the rear of the muffle

furnace with the door closed for approximately 6 minutes. The crucible and charcoal sample was removed from the furnace and allowed to cool in a desiccator for a time period of 1 h before being weighed. The percentage VM content was determined by using equation (2). The percentage ash content was determined as the residue after burning to constant weight at 750 °C. After the VM content had been determined the lids and uncovered crucibles were returned to the muffle furnace (750 °C, 6 h). The crucibles with lids in place were cooled in a desiccator for 1 h and weighed. The burning process was repeated until a 1 h period of heating resulted in a weight loss of 0.0005g or less. The percentage ash content was determined by using equation (3).

$$\%Moisture = [(A - B)/A] \times 100 \quad \textbf{(1)}$$

$$\%VolatileMatter = [(B - C)/B] \times 100 \quad \textbf{(2)}$$

$$\%Ash = (D/B) \times 100 \quad \textbf{(3)}$$

Where:

A = grams of air-dry sample used.
B = grams of sample after drying at 105 °C.
C = grams of sample after drying at 950 °C.
D = grams of residue after combustion at 750 °C.

The percentage VM content is a good indicator of the temperatures reached within the FC reactor. A low VM charcoal is the result of biomass being heated to a high temperature for a prolonged length of time. The concentration of ash present in charcoal is influenced by the degree of carbonization. A charcoal having a low percentage VM content corresponds to a material with an increased amount of lost mass. Increased carbonization has a concentrating effect on non-volatile extraneous compounds.

Using the proximate analysis results, charcoal yields can be calculated. Charcoal yield, y_{char}, as defined by equation (4) is commonly used to give a quick understanding of the efficiency of a given charcoal manufacturing process. Unfortunately, because charcoal is not a well defined chemical compound, this definition is inherently vague. A more useful value is the fixed carbon yield, y_{fC}, as defined by equation (5), which takes into account the composition of the charcoal sample as per the proximate analysis results.

$$y_{char} = m_{char} / m_{bio} \quad \textbf{(4)}$$

$$y_{fC} = y_{char} \times [\%\, fC / (100 - \%\, feedash)] \quad \textbf{(5)}$$

Where:

m_{char} = dry mass of product charcoal.
m_{bio} = dry mass of feedstock.
fC = percentage of fixed carbon content of the charcoal (100- *%VM* content - *%ash* content).
%feed ash = percentage ash content of the feed.

Table 4.1 illustrates the proximate analysis results for all the flash carbonized biocarbons.

Table 4.1: Proximate Analysis Results of 20-40 (425 - 850 μm) Mesh Charcoals

Feed	Section[a]	Proximate Analysis (%)[b]		
		VM	fC	ash
Corncob, 130404[c]	Middle	26.0	72.0	2.0
Corncob, 020704	Middle	16.9	80.8	2.3
Demin.[d] Corncob, 060804	Middle	19.8	79.3	0.9
BD[e] Corncob, 031104	Top	21.1	76.0	2.9
Kukui Nutshell, 020904	Middle	5.2	92.7	2.1
Macshell[f], 180304	Middle	7.6	91.7	0.7
Oak Wood, 090704	Middle	22.3	77.1	0.6
C & H Pure Cane Sugar, 131204	Top	1.8	98.2	0.0
β-D-Fructose, 180205	Top	6.8	93.1	0.1
Kraft Lignin, 220305	Top	5.7	90.4	3.9
Inulin, 120405	Top	2.5	96.7	0.8
α-D-Glucose, 250405	Top	5.1	94.7	0.2
BD Sucrose, 160505	Top	4.7	85.6	9.7
PD[g] Sucrose, 180505	Top	4.3	90.4	5.2

[a] *Refers to the position of the charcoal within the lab-scale FC canister.* [b] *Dry Basis - ASTM D1762-84 (Reapproved 1990).* [c] *Number corresponds to date produced dd/mm/yy.* [d] *Citric acid demineralized.* [e] *BD – Boron-doped.* [f] *Macadamia nutshell.* [g] *PD – Phosphorus-doped.*

During FC the predominant air flow is from top to bottom of the canister. Higher temperatures at the canister top are largely attributed to increased oxygen concentrations resulting from the location of the primary source of air supply. It should also be noted that a physical difference is often observed between 'top' and 'bottom' corncob charcoals. 'Bottom' portions of corncob charcoal are soft and spongy, whereas 'top' portions of corncob charcoal are hard and rigid. It is important to note that the different chemical components making up the physical structure of a corncob, i.e. cellulose, lignin, saccharides, may proceed through a melt phase at different temperatures. For example sucrose is a major intermediate product of photosynthesis of plants, and the major portion of assimilated carbon is transported in

this form[2]. We know that crystalline sucrose proceeds through a distinct liquid phase during FC.

4.2.1 Elemental Analysis Results of Select Charcoals

Elemental analysis of select biocarbons was carried out by Huffman Laboratories, Inc. Prior to ultimate analysis, samples were ground and homogenized. Table 4.2 illustrates elemental analysis results in addition to proximate analysis results.

Table 4.2: Ultimate and Proximate Analysis Results of Select Charcoals

Feed	Section[a]	Proximate Analysis (%)[b]			Ultimate Analysis (wt %)[c]				
		VM	Ash	fC	C	H	O	N	S
Corncob, 040504[d]	Middle	35.0	1.9	63.1	72.74	4.59	20.67	0.53	0.04
Oak Wood, 090704	Middle	23.4	0.4	76.1	80.52	3.66	16.12	0.16	0.01
Corncob, 040504	Top	16.2	2.8	81.0	82.31	3.17	12.10	0.64	0.05
Macshell, 180304	Top	13.3	0.9	85.8	86.57	3.06	9.67	0.58	0.04
Corncob, 140104	Middle	7.2	3.3	89.5	86.97	2.66	6.58	0.74	0.04
Macshell, 180304	Bottom	6.0	0.8	93.2	91.82	2.71	5.20	0.44	0.03

[a] Refers to the position of the charcoal within the lab-scale FC canister. [b] Dry Basis - ASTM D1762-84 (Reapproved 1990). [c] Dry basis values measured by Huffman Laboratories, Inc. [d] Number corresponds to date produced dd/mm/yy.

Elemental analysis results indicate that biocarbons are very low in elements sulfur and nitrogen. As the VM content is reduced the percentage carbon increases and the percentage oxygen decreases. This indicates that oxygen is removed as VM from charcoals exposed to increased heat treatment time and temperature. Oxygen content is determined by direct measurement in accordance to ASTM D5622. A sample is pyrolyzed at 1200 °C in a carbon pyrolysis tube, converting oxygen in the sample to

CO and CO_2. Molecular CO and CO_2 are subsequently measured by non-dispersive infrared detection via a Leco RO-478 Oxygen Analyzer.

Charcoal is an extremely reactive material and according to the Code of Federal Regulations (49 CFR Ch. I 172.101) is classed as a "spontaneously combustible material"[3]. Charcoal has been implicated as the cause of a number of household fires. The Hawaii County Police Department issued a media release concerning a Hilo home which was extensively damaged (02 July 2000) by fire after a bucket of wet charcoal spontaneously ignited[4]. Charcoals reactivity causes it to absorb and react with the ambient atmosphere. The tendency of carbon to chemisorb oxygen is greater than the tendency to absorb any other species. The reaction of oxygen and carbon has been studied at length[5-8], however the precise nature of carbon-oxygen structures is not completely established. Non-graphitizing carbons described by Franklin[9] are disorder graphitic type structures having large edge areas and in addition may contain various defects, dislocations, and discontinuities. Non-graphitizing carbons are also described as being porous and having a low density. These structural properties provide large areas for oxygen chemisorption. Molecular oxygen is either physically reversibly adsorbed or it is chemisorbed on the surface. In general terms, low temperature oxygen adsorption is completely reversible, however, at increased temperatures chemisorption of oxygen is enhanced resulting in the formation of oxygen surface compounds. Carbon-oxygen groups are also formed from reaction with oxidizing gases such as ozone, nitric oxide, and carbon dioxide, as well as reactions with oxidizing solutions[7]. Figure 4.2 illustrates possible oxygen functional groups on a non-graphitizing carbon.

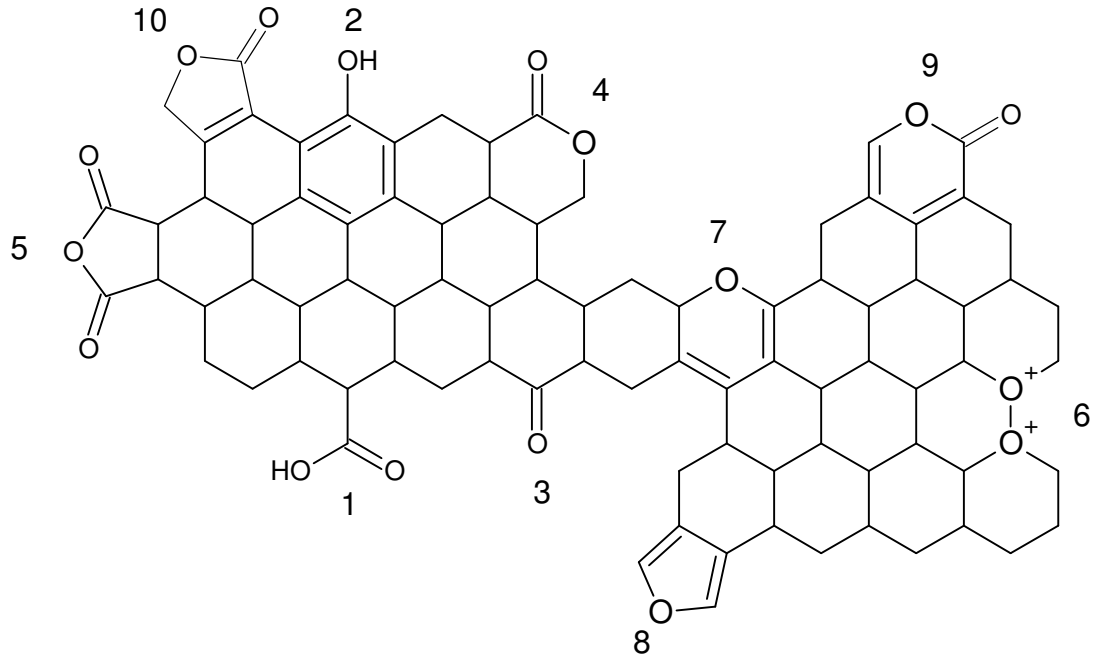

Figure 4.2: *Possible Oxygen Functional Groups on a Non-Graphitizing Carbon - adapted from ref [7]. 1 carboxylic acid. 2 phenol. 3 quinone. 4 lactone. 5 carboxyl anhydride. 6 cyclic peroxide. 7 2H-pyran. 8 furan. 9 2H-pyran-2-one (α-pyrone). 10 2(5H)-furanone.*

It is important to note that the nature and extent of carbon-oxygen surface complexes of a given carbon is affected by its specific surface area, particle size and ash content, as well as temperature and degree of carbonization[7]. Szymański *et al*[10] assembled a Table which shows thermal decomposition temperature ranges associated with various individual carbon surface oxides. Carboxylic groups decompose to CO_2 at the lowest temperature region (100-400 °C), closely followed by carboxylic anhydrides and lactones (427-657 °C). The most thermally stable carbon-oxygen groups are pyrone structures (900-1200 °C) followed by ethers, carbonylic and quinonic groups, and phenolic and hydroquinonic groups. In organic chemistry monocyclic γ-pyrones have been well characterized compared to alternate pyrone type structures including bicyclic and tricyclic pyrones[11, 12].

Note that all the biocarbons contain substantial amounts of oxygen that cannot be ignored in a model of their structure. Some of the biocarbons also contain small amounts of sulfur and nitrogen.

4.2.2 Specific Surface Area Analysis of Flash Carbonized Corncob Charcoal

Surface areas of carbons have received a great deal of attention since the discovery and application of various activated carbons; the surface area of activated carbons are typically on order or ~1000 m^2/g. Specific surface area information relevant to ordinary biomass charcoals is however small by comparison. When a porous solid interacts with a gas or vapor within a confined space the solid begins to adsorb the gas. Adsorption of the gas or vapor is noted through an observed decrease in the pressure of the gas. After a given amount of time no additional amount of gas is adsorbed, denoting that the closed system is at equilibrium. By applying ideal gas laws, the amount of gas adsorbed can be determined via the fall in pressure.

Adsorption of a gas or vapor on a solid is a result of the interaction between gaseous molecules and the solids surface. This interaction is due to chemical or physical forces. The amount of gas adsorbed by the solid is dependent on temperature, the adsorbate pressure, and the nature of both the solid and the gas[13]. A graphical representation (adsorption isotherm) of this relationship is therefore obtained by determining the quantity of gas adsorbed over a number of relative pressures under equilibrium conditions at a constant temperature. Similarly, desorption isotherms can be obtained by measuring the quantities of gas removed from the solid as the relative pressure is lowered. There are five types (I-V) of adsorption isotherms according to the Brunauer classification[14]. Isotherms of type IV and V possess a prominent hysteresis loop. Hysteresis is defined as the retardation of an effect[15]. In the case of an adsorption/desorption isotherm the adsorbate is not removed from the solid at the same rate as it was adsorbed at precisely the same relative pressures.

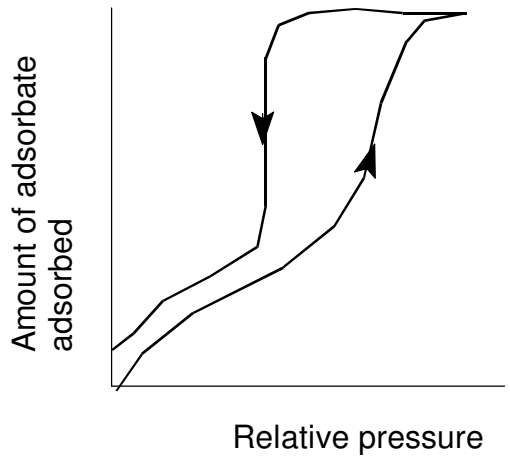

Figure 4.3: *Type H2 Hysteresis Loop in Accordance to the IUPAC classification – adapted from ref [16].*

The specific surface area of a solid includes internal surface areas comprised of crack walls, pores, and cavities that are deeper than they are wide. Pores are classified according to their width. The basis of this classification system comes from the fact that each of the size ranges corresponds to characteristic adsorption effects evident from the isotherm. Micropores have a pore width of less than 2 nm, mesopores have a pore width between 2 nm and 50 nm, and macropores have a pore width of greater than 50 nm[13].

Charcoals were analyzed using Quantachrome's Autosorb-1 instrument. Charcoal samples were outgassed under vacuum (212 °C, 4 h) prior to nitrogen adsorption at liquid nitrogen temperature, ~ -196°C. A limited linear region of the adsorption isotherm, P/P_0 = 0.01 – 0.1, was applied to the BET method to determine specific surface areas. To validate the method a surface area determination was performed on a commercial sample of Barnebey and Sutcliffe (B&S) coconut shell activated carbon and a low-surface area aluminum oxide standard. Results (1119 and 89 m^2/g respectively) were close to the accepted values (1106 m^2/g and 97 m^2/g).

20-40 (425 - 850 μm) Mesh corncob charcoal samples with varying percentages of VM content were selected and analyzed. Samples were also selected on the basis of their position within the lab-scale FC reactor (refer to Table 4.3).

Table 4.3: Specific Surface Area and Proximate Analysis Results for 20-40 Mesh Flash Carbonized Charcoals

Sample ID	Section[a]	% VM	% Ash	Specific Surface Area m^2/g at P/P_0 = 0.01-0.1
Corncob, 270105[b]	Top	3.1	3.7	447
Corncob, 270105	Middle	11.2	4.1	156
Corncob, 270105	Bottom	14.6	3.8	-[c]
Corncob, 130404	Bottom	16.4	6.9	-
Corncob, 171203	Bottom	4.1	1.8	247
Corncob, 130404	Top	15.2	2.2	60
Corncob, 220305	Top	19.7	2.5	-
Fisher Scientific Glass beads 11-312A ~3mm	NA[d]	NM[e]	NM	-
B & S Activated Coconut Charcoal L# L-925	NA	NM	NM	1119
Al_2O_3 low surface area standard	NA	NM	NM	89

[a] Section refers to position of the feedstock within the lab-scale FC reactor. [b] Date charcoal produced ddmmyy. [c] Isotherm shape poor resulting in an inaccurate low specific surface area value. [d] Not Applicable. [e] Not Measured.

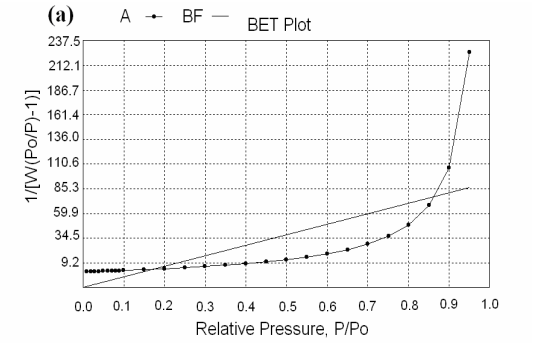
(a)
A
BF
BET Plot
1/[W(Po/P)-1)]
237.5
212.1
186.7
161.4
136.0
110.6
85.3
59.9
34.5
9.2
0.0 0.1 0.2 0.3 0.4 0.5 0.6 0.7 0.8 0.9 1.0
Relative Pressure, P/Po

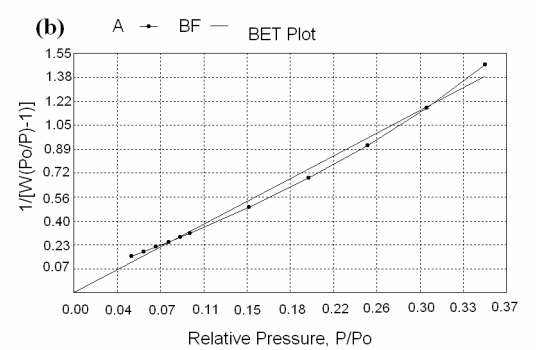
(b)
A
BF
BET Plot
1/[W(Po/P)-1)]
1.55
1.38
1.22
1.05
0.89
0.72
0.56
0.40
0.23
0.07
0.00 0.04 0.07 0.11 0.15 0.18 0.22 0.26 0.30 0.33 0.37
Relative Pressure, P/Po

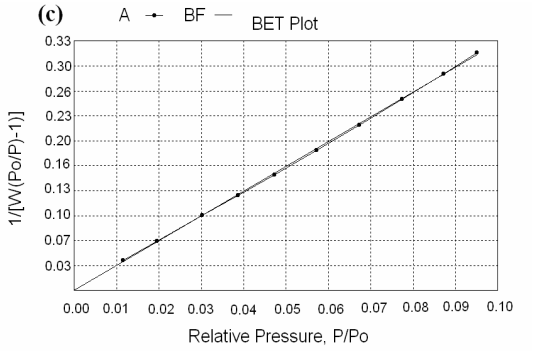
(c)
A
BF
BET Plot
1/[W(Po/P)-1)]
0.33
0.30
0.26
0.23
0.20
0.16
0.13
0.10
0.07
0.03
0.00 0.01 0.02 0.03 0.04 0.05 0.06 0.07 0.08 0.09 0.10
Relative Pressure, P/Po

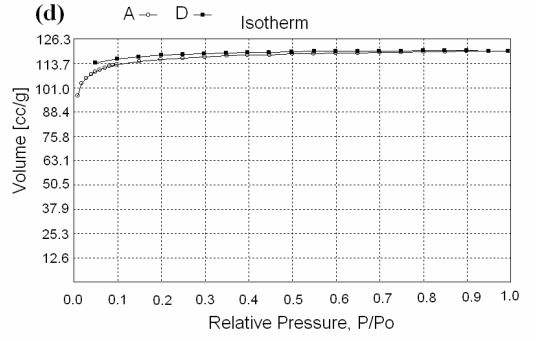
(d)
A
D
Isotherm
Volume [cc/g]
126.3
113.7
101.0
88.4
75.8
63.1
50.5
37.9
25.3
12.6
0.0 0.1 0.2 0.3 0.4 0.5 0.6 0.7 0.8 0.9 1.0
Relative Pressure, P/Po

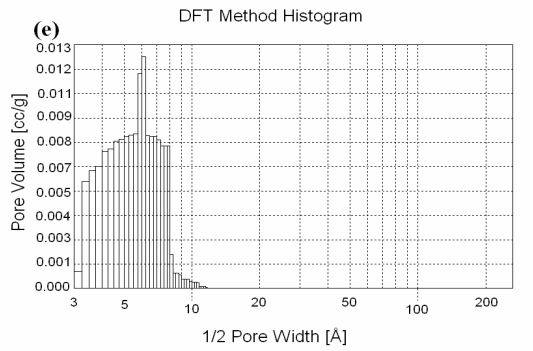
DFT Method Histogram
(e)
Pore Volume [cc/g]
0.013
0.012
0.011
0.009
0.008
0.007
0.005
0.004
0.003
0.001
0.000
3 5 10 20 50 100 200
1/2 Pore Width [Å]

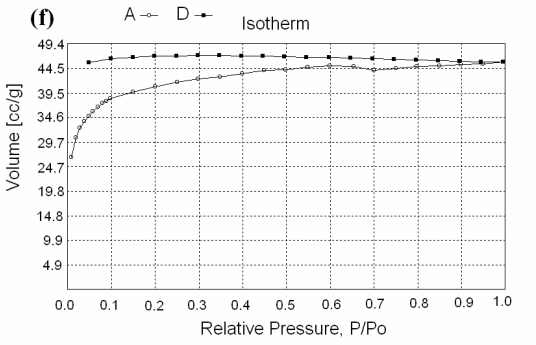
(f)
A
D
Isotherm
Volume [cc/g]
49.4
44.5
39.5
34.6
29.7
24.7
19.8
14.8
9.9
4.9
0.0 0.1 0.2 0.3 0.4 0.5 0.6 0.7 0.8 0.9 1.0
Relative Pressure, P/Po

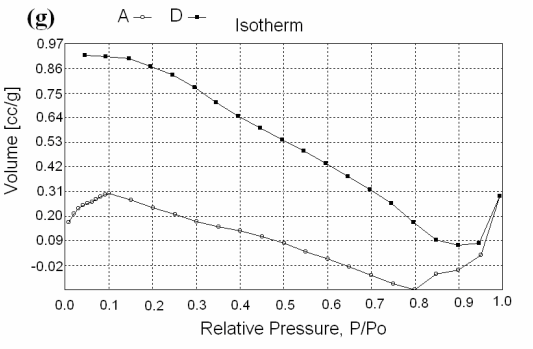
(g)
A
D
Isotherm
Volume [cc/g]
0.97
0.86
0.75
0.64
0.53
0.42
0.31
0.20
0.09
-0.02
0.0 0.1 0.2 0.3 0.4 0.5 0.6 0.7 0.8 0.9 1.0
Relative Pressure, P/Po

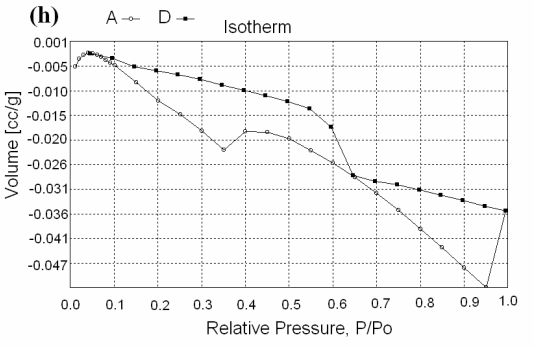
(h)
A
D
Isotherm
Volume [cc/g]
0.001
-0.005
-0.010
-0.015
-0.020
-0.026
-0.031
-0.036
-0.041
-0.047
0.0 0.1 0.2 0.3 0.4 0.5 0.6 0.7 0.8 0.9 1.0
Relative Pressure, P/Po

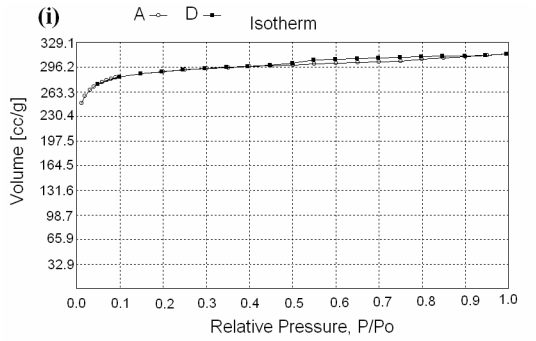

Figure 4.4: *BET Plots and Adsorption/Desorption Isotherms for a Series of Charcoals. (a) BET plot of carbonized (950 °C) boron-doped sucrose charcoal over pressure region P/P_0 = 0.01 – 0.95. (b) BET plot of B&S Activated Coconut Charcoal (mesh 12 × 30) over pressure region P/P_0 = 0.05 – 0.35. (c) BET plot of B&S Activated Coconut Charcoal (mesh 12 × 30) over pressure region P/P_0 = 0.01 – 0.1. (d) Adsorption/desorption isotherm of 20-40 Mesh 270105 'Top' corncob charcoal over pressure region P/P_0 = 0.01 – 1.0. (e) Density Functional Theory (DFT) histogram of 20-40 Mesh 270105 'Top' corncob charcoal calculated from data obtained over pressure region P/P_0 = 0.01 – 1.0. (f) Adsorption/desorption isotherm of 20-40 Mesh 270105 'Middle' corncob charcoal over pressure region P/P_0 = 0.01 – 1.0. (g) Adsorption/desorption isotherm of 20-40 Mesh 270105 'Bottom' corncob charcoal over pressure region P/P_0 = 0.01 – 1.0. (h) Adsorption/desorption isotherm of Fisher Scientific Glass beads over pressure region P/P_0 = 0.01 – 1.0. (i) Adsorption/desorption isotherm of B&S Activated Coconut Charcoal over pressure region P/P_0 = 0.01 – 1.0.*

Low VM corncob charcoal isotherms are type I in shape (refer to Fig. 4.4(d)) indicative of a microporous solid. For such materials the accessible micropore volume limits the uptake of nitrogen[17]. Calculating the specific surface area via the multipoint BET method requires a linear plot of $1/[W(P_0/P)-1]$ Vs P/P_0. The linear region using nitrogen as the adsorbate is normally confined to a limited region of the adsorption isotherm, ~ P/P_0 = 0.05 – 0.35 (refer to Fig. 4.4(a)). The linear region is shifted to lower relative pressures for microporous materials[17]. An ideal linear BET plot is not obtained over the pressure region P/P_0 = 0.05 – 0.35 (refer to Fig. 4.4(b)) therefore specific surface areas were calculated over the lower pressure region of P/P_0

= 0.01 – 0.1. It is also observed that the specific surface area results for the standard activated carbon differ significantly between pressure regions P/P_0 = 0.05 – 0.35 and P/P_0 = 0.01 – 0.1. The specific surface area result obtained using P/P_0 = 0.01 – 0.1 is nearly exactly what is reported by the B & S corporation, whereas the surface area result obtained using the pressure region P/P_0 = 0.05 – 0.35 is significantly lower, ~843 m^2/g.

The DFT histogram (refer to Fig. 4.4(e)) displays pore widths plotted against pore volume. From this chart it is clear that an extensive amount of pore volume is the result of pores with a half pore width between 3 and 10 Å. Pore widths of this size fall into the micropore classification.

The type of adsorbate used in physisorption surface area analysis can have an effect on the resulting specific surface areas. Nitrogen is the most commonly used adsorbate however its use has associated drawbacks. The most well known disadvantage of nitrogen adsorption is that diffusion of nitrogen into carbon micropores is very slow. Another disadvantage is its inability to access very small micropores[18]. Another commonly used adsorbate for surface area determinations of microporous carbons is carbon dioxide. Carbon dioxide is a small molecule with no permanent dipole moment and has minimized diffusion effects at 298 K[19]. The properties of carbon dioxide also allow for ultramicropores (pores smaller than 7 Å) to be more easily analyzed[18].

Results represented in Table 4.3 illustrate a clear link between the percentage VM content of a charcoal and its resulting specific surface area. As the percentage VM content is increased the specific surface area decreases. This trend is more distinctly represented by Figures 4.4(d), 4.4(f), and 4.4(g). A recent paper reports similar surface area results from analysis of wood charcoal as a function of HTT[20]. As the percentage VM content increases representative charcoal isotherms become more largely atypical to the point where such a small surface area is present that the instrument has trouble producing an accurate isotherm. To establish that the negative sloping isotherms are a result of a low specific surface area, Fisher Scientific glass beads (~3mm ∅) were analyzed. It is assumed that glass beads are a non-porous

material with a specific surface area limited to the external surface. With this assumption the estimated specific surface area of the glass beads analyzed equates to $0.005 m^2/g$. The isotherm obtained from the analysis of Fisher Scientific glass beads, Fig. 4.4(h), is far from typical but does contain similarities with that of high percentage VM flash carbonized corncob charcoals. At low relative pressures an expected positive adsorption of nitrogen is observed. This however quickly changes to a systematic negative adsorption. At higher relative pressures, $\sim P/P_0 = 0.9$, a positive adsorption of nitrogen is again observed, although the volume is very small. It should be noted that a polymeric material was previously analyzed resulting in a specific surface area of $0.5 m^2/g$. The isotherm for this material did not appear atypical. In order to obtain accurate surface areas of non-porous materials a large amount of sample is beneficial. However, due to the low density of corncob, no more charcoal sample could be added to the largest quantachrome glass sample container.

A corncob charcoal with a percentage VM content of 15.2% selected from the 'top' section of the lab-scale FC reactor was analyzed via the autosorb 1. A specific surface area of 60 m^2/g was obtained. In comparison a corncob charcoal sample with a similar percentage VM content (14.6%) selected from the 'bottom' section of the lab-scale canister produces an atypical isotherm and hence an inaccurate surface area value. As previously discussed the atypical isotherm is attributed to a non-porous low surface area material. This phenomenon may indicate that there is a difference in porosity between charcoals produced at the 'top' and 'bottom' portions of the canister. The similar VM content denotes that both chars have been subjected to the same degree of FC. A 'top' corncob charcoal with a VM content of 19.7% produced an abnormal isotherm. As discussed previously a physical difference is often observed between 'top' and 'bottom' corncob charcoals. 'Bottom' portions of corncob charcoal are soft and spongy indicating secondary char formation, whereas 'top' portions of corncob charcoal are hard and rigid.

The larger specific surface area observed for low VM corncob charcoals are attributed to an increase in pore accessibility. Upon heat treatment VM is removed exposing previously inaccessible pores. High heat treatment of charcoals may also result in the formation of cracks and fissures which would further contribute to the

specific surface area. As explained in section 1.2, FC technology provides improved yields of charcoal due to increased secondary carbon formation. It is therefore hypothesized that pyrolytic tars and volatile organic matter produced from biomass carbonization at the top of the lab-scale reactor canister are forced downwards by the primary airflow. The hot VM is then able to condense and carbonize in the cooler porous 'bottom' charcoal. This phenomenon results in a reduction in surface area due to the blocking of pores. A Hitachi S-4100 Field Emission Scanning Electron Microscope with X-ray analyzer was employed to investigate the various observed specific surface area phenomena.

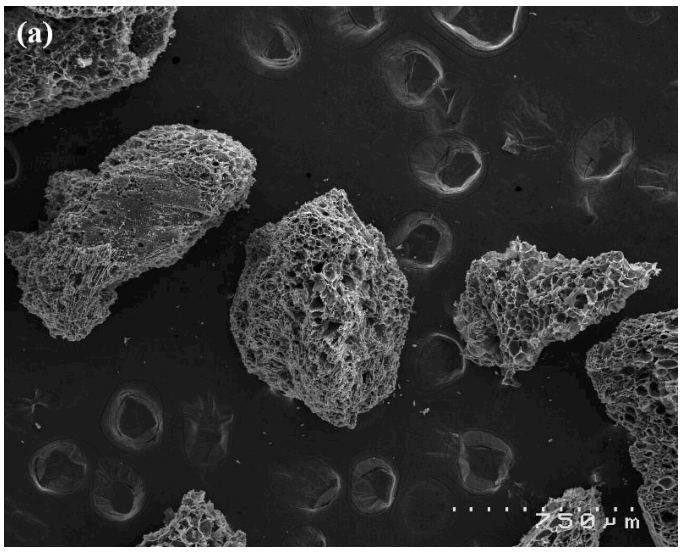

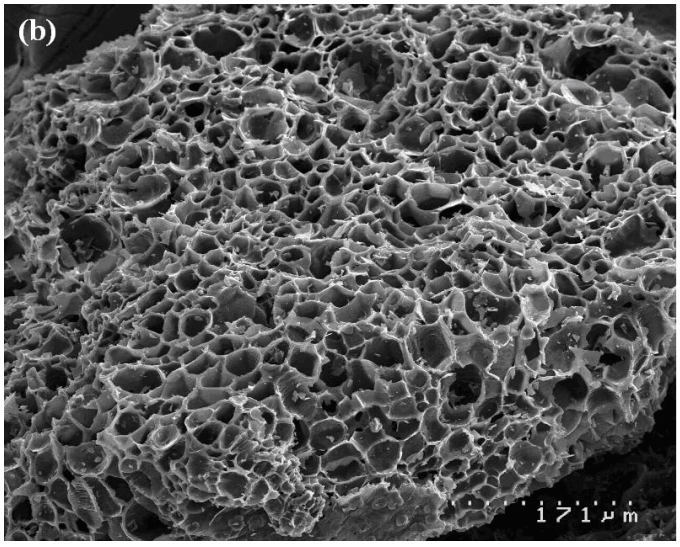

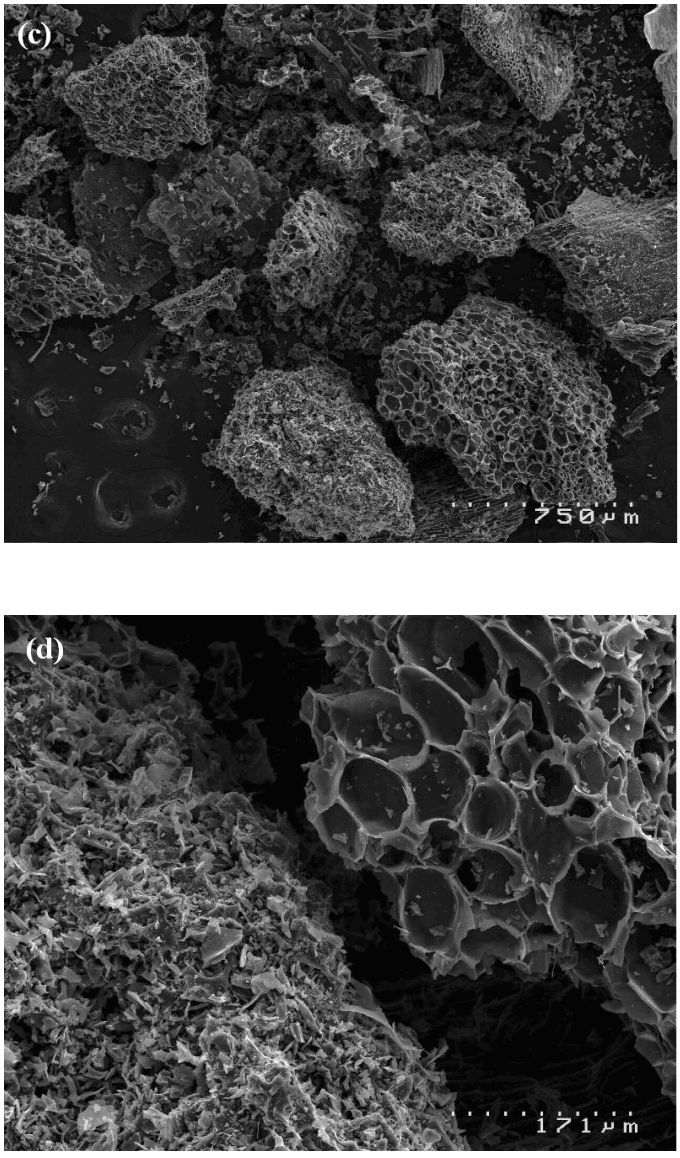

Figure 4.5: *SEM Micrographs of Corncob Charcoal. (a, b) 20-40 Mesh corncob charcoal 270105 'Top'. (c, d) 20-40 Mesh corncob charcoal 270105 'Bottom'.*

SEM micrographs 4.5(a) and 4.5(b) show a relatively clean porous material. It is important to note that the pores observed would not contribute much to the overall specific surface area of the material. As mentioned previously corncob charcoal appears to be microporous (pore size <2nm) in nature. SEM observed pores are significantly larger than the largest micropore dimensions. SEM micrographs 4.5(c) and 4.5(d) appear more disordered with larger particles covered with smaller particle debris. This is more clearly represented in Figure 4.5(d) whereby a distinct contrast in particle types is illustrated. The debris covering some particles may be an indicator of secondary carbonization.

It is also interesting to compare the isotherms obtained by corncob charcoal and that of activated coconut carbon. The isotherm obtained from the activated coconut carbon has a closed hysteresis loop (refer to Fig. 4.5(i)) In contrast the desorption curve for low VM corncob charcoals remains parallel (refer to Fig. 4.5 (d) (non-equilibrium isotherm) to the adsorption curve even at low pressures, i.e. the amount of nitrogen desorbed is distinctly different from the amount of nitrogen adsorbed at the same relative pressure. A corncob charcoal sample was analyzed using longer equilibration times, however the same parallel desorption curve resulted. Surface area analysis performed by W. J. Braida *et al*[21] on maple wood charcoal produced very similar nitrogen and argon isotherms. Braida *et al* attributed the irreversible isotherm to severe diffusion limitations through constricted pores and to structural rearrangement/relaxations of adsorbent during sorption. The second factor described by Braida is also termed low-pressure hysteresis. Low-pressure hysteresis is attributed to swelling and distortions in structure caused by adsorption and condensation of adsorbate. Since the distortions are not perfectly elastic, some adsorbate molecules become trapped and can escape only very slowly or not at all. The degree to which a solid expands during adsorption depends on the overall rigidity of the sample[13]. Braida *et al* also produced adsorption isotherms using carbon dioxide as the adsorbate. The resulting hysteresis was much less pronounced and was attributed to the adsorbates enhanced diffusion properties. Figures 4.4(d) and 4.4(g) illustrate a great difference in hysteresis. The low VM corncob charcoal has minimal hysteresis compared to the high VM corncob charcoal. This may indicate a difference in structure, i.e. the low VM corncob charcoal may be more rigid and may contain more accessible pores. Charcoal hysteresis caused by benzene adsorption was also investigated by Braida *et al*[21]. It was observed that upon adsorption of benzene, the charcoal sample swelled thus causing a deformation of the charcoal pore structure. The proposed mechanism behind this phenomenon involved the adsorption of benzene into open pores which subsequently caused the rearrangement of polyaromatic sheets resulting in pore expansion. Expansion of pores opened up new pathways for more benzene molecules to penetrate. In some circumstances the new pathways were closed after the adsorbate entered, trapping it until further rearrangement occurred. Expansion of the carbon matrix is not expected to be reversible due to the assumed low mobility of polyaromatic sheets.

The type of hysteresis displayed by a range of charcoals indicates that the material is appreciably flexible. This information should be kept in mind when proposing charcoal structures.

4.3 Carbonization

Carbonization is generally thought of as an aromatic growth and polymerization process, resulting in carbon enrichment and the development of porosity as VM is removed. Smaller polyaromatic hydrocarbons anneal together and rearrange at high heat treatment temperatures forming larger more condensed aromatic clusters of graphitic nature. A factor that makes carbonization such a complex process is the presence of several polymerization sites available in an aromatic molecule. For instance there are eleven possible reaction products from the simple dimerization of anthracene. Further complications in carbonization chemistry eventuate as aromatics polymerize in two dimensions. The presence of oxygen in carbonaceous structures has also been found to affect thermal reactions involved in the carbonization process. Severe oxidation has been found to significantly reduce the graphitizibility of pitch[22].

Charcoals were carbonized within a closed porcelain crucible in a muffle furnace (Barnstead Thermolyne FB1215M). In a typical carbonization experiment 5-10 g of 20-40 Mesh charcoal was added to a Coors crucible, lidded, and subjected to a VM analysis using ASTM method D1762-84. The ASTM method was modified only by length of time for which the charcoal-containing crucible was positioned at the back of the furnace; in this case 30 minutes instead of 6.

It is important to note that a couple of weaknesses are associated with the use of the muffle furnace technique in obtaining low VM biocarbons. Firstly, the muffle furnace thermocouple reports its own temperature, which is neither the furnace temperature, nor the temperature of the carbon within the closed crucible. Secondly, the closed crucible is not 100% air tight and therefore carbonization conditions are not strictly in an inert atmosphere[1]. However, despite these shortcomings the use of the muffle furnace in obtaining carbonized charcoals is adequate.

4.3.1 Proximate Analysis Results of Select Carbonized Charcoals

Table 4.4 below illustrates the proximate analysis results for all relevant carbonized biocarbons:

Table 4.4: Proximate Analysis Results of 20-40 Mesh (425 - 850 μm) Carbons

Feed	Proximate Analysis (%)[a]				
	Section[b]	HTT[c], °C	VM	fC	Ash
Corncob, 130404[d]	Middle	950	3.2	94.3	2.5
Corncob, 130404	Top	950	2.2	95.2	2.6
Corncob, 130404	Middle	1050	2.5	91.4	6.1
Demineralized Corncob, 060804	Middle	950	1.7	97.0	1.3
Boron-doped Corncob, 031104	Top	950	1.5	95.0	3.5
Kukui Nutshell, 020904	Middle	950	2.6	95.0	2.4
C & H Pure Cane Sugar, 131204	Top	950	1.4	98.5	0.1
β-D-Fructose, 180205	Top	950	1.7	98.1	0.2
β-D-Fructose, 180205	Top	1050	1.6	98.3	0.1
α-D-Glucose, 250405	Top	950	1.6	98.3	0.1
Inulin, 120405	Top	950	1.4	98.1	0.5
Kraft Lignin, 220305	Top	950	2.7	93.2	4.1
Kraft Lignin, 220305[e]	Top	1050	2.8	93.1	4.1
Boron-doped Sucrose, 160505	Top	950	3.2	86.6	10.2
Phosphorus Doped Sucrose, 180505	Top	950	2.7	92.1	5.2
Desulco 9012 Carbon	-	>2760	0.7	99.2	0.1

[a] Dry Basis - ASTM D1762-84 (Reapproved 1990). [b] Refers to the position of the charcoal within the lab-scale FC canister. [c] Heat Treatment Temperature. [d] Number corresponds to date produced dd/mm/yy. [e] Particle size <425 μm but >212 μm.

All carbons have very low VM contents, ranging between 1.4 and 3.2 %. There also appears to be very little difference between carbons heat treated at 950 °C and carbons heat treated at 1050 °C; a slight decrease in the percentage VM content and a slight increase in the percentage ash content for biocarbons carbonized at 1050 °C

compared to biocarbons carbonized at 950 °C. All heat treated biocarbons have a high fixed carbon content.

4.3.2 Electrical and Physical Properties of Select Carbonized Charcoals

As mentioned previously graphite is a two-dimensional solid, composed of a series of stacked parallel layer planes, having trigonal sp^2 bonding[23], and is often referred to as a semi metal.

Based on Franklin's[9] model, heat treated carbon based materials form either graphitizing carbons or non-graphitizing carbons. The carbons we prepared are classified as non-graphitizing carbons since they are derived from feedstocks high in oxygen and hence are supposed to consist of randomly orientated cross-linked small graphitic crystallite. It is assumed that it is the graphitic nature of the heat treated carbon material giving rise to its ability to conduct electricity. It is important to note however that carbon based polymers are also excellent conductors of electricity. Polyacetylene (Fig. 4.6(a)), polythiophene (Fig. 4.6(b)) and poly(paraphenylene) (Fig. 4.6(c)) have electrical resistivities of ~6 x 10^{-6} Ω·cm, ~0.001 Ω·cm, and ~0.001 Ω·cm respectively[24].

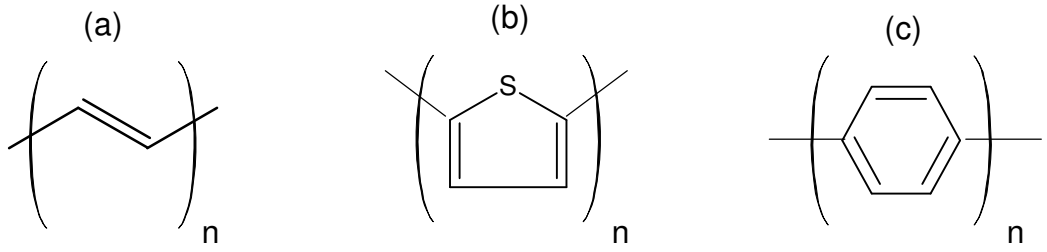

Figure 4.6: *Structural Examples of Some Common Carbon Based Polymers. (a) Polyacetylene. (b) Polythiophene. (c) Poly(paraphenylene).*

Electrical resistivity is defined as a measure of the resisting power of a specified material to the flow of an electric current[25] and is usually obtained via application of equation (6) below:

$$\rho = RA/l \quad \textbf{(6)}$$

Where:

ρ = is the static resistivity (measured in ohm metres)
R = measured resistance (Ω)
A = cross-sectional area of the specimen (cm^2) – in our case cross-sectional area of a packed bed of biocarbon.
l = length of the specimen (cm) – in our case the measured length between the two probes.

The electrical resistivity of various carbonized biocarbon samples was determined by a two-probe packed-bed technique at room temperature. The apparatus and methodology used is analogous the set up employed by Mochidzuki *et al*[1]. As shown in Figure 4.7, the upper electrode is forced down upon the biocarbon bed by a pneumatic piston. The electrical resistance of the compressed bed is measured with a precision, hand-held milliohmmeter (ISOTK M210). This meter has a resolution of 0.001 Ω from 0 to 1.990 Ω, a resolution of 0.01 Ω from 1.99 to 19.90 Ω, and a resolution of 0.1 Ω from 19.9 to 199.9 Ω. It should be noted that the measurement of the bed height is adjusted by the zero-offset (i.e. a blank measurement of the apparatus prior to sample analysis). In a typical electrical resistivity experiment, 20-40 Mesh carbonized biocarbon (1 g DB) was placed into the alumina tube. The upper electrode was lowered gently into the alumina tube and once in place the remainder of the apparatus was assembled. The pneumatic piston was then operated generating required pressures of 0-500 psig. Resistance is at a minimum at the maximum pressure of 500 psig which equates to a working pressure of ~10000 kPa. A resistivity value is given at the maximum working pressure of 10000 kPa after two or more compressions.

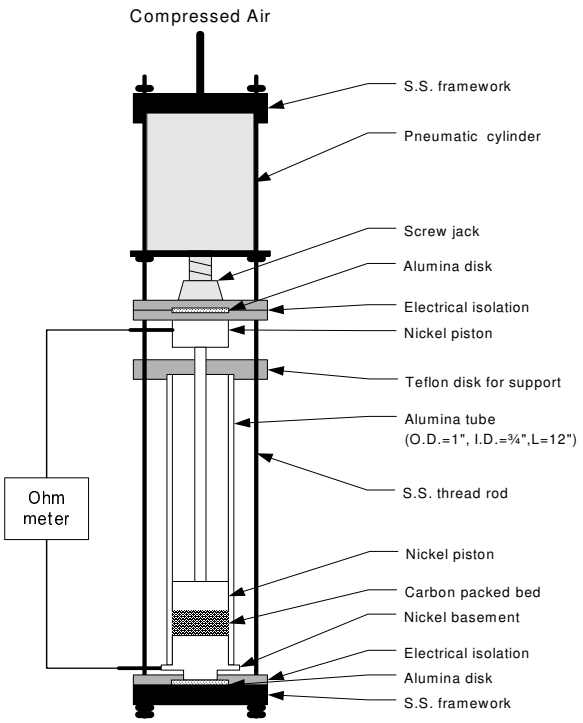

Figure 4.7: *Apparatus Employed to Measure the Electrical Resistivity of a Packed Bed of Carbonized Charcoal.*

The electrical resistivity of packed beds depends on the intrinsic properties of the particles, the property of the contacts between the particles, the arrangement of the particles and the packed bed density. The electrical resistivity of packed beds is significantly reduced as the compaction pressure is increased. Increasing the bed pressure increases the material density and increases the number of interparticle contacts[26].

As mentioned previously in section 4.3, 20-40 Mesh charcoal samples were carbonized at a desired HTT (nominally 950 °C) for 30 minutes. This method was employed due to previous research in the R3 laboratory located at the Hawaii Natural Energy Institute (HNEI) indicating that soak times greater than 30 minutes did not significantly affect the electrical resistivity, (refer to Fig. 4.8).

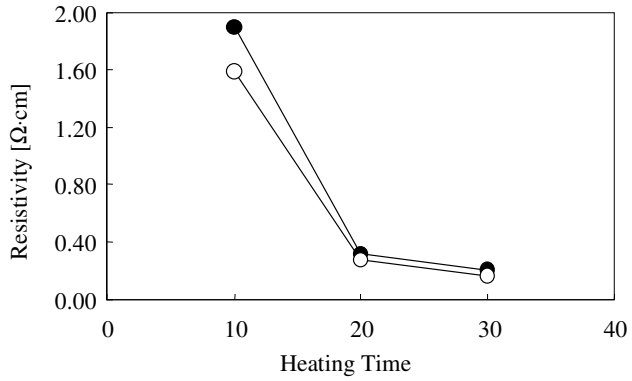

Figure 4.8: *Graphical Representation Showing the Result of Charcoal Resistivity Vs. Heating Time (Furnace temperature: 950 ℃) (○); resistivity of 425-850 μm, (●); resistivity of <425 μm.*

The electrical resistivity and density measurements for carbons are expressed at the maximum working bed pressure of ~10000 kPa after two or more compressions. Previous research performed by the R3 laboratory indicated that measurements after one compression were not reliable, and that further compressions were required in order to obtain reproducible values. This is more clearly illustrated in Figures 4.9(a), 4.9(b) and Table 4.5.

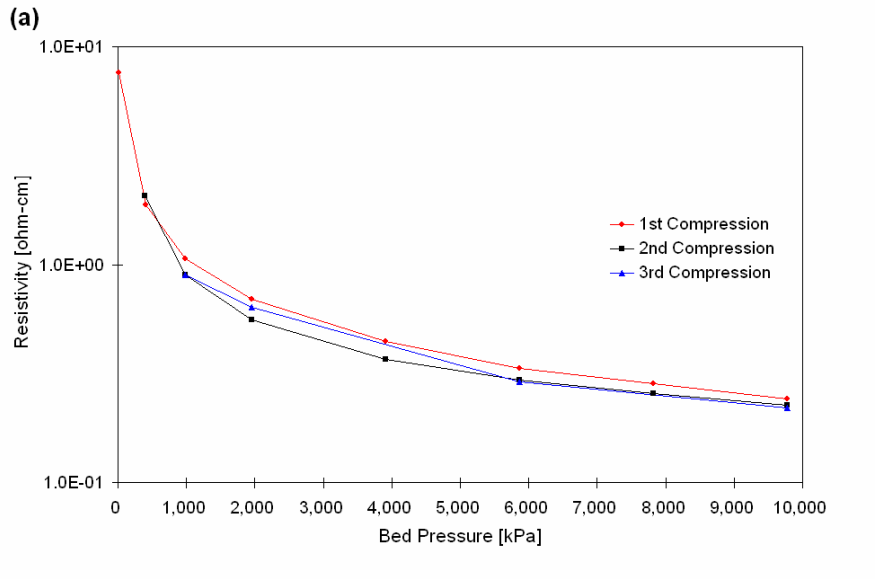

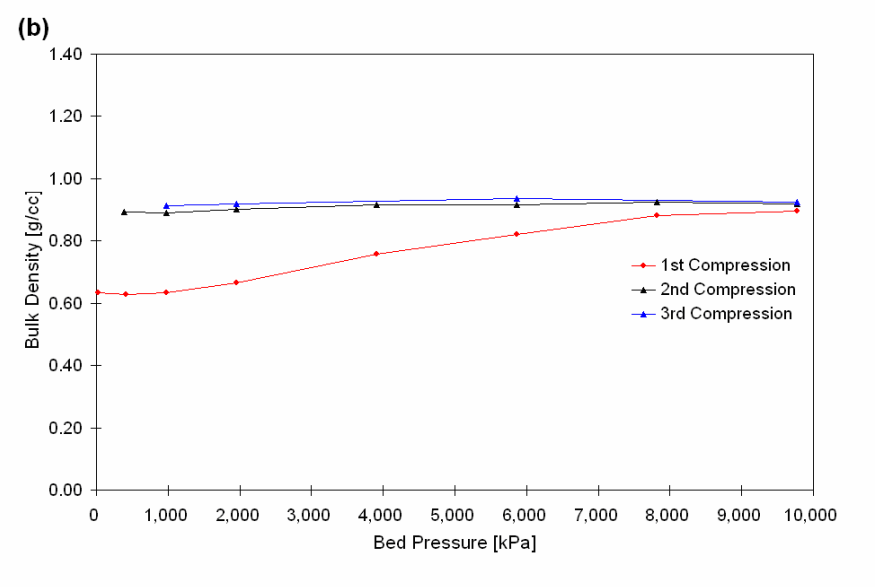

Figure 4.9: *Graphical Representation Showing (a) Electrical Resistivity Vs Bed Pressure for Carbonized (950 °C) 20-40 Mesh Fructose Carbon. (b) Density Vs Bed Pressure for Carbonized (950 °C) 20-40 Mesh Fructose Carbon.*

Table 4.5: Effects of Compression Number on the Electrical Resistivity and Density of Carbonized (950 °C) 20-40 Mesh Fructose Carbon

Compression	P(w[a])[kPa]	Electrical Resistivity (Ω·cm)	Density (g/cm^3)
1st	9779	0.23	0.86
2nd	9779	0.21	0.89
3rd	9779	0.21	0.92

[a] *Working bed pressure*

From the above charts and Table it is clear that values from the first compression are not representative. It is hypothesized that the first bed compression may cause particle fracture resulting in a smaller particle size distribution. The smaller particles may subsequently pack more consistently after the initial release of pressure.

Previous research performed in the R3 laboratory also indicates that fine particle packed beds have increased densities compared to coarse particle packed beds. This suggests that fine particles are more easily compressed than coarse particles. The

fracturing of particles upon compression may therefore account for the commonly observed increase in density with extended compressions.

20-40 Mesh particle size was selected for electrical resistivity measurements as again previous research in the R3 laboratory indicated a correlation between particle size and resistivity. It was observed that a coarse particle packed bed resulted in decreased electrical resistivities compared to a fine particle packed bed (refer to Table 4.6).

Table 4.6: Affect of Particle Size on the Electrical Resistivity and Density of Corncob Carbon

Particle Size	HTT (°C)	Soak Time (min.)	P (w[a]) [kPa]	Bed Length (cm)	Resistance (Ω)	Resistivity (Ω·cm)	Density (g/cm^3)
20-40	950	10	9547	0.6425	0.358	1.59	0.546
<425 µm	950	10	9551	0.4969	0.330	1.89	0.706
20-40	950	20	9602	0.6509	0.063	0.28	0.539
<425 µm	950	20	9543	0.5324	0.059	0.32	0.659
20-40	950	30	9797	0.6213	0.036	0.16	0.580
<425 µm	950	30	9585	0.5274	0.039	0.21	0.665

[a] *Working bed pressure*

From Table 4.6 it appears that fine particle biocarbon packed beds have a decreased electrical resistance but a greater electrical resistivity compared to coarse particle packed beds. It is supposed that fine particles pack more intimately, therefore reducing the amount of possible poor conducting air gaps. This results in increased interparticle contact which facilitates the flow of electricity. It is also observed that the corrected biocarbon packed bed length is significantly smaller for fine particle beds compared to packed coarse particle beds which accounts for the lowered resistance. This property adds additional robustness to the claim that fine particle beds are more easily compressed than coarse particle beds. It is known that oxygen chemisorption can increase the electrical resistivity of a carbon[1]. Lefebvre *et al*[26] remarks that the electrical resistivity of powder compacts is strongly affected by the

amount of non-conducting particle interfaces. It is therefore proposed that smaller particles having larger surface areas are more heavily oxidized, resulting in an increased amount of non-conducting particle interfaces, consequently causing an increase in electrical resistivity. Results obtained are in contrast to earlier reported biocarbon packed bed electrical resistivity measurements[1], in that the electrical resistivity of a packed bed appears to be dependent on both the particle size and apparent bulk density of the bed. Table 4.7 illustrates the electrical and physical properties for all the carbonized biocarbons:

Table 4.7: Electrical and Physical Properties of 20-40 (425 - 850 μm) Mesh Carbonized Charcoals Employed in this Work

Feed	HTT[a], °C	Section[b]	Surface Area[c], m^2/g,	Pore Volume, mL/g	Resistivity[d], Ω·cm	Density[d], g/cm^3
Corncob, 130404[e]	950	Middle	331	0.146	0.19 ± 0.05	0.60 ± 0.07
Corncob, 130404	950	Top	419	0.178	NM[f]	NM
Corncob, 130404	1050	Middle	187	0.084	0.13	0.56
Demin[g]. Corncob, 060804	950	Middle	403	0.170	0.21 ± 0.04	0.52 ± 0.04
BD[h] Corncob, 031104	950	Top	314	0.144	0.20	0.54
Kukui Nutshell, 020904	950	Middle	139	0.069	0.17	0.83
C & H Sugar, 131204	950	Top	172	0.080	0.27 ± 0.03	0.99 ± 0.12
C & H Sugar, 131204	FC[i]	Top	76	0.049	22.99	1.07
β-D-Fructose, 180205	950	Top	199	0.137	0.22 ± 0.01	0.92 ± 0.00
β-D-Fructose, 180205	1050	Top	NM	NM	0.12	0.97
α-D-Glucose, 250405	950	Top	217	0.110	0.19	0.85
Inulin, 120405	950	Top	261	0.140	0.22	0.91
KL[j], 220305	950	Top	248	0.106	0.21	0.80
KL, 220305[k]	1050	Top	NM	NM	0.17	0.90
BD Sucrose, 160505	950	Top	96	0.044	0.14	0.96
PD[l] Sucrose, 180505	950	Top	235	0.107	0.19	0.94
Desulco 9012 Carbon	>2760	NA[m]	NM	NM	0.03	1.09

Feed	HTT[a], °C	Section[b]	Surface Area[c], m^2/g,	Pore Volume, mL/g	Resistivity[d], Ω·cm	Density[d], g/cm^3
Synthetic Graphite Powder (1-2 μm)		NA	NM	NM	0.03[j]	1.41[n]

[a] Heat Treatment Temperature. [b] Refers to the position of the charcoal within the lab-scale FC canister. [c] BET surface area calculated over the pressure region P/P_0 = 0.01-0.1. [d] Resistivity and density values obtained from the maximum of the second or greater pressurization. [e] Number corresponds to date produced dd/mm/yy. [f] Not Measured. [g] Citric acid demineralized. [h] Boron-doped (BD). [i] Flash carbonized (FC). [j] Kraft Lignin (KL). [k] Particle size <425 μm but >212 μm. [l] Phosphorus-Doped (PD). [m] Non Applicable. [n] Values obtained from reference [1].

The electrical resistivity of a packed bed of untreated biocarbon carbonized at 950 °C ranges from 0.17-0.22 Ω·cm, excluding sucrose carbon (0.27 Ω·cm). This result indicates that differing feedstock based charcoals, once heat treated at 950 °C, appear to have similar electrical properties. It is important to note that the electrical resistivity of carbonized charcoals is only six to seven times greater than the resistivity of powdered synthetic graphite, (~0.03 Ω·cm). Biocarbons heat treated at 1050 °C have reduced electrical resistivities ranging from 0.12-0.17 Ω·cm. The reduction in resistivity is associated with the further release of volatile organic matter and additional structural rearrangement. Additional release of VM upon increased HTT is noted via the proximate analysis results illustrated in Table 4.4. The importance of heat treatment in obtaining electrically conductive biocarbons is illustrated with reference to the prepared sucrose carbon. A portion of sucrose charcoal was subjected to an electrical resistivity measurement prior to carbonization. The sucrose charcoal has a VM content comparable to the sucrose carbon, 1.8% compared to 1.4% however the electrical resistivity of the sucrose carbon is significantly (eighty five times) lower. This indicates that upon carbonization loss of VM and perhaps more importantly structural rearrangement are the fundamental processes required to produce a highly conductive biocarbon.

Carbon literature contains speculation on the potential effects of mineral impurities on the electrical resistivity of carbon. Impurities may act as donors or accepters and thereby improve the electrical conductivity of the carbon semiconductor[1]. Therefore in addition to evaluating possible differences in the electrical properties of various feedstock based biocarbons, the affect of mineral matter on electrical resistivity of heat treated charcoals was also considered. The electrical resistivity of pure carbons derived from D-glucose, D-fructose, sucrose, and inulin are compared to carbons derived from corncob, kukui nutshell, and Kraft lignin which contain inorganic mineral matter. As previously mentioned charcoals carbonized at 950 °C have electrical resistivities ranging from 0.17-0.22 Ω·cm. This result indicates that mineral matter at concentrations ranging between 2.4-6.1%, typical of biomass, does not affect the electrical resistivity of carbonized biocarbons. A more detailed analysis of specific minerals usually located in biomass based charcoals is offered in section 7.18.

Non-graphitizing carbons typically form solid chars without proceeding through a prominent liquid phase, while graphitizing carbons usually form a liquid on heating to temperatures around 400-500 °C. It is believed that the distinct liquid phase which graphitizing carbons experience upon carbonization allows for the necessary formation of orientated regions[27].

It is observed that kukui nutshell carbon has a slightly lower electrical resistivity compared to alternate prepared biocarbons. It is known that the kukui nutshell contains large amounts of oil that forms a coke during pyrolysis[1]. The transient liquid phase of the coke may provide ideal conditions for the formation of a graphitizing carbon. It is therefore proposed that a lower electrical resistivity for kukui nutshell carbon may be the result of an increased proportion of true graphitic structure.

As mentioned previously charcoal retains the form and structure of its biomass precursor. For example corncob, a light porous feedstock, produces a low density easily friable porous carbon, ~0.52-0.60 g/cm^3. Alternatively a hard dense nutshell,

such as the kukui nutshell, produces a hard dense carbon, ~0.83 g/cm^3. All of the pure carbons having gone through a distinct liquid phase upon pyrolysis produced high density carbons with density values ranging between 0.85 and 0.99 g/cm^3. Franklin[9] remarks that graphitizing carbons have relatively high densities, ca. 1.99-2.25 g/cm^3.

Carbonized corncob charcoal has a surprisingly high specific surface area, ca. 300-400 m^2/g, and resultant low density. Corncob does not go through a distinct liquid phase upon pyrolysis and retains much of its primary structural features (refer to SEM Fig. 4.1(a)). Carbonized kukui nutshell charcoal has a considerably lower specific surface area (139 m^2/g) compared to corncob carbon. The lower surface area of kukui nutshell charcoal has been previously attributed to the feedstock containing high amounts of oil which forms a low surface area coke during pyrolysis[1].

The specific surface area of carbons derived from D-glucose, D-fructose, sucrose, inulin and Kraft lignin are much lower (172-261 m^2/g) than carbonized corncob carbon. This is attributed to the fact that precursors D-glucose, D-fructose, sucrose, inulin, and Kraft lignin all go through a distinct liquid phase upon pyrolysis. Note that the surface area result for Kraft lignin carbon is significantly greater than the surface area measurement reported by R. K. Sharma *et al*[28]; ca. 5m^2/g for a lignin char heat treated to 400 °C. It was supposed that the high temperatures were detrimental to the pore structure of the char. Feedstock materials which proceed through a distinct liquid phase during pyrolysis loose their gross morphology as depicted in Figures 4.1 (b-f) and 4.10 (a-c). Liquids have a definite volume, lack porosity, and assume the shape of their containers. The solid char resulting from additional heat treatment of the intermediate liquid phase appears amorphous and is likened to glass. The pore volume of carbonized charcoals ranges between 0.044-0.170 mL/g, with the melt carbons typically having lower pore volumes compared to corncob carbon.

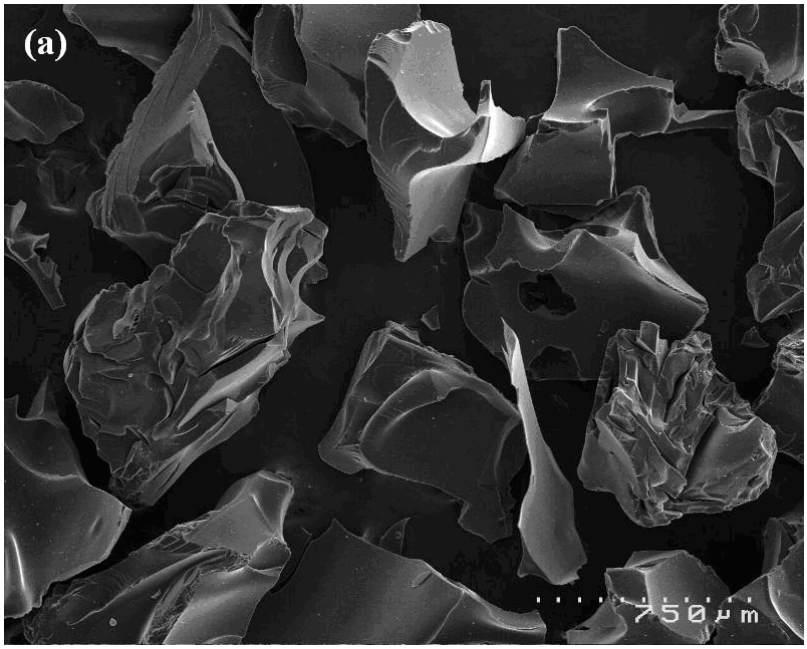
(a)
750µm

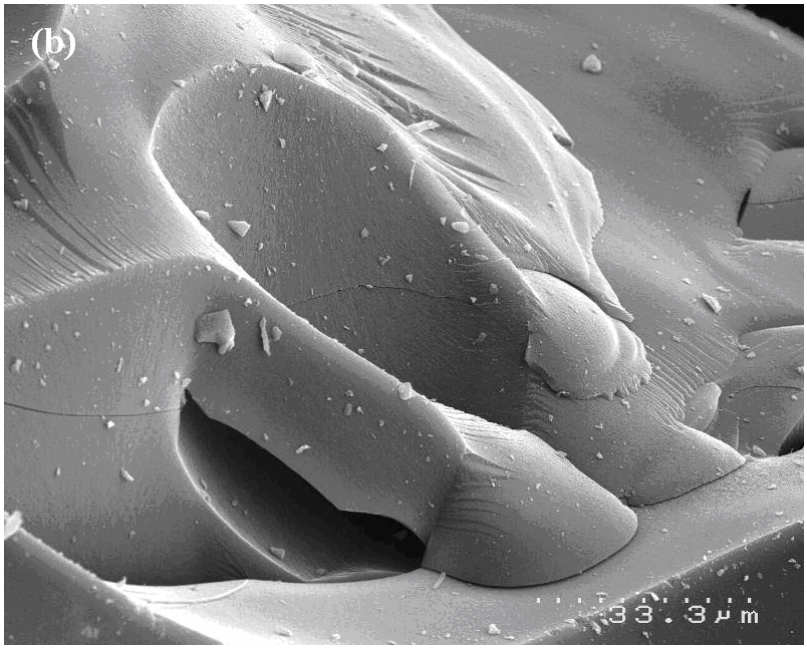
(b)
33.3µm

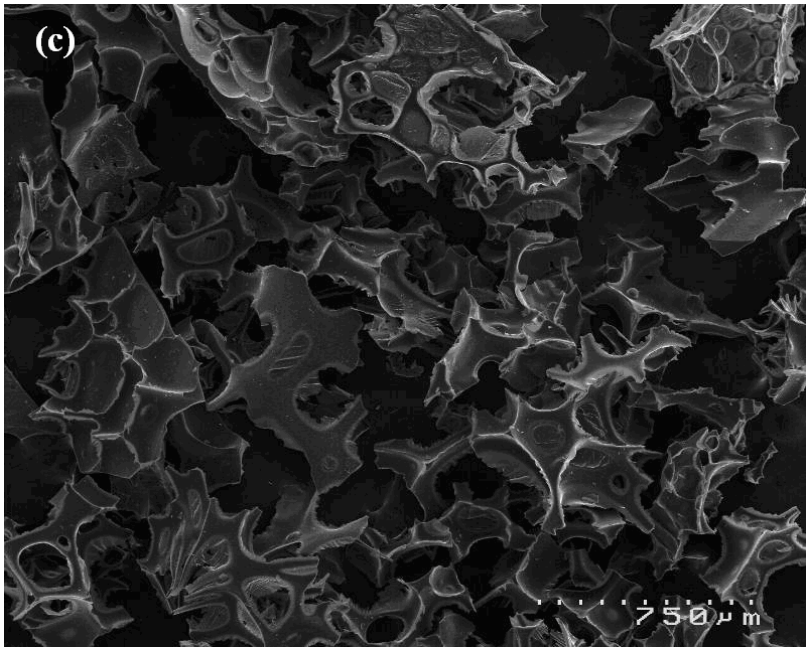

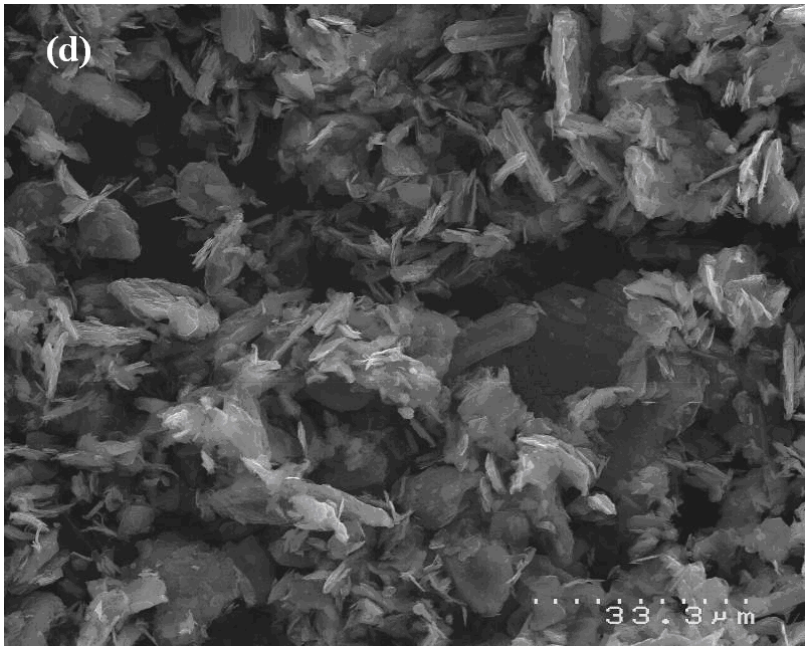

Figure 4.10: *SEM Photographs of Select Biocarbons and Synthetic Graphite. (a, b) 20-40 Mesh fructose charcoal. (c) 20-40 Mesh Kraft lignin charcoal. (d) 1-2 µm Synthetic graphite.*

Again it is important to note that the area of the outer surface – the geometric surface – is virtually negligible in comparison to the internal pore wall surface area. During carbonization inaccessible pores become cleared of various carbonaceous compounds and non-organized carbon. Carbon may also be removed partially from the graphitic

layers of elementary crystallites[29]. SEM photographs (4.10(a-c)) depict an amorphous glass-like material with no visible signs of porosity. The SEM photograph of synthetic graphite (4.10(d)) also shows a material having a smooth glass like appearance and lacking visible porosity.

The isotherms resulting from all carbonized charcoals were typical of microporous materials and are subsequently classified as type I in accordance to the Braunauer classification[13] (refer to Fig. 4.11(a-c)). The representative DFT histogram (refer to Fig. 4.11(d)) of a carbonized charcoal illustrates that the specific surface area is the result of the majority of pores having a half pore width between 3 and 10 Å. Pore widths of this size consequently fall into the micropore classification.

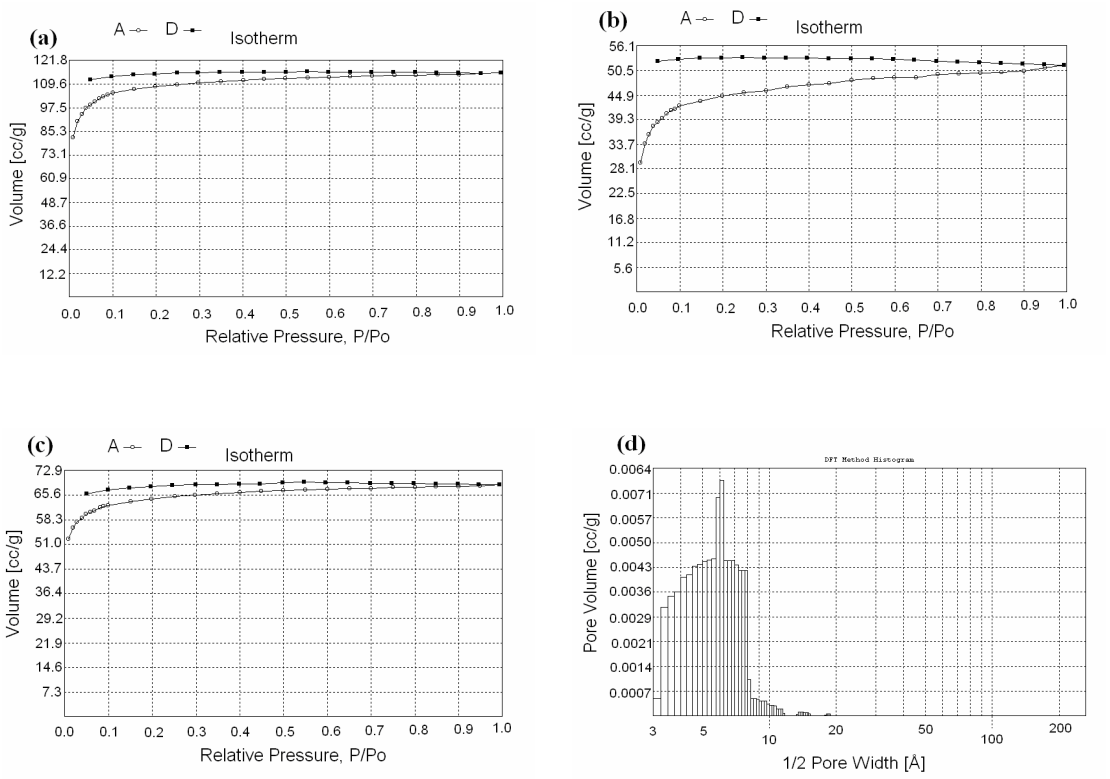

Figure 4.11: *Adsorption/Desorption Isotherms and a DFT plot of Carbonized Charcoals. (a) Adsorption/Desorption Isotherm of (950 °C) 20-40 Mesh Corncob Charcoal Over pressure region P/P_0 = 0.01 – 1.0. (b) Adsorption/desorption isotherm of carbonized (950 °C) 20-40 Mesh sucrose charcoal over pressure region P/P_0 = 0.01 – 1.0. (c) Adsorption/desorption isotherm of carbonized (950 °C) 20-40*

Mesh Kraft lignin charcoal over pressure region P/P_0 = 0.01 – 1.0. (d) Density Functional Theory (DFT) histogram of carbonized (950 °C) 20-40 Mesh Kraft lignin charcoal calculated from data obtained over pressure region P/P_0 = 0.01 – 1.0.

The phenomena of low-pressure hysteresis is again present for carbonized charcoals. With the possible exception of the sucrose carbon, the hysteresis is not as pronounced as previously observed for high VM charcoals. Recall that low-pressure hysteresis is mainly the result of severe diffusion limitations through constricted pores. Sucrose carbon has the lowest specific surface area and the lowest pore volume compared to the other melt carbons. The lower pore volume associated with the sucrose carbon may indicate a higher proportion of narrow slit shaped pores known to impede diffusion of the adsorbate[20].

It is remarked that the melt carbons have a high density with values being almost double that of corncob carbon. This is further evidence that carbons derived from D-glucose, D-fructose, sucrose, inulin, and Kraft lignin have reduced porosities compared to carbons which do not go through a distinct liquid phase during pyrolysis. According to Franklin[9], graphitizing carbons are non-porous with relatively high densities. It is also remarked that natural and synthetic graphite are dense materials having insignificant specific surface areas, ~3.0 m^2/g[30].

In summary, these results show that all carbons possess large surface areas and substantial microporosity that cannot be ignored in a model of their structure. Furthermore all carbonized charcoal powders conduct electricity almost as well as graphite powders.

1. Mochidzuki, K.; Soutric, F.; Tadokoro, K.; M. J. Antal, J.; Tóth, M.; Zelei, B.; Várhegyi, G., Electrical and Physical Properties of Carbonized Charcoals. *Ind. Eng. Chem. Res.* **2003,** 42, 5140-5151.

2. Usuda, H.; Edwards, G. E., Localization of Glycerate Kinase and Some Enzymes for Sucrose Synthesis in C_3 and C_4 Plants. *Plant Physiol.* **1980,** 65, 1017-1022.

3. Government, F., Code of Federal Regulations - Title 49-Transportation. In 2004; p 148.

4. Department, H. C. P., Hilo Fire 07/02/00. In 2000.

5. Puri, B. R.; Singh, D. D.; Nath, J.; Sharma, L. R., Chemisorption of Oxygen on Activated Charcoal and Sorption of Acids and Bases. *Industrial and Engineering Chemistry* **1958,** 50, (7), 1071.

6. Loebenstein, W. V.; Deitz, V. R., Oxygen Chemisorption on Carbon Adsorbents. *The Journal of Physical Chemistry* **1955,** 59, (6), 481.

7. Marsh, H.; Heintz, E. A.; Rodriguez-Reinoso, F., *Introduction to Carbon Technologies*. 1997.

8. Rowell, R., *The Chemistry of Solid Wood*. 1983.

9. Franklin, R. E., Crystallite Growth in Graphitizing and Non-Graphitizing Carbons. *Proc. R. Soc. London A* **1951,** 209, 196.

10. Szymański, G. S.; Karpiński, Z.; Biniak, S., The Effect of the Gradual Thermal Decomposition of Surface Oxygen Species on the Chemical and Catalytic Properties of Oxidized Activated Carbon. *Carbon* **2002,** 40, (14), 2627-2639.

11. Montes-Morán, M. A.; Suárez, D.; Menéndez, J. A.; Fuente, E., On the Nature of Basic Sites on Carbon Surfaces: An Overview. *Carbon* **2004,** 42, 1219-1225.

12. Suárez, D.; Menéndez, J. A.; Fuente, E.; Montes-Morán, M. A., Contribution of Pyrone-Type Structures to Carbon Basicity: An ab Initio Study. *Langmuir* **1999,** 15, 3897-3904.

13. Gregg, S. J.; Sing, K. S. W., *Adsorption, Surface Area and Porosity*. Second ed.; Academic Press: 1982.

14. Braunauer, S.; Deming, L. S.; Deming, W. E.; Teller, E., On a Theory of the van der Waals Adsorption of Gases. *J. Am. Chem. Soc.* **1940,** 62, 1723-1732.

15. R. J. Lewis, S., *Hawley's Condensed Chemical Dictionary*. 12th ed.; Van Nostrand Reinhold: 1993.

16. Lu, G. Q.; Zhao, X. S., *Nanoporous Materials - Science and Engineering*. Imperial College Press: 2004.

17. Quantachrome, *Quantachrome Corporation Autosorb 1 Gas Sorption System*. 1996; Vol. 1/96 AS-1 P/N 05061.

18. Quantachrome, *Powder Tech Note 35*. p 1-5.

19. Marsh, H.; Rand, B., The Characterization of Microporous Carbons by Means of the Dubinin-Radushkevich Equation. *Journal of Colloid and Interface Science* **1970,** 33, (1), 101-116.

20. Pattaraprakorn, W.; Nakamura, R.; Aida, T.; Niiyama, H., Adsorption of CO_2 and N_2 onto Charcoal Treated at Different Temperatures. *Journal of Chemical Engineering of Japan* **2005,** 38, (5), 366-372.

21. Braida, W. J.; Pignatello, J. J.; Lu, Y.; Ravikovitch, P. I.; Neimark, A. V.; Xing, B., Sorption Hysteresis of Benzene in Charcoal Particles. *Environ. Sci. Technol.* **2003,** 37, 409-417.

22. Lewis, I. C., Chemistry of Carbonization. *Carbon* **1982,** 20, (6), 519-529.

23. Pierson, H. O., *Handbook of Carbon, Graphite, Diamond and Fullerenes - Properties, Processing and Applications*. William Andrew Publishing/Notes: 1994.

24. Dai, L., Part I: From Conducting Polymers to Carbon Nanotubes: A Revolution of Sensors Based on Architectural Diversity of the π-Conjugated Structure. *Energeia* **2005,** 16, (2).

25. *The Reader's Digest Oxford Complete Wordfinder*. The Reader's Digest Association Limited: 1993.

26. Lefebvre, L. P.; Pleizier, G.; Deslandes, Y., Electrical Resistivity of Green Powder Compacts. *Powder Metallurgy* **2001,** 44, (3), 259.

27. Harris, P. J. F., Structure of Non-Graphitizing Carbons. *International Materials Reviews* **1997,** 42, (5), 206-218.

28. Sharma, R. K.; Wooten, J. B.; Baliga, V. L.; Lin, X.; Chan, W. G.; Hajaligol, M. R., Characterization of Chars from Pyrolysis of Lignin. *Fuel* **2004,** 83, 1469-1482.

29. Wigmans, T., *Fundamentals and Practical Implications of Activated Carbon Production by Partial Gasification of Carbonaceous Materials*. NORIT Activated Carbon.

30. CARBONS, A. Graphite and Carbon Grades For Conductive Plastic and Polymer Applications. http://www.asbury.com

5.0 Structural Analysis of Biocarbons

Section 2.0 illustrates the complex process of char formation, of which many of the pyrolysis steps are not well defined. Analytical techniques often employed by researchers to follow the plethora of reactions involved in biomass pyrolysis include: FTIR, ^{13}C CPMAS NMR, Py-GC-MS, XRD, ESR, and TG. A large amount of information has been obtained, yet an accurate model of the structure of charcoal still remains in debate. Like previous researchers, instrumental techniques including ESR, XRD, ^{13}C CPMAS NMR, and TG have been employed in this work in the hope of obtaining additional information on the nature of the biomass charcoal's atomic structure. In addition to the above analytical techniques Matrix Assisted Laser Desorption Ionization (MALDI) was explored as a viable analysis tool for obtaining char structural information.

5.1 Electron Spin Resonance (ESR)

Electron spin resonance or paramagnetic resonance is a spectroscopic technique used to study molecules which contain unpaired electrons. These molecules may be found as stable entities but more often are encountered as intermediates in chemical reactions[1]. The technique ESR involves energy transitions between electron spin states in an applied magnetic field initiated by electromagnetic energy, typically in the microwave range of frequencies. Monochromatic radiation is directed upon a given sample housed within an appropriate cell. Adsorption of energy takes place only when the energy of a quantum of incident radiation is equivalent to the energy-level separation distinct for the paramagnetic molecules within the sample. A single energy transition or a set of degenerate transitions are referred to as a line. The shapes of ESR lines are often described by comparison with lorentzian and Gaussian line shapes and are commonly presented in the first or second derivative mode[1].

A significant literature exists describing the structural characterization of carbonaceous materials using ESR[2-7]; a large amount of this literature predates the 1970's. General conclusions are that line width changes with increasing

carbonization temperatures; at low charring temperatures line widths are on the order of 10 G, compared to line widths as small as a few tenths of a gauss at carbonization temperatures ranging between 500 °C and 700 °C; at higher temperatures still, the lines again broaden and in some cases become unobservably weak[2]. Urbański *et al*[5] showed that the pyrolysis of pure cellulose resulted in the formation of free radicals. Free radicals are thought to be the cause of charcoal's remarkable property of facilitating burning mixtures. Furthermore, Urbański recognized that the concentration of free radicals resulting from cellulose pyrolysis was dependent upon carbonization temperature with the maximum concentration of free electrons being noted at 475 °C. At temperatures exceeding 475 °C the free radical concentration was found to decrease. It was also noted that grinding charcoal produced increased concentrations of free radicals. Findings by Asada *et al*[7] substantiate the above results.

A select number of biocarbons having a particle size of <212 μm were analyzed on a Varian E104A X-Band spectrometer operating at 9 GHz. Biocarbon powders were placed in 4 mm o.d. borosilicate tubes, and examined at 25 °C. ESR spectra were calibrated against the stable radical diphenylpicrylhydrazyl (DPPH) at g = 2.0036. Table 5.1 and Figures 5.1(a-d) illustrate results from a series of ESR analyses of select biocarbons. An ESR spectrum of a blank borosilicate tube was obtained to rule out possible influences of glass contaminants on subsequent biocarbon spectra.

Table 5.1: ESR Results Obtained From Select <212 μm Charcoal Powders

Sample ID	Section[a]	HTT (°C)[b]	Peak-peak distance (G)	Relative intensity[c]
Corncob 020704[d]	Middle	NA	5	63
Corncob 020704	Middle	750	-*[e]	
Corncob 020704	Middle	950	4 -[f]	0
Demin. Corncob	Middle	NA	4.8	86
Demin. Corncob[g]	Middle	NA	5.3	30
BD Corncob	Top	NA	5.3	24

Sample ID	Section[a]	HTT (°C)[b]	Peak-peak distance (G)	Relative intensity[c]
Macshell	Middle	NA	5.3	82
Oak Wood	Middle	NA	5.3	100
Sucrose	Top	NA	11	1
			-*	
			1150	50
Sucrose	Top	950	5.5	0
			1600	15
BD Sucrose	Top	950	-	
			175	1
PD Sucrose	Top	950	4.5	0
			1300	1
β-D-Fructose	Top	950	5	0
			875	33
Inulin	Top	950	5	0
			1075	53
Kraft Lignin	Top	950	5.0	0
			450	5
AC[h]		NA	5.5	1
			350	2
Syn. Graphite		>3000	2	0
			525	5

[a] Refers to the position of the charcoal within the lab-scale FC canister. [b] Heat Treatment Temperature. [c] Area of ESR signal relative to that of oak wood charcoal = 100.. [d] Number corresponds to date produced dd/mm/yy. [e] - unable to measure due to superimposed peaks. [f] – no measurable signal. [g] Particle size 20-40. [h] Activated Coconut Carbon (AC).*

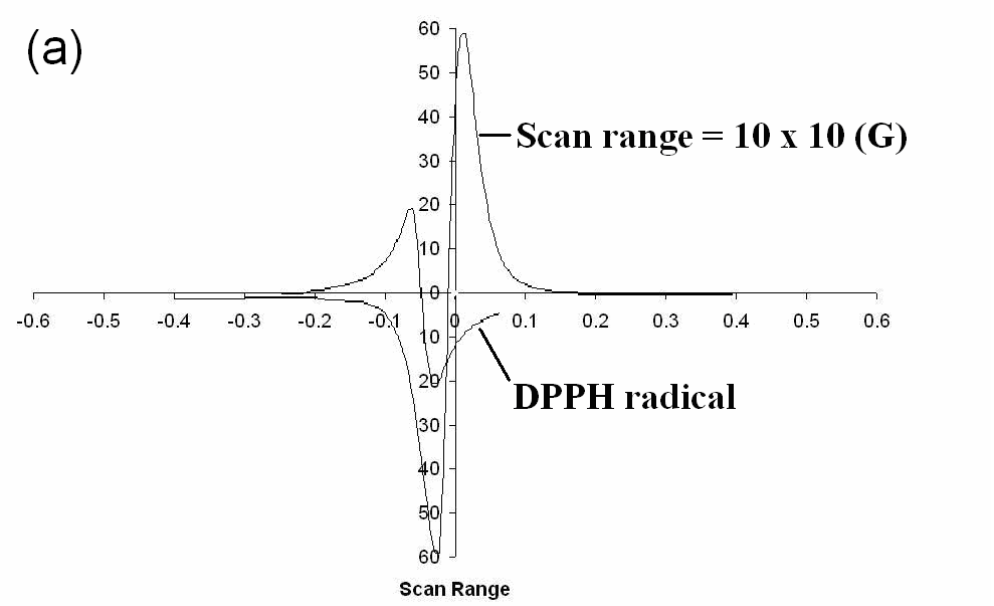
(a)
Scan range = 10 x 10 (G)
DPPH radical
Scan Range

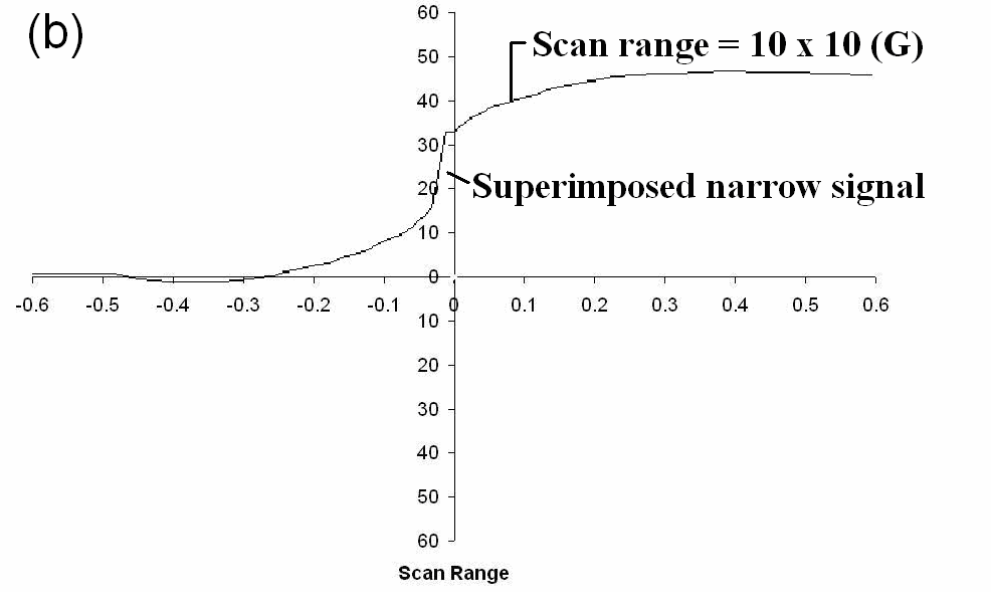
(b)
Scan range = 10 x 10 (G)
Superimposed narrow signal
Scan Range

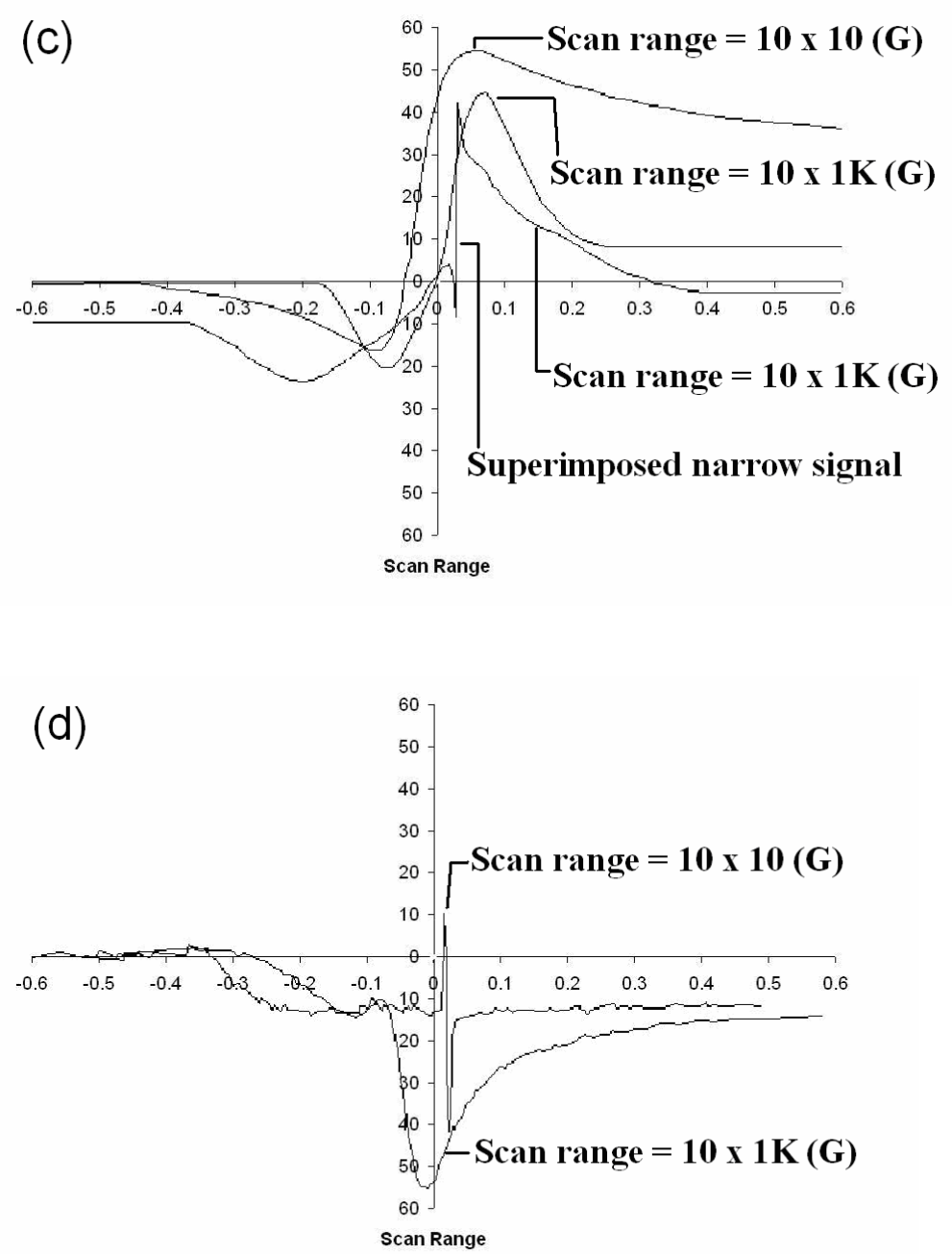

Figure 5.1: *ESR Spectra of Select Biocarbons. (a) 'Middle' 020704 corncob charcoal. (b) Carbonized (750 °C) 'Middle' 020704 corncob charcoal. (c) 'Top' 131204 sucrose charcoal. (d) Synthetic graphite.*

All measured absorbance signals are the first derivative (refer to Fig. 5.1(a)) and have a g-value close to 2.0036. This g-value is typical of a light atom, undoubtedly a carbon-centered organic radical. ESR results also indicate that biocarbons contain two major free radical types; at lower carbonization temperatures a sharp narrow

signal is observed (2-5 G), whereas at high heat treatment temperatures an extremely broad signal is realized (350-1300 G). It also appears that the two types of radicals are not mutually exclusive, for example the ESR spectra resulting from corncob charcoal carbonized at 750 °C (refer to Fig. 5.1(b)) and sucrose charcoal (refer to Fig. 5.1(c)) display what appears to be a narrow signal superimposed upon a larger broader signal. The narrow line width observed for chars heat treated at temperatures between 400-700 °C is explained via an increase in spin concentration and aromaticity giving rise to exchange narrowing. The accepted theory for the broadening of lines for chars exposed to higher temperatures (750-1000 °C) involves the interaction of free radicals with conduction electrons or charge carriers [2]. It is well known that paramagnetic gases, char oxidation, and paramagnetic metals cause line broadening [2, 8].

The relative area of each respective ESR signal was calculated from respective peak amplitudes and peak widths. ESR results indicate that oak wood charcoal contains the highest relative free radical concentration, followed closely by demineralized corncob charcoal and macadamia nutshell charcoal. The radical concentrations associated with such charcoal's appear to be derived exclusively from carbon radicals which afford a narrow signal. The free radical concentrations associated with carbons prepared from sucrose, D-fructose, inulin, and to a lesser extent Kraft lignin are reduced by as much as 5-53% relative to oak wood charcoal. It is interesting to note however that only carbon radicals which afford a broad signal contribute to the carbons free radical population. Similar to Urbański's work the qualitative ESR results indicate a decrease in total carbon radical concentration with increasing HTT.

In addition to differences in signal breadth between the various biocarbons observable variances in line shape are also apparent. The majority of signals are symmetric as in Figure 5.1(a), however in the case of sucrose charcoal (refer to Fig. 5.1(c)) and synthetic graphite (refer to Fig. 5.1(d)) line shapes are asymmetric; a grossly exaggerated right hand side compared to its left hand side is observed. It is remarked that ESR signals derived from fullerene soots are symmetric and remain largely unaltered when exposed to oxygen[9]. Unambiguous line shapes corresponding to heat treated corncob carbon, activated coconut carbon, and carbons derived from sucrose

(untreated and doped) and Kraft lignin were difficult to obtain due to a low signal to noise ratio, (refer to appendix 9.2). This may be a result of extreme signal broadening.

5.2 X-ray Diffraction (XRD)

XRD is an analytical technique often employed to determine the atomic and molecular structure of solid crystalline materials by measuring patterns of scattered x-rays after they pass through an ideal specimen. When x-ray radiation falls on a substance scattered radiation of two types, compton modified scattering incoherent with respect to the primary beam, and unmodified scattering coherent with the primary beam, spreads out spherically from all the atoms in the sample. An interference effect as a consequence of unmodified scattered radiation from the different atoms within the substance causes the intensity of scattered unmodified radiation to vary in different directions. A diagram of this intensity variation is called a diffractogram. The material's diffractogram pattern is dependent on the kinds of atoms and their arrangement in the substance, i.e. the unit cell[10].

As previously discussed in section 2.2, carbon in the form of charcoal is typically described as microcrystalline graphite. The basis for this statement was early XRD analyses of a variety of graphites and amorphous carbons. Select amorphous carbons gave bands in identical positions with certain lines associated with crystalline graphite, however at the time is was deemed doubtful that the technique was sufficiently accurate to permit precise measurement of band width and position[11]. Indeed some years later it was stated by perhaps the world's foremost authority on carbons that it is too often supposed that all amorphous carbons contain minute crystallites of graphite[12]. Franklin went on to demonstrate using XRD that two distinct classes of carbon are produced from the pyrolysis of organic materials, graphitizing carbons and non-graphitizing carbons. Non-graphitizing carbons like those derived from carbohydrates show no trace of homogeneous development of true graphitic structure, even after heating to 3000 °C. A number of attempts have also been made to describe amorphous carbons by taking crystalline graphite and reducing the particle size whilst following the XRD diffractogram pattern[11, 13]. Fine grinding

of graphite was found to markedly decrease the crystallite size causing the sharp intense (002) graphitic peak observed at 26.6 ° (2 θ) to decrease, ultimately leading to the final XRD spectrum to resemble a turbostratic carbon. More recent XRD analyses of a variety of biocarbons led to broad featureless peaks in the region of the sharp intense (002) peak associated with crystalline graphite[14]. The broad biocarbon peaks were also noted as bearing little resemblance to the turbostratic carbon displayed by Walker and Seeley[13]. It appears obvious that despite numerous previous attempts, utilizing XRD, to prove that amorphous carbon is the ultimate form of the graphite series, enough evidence remains to suggest microcrystalline graphite is not the major constituent of amorphous non-graphitizing carbon.

XRD measurements were performed using a Philips X'Pert MPD system equipped with a Cu monochromator and a MiniProp detector. The generator was set at 45 kV and 40 mA, PDS at 0.1 mm, and PRS at 0.2 mm. All scans were run over the 2θ range of 1.5-70°, using a step size of 0.03° (2θ), and a scan speed of 1.5 s/step. Collected data was subsequently treated using X'Pert HighScore software. Treatment steps involved: 1) a 20 point Fast Fourier Transform smooth, 2) $K\alpha_2$ stripping utilizing the Rachinger technique, 3) Peak location by means of a minimum 2nd derivative peak finder technique, and 4) Profile fitting via application of a Pseudo-Voigt profile function to the measured data. A Scherrer calculator which formed part of the software was employed to determine crystallite size (Å) and lattice strain (%).

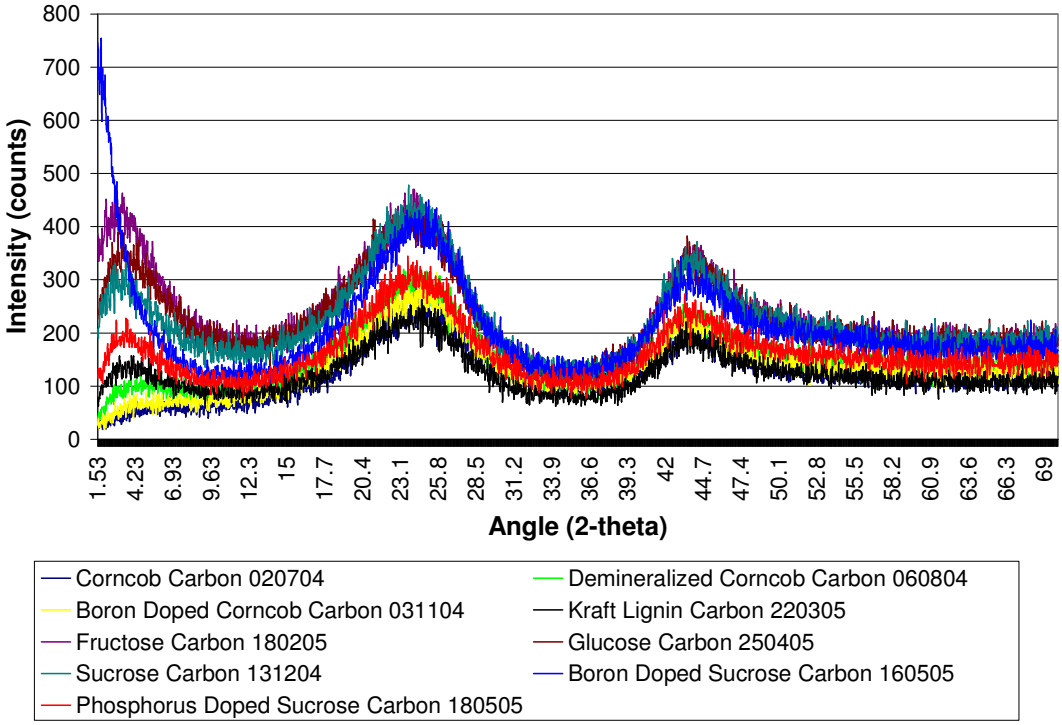

Figure 5.2: *XRD Diffractogram of a Variety of <212 μm Heat Treated (950 °C) Biocarbons.*

XRD diffractogram patterns displayed in Fig. 5.2 are indicative of an amorphous material having some degree of short range order. All heat treated biocarbons have analogous diffractogram patterns, however small observable differences are noted between biocarbon samples with respect to peak intensity and peak shape. Peak shape is not only affected by the degree of crystallinity but also by crystal size; as the crystal size is reduced, diffraction peaks become increasingly broad. In addition to peak broadening the effects of stress can further complicate the picture by causing observable shifts in the location of the diffraction peaks[15]. The initial low angle scattering peak maxima varies for the carbons. The low angle peak may be evidence of a regular microporous structure, reinforcing previous specific BET surface area results. Note that work performed by Pfeifer *et al*[16] on a series of activated carbons evidenced a material wherein the pore space resulted from an extended fractal network of channels having widths of between 15-20Å. The change in initial low angle base line intensity with carbon types may indicate the early presence of an underlying amorphous structure. Carbons derived from corncob and Kraft lignin have low initial intensities compared to carbons derived from pure sugars. It is

recognized from SEM photographs and from normal visual inspection that carbons derived from pure sugars, such as sucrose and D-fructose appear more glass-like as opposed to carbons derived from feedstock's corncob and wood. An alternate possibility for the variation in initial angle intensity may be due to sample preparation. Prior to XRD analysis, carbon samples are packed into a depression within a stainless steel sample holder. An ideally prepared sample requires the carbon material to be packed in the depression as flat as possible. X-rays are then directed upon the sample with the diffracted rays being captured by the detector. X-rays directed at low angles have an increased chance of reaching the detector with high intensity due to minimal diffraction. It is therefore supposed that the high initial angle intensity associated with boron-doped sucrose carbon is a result of minimal diffraction. It is also recognized that packing of the various carbon materials into the stainless steel sample holder is affected by the physical properties of the carbon. Corncob carbon is noticeably softer than carbons derived from pure sugars and is more easily reduced to smaller more compressible particles. Packing of corncob carbon ensuring a flat level surface is therefore more easily obtainable. Deviation from a level surface may result in increased minimal diffraction.

Figure 5.3 is an XRD diffractogram comparing synthetic graphite with heat treated fructose charcoal. The broad featureless peaks represented by the D-fructose carbon bear little resemblance to the sharp intense peaks associated with synthetic graphite. In addition, the well defined 002 synthetic graphite peak appears at a higher angle compared to the analogous 002 peak maxima associated with the fructose carbon. Furthermore the small peak around 54° (2θ) displayed by synthetic graphite is absent in all heat treated carbon diffractogram patterns. It is however recognized that peak intensity decreases with increasing angle in accordance to Lorentz effects. The lack of an XRD peak at 54° (2θ) for the series of heat treated biocarbons may be due to Lorentz effects on already low intensity broad peaks.

A wider angle scattering diffractogram was also obtained for Kraft lignin carbon. Figure 5.4 displays this XRD pattern in comparison with the standard angle Kraft lignin carbon diffractogram pattern. An additional broad peak occurs at 80° (2θ) which appears to be superimposed upon a still larger broad amorphous peak. This

additional peak located at a higher angle illustrates that the Lorentz effects are not a definitive reason for the lack of an XRD peak at 54° (2θ). It is therefore recognized that the atomic structure of graphite can vary due to the manner in which the layer planes are stacked. There are two slightly different ways of stacking, hexagonal, which is the most common stacking sequence, and rhombohedral. Rhombohedral graphite is thermodynamically unstable and is always found in combination with hexagonal graphite. Rhombohedral graphite usually reverts to hexagonal graphite upon heat treatment above 1300 °C[17]. The absent XRD peak for heat treated carbons may therefore indicate the presence of rhombohedral graphite.

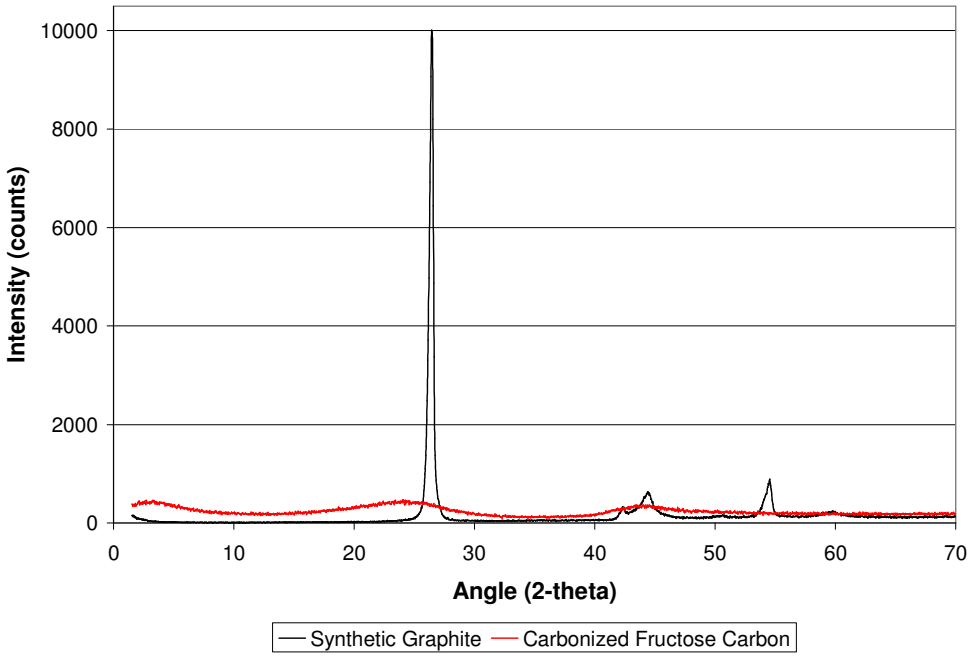

Figure 5.3*: X-ray diffractogram pattern showing well defined sharp peaks associated with synthetic graphite compared to broad featureless peaks associated with carbonized Kraft lignin charcoal.*

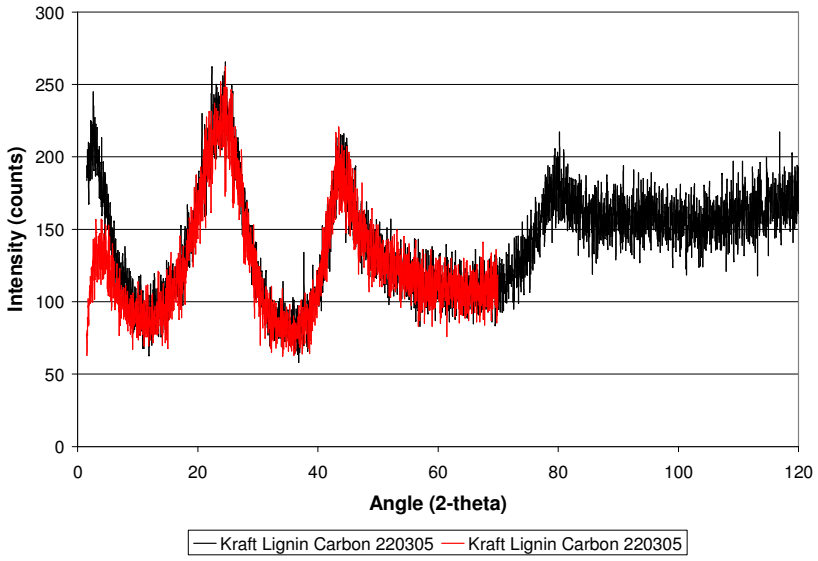

Figure 5.4: *XRD Diffractogram Comparing Carbonized (950 °C) Kraft Lignin Carbon at High Angle and at Low Angle.*

Table 5.2: Results of the XRD Analyses of Heat Treated (950 °C) Carbons

Carbon type	(002) peak position, deg (2θ)	fwhm,[a] deg (2θ)	τ[b], Å	ε[c], (%)	*d*(002)[d], Å	γ_a[e], (%)
Glucose	25.05	4.00	20	7.85	3.55	63
Fructose	24.52	4.00	20	8.03	3.63	86
Sucrose	24.76	4.00	20	7.95	3.59	86
Inulin	25.14	4.00	20	7.83	3.54	67
Kraft Lignin	25.16	4.00	20	7.82	3.54	59
Corncob	24.97	4.00	20	7.88	3.56	75
Demin. Corncob	24.85	4.00	20	7.92	3.58	76
BD[f] corncob	25.44	4.00	20	7.73	3.50	61
BD sucrose	25.61	4.00	20	7.68	3.48	65
PD[g] sucrose	25.11	4.00	20	7.84	3.54	68
Syn. Graphite	26.38	0.53	255	0.98	3.38	100

[a] fwhm: full width at the half maximum peak height of reflection (002). [b] τ: crystallite size. [c] ε: lattice strain. [d] d(002): distance between crystallite planes in the 002 direction. [e] γ_a: estimated aromaticity (refer to ref. [18]). [f] Boron-doped. [g] Phosphorus doped.

Data shown in Table 5.2 reinforces what is previously noted in Figure 5.2; all carbons appear to have similar crystal properties, in particular when analyzing the (002) reflection. As expected from broad diffractogram peaks the crystallite sizes recognized in heat treated biocarbons are significantly smaller in comparison to synthetic graphite, ca. 20 and 255 Å respectively. The percentage lattice strain for heat treated biocarbons is also greater compared to synthetic graphite (~8% and ~1% respectively), which may account for the shift in (002) peak position. The distance between graphitic planes in the (002) direction for heat treated carbons does not significantly vary from carbon to carbon, however the spacing noted in heat treated biocarbons is notably greater than the spacing determined for synthetic graphite, 3.55 ± 0.04 Å and 3.38 Å respectively. It is also remarked that a significant decrease in interlayer spacing is not observed for doped carbons compared to untreated carbons derived from analogous feedstocks. Thus it appears that reduced electrical resistivities associated with doped carbons is not a result of enhanced graphitizibility, but due rather to the possible increase in positive hole movement and suppressed carbon oxidation. In addition previous XRD evidence associated with carbons derived from macadamia nutshell indicated the presence of graphitic domains only 2 or three layers thick in the (002) direction[14]. Table 5.2 also illustrates estimated aromaticity values for respective carbons. The average estimated aromaticity value associated with heat treated biocarbons equates to 71 ± 10%. Obtained aromaticity values are somewhat lower than previously calculated values, which approach 99%[14], and appear more consistent with values obtained from heat treated (1200 °C) coals, 75 – 82%[18]. It is important to note that the degree of aromaticity is dependent upon the contribution from the γ band. It was noted that at times it was difficult to resolve the γ band using the X'Pert HighScore software due to some biocarbons offering more symmetrical (002) peaks than others.

In summary, these results show that the graphitic regions in carbonized charcoal are comparable in size to the carbon's micropores. There is no evidence to suggest that carbonized charcoal contains an extensive network of graphene sheets. This differs from the HRTEM findings reported by Baliaga *et al*[19] which appear to indicate extensive graphene sheet development in a char derived from pectin heat treated at 800 °C.

5.3 ^{13}C Cross-Polarization Magic-Angle Spinning Nuclear Magnetic Resonance (^{13}C CPMAS NMR)

NMR measurements were performed on a Bruker DRX 200 spectrometer equipped with a 7 mm doubly tuned (H/X) solids probe and ZrO rotors with Teflon caps. ^{13}C spectra were obtained at ~35 kHz decoupling field. A 5 µs ^{1}H prep pulse, 2.5 second recycle delay and 5 ms contact time were employed for all charcoals and carbons. Figures 5.5 (a-d) illustrate the outcome of various NMR experiments.

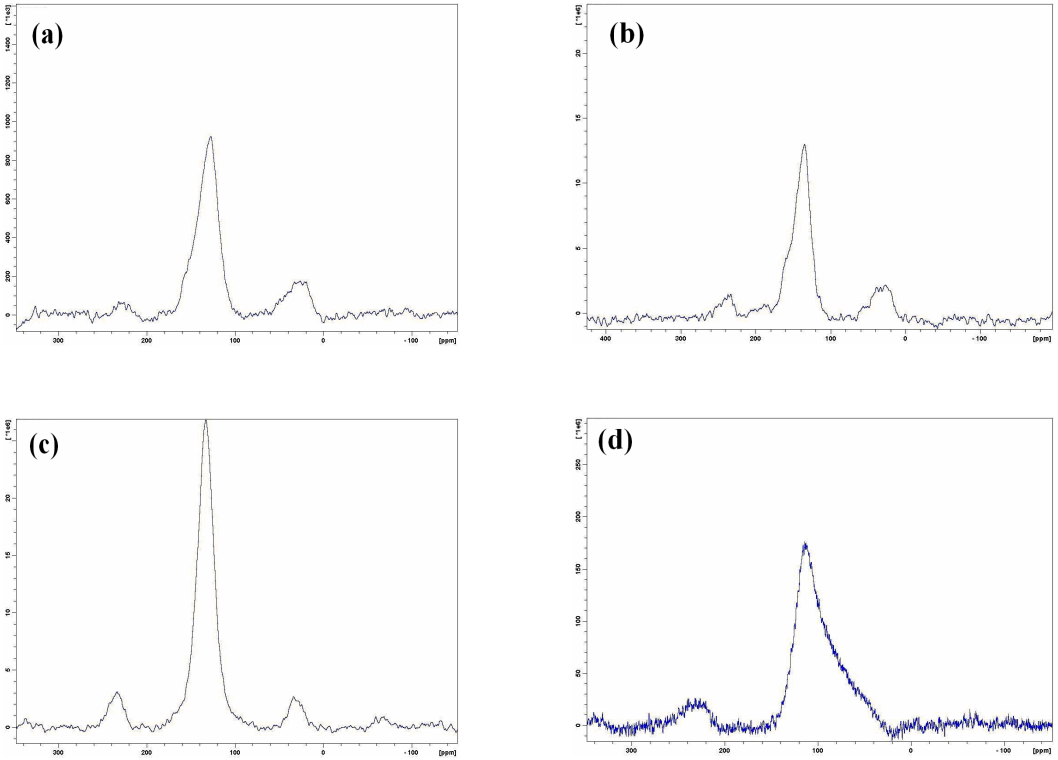

Figure 5.5: *NMR Spectra of Select Biocarbons. (a) <212 µm 'Middle' 020704 corncob charcoal (HP decoupled). (b) <212 µm 'Middle' 020704 corncob charcoal. (c) Carbonized (750 °C) <212 µm 'Middle' 020704 corncob charcoal. (d) Carbonized (950 °C) <212 µm 'Middle' 020704 corncob charcoal.*

All NMR spectra show a broad peak centered at a chemical shift of between 120 and 140 ppm, indicative of conjugated carbon-carbon species and aromatic compounds. In addition all NMR spectra show smaller peaks at approximately ± 100 ppm of the larger more intense peak. These extra signals represent spinning sidebands and are positioned at ± 100 ppm due to spinning at 5 kHz on a 200 MHz instrument. Figure 5.5(a) and (b) both represent ^{13}C NMR spectra resulting from corncob charcoal, however Figure 5.5(a) illustrates a ^{13}C HP decoupled NMR spectra. Comparison of the two spectra types reveals minimal differences in peak shape and position. As a result direct ^{13}C observation was employed for subsequent NMR experiments due to its considerably faster analysis times. The NMR peak shape of corncob charcoal is not completely symmetric having what appears to be a superimposed smaller peak upfield from the predominant aromatic peak. A side peak of this type is typically associated with carboxyl and phenolic carbons. The assymetric NMR peak shape associated with corncob charcoal is a not uncommon feature and is comparable to NMR spectra obtained from tabacco, pectin, and lignin chars which have been subjected to similar HTT's[20-22]. The NMR spectra representing corncob charcoal carbonized at a HTT of 750 °C (Fig. 37(c)) appears to have a more intense symmetrical aromatic peak compared to flash carbonized corncob charcoal. This may be interpreted as a loss of oxygen functionality with increasing carbonization temperature via dehydration, decarbonylation, and decarboxylation reactions, resulting in condensation and aromatic growth. Note that numerous studies utilizing ^{13}C NMR have investigated the change in coal structure progressing from low rank coals (peat) to high rank coals (bituminous and anthracite)[23-25]. In general a collapse of sharp peaks into broad, less-resolved peaks is observed with increasing coal rank. An anthracite coal sample (19 'Lockatong stem[23]) displays a very similar ^{13}C NMR spectrum compared with FC corncob charcoal, i.e. a single broad aromatic peak centered at 125 ppm. It is interesting to note that the anthracite coal has an increased H/C ratio relative to FC corncob charcoal (0.4 compared to 0.04) but has a reduced O/C ratio (0.03 compared to 0.15). The NMR spectrum of a coal sample (14 'Morrison stem') which has a similar H/C and O/C ratio as FC cob charcoal displays an additional broad peak downfield of the prominent aromatic peak (25 ppm). This peak is often associated with paraffinic and methoxy carbon. Therefore it appears

that FC corncob of moderate VM content (~16.2%) has a greater degree of aromaticity compared to coals of similar chemical composition.

Obtaining a good NMR spectrum for corncob charcoal carbonized at 950 °C was more difficult compared to the previous cob chars. The difficulty was related to adjusting the tune and match on the probe. Additional analyses of low VM carbons via NMR were not undertaken due to the fear of arcing and subsequent damage to the probe.

5.4 Thermogravimetry-Mass Spectroscopy (TG-MS)

Thermogravimetry (TG or TGA) is an analytical technique which involves the careful measurement of a substance's mass as a function of temperature whilst the material is subjected to a controlled temperature program. With today's instruments materials can be heated or cooled under alternate atmospheres in the temperature range from -160 to 1600 °C at rates of fractions of a degree per minute up to 100 °C min^{-1}. Typical sample masses exposed to a controlled temperature program range from 10-100 mg, with most instruments offering a high level of accuracy and precision c.a. ±1% in the microgram range. It is remarked that TG has the ability to offer a large amount of meaningful data however it is subject to a number of experimental variables and thus requires considerable care during interpretation[26]. Thermogravimetric data is usually displayed as a plot of the mass against time or temperature. Alternatively changes in mass can be presented as the derivative thermogravimetric curve (DTG) which has the additional benefit of being able to display subtle changes in mass which are sometimes barely discernible on a TG curve[26]. When TG is coupled with mass spectrometry it becomes a remarkable tool for investigating and identifying chemical compositions of unknown materials. With knowledge of evolved compounds and associated mass losses a skilful chemist can make some good guesses as to the material's original chemical composition and structure.

Thermogravimetry experiments were carried out at the Hungarian Academy of Sciences and involved the collective input of the following authors: Gábor Várhegyi, Erika Mészáros, Emma Jakab, and Michael Jerry Antal.

The TG-MS system employed consisted of a Perkin Elmer TGS-2 thermobalance coupled to a Hiden HAL 301 F/PIC quadrupole mass spectrometer via a heated capillary transfer line. A combustion kinetics study (refer to section 7.2.6) and a structural elucidation study was performed. A number of alternate carbonized charcoals were investigated using TG-MS with the aim of answering the question "Do all carbonized charcoals have the same chemical structure?". In this investigation measurements were carried out using argon purge gas with a flow rate of 140 mL/min^{-1}. Sample masses employed throughout the investigation were somewhat dependent on the VM content of the respective charcoals, and hence ranged between 7 – 17 mg. Charcoal samples were heated from 20 °C to 1000 °C at a heating rate of 20 °C min^{-1} in a platinum sample pan. The mass spectrometer was operated in electron impact ionization mode at 70 eV, with ion intensities normalized to both sample mass and to the intensity of the ^{38}Ar isotope carrier gas[27].

The TG-MS study associated with elucidating structure related information from carbonized charcoals initially involved principal component analysis (PCA). PCA is a useful tool for differentiating similarities and differences in the thermal behavior of charcoals. The principle component score plot illustrated as Figure 5.6 simply indicates that the VM content of a charcoal is a key determinant of its thermal properties as quantified by TG-MS. Charcoals of high VM content, oak wood and middle corncob charcoal (27% and 24% respectively), exhibit similar thermal behavior. Another separate group are the collection of charcoals which posses low VM contents (4.3 – 5 wt%). Charcoals with intermediate VM contents (9 – 12%) are positioned nearby but in the general direction of the high VM charcoals.

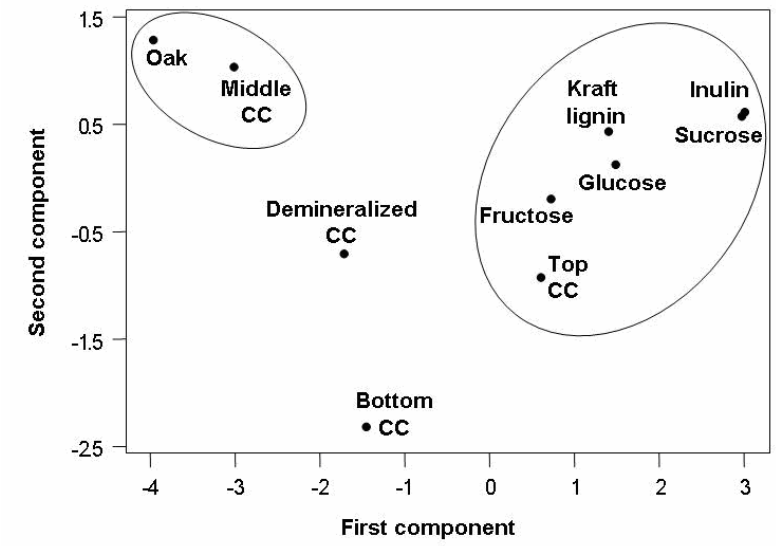

Figure 5.6: *Principal Component Score Plot of Alternate Derived Feedstock Biocarbons.*

After PCA analysis, TG/DTG data was examined on an individual charcoal type basis, combined plots of high VM charcoals (a) and low VM charcoals (b) are displayed in Fig. 5.7:

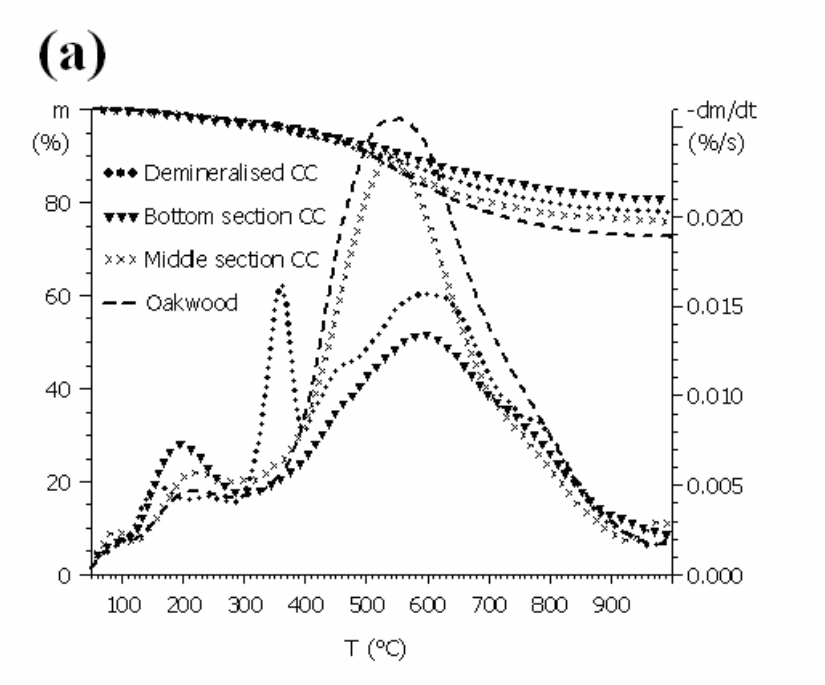

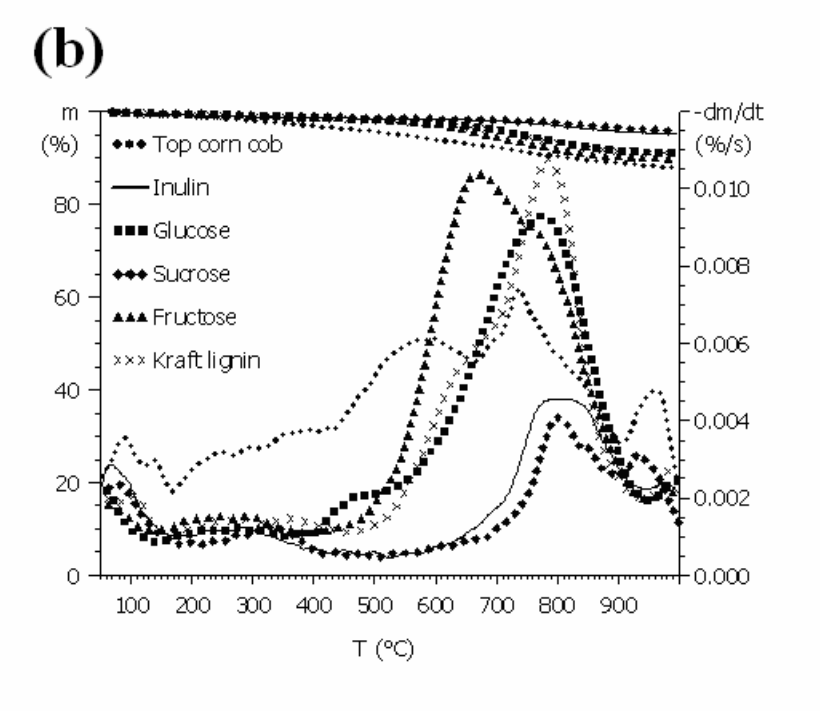

Figure 5.7: *TG and DTG Curves of High VM (a) and Low VM (b) Charcoals.*

The major decomposition peak associated with high VM charcoals occurs between temperatures 500 - 600 °C, whereas the major decomposition peak associated with low VM charcoals is significantly higher ca. 750 - 800 °C. The fructose charcoal is noted as decomposing over a broader temperature range (500 - 950 °C). It is also remarked that the low VM cob charcoal appears to behave in a different manner compared to the other low VM biocarbons. Decomposition products of the various charcoals were also monitored using mass spectrometry. Evolution profiles of both high (Fig. 5.8 (a)-(d)) and low VM charcoals (Fig. 5.8 (e)-(j)) are displayed below:

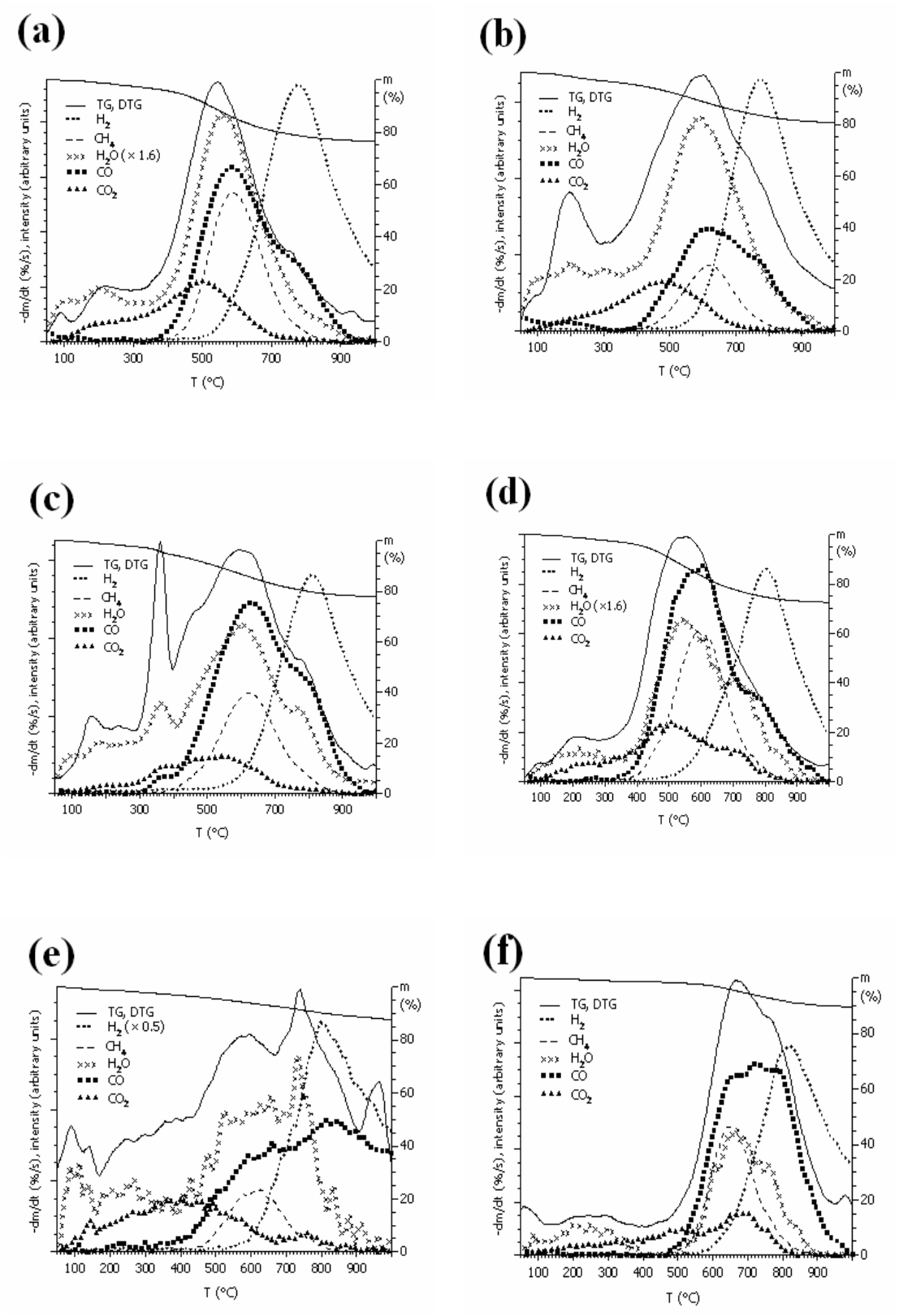
(a)
TG, DTG
H2
CH4
H2O (×1.6)
CO
CO2
-dm/dt (%/s), intensity (arbitrary units)
m (%)
T (°C)
(b)
TG, DTG
H2
CH4
H2O
CO
CO2
-dm/dt (%/s), intensity (arbitrary units)
m (%)
T (°C)
(c)
TG, DTG
H2
CH4
H2O
CO
CO2
-dm/dt (%/s), intensity (arbitrary units)
m (%)
T (°C)
(d)
TG, DTG
H2
CH4
H2O (×1.6)
CO
CO2
-dm/dt (%/s), intensity (arbitrary units)
m (%)
T (°C)
(e)
TG, DTG
H2 (×0.5)
CH4
H2O
CO
CO2
-dm/dt (%/s), intensity (arbitrary units)
m (%)
T (°C)
(f)
TG, DTG
H2
CH4
H2O
CO
CO2
-dm/dt (%/s), intensity (arbitrary units)
m (%)
T (°C)

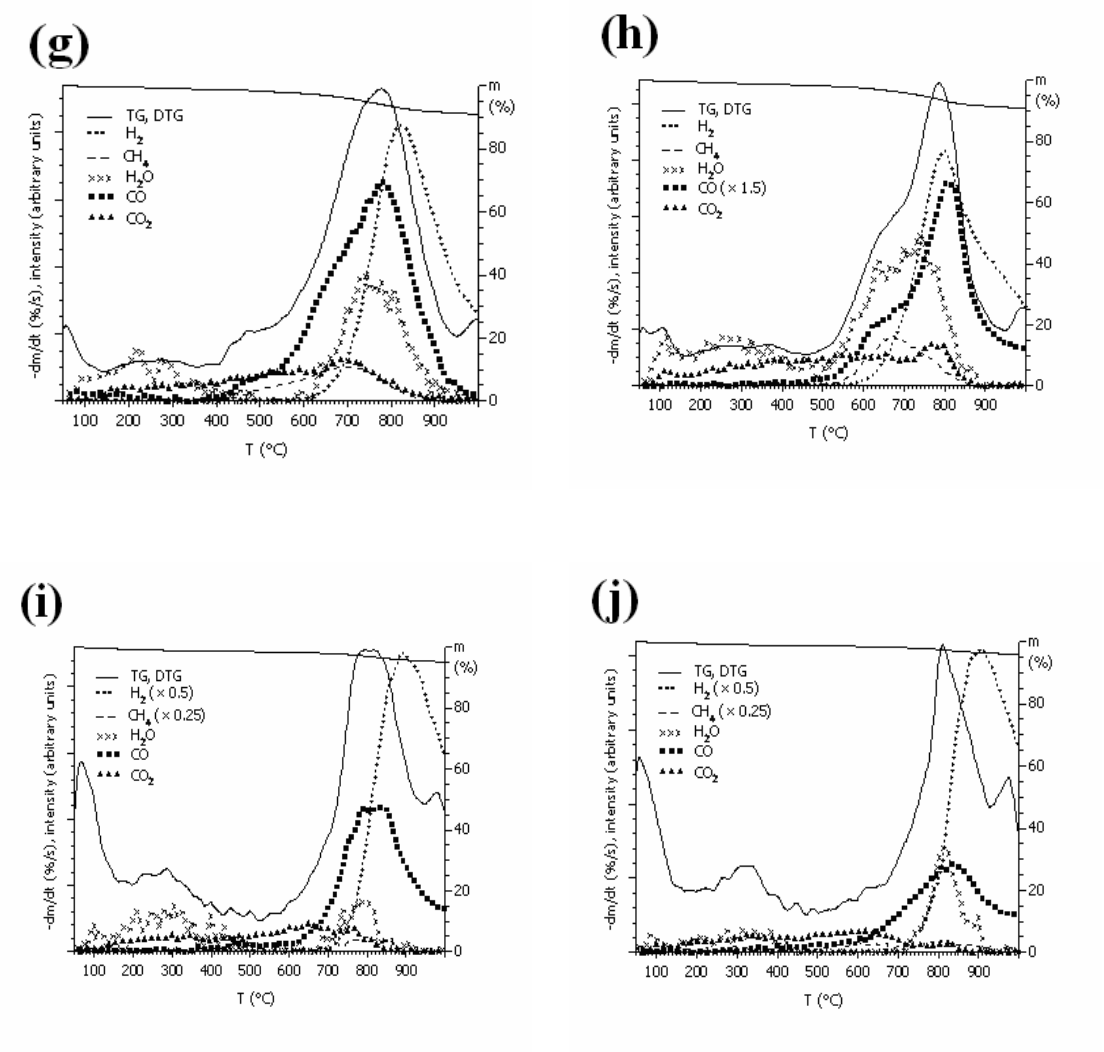

Figure 5.8: *TG, DTG Curves and Evolution Profiles of the Main Volatile Products Formed from Select Biocarbons. Middle section corncob (a), bottom section corncob (b), demineralized corncob (c), oak wood charcoal (d), top section corncob (e) fructose (f), α-D-glucose (g), Kraft lignin (h), inulin (i), and (j) sucrose charcoal.*

The products that evolved from all charcoals included hydrogen, methane, water, carbon monoxide, and carbon dioxide. Low temperature thermal decomposition of all charcoals involved the evolution of mainly water and carbon dioxide. It is important to note that the initial evolution of water and carbon dioxide may be the result of chemisorbed or physisorbed species. High VM charcoals once exposed to temperatures in excess of 300 °C begin to evolve gases carbon monoxide and methane. At temperatures above 500 °C the evolution of hydrogen gas begins.

Concerning the low VM charcoals, the temperature range for which products can be detected is similar to the high VM charcoals however the initiation of hydrogen evolution in low VM chars occurs at a somewhat increased temperature. Other evolved chemical species were also detected upon thermal decomposition of high VM charcoals. Aliphatic fragments including $C_2H_3^+$ were detected in both oak wood charcoal and middle section corncob charcoal. In addition CH_3CO fragments and HCHO were detected suggesting the presence of aldehydes and other oxygen containing compounds. Evolved aromatic compounds released in the same temperature range include toluene and phenol, whereas benzene was noted to evolve at higher temperatures. At temperatures below 400 °C various other evolved compounds were detected with respect to the sample of demineralized corncob charcoal. A sharp peak was noted at approximately 150 °C and is associated with methyl acetate, a pyrolytic remnant of the citric acid wash. The peak noted at 360 °C represents oxygenated furan compounds and their derivatives. TG-MS evidence thus far indicates that charcoals of varying VM content are indeed structurally different. In addition subtle variations in the concentration of evolved products, specifically CO, indicate the possibility of further structural differences between heat treated charcoals. As remarked in previous sections charcoals derived from D-glucose, D-fructose, sucrose, inulin, and Kraft lignin proceed through a distinct liquid phase during pyrolysis. Yet despite this similarity it was observed that inulin, sucrose, and Kraft lignin derived charcoals continue to evolve carbon monoxide at high temperatures (>1000 °C), distinct from glucose and fructose derived charcoals. At a temperature in excess of 800 °C biocarbons derived from corncob and oak wood which do not proceed through a distinct liquid phase during pyrolysis, behave in a near identical manner as the melt charcoals. However, only the untreated corncob charcoal's, and in particular the 'top' corncob charcoal sample, continue to evolve carbon monoxide at a temperature greater than 1000 °C. Evidence from ash analysis suggests there is a correlation between the ash content of a biocarbon and its propensity to persistently emit CO at higher temperatures. There are two exceptions: the demineralized corncob and oak wood carbons[27].

5.5 Matrix Assisted Laser Desorption Ionization Time of Flight Mass Spectrometry (MALDI-TOF MS)

Laser desorption ionization (LDI) was first introduced in the 1960's to generate ions in mass spectrometers. Traditionally mass spectroscopic techniques have been limited to investigations involving low molecular weight species however, with the development of matrix-assisted LDI high molecular weight molecules and polymers have become amenable to analysis (e.g. polystyrene with masses of 1,500,000 amu[5]). This development has since lead to an explosive growth in popularity for MALDI[28, 29]. Upon pulsed laser irradiation a dense cloud of analyte, matrix, and excited matrix molecules is formed, which expands supersonically into a vacuum. Irradiation in this way enables efficient and controllable energy transfer which safeguards analyte molecules of interest from thermal decomposition. MALDI is hence classified as a 'soft' ionization technique and has the major advantage of producing primarily singly charged ions. Depending on the polarity chosen for the extraction field both singly charged positive or negative ions are observed, however regardless of whether the original species was singly or multiply charged the magnitude is always ± 1[28, 29]. Correct choice of the matrix is considered crucial for obtaining reliable MALDI mass spectra. With regard to analyzing insoluble carbonaceous materials the matrix compound 7,7,8,8-tetracyanoquinodimethane (TCNQ) has seen some success[30, 31]. A solvent free sample preparation technique involving mechanical homogenization of the analyte and matrix is utilized as an alternative to co-crystallization due to the high insolubility of carbonaceous materials[30, 31]. MALDI MS has also been used to successfully identify fullerenes. In this case a matrix is typically not necessary with simple dissolution in toluene being suitable.

Recently Šedo *et al*[32] carried out a study involving the laser desorption-ionization of numerous carbon forms; graphite, synthetic diamond, carbon nanotubes, and glassy carbon[6]. It was recognized that in positive linear mode, after exceeding a material

[5] Atomic Mass Unit (amu)

[6] Glassy carbon produced via the thermal degradation of cross-linked resins at 2200 °C.

dependent threshold laser power, singly charged carbon clusters $[C_n]^+$ with n = 1-31 were formed. Increase in the laser power above a second threshold value resulted in the formation of an additional set of very heavy odd-numbered carbon clusters. Laser desorption-ionization in negative linear mode afforded only one cluster ion family ($[C_n]^-$) whereby n = 1-19. Post source decay (PSD) techniques and the reflectron were also utilized to eliminate the possibility that carbon materials studied contained stable fullerene structures. PSD of carbon clusters examined resulted in the loss of neutral C_3 molecules, whereas PSD of fullerene afforded the expected loss of neutral C_2 particles.

Mass spectra were measured on a Bruker Autoflex II MALDI-TOF/TOF mass spectrometer equipped with a nitrogen laser (λ = 337 nm) operating at a frequency of 16.7 Hz. Generated ions were accelerated at 20 kV and the detector voltage was 1.5 kV. In order to avoid detector saturation, ions less than or equal to 40 Da were suppressed. A pulsed ion extraction rate of 100 ns was employed for enhanced spectral resolution. Biocarbon samples were suspended in toluene and subsequently spotted onto a polished steel target plate. Spectra were acquired in both linear and reflectron mode and in both positive and negative mode. The mass spectrometer was calibrated prior to measurement using a fullerene (C_{60}) standard. A minimum of 300 shots were summed. Precursor ions collected for LIFT application were accelerated to 6 kV and selected in a timed ion gate. In the LIFT-cell the fragments were further accelerated to 19 kV. The reflector potential was 23.5 kV.

In this laboratory synthetic graphite analyzed in positive linear mode (35% laser power) afforded analogous low *m/z* carbon clusters noted by Šedo *et al* ($[C_n]^+$ where n = 1-27) (refer to Fig. 5.8a), however despite raising the laser power to significant levels (70%), carbon cluster sets greater than C_{36} were not observed. Spectra resulting from positive linear mode analyses of biocarbon materials differed from those obtained from synthetic graphite since they contained no cluster series at low laser power but instead afforded discrete ions (see Fig. 5.8b-c). Spectra associated with biocarbons evolved with laser power; at 25% the ion *m/z* 701 predominates, a peak in this region is noted and dismissed as contaminant by Šedo *et al*; at 28% *m/z* ions 317, 429, 453, and 465 appeared and intensified with increasing laser power;

finally at laser powers ≥ 40% low *m/z* carbon clusters were observed. In addition to the predominant ion *m/z* 701, laser desorption-ionization of the melt biocarbons also afforded ion *m/z* 685. This may be interpreted as the difference of an oxygen atom. Positive linear mode analysis of biocarbon materials and synthetic graphite resulted in no *m/z* 720 ion indicative of C_{60} fullerene. Furthermore the LIFT spectrum associated with standard C_{60} differed significantly from any prominent biocarbon peaks analyzed (*m/z* 701, 685); neutral C_2 particles were lost compared to the preferred loss of neutral C_3 molecules observed for biocarbon ions.

In agreement to the results obtained by Šedo *et al*, negative linear mode analyses of biocarbon materials afforded only one carbon cluster family, ($[C_n]^-$ where n = 1-14). However like positive mode analysis additional ions of discrete stability were apparent, of which ions 205 and 473 dominate (see Fig. 5.8d). During MALDI analysis of biocarbons it was noted that the polished target plate became contaminated with char related ions. Contamination of the target plate got progressively worse with increased use and was more noticeable in negative mode.

These results indicate distinct structural differences between biocarbons and synthetic graphite. Biocarbons appear to contain structures of distinct stability which are readily desorbed as ions. One very likely reason for the ease of desorption may be the presence of readily protonated covalently bonded oxygen atoms throughout the highly carbonaceous material. The presence of low *m/z* carbon clusters associated with biocarbons at high laser power may be indicative of microcrystalline graphite, adding further weight to the XRD evidence.

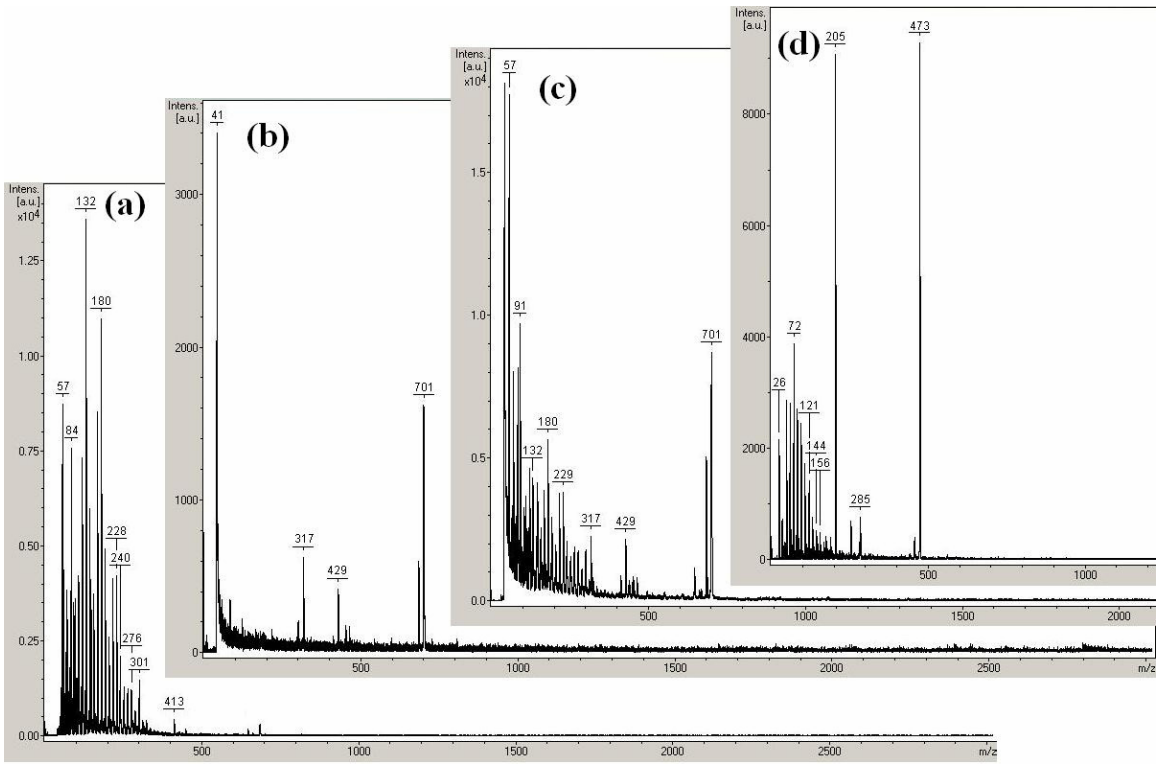

Figure 5.9: *Linear Mode MALDI-TOF MS of Select Biocarbons. (a) positive mode 35% laser power synthetic graphite. (b) positive mode 30% laser power D-fructose carbon. (c) positive mode 45% laser power D-fructose carbon. (d) negative mode 35% laser power inulin carbon.*

In summary, these results show that biocarbons contain no fullerene structures. Instead biocarbons contain structures that readily desorb ions with *m/z* values of 701, 685, 465, 453, 429, and 317. The MALDI-TOF spectra of biocarbons have little in common with that of graphite. A model of the structure of carbonized charcoal should be consistent with these MALDI-TOF spectra.

5.6 Elemental Analyses of Select Carbons

As in section 4.2 elemental analysis of select carbons was measured by Huffman Laboratories, Inc. Table 5.3 illustrates the results.

Table 5.3: Elemental Analyses of Select Carbons (dry-basis), Measured by Huffman Laboratories, Inc., USA

	C (wt %)	H (wt %)	O (wt %)	N (wt %)	S (wt %)	ash (wt %)
Oak wood	96.19	0.65	1.54	0.20	<0.05	1.02
Middle CC	94.01	0.71	1.92	0.56	<0.05	2.67
Bottom CC	92.92	0.64	2.19	0.64	<0.05	3.47
Top CC	92.99	0.72	2.25	0.54	0.06	3.11
Fructose	96.62	0.75	2.24	0.13	<0.05	0.15
Kraft lignin	91.31	0.68	4.62	0.51	1.44	3.70
Glucose	96.33	0.74	2.53	0.11	<0.05	0.17
Inulin	96.10	0.71	2.61	0.13	<0.05	0.42
Sucrose	96.70	0.76	2.17	0.12	<0.05	0.04

With the exception of Kraft lignin results shown in Table 5.3 all prepared carbons are sulfur poor. In addition all carbons appear to contain low amounts of the elements nitrogen and hydrogen. The percentage ash results show carbons derived from D-fructose, D-glucose, and sucrose to be very pure, moreover the prepared carbons contain between 1.5 and 4.6 wt.% oxygen and are exceedingly carbon rich. Elemental results in combination with detected ions observed from MALDI analyses afford the opportunity for some educated guesses to be made as to the possible atomic structures present in carbons. Discussion of putative structures is offered in the following section.

1. Wertz, J. E.; Bolton, J. R., *Electron Spin Resonance - Elementary Theory and Practical Applications*. McGraw-Hill Inc.: 1986; p 481.

2. Singer, L. S., A Review of Electron Spin Resonance in Carbonaceous Materials. *Fifth Carbon Conference* **1961,** 2, 37-64.

3. Mrozowski, S., Further Studies of Electron Spin Resonance in Chars, Carbons, and Graphites. *Fifth Carbon Conference* **1962,** 2, 79-88.

4. Singer, L. S.; Wagoner, G., Electron Spin Resonance in High-Temperature Carbons and Graphites*. *Fifth Carbon Conference* **1961,** 2, 63-71.

5. Urbanski, T.; Benbenek, S.; Bedynski, S.; Wasilewski, A., Free Radicals in Charcoal and the Combustion of Compositions Containing Charcoal. *Explosivstoffe* **1970**.

6. Zheng, S.; Feng, J.-W.; Maciel, G. E., In Situ High-Temperature EPR Investigation of the Charring of Tobacco and the O_2-Induced and H_2O-Induced Behavior of the Char. *Energy & Fuels* **2005,** 19, 2247-2253.

7. Asada, T.; Ishihara, S.; Yamane, T.; Toba, A.; Yamada, A.; Oikawa, K., Science of Bamboo Charcoal: Study on Carbonizing Temperature of Bamboo Charcoal and Removal Capability of Harmful Gases. *Journal of Health Science* **2002,** 48, (6), 473-479.

8. Jordan, B. F.; Baudelet, C.; Gallez, B., Carbon-Centered Radicals as Oxygen Sensors for in Vivo Electron Paramagnetic Resonance: Screening for an Optimal Probe Among Commercially Available Charcoals. *Magnetic Resonance Materials in Physics, Biology and Medicine* **1998,** 7, 121-129.

9. Dunne, L. J.; Sarkar, A. K.; Kroto, H. W.; Munn, J.; Kathirgamanathan, P.; Heinen, U.; Fernandez, J.; Hare, J.; Reid, D. G.; Clark, A. D., Electrical, Magnetic and Structural Characterization of Fullerene Soots. *J. Phys.: Condens. Matter* **1996,** 8, 2127-2141.

10. *McGraw-Hill Encyclopedia of Science and Technology*. 8th ed.; McGraw-Hill: 1997; Vol. 19.

11. Randall, J. T., *The Diffraction of X-Rays and Electrons by Amorphous Solids, Liquids, and Gases*. John Wiley & Sons, Inc.: 1934.

12. Franklin, R. E., The Structure of Graphitic Carbons. *Acta Cryst.* **1951,** 4, 253.

13. P. L. Walker, J.; Seeley, S. B., Fine Grinding of Ceylon Natural Graphite. *Proceedings of the Third Biennial Carbon Conference* **1957**, 481-494.

14. Mochidzuki, K.; Soutric, F.; Tadokoro, K.; M. J. Antal, J.; Tóth, M.; Zelei, B.; Várhegyi, G., Electrical and Physical Properties of Carbonized Charcoals. *Ind. Eng. Chem. Res.* **2003,** 42, 5140-5151.

15. Jenkins, R.; Synder, R. L., *Introduction to X-ray Powder Diffractometry*. John Wiley & Sons Inc.: 1996; Vol. 138, p 403.

16. Pfeifer, P.; Ehrburger-Dolle, F.; Rieker, T. P.; Gonzalez, M. T.; Fofman, W. P.; Molina-Sabio, M.; Rogriguez-Reinoso, F.; Schmidt, P. W.; Voss, D. J., Nearly Space-Filling Fractal Networks of Carbon Nanopores. *Phys. Rev. Lett.* **2002,** 88, (115502).

17. Pierson, H. O., *Handbook of Carbon, Graphite, Diamond and Fullerenes - Properties, Processing and Applications*. William Andrew Publishing/Notes: 1994.

18. Lu, L.; Sahajwalla, V.; Harris, D., Characteristics of Chars Prepared from Various Pulverized Coals at Different Temperatures Using Drop-Tube Furnace. *Energy & Fuels* **2000,** 14, 869 - 876.

19. Baliga, V.; Sharma, R.; Miser, D.; McGrath, T.; Hajaligol, M., Physical Characterization of Pyrolyzed Tobacco and Tobacco Components. *J. Anal. Appl. Pyrolysis* **2003,** 66, 191-215.

20. Sharma, R. K.; Wooten, J. B.; Baliga, V. L.; Lin, X.; Chan, W. G.; Hajaligol, M. R., Characterization of Chars from Pyrolysis of Lignin. *Fuel* **2004,** 83, 1469-1482.

21. Sharma, R. K.; Wooten, J. B.; Baliga, V. L.; Martoglio-Smith, P. A.; Hajaligol, M. R., Characterization of Char from the Pyrolysis of Tabacco. *J. Agric. Food. Chem.* **2002,** 50, 771-783.

22. Sharma, R. K.; Wooten, J. B.; Baliga, V. L.; Hajaligol, M. R., Characterization of Chars from Biomass-Derived Materials: Pectin Chars. *Fuel* **2001,** 80, 1825-1836.

23. Hatcher, P. G., Dipolar-Dephasing ^{13}C NMR Studies of Decomposed Wood and Coalified Xylem Tissue: Evidence of Chemical Structural Changes Associated with Defunctionalization of Lignin Structural Units during Coalification. *Energy & Fuels* **1988,** 2, (1), 48-58.

24. Wind, R. A.; Duijvestijn, M. J.; Lugt, C. v. d.; Smidt, J.; Vriend, H., An Investigation of Coal by Means of ESR, ^{1}H NMR, ^{13}C NMR and Dynamic Nuclear Polarization. *Fuel* **1987,** 66, 876-885.

25. Orem, W. H.; Finkelman, R. B., Coal Formation and Geochemistry. *Treatise on Geochemistry* 7, 191-222.

26. Meyers, R. A., *Encyclopedia of Analytical Chemistry - Applications, Theory and Instrumentation*. John Wiley & Sons, Ltd.: 2000; Vol. 15.

27. Mészáros, E.; Jakab, E.; Várhegyi, G.; Bourke, J.; M. J. Antal, J., Do All Carbonized Charcoals Have The Same Chemical Structure? *Tentative Reference* **2007**.

28. Pasch, H.; Schrepp, W., *MALDI-TOF Mass Spectrometry of Synthetic Polymers*. Springer: 2003; p 298.

29. Henderson, W.; ndoe, J. S. M., *Mass Spectrometry of Inorganic and Organometallic Compounds - Tools - Techniques - Tips*. John Wiley & Sons, Ltd: 2005.

30. Edwards, W. F.; Jin, L.; Thies, M. C., MALDI-TOF Mass Spectrometry: Obtaining Reliable Mass Spectra for Insoluble Carbonaceous Pitches. *Carbon* **2003,** 41, 2761-2768.

31. Przybilla, L.; Brand, J. D.; Yoshimura, K.; Räder, H. J.; Mullen, K., MALDI-TOF Mass Spectrometry of Insoluble Giant Polycyclic Aromatic Hydrocarbons by a New Method of Sample Preparation. *Anal. Chem* **2000,** 72, 4591-4597.

32. Šedo, O.; Alberti, M.; Janča, J.; Havel, J., Laser Desorption-Ionization Time of Flight Mass Spectrometry of Various Carbon Materials. *Carbon* **2006,** 44, 840-847.

6.0 A Model of the Structure of Carbonized Charcoal

From the numerous analytical techniques employed in this work, a number of insights are obtained about the possible chemical structure of biocarbons. We know from surface area measurements that carbonized charcoals are microporous, containing pores with half pore widths of between 3 and 10 Å. Therefore our proposed model has to account for these pores and their subsequent contribution to surface area. One way to account for the presence of micropores is to acknowledge the possibility of voids within hexagonal planes, (see Fig. 6.1(b)-(d)). The presence of holes within condensed hexagonal planes would also create positions for free radicals and dangling bonds which would subsequently contribute to the well known chemisorption property noted in biocarbons. In addition the packing of disorganized small graphitic and non-graphitic particles would allow for numerous atomic size interstices to be formed. Techniques including electrical resistivity, XRD, and NMR all indicate that carbonized charcoals are comprised of highly conjugated aromatic compounds. XRD further indicates that up to 71% of the heat treated carbon material is made up of microcrystalline graphite (Fig. 6.1 (a)). It is known that carbon compounds which contain five-membered rings, such as fullerene, decompose to structures composed of more thermodynamically stable six membered rings. Therefore the proposed model should contain microcrystalline graphite up to at least 71%, interspersed with non-graphitic condensed six membered rings. Note that the included microcrystalline graphite contains only three layers which is consistent with alternate XRD analysis. However, the model must account for the significant amount of oxygen detected in our carbonized charcoals. Results obtained from MALDI analyses indicate the presence of readily-formed ions, the most dominant of which include *m/z* 701, 685, 429, and 317. Putative structures of such ions are presented in Fig. 6.1 (b)-(g).

(a)

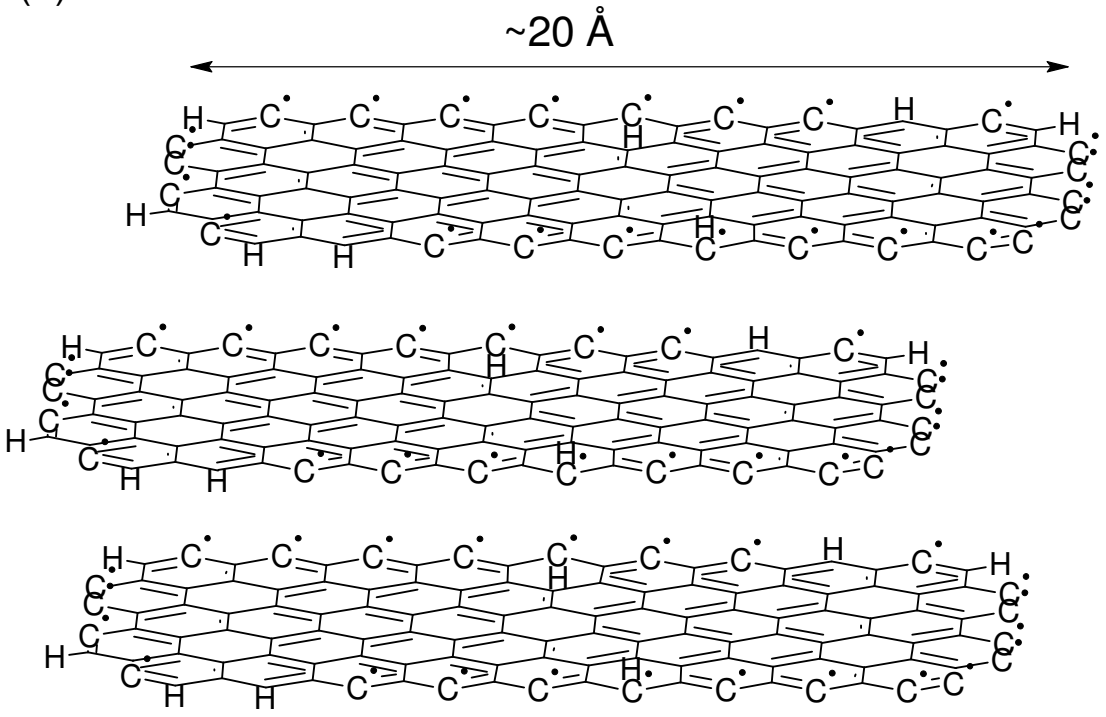

Microcrystalline Graphite
Composition = C(99.45%) H(0.55%)

(b)

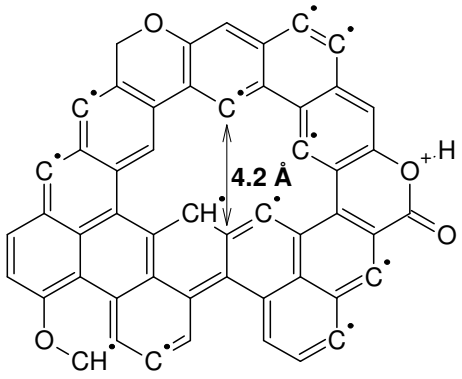

Molecular Formula = $C_{52}H_{13}O_4$
Formula Weight = 701.657
Composition = C(89.01%) H(1.87%) O(9.12%)

(c)

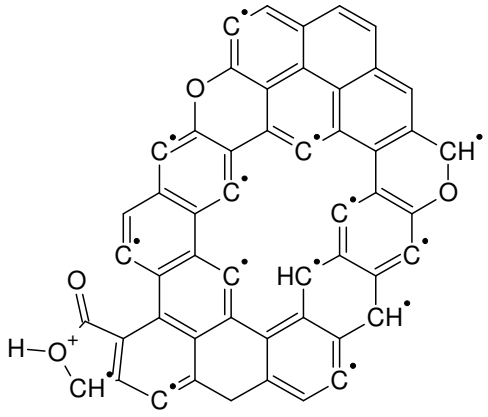

Molecular Formula = $C_{52}H_{13}O_4$
Formula Weight = 701.657
Composition = C(89.01%) H(1.87%) O(9.12%)

(d)

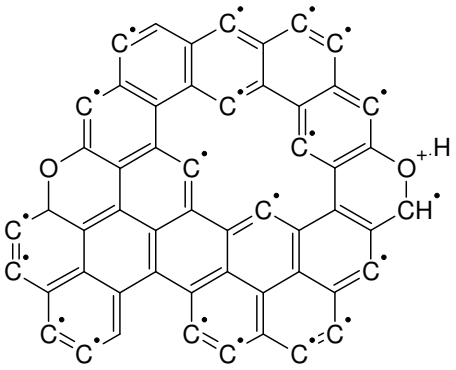

Molecular Formula = $C_{54}H_5O_2$
Formula Weight = 685.616
Composition = C(94.60%) H(0.74%) O(4.67%)

(e)

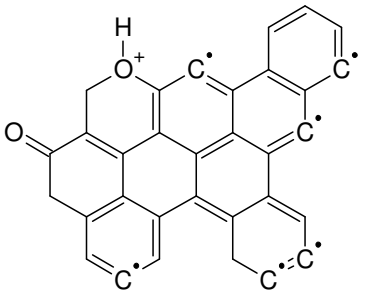

Molecular Formula = $C_{32}H_{13}O_2$
Formula Weight = 429.444
Composition = C(89.50%) H(3.05%) O(7.45%)

(f)

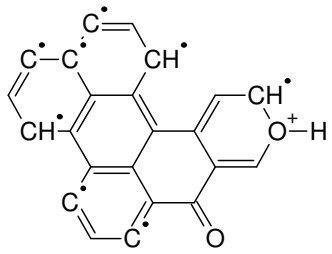

Molecular Formula = $C_{23}H_9O_2$
Formula Weight = 317.316
Composition = C(87.06%) H(2.86%) O(10.08%)

(g)

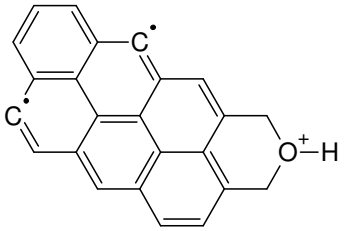

Molecular Formula = $C_{24}H_{13}O$
Formula Weight = 317.359
Composition = C(90.83%) H(4.13%) O(5.04%)

Figure 6.1: *Putative Carbonaceous Structures Constituting Biocarbons.*

The structures incorporate the presence of carbon radicals at the planar fringes, in addition to pyran, pyrone, and furanone moieties. The elemental compositions of the putative ions differ slightly from the overall elemental analyses of the carbonized charcoals (refer to Table 5.3, section 5.6). However since 71% of heat treated charcoal is composed of microcrystalline graphite subsequent incorporation of this amount of carbon brings the elemental compositions into line with the actual analysis, (Fig. 6.2). Obviously there are many possible ways in which to fuse hexagonal rings together in order to obtain structures which both fit MALDI results and determined elemental compositions; Figure 6.2 is but one representation serving as a basic

skeletal model. Furthermore this model is necessarily incomplete due to a lack of results detailing how the putative ions and microcrystalline graphite relate to each other through covalent or other bonding. As mentioned previously a related thermogravimetric study concluded that there are at least 3 different classes of non-graphitizing biocarbons. The heat treated biocarbon model can therefore be adapted to fit alternate structures of carbons, for instance Kraft lignin carbon. TG-MS work shows this carbon is one which contains significant amounts of sulfur and which persistently evolves CO at high temperatures. Sulfur heteroatoms could be incorporated into smaller carbonaceous particles. Persistent CO evolution could be explained by the presence of highly stable pyrone structures which require high thermal energies before CO and CO_2 is released. Biocarbons that do not persistently evolve CO over temperatures 800-1000 °C may contain thermally less stable carbon-oxygen structures, such as lactones, peroxides, and phenolic groups. The carbonized charcoal model may also be adapted to describe a high VM charcoal. An increased percentage of various oxygenated carbonaceous particles would be present relative to microcrystalline graphite, perhaps consisting of more furanone type structures. Lack of atomic size pores within hexagonal carbon layers as well as blocked pores due to increased VM content would also explain a reduction in surface area.

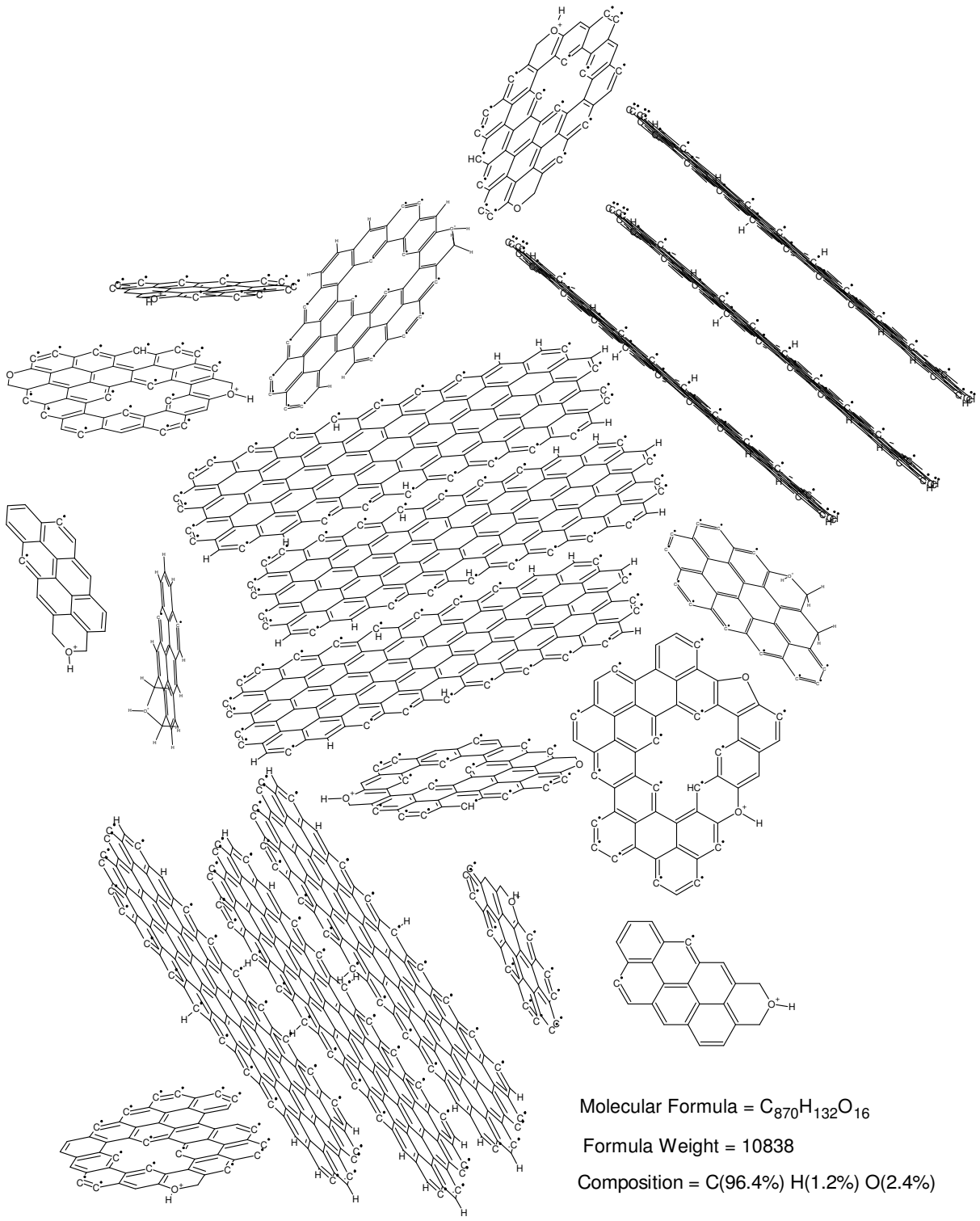

Figure 6.2: *Postulated New Heat Treated Biocarbon Model.*

7.0 Mineral Matter in Biomass and Biomass Charcoal's

7.1 Introduction

In recent years there has been increased attention to the use of biomass fired power boilers for electricity production. It is now well established that inorganic residues resulting from biomass combustion in power boilers cause such noxious effects as fouling, slagging, corrosion, bed agglomeration, and the poisoning of catalysts. These negative effects have hence initiated a great deal of research in the area of biomass demineralization. In addition it is recognized in the metallurgical industry that carbon forms low in ash, in particular low in minerals sulfur and phosphorus, are preferred reductants. Moreover, the demand for silicon, especially high purity silicon is very high. This form of silicon can only be produced using carbon with low impurities. The following chapter is divided into three main areas, the demineralization of corncob biomass and its subsequent charcoal properties, ash migration as a factor of the process of FC, and the effect of doping on heat treated charcoals.

7.2 Extraction of Minerals from Corncob

As mentioned previously in section 3.1 corncob is an abundant cheap renewable resource. In addition, the physical properties of corncob biomass, in particular its porosity, make it an ideal candidate for subsequent demineralization. Samples of corncob feedstock were provided courtesy of Prof. J. Brewbaker and the Waimanalo Research Farm of the University of Hawaii. In an attempt to establish ideal conditions required to remove efficiently and cost effectively inorganic minerals from biomass, various solvents and leaching techniques were trialed.

7.2.1 Hot Water Mineral Extraction of Whole Corncob

This experiment was designed to investigate the removal of inorganic minerals from whole corncob via a hot-water soak. Furthermore, the effect of soak-time on subsequent ash removal was also examined.

Five whole corncobs of similar size and mass were selected for demineralization. One corncob was set aside as a control, whilst the four remaining corncobs were placed into a closed 1 mm ø stainless steel Mesh cage. A large Teflon stir bar was added to the cage as a weight in order to counteract the buoyancy of the corncobs and to therefore ensure complete corncob submersion. A 10 L insulated silica glass wash cylinder was prepared with a given amount of pre-heated tap water (refer to Fig. 7.1). An electrical heating wire wound around the glass wash cylinder was used to heat the system to a controlled temperature of between 90-100 ℃. An adjustable valve located at the base of the wash cylinder was operated to produce a desired flow rate.

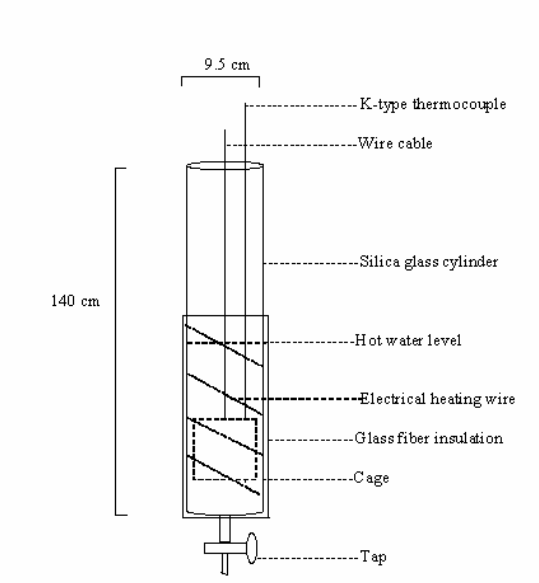

Figure 7.1: *Diagram of Wash Cylinder.*

Once the tap water reached a temperature of between 90 ˚C and 100 ˚C the cage containing the corncob was lowered into the wash cylinder and a stopwatch was initiated. The water temperature was checked every 10 minutes with the aid of a k-

type thermocouple and the lower valve adjusted giving a consistent outlet flow of water. The 'wash' water was measured using a 1 L measuring cylinder before being discarded in an attempt to estimate the volume of heated water used to wash each corncob. Due to water exiting the wash cylinder, the system was continually recharged with similar tempered tap water. A corncob was removed every 2 hours and placed into an oven set at 105 ˚C at atmospheric pressure. The dry corncob samples were subsequently removed from the oven and milled to a particle size of <1.0 mm prior to Total Biomass analysis as per ASTM method E1756-95, and Ash in Biomass analysis as per ASTM method E1755.

Results from this experiment are illustrated in Table 7.1.

Table 7.1: Percentage Ash Content of Whole Corncob after a Hot-Water Wash

Percolation time (minutes)	% ash content[a] (DWB)
0 (control)	1.46
120	2.02
240	1.25
360	1.06
480	0.67

[a] *Dry Basis - ASTM E 1755-95.*

A total of 17 L of 'wash' water was percolated through the corncob bed over a time period of 480 minutes. The percentage ash results obtained from the above experiment indicate that as soak-time and volume of wash water increases the percentage ash content of corncob decreases. However, despite washing a single corncob for eight hours, a significant quantity of inorganic ash still remains bound within the organic structure. Possible reasons for the poor reduction in ash content is primarily attributed to the poor solubility of inorganic mineral deposits and organically bound inorganic minerals, and to the type of bonding existing between inorganic minerals and the organic cob matrix. It is also possible that minerals present in the tap water may enter and non-reversibly bond to the newly ion exchanged cellulosic material.

Various shortcomings pertaining to the method outlined above became apparent throughout the duration of the experiment. It was observed that the volume of water flowing through the cylinder system was difficult to maintain at a constant rate. This lead to inconsistencies in the volume of water used per corncob, and consequently only an estimate of the total volume of 'wash' water used was calculated. It was also observed that the use of different milling equipment (i.e. the bench top Wiley mill and the laboratory blender) produced varying particle sizes. Corncob 1 (control) was milled using the bench top grinder, whereas corncobs 2-5 were milled using the laboratory blender. The laboratory blender had trouble grinding up the hard chaff which consequently led to less coarse chaff being included in the final sample. It was also apparent that the sample size was small and therefore percentage ash results may not be representative of a bulk corncob sample. Biomass is a largely heterogeneous material, and despite corncob 2 showing an increase in percentage ash content relative to the control, it is probable that leaching of minerals did occur, and that the initial percentage ash content of corncob 2 was greater than 2.02%. Experiments hereafter were designed to take into account and mitigate the various shortcomings experienced with this particular experiment.

7.2.2 Hot Deionized Water Mineral Extraction of Whole Corncob

This experiment was designed to investigate whether hot deionized (DI) water was a more effective solvent for removing inorganic minerals from whole corncob. Furthermore, the effect of water volume on ash removal was also considered. The apparatus used for the previous hot-water extraction was also employed for this experiment (refer to Fig. 7.1).

Four corncobs of similar size and mass were selected and allowed to equilibrate in ambient laboratory conditions for twenty four hours prior to being added into a closed 1 mm ø stainless steel Mesh cage. Using a 1 L measuring cylinder, 3 L of previously heated DI water was added to the glass wash cylinder. Once the DI water reached a controlled temperature of between 90 ˚C and 100 ˚C the cage containing the corncob was lowered into the wash cylinder and a stopwatch was initiated. The water temperature was checked every 20 minutes with the aid of a k-type thermocouple. A

corncob was removed from the hot stagnant water every 2 hours and placed into an oven set at 105 ˚C at atmospheric pressure. The dry corncob samples were subsequently removed from the oven and milled to a particle size of <1.0 mm with the aid of both the laboratory blender, and the bench top Wiley mill, prior to Total Biomass analysis as per ASTM method E1756-95, and Ash in Biomass analysis as per ASTM method E1755. The control for this experiment was the same ground cob material utilized in the previous hot-water extraction (7.2.1).

Results from this experiment are illustrated in Table 7.2.

Table 7.2: Percentage Ash Content of Whole Corncob after a Hot 3 L DI Water Soak

Soak-time (minutes)	% ash content[a] (DWB)
0 (control)	2.27
120	1.07
240	0.83
360	0.74
480	0.71

[a] *Dry Basis - ASTM E 1755-95.*

The percentage ash results obtained from the above experiment indicate that as soak-time increases the percentage ash content of corncob decreases. Furthermore, the results also indicate that within the first two hours much of the inorganic mineral matter is removed; the rate of ash removal thereafter continually diminishes as soak-time increases. The experimental outcome also suggests that the volume of solvent used is a less important factor compared to the soak-time. The percentage ash content of the control cob sample is significantly greater than the previously obtained control cob percentage ash value illustrating the non-homogeneity of biomass and possible weaknesses in sample preparation.

Despite washing a single corncob for eight hours, a significant quantity of inorganic ash still remains bound within the cob. Again the primary reason for poor ash

removal was attributed to the low solubility of some specific inorganic species present inside the cob matrix.

7.2.3 Ambient Temperature Citric Acid Mineral Extraction of Whole Corncob

This experiment was designed to investigate whether an ambient temperature citric acid solution was a more effective solvent for removing inorganic minerals from whole corncob compared to hot water treatments. It was anticipated that a more acidic solution would facilitate the removal of inorganic ions from the organic acid components (carboxyl) present in corncob, (refer to Fig. 7.2)

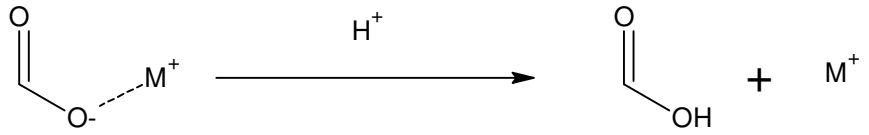

Figure 7.2: *Removal of a Metal Cation Bound to a Carboxylic Group by Means of Acid Hydrolysis.*

Citric acid was selected for three main reasons: 1) it is a known chelator with three functional carboxyl groups which can all donate a pair of electrons to a metal ion forming metal citrates, 2) it is a relatively strong polyprotic acid having low first and second pKA values, and 3) it is an organic acid, therefore any remaining citric acid in the cob structure would not add to mineral impurity amounts during FC.

Four corncobs of similar size and mass were selected and allowed to equilibrate in ambient laboratory conditions for twenty four hours. After the 24-hour period each of the corncobs were weighed using a two decimal electronic balance and physically adjusted to within a gram of each other without destroying the primary structure of the cob. Each corncob was then placed into a separately labeled 300 mL glass Pyrex beaker to which 200 mL of ambient temperature 0.1 $molL^{-1}$ citric acid solution was added. To counteract the cob buoyancy a clean piece of plastic tubing was used to submerge the cob in solution. Every two hours a corncob was removed from solution and washed thoroughly with ambient temperature DI water. To ensure complete

removal of acid a pH meter (Corning 340) was employed to analyze the wash water. Once the wash water pH measured at or above the initial pH value of DI water the cob was subsequently placed into an oven set at 105 ˚C at atmospheric pressure. The dry corncob samples were then removed from the oven, milled, and analyzed for Total Biomass and Ash in Biomass via ASTM methods E1756-95 and E1755 respectively. The control for this experiment was the same ground cob material utilized in the initial hot-water extraction.

Results from this experiment are illustrated in Table 7.3.

Table 7.3: Percentage Ash Content of Whole Corncob after a 200 mL Ambient Temperature 0.1 molL^{-1} Citric Acid Solution Soak

Soak-time (minutes)	% ash content[a] (DWB)
0 (control)	1.64
120	0.66
240	0.87
360	1.00
480	0.77

[a] *Dry Basis - ASTM E 1755-95.*

The percentage ash results obtained from the above experiment do not consistently follow a trend, however it appears that under the above experimental conditions the maximum amount of soluble and ion exchangeable minerals are removed from a whole corncob in only 2 hours. The use of an organic acid therefore appears to be much more efficient solvent for removing inorganic minerals from corncob. The main explanation regarding the scatter in percentage ash content of acid soaked corncob is attributed to the heterogeneous nature of biomass. In spite of the ostensible increase in efficiency a significant amount of inorganic ash still remains bound within the cob. Reasons for limited ash removal are as before, poor solubility of specific mineral species and possible mass transfer limitations.

7.2.4 Hot DI Water Mineral Extraction of Chopped Corncob

This experiment was designed to take into account the possible existence of mass transfer limitations. A percolation system analogous to the previous hot water extraction system was employed, (see section 7.2.1).

Whole corncobs were randomly selected, broken up into smaller pieces - typically 2-3 cm in length by 1 cm in diameter - and left out in ambient laboratory conditions for twenty four hours prior to being placed into a closed 1 mm Ø stainless steel Mesh cage. Using a 1 L measuring cylinder, 2.1 L of previously heated DI water was added to the glass wash cylinder. Once the DI water reached a controlled temperature of between 90 ˚C and 100 ˚C the cage containing the chopped cob was lowered into the wash cylinder and a stopwatch was initiated. The water temperature was checked every 20 minutes with the aid of a k-type thermocouple. The lower valve was also adjusted so that a flow rate of 10mL/min of hot DI water exiting the system was achieved. Due to hot DI water exiting the wash cylinder, the system was continually recharged with similar tempered DI water. A 3 L DI water limit was set for the duration of this experiment resulting in the remaining 900 mL of hot DI water being added to the system over 300 minutes. Grab samples of chopped corncob were removed from the steel cage every 75 minutes and placed into an oven set at 105 ˚C at atmospheric pressure. Like previous leaching experiments the dry corncob samples were subsequently removed from the oven, milled, and analyzed for percentage moisture content and percentage ash content. The control for this experiment was the same ground cob material utilized in the previous hot-water extractions.

Results from this experiment are illustrated in Table 7.4.

Table 7.4: Percentage Ash Content of Whole Corncob after a Hot 3 L DI Water Wash

Percolation time (minutes)	% ash content[a] (DWB)
0 (control)	1.58
75	0.92
150	0.90
225	0.83
300	0.59

[a] *Dry Basis - ASTM E 1755-95.*

The percentage ash results obtained from the above experiment indicate yet again that as soak-time increases the percentage ash content of chopped corncob decreases. Furthermore, the same phenomena regarding the rate of ash removal continually diminishing as soak-time increases is apparent. However, the evident ash removal plateau occurs at a somewhat lower percolation time, (75 min), compared to the previous hot DI water soak and the initial hot water wash experiment (360 min). This intuitively indicates that the increased surface area provided by the mechanical break up of whole corncobs allows for mineral matter to be removed in a distinctly shorter period of time. A lower percentage ash content (0.59%) was observed after a percolation time of 300 min compared 225 min (ca. 0.83%). This result is what one might naturally expect to occur however other likely reasons for this significant reduction include, (1) the heterogeneous nature of biomass, (2) a non-representative grab sample being removed and ashed, and (3) the physical loss of dry corncob mass or ash during the ash analysis procedure. Despite an observed increase in mineral removal efficiency, a significant amount of inorganic ash still appears to be bound within the cob structure. It seems clear that there is a portion of inorganic minerals present within the corncob structure which are inherently difficult to remove via simple non-aggressive ion exchange methods.

Like the initial hot water extraction experiment a shortcoming of the experimental procedure was noted. It was difficult to maintain a constant flow rate of 10 mL/min

consequently leading to small inconsistencies associated with the rate of hot DI water flow through the chopped corncob sample.

7.2.5 Hot Citric Acid Mineral Extraction of Chopped Corncob

This experiment was designed to investigate whether the entire ash load of chopped corncob could be removed using slightly more aggressive conditions. A percolation system analogous to the previous hot DI water extraction system was employed, (see section 7.2.4 and Fig. 7.1).

Whole corncobs were randomly selected, broken up into smaller pieces - typically 2-3 cm in length by 1 cm in diameter - and left out in ambient laboratory conditions for 24 hours. The chopped corncob was placed into a closed 1 mm ø stainless steel Mesh cage. Using a 1 L measuring cylinder, 1.9 L of previously heated 0.1 $molL^{-1}$ citric acid solution water was added to the glass wash cylinder. Once the citric acid solution reached a controlled temperature of between 90 ˚C and 100 ˚C the cage containing the chopped cob was lowered into the wash cylinder and a stopwatch was initiated. The citric acid solution temperature was checked every 20 minutes with the aid of a k-type thermocouple. The lower valve was also adjusted so that a flow rate of ~7 mL/min of hot citric acid solution was achieved. Due to hot citric acid solution exiting the wash cylinder, the system was continually recharged with similar tempered citric acid solution. A 3.2 L citric acid solution limit was set for the duration of this experiment resulting in the remaining 1.3 L of hot citric acid solution being added to the system over a 240 minute time period. Grab samples of chopped corncob were removed from the steel cage at T = 30 min, T = 60 min, T = 120 min, and T = 240 min. The acid wash was followed by a neutralization step involving the percolation of boiled and ambient temperature DI water through the cob bed (refer to Fig. 7.3). Like experiment 7.2.3 a pH meter was employed to analyze the wash water and hence determine the point of complete acid removal. Separate cob samples were then placed into an oven set at 105 ˚C at atmospheric pressure. The percentage moisture content and percentage ash content was then determined (refer to Table 7.5). The control for this experiment was the same ground cob material utilized in the initial hot-water extraction.

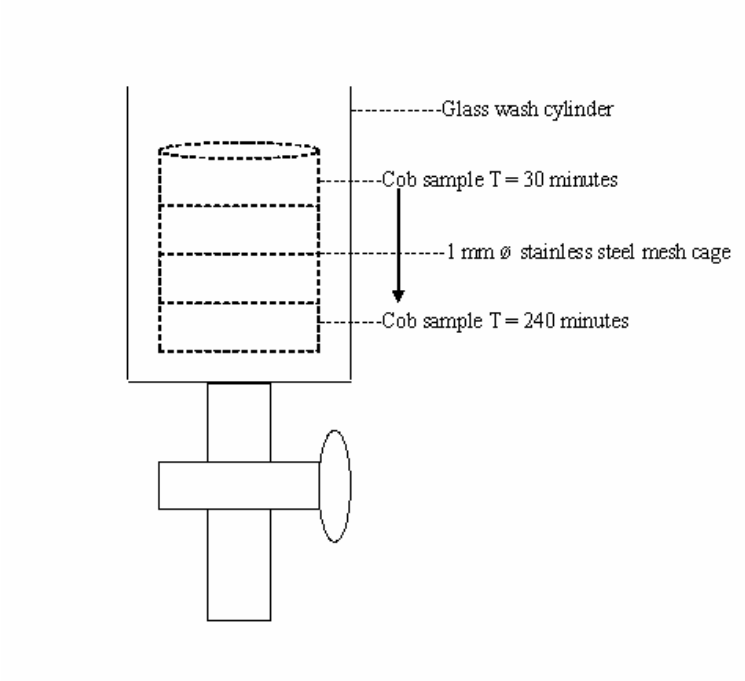

Figure 7.3: *Diagram Illustrating Neutralization of Citric Acid Demineralized Corncob Biomass.*

With minor alterations to the mineral extraction methodology outlined above an additional slightly more aggressive experiment was performed. 3.2 L of hot 0.1 $molL^{-1}$ citric acid solution was replaced with 3 L of hot 1.0 $molL^{-1}$ citric acid solution. An alternate flow rate of ~12.5 mL/min was also applied with grab samples of chopped corncob being removed from the steel cage at T = 30 min, T = 60 min, and T = 120 min. Neutralization of acid leached corncob was performed as above, however individual sample populations were divided into layers in reverse order, i.e. cob sample T = 120 min was at the steel cage top as opposed to being near the cage bottom as before. In addition, extra cob sample populations were removed from acid leached cob samples T = 30 min and T = 120 min prior to washing with DI water in order to evaluate the effect of the neutralization step (refer to Table 7.5).

Table 7.5: Percentage Ash Content of Chopped Corncob after Hot Citric Acid Treatments

Ash removal treatment	Percolation time (minutes)	% ash content[a] (DWB)
Hot 0.1 molL^{-1} citric acid solution treatment inclusive of neutralization step	0 (control)	2.67
	Control Average	1.63[b] ±[c] 0.51
	30	0.57 ± 0.01
	60	0.45 ± 0.02
	120	0.42 ± 0.02
	240	0.60 ± 0.02
Hot 1.0 molL^{-1} citric acid solution treatment inclusive of neutralization step	30	0.63
	60	0.52
	120	0.56
Hot 1.0 molL^{-1} citric acid solution treatment	30	0.63
	120	0.57

[a] *Dry Basis – ASTM E 1755-95.* [b] *average of 9 untreated corncob ash analyses.* [c] *± value indicates sample standard deviation*

The percentage ash results obtained from the above experiments follow the same trends as previous demineralization experiments. However, of importance is the fact that the evident ash removal plateau occurs at a slightly lower percolation time (60 min), and that the obtained percentage ash results are at a minimum compared to previous mineral extraction experiments. The above results also indicate that a more concentrated solution of citric acid does not remove additional minerals from cob biomass compared to a weaker citric acid solution. Also of special interest are the percentage ash results pertaining to the non-neutralized cob samples. Results indicate that washing chopped corncob with DI water following an acidic treatment does not remove additional mineral matter from the corncob structure. The percentage ash content of the control sample is higher than previous control ash results indicating that the powdered control sample is non-homogeneous. It is important to recognize

that the control cob material was the result of a single cob being ground and therefore may not be representative of bulk corncob. To assess the effectiveness of demineralization treatments, a representative untreated corncob percentage ash content is required. An average percentage ash content of untreated corncob was therefore determined using data from above and data obtained by previous analysts. In order to assess the reproducibility of the ash analysis procedure, corncob samples subjected to a hot 0.1 $molL^{-1}$ citric acid solution treatment were analyzed in triplicate. The standard deviation obtained from the triplicate analyses was very small indicating good reproducibility of data and a homogeneous sample population. Using the triplicate analysis results, the statistical technique one-way Analysis of Variance (ANOVA) was employed to investigate possible statistical differences within treated corncob sample populations, i.e. is the percentage ash result obtained at percolation time 30 min statistically different from the percentage ash result obtained at percolation time 240 min. ANOVA was also used to confirm whether a statistical difference existed between the ash contents of treated corncob and untreated corncob (refer to Table 7.6(a) and (b)). Prior to ANOVA a Grubbs' outlier test was performed on the control corncob measurements to ensure that all measurements came from the same sample population. The Grubb's test compares the deviation of the suspect value from the sample mean with the standard deviation of the sample (refer to equation (7) below)[1].

$$G = \left| suspect\ value - \bar{x} \right| / s \qquad \textbf{(7)}$$

The critical value for G at P = 0.05 is 2.13. This value is greater than the calculated G-value of 1.91 obtained from including the suspect percentage ash value 2.67 in the data set. This result indicates that the suspect value is part of the same sample population. Because the suspect percentage ash value (2.67%) deviated from the mean percentage ash value (1.69%) by the largest quantity, all other control ash measurements must come from the same sample population.

Ideal one-way ANOVA requires an equal number of replicates for each given treatment, but this is not essential. Advanced computer programs can overcome the

problem of unequal replicates by entering "missing-values". The mean percentage ash content of untreated corncob was calculated from 8 replications, therefore the lowest three percentage ash content values were compared to treated corncob percentage ash contents. If a significant difference was observed using the lowest control ash data, then a significant difference would also occur with the inclusion of the entire control percentage ash population.

Table 7.6(a): Summary Data with respect to Hot 0.1 molL^{-1} Citric Acid Treatment of Chopped Corncob required for One-Way ANOVA

Groups	Count	Sum	Average	Variance
% ash content of untreated corncob biomass	3.00	3.87	1.29	9.10E-03
% ash content of chopped corncob following a 30 minute hot 0.1 molL^{-1} citric acid solution treatment	3.00	1.71	0.57	1.57E-04
% ash content of chopped corncob following a 60 minute hot 0.1 molL^{-1} citric acid solution treatment	3.00	1.36	0.45	2.78E-04
% ash content of chopped corncob following a 120 minute hot 0.1 molL^{-1} citric acid solution treatment	3.00	1.25	0.42	4.60E-04
% ash content of chopped corncob following a 240 minute hot 0.1 molL^{-1} citric acid solution treatment	3.00	1.81	0.60	4.89E-04

Table 7.6(b): ANOVA Results with respect to Hot 0.1 molL^{-1} Citric Acid Demineralization of Chopped Corncob

Source of Variation	SS	df	MS	F	P-value	F crit
Between Groups	1.53	4.00	0.38	182.02	2.71E-09	3.48
Within Groups	0.02	10.00	2.10E-03			
Total	1.55	14.00				

The calculated F value obtained from a one-sided F-test is much greater than the critical value of F therefore the null hypothesis is rejected; the sample means are significantly different. The above ANOVA Table also gives the P-value, which is the probability that our calculated F value would be obtained by chance (random error) alone. This probability is extremely small providing an additional reason for the rejection of the null hypothesis. A significant result in one-way ANOVA can arise

for several reasons: for example, one mean may differ from all the others, all the means may differ from each other, or the means may fall into two distinct groups. A novel way for determining the reason for a significant result is to compare the difference between ordered adjacent mean values with the least significant difference as given by equation (8)[1]:

$$s\sqrt{\left(\frac{2}{n}\right)} \times t_{h(n-1)} \qquad \textbf{(8)}$$

Where s is the within-sample estimate of σ_0, and $t_{h(n-1)}$ is the critical value of t having a number of degrees of freedom of this estimate at a 95 % confidence interval. The calculated lest significant difference (LSD) from the above data equates to 8.34E-02. Table 7.7 illustrates the possible significant differences between the alternate percentage ash sample means.

Table 7.7: Significant Differences between Percentage Ash Population Means of Untreated and Citric Acid Treated Corncob Biomass

Comparison of % ash population means[a]	Calculated difference between population means	Significant difference, (Y/N)[c]
Untreated corncob Vs 30 min acid treated cob (a.t.c)[b]	0.72	Y
Untreated corncob Vs 60 min a.t.c	0.84	Y
Untreated corncob Vs 120 min a.t.c	0.87	Y
Untreated corncob Vs 240 min a.t.c	0.69	Y
30 min a.t.c Vs 60 min a.t.c	0.11	Y
30 min a.t.c Vs 120 min a.t.c	0.15	Y
30 min a.t.c Vs 240 min a.t.c	0.03	N
60 min a.t.c Vs 120 min a.t.c	0.04	N
60 min a.t.c Vs 240 min a.t.c	0.15	Y
120 min a.t.c Vs 240 min a.t.c	0.19	Y

[a] Dry Basis – ASTM E 1755-95. [b] (a.t.c) refers to acid treated cob. [c] (Y/N) refers to yes/no.

Comparing the LSD value 8.34E-02 with values calculated in column 2 of Table 7.7, a definite significant difference exists with respect to the percentage ash content of untreated corncob and all hot citric acid treated corncob samples. It is also remarked that there appears to be a significant difference between corncob samples subjected to acid leaching periods of 60 and 120 minutes compared to corncob leached for 30 minutes. No significant difference exists between corncob samples acid leached for 60 and 120 minutes respectively. Furthermore no significant difference is present between the corncob sample subjected to an acid leaching period of 240 minutes and the corncob sample leached for 30 minutes. However it is important to note that the LSD is not entirely rigorous and it can be shown that it leads to too many significant differences[1]. With this in mind a follow-up test known as the multiple range test was performed. The multiple range test is similar to the LSD test, however instead of multiplying $s\sqrt{(2/n)}$ by $t_{h(n-1)}$ a Q value obtained from the "The Studentized Range" Table is used. The Q value changes as we compare means, for instance upon comparing the highest mean with the lowest mean a Q value is selected at 5 treatments (5 distinct population means involved) having 10 degrees of freedom, however upon comparing the highest mean with the second lowest mean a Q value is selected at 4 treatments again having 10 degrees of freedom. The degrees of freedom (df) do not change – it is always the df of the residual (error) mean square. Table 7.8(a) and 7.8(b) illustrate the calculated multiple range values ($Q x \sigma_d$) and their subsequent comparison to calculated differences between percentage ash population means.

Table 7.8(a): Calculated Multiple Range Values with respect to Hot 0.1 molL^{-1} Citric Acid Demineralization of Corncob

No. of treatments	Q value obtained from "The Studentized Range" table	Multiple range value ($Q x \sigma_d$)
5	4.66	0.17
4	4.33	0.16
3	3.88	0.15
2	3.15	0.12

Table 7.8(b): Calculated Differences between Population Means with respect to Hot 0.1 molL^{-1} Citric Acid Demineralization of Corncob

Mean % ash content[a]					
1.29 (control)					
0.60 (240 min.)					0.69*[b]
0.57 (30 min.)				0.03	0.72*
0.45 (60 min.)			0.11	0.15	0.84*
0.42 (120 min.)		0.04	0.15	0.19*	0.87*
Mean % ash content	0.42 (120 min.)	0.45 (60 min.)	0.57 (30 min.)	0.60 (240 min.)	1.29 (control)

[a] *Dry Basis – ASTM E 1755-95.* [b] ** refers to a calculated significant difference.*

By comparing the appropriate multiple range value with calculated values in Table 7.8 (b) a definite significant difference exists regarding the percentage ash content of untreated corncob and all hot citric acid treated corncob samples, i.e. the calculated multiple range value at 5 treatments equates to 0.17, the difference between the mean corncob control percentage ash result and the means of the treated corncob percentage ash results is greater than 0.17 and hence a statistical difference is noted. Likewise there appears to be a statistical difference between the mean percentage ash result obtained from acid leaching cob for 240 min compared to the mean percentage ash result obtained from acid leaching cob for 120 min; the calculated difference between these means (0.19) is greater than the appropriate multiple range value (0.16). The more rigorous multiple range test indicates no additional significant differences between alternate percentage ash means which is in contrast to previously noted significant differences calculated using the LSD. Using the above results we can conclude that corncob subjected to a hot 0.1 molL^{-1} citric acid solution treatment obtains significantly reduced ash contents compared to untreated corncob. We can also conclude that that the maximum amount of minerals under hot 0.1 molL^{-1} citric acid solution treatment conditions are removed at a minimum time of 30 minutes. In stating this, the calculated multiple range value equals the calculated difference in means between sample populations 30 minute and 120 minute indicating that this difference is only very marginally insignificant. If additional ash analysis

replications were performed there is a possibility that a significant difference would eventuate.

With an average percentage ash content representative of untreated corncob the effectiveness of each demineralization treatment can therefore be evaluated. Table 7.9 illustrates the percentage effectiveness of the various ash removal treatments performed on corncob biomass.

Table 7.9: Demineralization Treatment Effectiveness on Corncob Biomass

Ash removal treatment	Percolation/soak time (minutes)	Ash removal percentage effectiveness[a]
Hot water extraction	120	-20
	240	26
	360	37
	480	60
Hot DI water extraction	120	37
	240	51
	360	56
	480	58
Ambient temperature 0.1 $molL^{-1}$ citric acid solution	120	61
	240	48
	360	41
	480	59
Hot DI water extraction (chopped corncob)	75	45
	150	47
	225	51
	300	65
Hot 0.1 $molL^{-1}$ citric acid solution	30	66

Ash removal treatment	Percolation/soak time (minutes)	Ash removal percentage effectiveness[a]
(chopped corncob)		
	60	73
	120	65
	240	64
Hot 1.0 molL^{-1} citric acid solution (chopped corncob)	30	63
	60	69
	120	67

[a] *% Effectiveness refers to the percentage of ash removed from corncob with respect to the average untreated corncob percentage ash result (1.69 %).*

Results from Table 7.9 indicate that the most effective and consistent demineralization treatment for removing minerals from corncob biomass involves a hot 0.1 molL^{-1} citric acid percolation treatment.

Although chopped corncob percentage ash contents resulting from a hot 0.1 molL^{-1} citric acid solution treatment are at a minimum, a significant quantity of inorganic mineral matter still remains within the corncob biomass. It is remarked that ash reductions of up to 90 % were obtained by Piskorz *et al*[2] after aggressive treatment conditions involving strong mineral acids. It therefore appears that in order to remove the entire ash load from corncob biomass more aggressive conditions are required. This would ultimately affect the cost effectiveness' of the demineralization procedure and for this reason it was deemed that a hot 0.1 molL^{-1} citric acid solution treatment would be utilized to demineralize alternate feedstock types and to produce a bulk amount of demineralized chopped corncob.

7.2.6 Production and Properties of Demineralized Corncob Charcoal

A scaled up 0.1 $molL^{-1}$ citric acid solution treatment was employed to produce a large quantity of demineralized chopped corncob feedstock which was to be converted into a low ash charcoal via FC. 750 g of laboratory equilibrated chopped corncob was partially demineralized by use of a 10 L insulated silica glass wash cylinder and 7 L of hot ~90 °C 0.1 $molL^{-1}$ citric acid solution. A continuous flow of hot citric acid was percolated through the cob bed for 120 min. Buoyancy of the chopped corncob was counteracted by a weighted 1 mm Ø stainless steel cage. The acid wash was followed by a neutralization step which involved the percolation of boiled and ambient temperature deionized water through the cob bed. It is important to note that the color of the percolated citric acid was bright orange indicating the possibility of extractives being removed in addition to inorganic minerals. After washing with DI water the entire corncob sample was removed from the cylinder and placed into an oven set at 105 ℃ at atmospheric pressure for overnight drying. A grab sample of the dry corncob sample was milled to a particle size of <1.0 mm prior to Total Biomass analysis as per ASTM method E1756-95, and Ash in Biomass analysis as per ASTM method E1755. The remaining cob sample was prepared for FC. 0.54 kg of demineralized chopped corncob biomass was flash carbonized at an elevated pressure of 1.48 Mpa. The run was terminated after 1.16 kg of air was delivered at a flow of 0.03 kg/min. Biomass and associated charcoal percentage ash results are illustrated in the Table 7.10.

Table 7.10: Mean Percentage Ash Content of Untreated and Demineralized Corncob Feed and their Respective Charcoals

Feed	Mean % Ash Content[a] in Biomass	Mean % Ash Content[b] in Flash Carbonized Charcoal			
		Top[c]	Middle	Bottom	Overall
Corncob	1.69 ± 0.52	2.28 ± 0.94[d]	1.78 ± 0.41	2.65 ± 1.44	2.13 ± 0.43
Demin. Corncob 060804[e]	0.56 ± 0.04	0.94 ± 0.02	0.86 ± 0.02	1.16 ± 0.00	0.94[f]

[a] Dry Basis – ASTM E 1755-95. [b] Dry Basis – ASTM D1762-84 (Reapproved 1990). [c] 'Top', 'Middle', and 'Bottom' refers to the canister section from which charcoal was sampled. It is important to note that for demineralized corncob charcoal, 'Top', 'Middle', and 'Bottom' portions refers to three split portions in the top half of the canister only. [d] ± value indicates sample standard deviation. [e] Number corresponds to date produced dd/mm/yy. [f] No standard deviation is offered for the 'overall' demineralized corncob run as only one demineralized corncob run has been performed to date.

From Table 7.10 it is clear that the large scale demineralization procedure effectively reduced the percentage ash content of corncob biomass to an amount comparable to previous small scale citric acid treatments. The calculated standard deviation for the demineralized corncob biomass ash content is very small and is attributed to a single small homogeneous sample population being analyzed. A larger standard deviation with regard to the percentage ash content of untreated corncob biomass is observed and is attributed to a variety of corncob populations (average of 9 results) being sampled and analyzed between years 2004 and 2005. An increase in the ash content is observed for all biomass charcoals and is the result of a concentration effect, i.e. combustible mass is lost via the carbonization process whereas the mineral content remains largely unaffected. The percentage ash content for demineralized corncob

charcoal is significantly lower than the percentage ash content for untreated corncob charcoal. Again the standard deviation for the demineralized corncob charcoal percentage ash content is small and is largely attributed to a small sample size. The average percentage ash content of untreated corncob charcoal was determined using results from 8 separate FC runs. The 8 separate corncob only runs were selected on the basis of observations made after each FC experiment; ~1/3 of corncob run results were ignored due to being under or over carbonized. Table 7.11 illustrates relevant proximate analysis results for select 20-40 Mesh flash carbonized charcoals.

Table 7.11: Proximate Analysis Results of Select 20-40 Mesh Untreated and Demineralized Corncob Charcoals

Feed	Section[b]	Proximate Analysis (%)[a]		
		VM	fC	Ash
Corncob	Top	15.2	82.6	2.2
Charcoal	Middle	26.0	72.0	2.0
130404[c]	Bottom	20.6	75.9	3.5
	Overall[d]	**22.9**	**74.8**	**2.3**
Corncob	Top	19.7	77.8	2.5
Charcoal	Middle	11.9	85.1	3.0
220305	Bottom	12.7	82.7	4.7
	Overall	**15.5**	**81.4**	**3.1**
Demineralized	Top	2.5	96.5	0.9
Corncob	Middle	19.8	79.4	0.9
Charcoal	Bottom	26.1	72.7	1.2
060804	**Overall**	**13.7**	**85.4**	**0.9**

[a] Dry Basis – ASTM D1762-84 (Reapproved 1990). [b] Refers to the position of the charcoal within the lab-scale FC canister. [c] Number corresponds to date produced dd/mm/yy. [d] Weighted average.

Proximate analysis results indicate differences in charcoal properties according to the biomasses original position within the lab-scale reactor canister. The 'top' portion of corncob charcoal has a lower percentage VM content in comparison to the 'middle'

and 'bottom' portions. This physical property indicates a higher temperature being present for a longer period of time at the top of the reactor canister. Recently the propagation of the flaming pyrolysis reaction unique to FC was investigated[3]. From the spatial distribution of products' properties obtained from various FC experiments, conformation that the carbonization reaction propagated upward from the bottom of the bed to its top was obtained, and in addition it was revealed that the charcoal products were further carbonized and combusted from the top downward after the entire bed was converted into charcoal. Furthermore at higher operating pressures there appeared to be an increase in the upward speed of the flame through the bed.

The concentration of ash present in charcoal is influenced by the degree of carbonization. This may explain the higher percentage ash content for the 'top' portion of low VM corncob charcoal. High carbonization temperatures may also result in the increased release of volatile inorganic minerals sulfur, chlorine, and to some extent potassium[4]. As identified in section 4.2.2 charcoals with low VM contents have increased specific surface areas. In addition, the porosity of the charcoal product was also related to the charcoal's location within the lab-sale FC canister. Moreover it has been well established that inorganic minerals present in carbonaceous materials affect the development of surface area[5-7]. Alkali compounds are known to promote the formation of slit-shaped pores whereas transition metals and alkali earth compounds enhance mesopore formation[5]. The 'middle' portion of corncob charcoal has a high VM content indicating that lower carbonization temperatures were reached in this section of the canister. A surface area analysis was performed (see Table 7.12) on the 'middle' portion of 20-40 Mesh demineralized corncob charcoal and compared to corncob charcoal products having similar VM contents.

Table 7.12: Physical Properties of Select 20-40 Mesh Untreated and Demineralized Corncob Charcoals

Feed	Section[a]	Surface Area[b], m^2/g,	Pore Volume, mL/g
Corncob Charcoal 130404[c]	Bottom	-[d]	-
Corncob Charcoal 220305	Top	9.0	0.002
Demineralized Corncob Charcoal 060804	Middle	58	0.030

[a] Refers to the position of the charcoal within the lab-scale FC canister. [b] BET surface area calculated over the pressure region P/P_0 = 0.01-0.1. [c] Number corresponds to date produced dd/mm/yy. [d] – isotherm shape poor resulting in an inaccurate specific surface area value.

As in section 4.2.2 the porosity of select charcoal samples was determined via a Quantachrome Autosorb-1 gas sorption analyzer. After pretreatment under vacuum (210°C, 4 h), the adsorption and desorption isotherms of charcoal samples were obtained using nitrogen as an adsorbate. From the resulting isotherm the Brunauer-Emmett-Teller (BET) specific surface area and total pore volume of the charcoal samples was calculated. It is important to note that the demineralized corncob biomass was positioned in the upper half of the reactor canister during FC. The 'middle' demineralized corncob charcoal portion is therefore more ideally compared to a 'top' portion of corncob charcoal obtained from a regular whole corncob run. The demineralized corncob charcoal is observed to have an increased specific surface area and total pore volume (58 m^2/g and 0.030 mL/g respectively) compared to untreated corncob charcoal (9 m^2/g and 0.002 mL/g). An increase in the specific surface area for demineralized corncob charcoal may be the result of a reduced ash content, or the possible enhancement of pore volumes due to the removal of specific mineral types. Deashing of the biomass feedstock often increases the surface area of its carbon derivative[8].

The adsorption-desorption isotherm for 20-40 Mesh 'middle' demineralized corncob charcoal (see Fig. 7.4) is in a state of under-equilibrium. The desorption curve is grossly distinct from the adsorption curve at the same relative pressures. This can be attributed to the material containing very tiny pores that are not easily accessible for nitrogen gas.

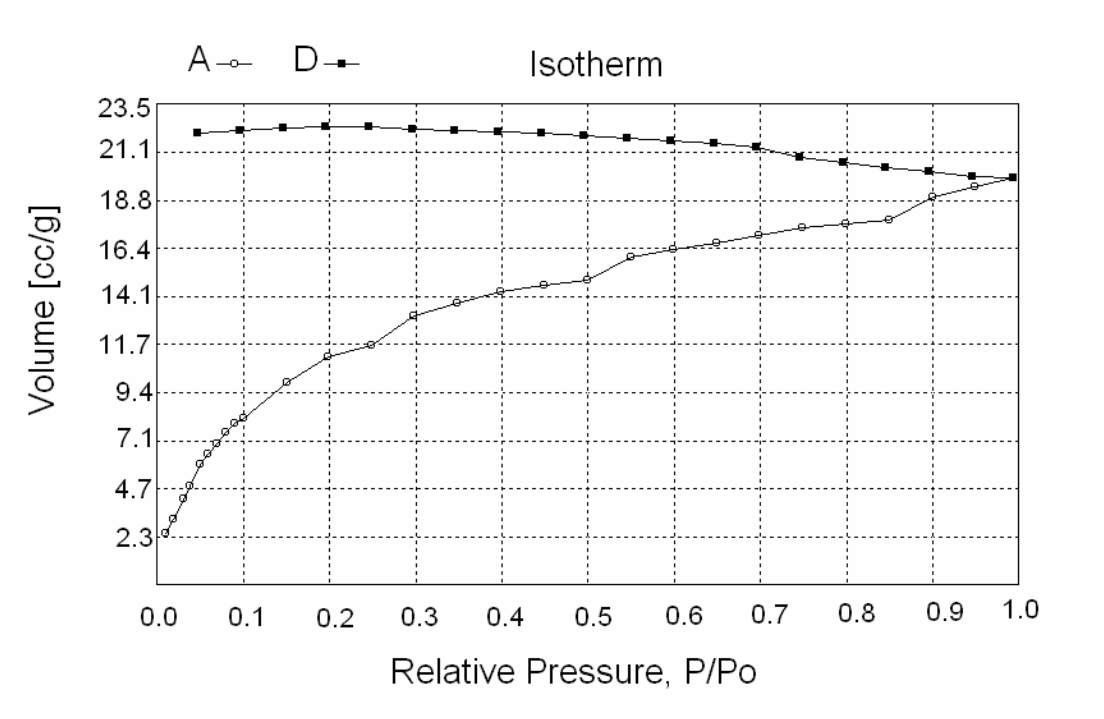

Figure 7.4: *Adsorption-Desorption Isotherm of 20-40 Mesh 060804 'Middle' Demineralized Corncob Charcoal obtained over pressure region P/P_0 0.01-1.0.*

A portion of 20-40 Mesh 'middle' demineralized cob charcoal was carbonized (950 °C, 30 min) prior to an electrical resistivity measurement and specific surface area analysis. Proximate analysis, electrical resistivity, and surface area results can be noted in Table 4.4 of section 4.3.1 and Table 4.7 of section 4.3.2 respectively. The electrical resistivity of demineralized corncob carbon is analogous to the electrical resistivity of untreated cob carbon, 0.21 Ω·cm compared to 0.19 Ω·cm respectively. This result indicates that the removal of typical biomass minerals does not affect the resultant carbons electrical properties. The result also goes some way in supporting the finding that mineral matter generally found in biomass-based materials does not influence the electrical properties of their subsequent carbons. The BET specific

surface area of demineralized cob carbon is comparable to the surface area obtained from untreated cob carbon, 403 m^2/g and 419 m^2/g respectively. This result indicates that the influence of mineral matter upon surface area in carbonaceous materials is negligible after high heat treatment.

The combustion properties of untreated and partially demineralized cob chars in the kinetic regime was studied using a large number of thermogravimetric experiments within a wide range of experimental conditions[9]. The complexities of biomass derived charcoal combustion arise from biocarbon chemical, structural and physical inhomogeneities, as well as mineral content and composition. As a result the combustion process cannot be accurately described by a single reaction, and was instead modeled on a devolatilization step and two burn-off[7] reactions. Results from the numerous thermogravimetric experiments indicated that the level of grinding had considerable affect on combustion reactivity. It was however noted that the burn-off of the partially demineralized char was not affected by grinding at all. This phenomenon was explained by the negligible influence grinding has on the already high specific surface area of the partially demineralized cob charcoal compared to untreated corncob charcoal; grinding usually increases the external surface area only. Of particular interest was the fact that in spite of the higher surface area, the partially demineralized cob charcoal evidenced much lower combustion reactivity; in linear heating rate experiments burn-off terminated ~130-160 °C higher relative to analogous experiments with untreated cob chars. The difference in combustion is explained by the well-known catalytic effect exerted by acid-soluble inorganic minerals[9].

7.3 Hot Citric Acid Mineral Extraction from a Hardwood

This experiment was designed to investigate the effectiveness of leaching inorganic minerals from a hardwood as opposed to herbaceous corncob. Literature indicates that the percentage ash content of woods are significantly reduced compared to most

[7] Burn-off is associated with the self-heating (ignition) of a sample which leads to combustion at a high reaction rates.

Gramineae species, oak wood has a percentage ash content equating to 0.19%[10]. A percolation system analogous to the hot DI water extraction system was employed. The methodology utilizing hot 0.1 $molL^{-1}$ citric acid solution to extract inorganic minerals was followed (refer to section 7.2.5)

Large pieces of debarked treated Cowboy oak wood were randomly selected and cut into manageable pieces using an electric saw ("Sawzall"). The oak wood was further broken up into smaller pieces - typically 2-3 cm in length by 1 cm in diameter – and left out in ambient laboratory conditions for twenty four hours. Using a 1 L measuring cylinder, 3 L of hot 0.1 $molL^{-1}$ citric acid solution was percolated through a 1 mm Ø stainless steel Mesh cage (flow rate ~6.25mL/min) containing chopped oak wood. As before, the citric acid solution was maintained at a temperature between 90 °C and 100 °C and chopped oak wood grab samples were removed at T = 30 min, T = 60 min, T = 120 min, and finally at T = 240 min. Despite previous corncob demineralization experiments indicating that at a very maximum 120 minutes of leaching time is all that is required to remove the greatest amount of minerals under the hot citric acid conditions, a longer leach time was employed to account for possible enhanced mass transfer limitations associated with the denser feedstock. Furthermore, despite previous demineralization results indicating that a DI water wash after acid leaching played no further role in removing inorganic minerals, the acid leached oak wood was subjected to a neutralization step aimed at removing excess acid. Oak wood samples were placed in the cage in the following order: longest acid leached oak wood sample (240 minute) at the cages top sequentially followed by the next longest acid leached oak wood sample (120 minute) and so on. Boiled and ambient temperature DI water was then percolated through the chopped oak wood cage, after which the oak wood samples were removed and dried in an oven set at 105 °C.

Percentage ash results from the above experiment are illustrated in Table 7.13.

Table 7.13: Percentage Ash Content of Chopped Debarked Cowboy Oak Wood after a Hot 0.1 molL^{-1} Citric Acid Wash

Percolation time (minutes)	% ash content[a] (DWB)	Ash removal percentage effectiveness[b]
0 (control)	0.79 ± 0.09	-
30	0.44	44
60	0.46	42
120	0.46	42
240	0.52	34

[a] *Dry Basis – ASTM E 1755-95.* [b] *% Effectiveness refers to the percentage of ash removed from oak wood with respect to the average untreated oak wood percentage ash result (0.79 %).*

The percentage ash results obtained are analogous to previous ash content results associated with the hot citric acid demineralization of chopped corncob. Evidently the ash removal plateau occurs after only 30 minutes, the lowest percolation time yet with regard to removing the maximum amount of inorganic minerals under hot citric acid conditions. However, when comparing the ash removal percentage effectiveness values between oak wood and corncob it is evident that removing inorganic minerals from oak wood is substantially more difficult compared to corncob, 44% compared to 73%. Possible reasons for quick yet poor effective removal of ash from oak wood may include: 1) poor mass transfer of inorganic minerals out of the dense oak wood; citric acid soluble/exchangeable minerals at the woods surface are easily removed leaving the remaining majority of ash in the innermost portions of the wood structure unaffected, and 2) different inorganic mineral species are present in enhanced concentrations compared to corncob; hardwoods may contain a higher percentage of insoluble structural related minerals such as calcium and silicon as opposed to corncob. The percentage ash results of citric acid leached oak wood are consistently low, ranging between 0.44 and 0.52%. Despite a minimum observed ash content result of 0.42% being obtained from hot citric acid leached cob, the subsequent scaled-up and more representative acid leaching corncob experiment resulted in a corncob ash content of 0.56 ± 0.04%. Acknowledging this, the oak wood biomass

appears to have a better chance at obtaining a slightly decreased consistent ash level of between 0.4-0.5% after a hot citric acid treatment compared to corncob.

7.4 Hot Citric Acid Mineral Extraction from a Softwood

This experiment was designed to investigate the effectiveness of leaching inorganic minerals from a softwood as opposed to a hard wood or a herbaceous corncob. Referring to section 3.0, biomass materials corncob, oak wood (hardwood), and iron wood (softwood) are significantly different with regard to their physical and chemical structure. Removing inorganic minerals from a sample of debarked iron wood (part of the pine tree family) was achieved using the same procedure employed to demineralize a portion of oak wood. Percentage ash results from this experiment are illustrated in Table 7.14.

Table 7.14: Percentage Ash Content of Chopped Debarked Iron Wood after a Hot 0.1 molL^{-1} Citric Acid Wash

Percolation time (minutes)	% ash content[a] (DWB)	Ash removal percentage effectiveness[b]
0 (bark)	11.19	-
0 (control)	1.82	-
30	1.35	26
60	1.29	29
120	1.22	33
240	1.35	26

[a] *Dry Basis – ASTM E 1755-95.* [b] *% Effectiveness refers to the percentage of ash removed from oak wood with respect to the average untreated oak wood percentage ash result (1.82 %).*

Out of all the hot citric acid demineralization experiments, the percentage ash contents obtained from leaching ironwood are the highest yet. However, of similarity with alternate hot citric acid demineralization experiments, ash removal continually diminishes as soak-time increases. After two hours of hot citric acid leaching, further

percolation of acid does not appear to remove additional amounts of inorganic minerals from the organic iron wood structure. Furthermore, like the previous oak wood demineralization experiment the ash removal percentage effectiveness is poor compared to corncob, 33% compared to 73%. Moreover, the ash removal percentage effectiveness associated with iron wood is significantly lower compared to ash removal percentage effectiveness associated with oak wood. These percentage ash results further substantiate assertions that leaching inorganic minerals from dense materials is far more difficult than leaching inorganic minerals from porous materials.

Explanations for the poor removal of inorganic minerals using a hot citric acid wash are as before, poor mass transfer of inorganic minerals out of the dense wood structure, and the presence of enhanced concentrations of non-soluble inorganic mineral species. Untreated debarked iron wood has a moderately high percentage ash content (1.82%) comparable to that of untreated corncob. One possible reason for the atypically high ash content of iron wood may be due to the preparative procedure employed to obtain a debarked iron wood sample. The sample of iron wood utilized for demineralization was obtained from a felled tree and was subsequently hand stripped of its bark. A thin layer of red tissue remaining on the heart wood subsequent to debarking may have contributed a large proportion of insoluble minerals to the overall percentage ash content; iron wood bark has a very high percentage ash content, ~11.2%.

It was also observed that the citric acid residue after the demineralization of iron wood was bright orange, comparable to the color obtained after citric acid demineralization of corncob. The orange color was distinct from the light yellow citric acid wash resulting from Cowboy oak wood demineralization and is thought to be the result of red colored extractives being removed in addition to inorganic minerals during citric acid demineralization; note that the residual bark tissue on the iron wood samples was red as was the color of untreated corncob.

Figure 7.5 is a chart summarizing the demineralization results for all feedstocks subjected to an ash removal experiment.

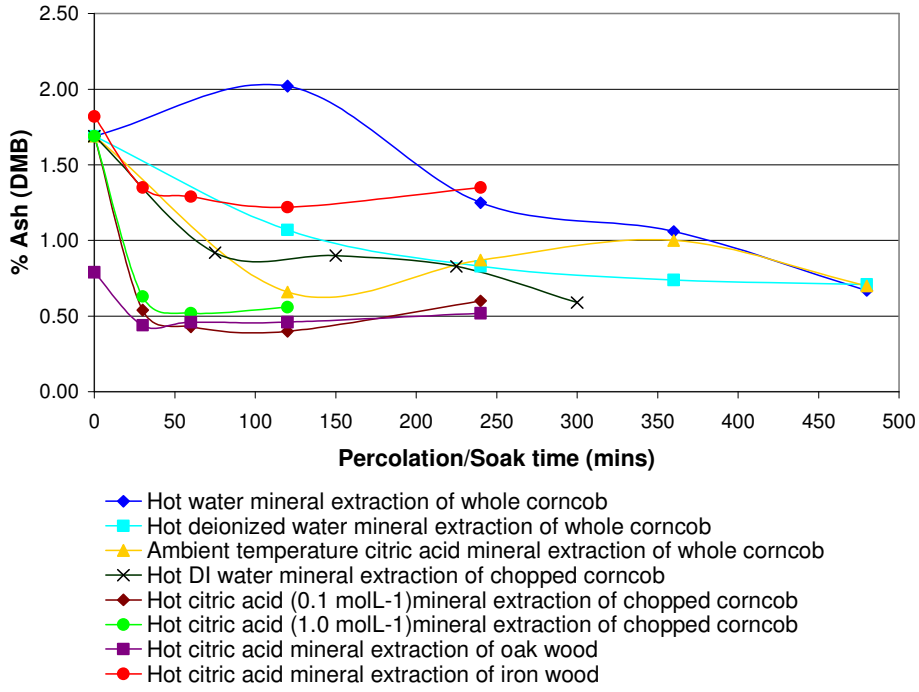

Figure 7.5: *Chart Showing the Remaining Ash Content of Various Biomass Feedstocks Subsequent to Demineralization.*

The chart clearly indicates that the best demineralization results were obtained by percolating a hot 0.1 $molL^{-1}$ citric acid solution through a portion of chopped corncob. The phenomenon regarding the rate of ash removal continually diminishing as soak-time increases is evident in the above graph with obvious plateaus being apparent for most demineralization treatments. The hot citric acid treatment of corncob appears to remove more minerals relative to the control (untreated corncob) compared to wood samples oak wood and iron wood. The following section, (7.5) describes efforts to determine elemental compositions of respective biomass ash residues. It is hoped that data from such analyses will help explain the reason behind incomplete ash removal and why mineral removal is more difficult for wooded biomass compared to gramineae biomass.

7.5 Inductively Coupled Plasma Mass Spectroscopy (ICP-MS) Analyses of Biomass Ash Residues

Biomass ash residues resulting from ASTM method E 1755-95 were digested using hot concentrated nitric acid, filtered, diluted, and made up to volume using 18 mega-ohm water. Sample solutions were run on a Perkin Elmer Elan DRC II ICP-MS equipped with an ASX-320 autosampler. Prior to sample analysis a series of blanks and mineral standards were run in order to obtain the required calibration curves. It is important to note that some ash samples did not fully dissolve during digestion. The remaining particulate is supposed to consist primarily of silicon and carbon remnants.

Table 7.15: Mineral Composition of Select Biomass Ash Residues Via ICP-MS (ppb)

Mineral	CC[a]	Demin. CC	Red.[b] (%)	OW[c]	Demin. OW	Red. (%)	IW[d]	Demin. IW	Red. (%)
B	73	44	40	193	102	47	94	77	18
Na	611	133	78	450	233	48	1120	498	55
Mg	10899	2636	76	2364	1624	31	12655	6775	46
Al	767	940	-23	639	112	82	161	57	64
Si	305	313	-2	494	336	32	156	71	55
P	10912	5435	50	1648	1071	35	9551	3946	59
K	S[e]	920		14886	8421	43	13575	3600	73
Ca	2444	981	60	24519	21195	14	81093	58300	28
Fe	7072	2648	63	36092	648	98	6509	206	97
Mn	374	85	77	1418	922	35	1546	816	47
Cu^{65}	2585	889	66	387	9828	-2439	8061	3427	57
Zn^{66}	3850	419	89	284	3139	-1004	3015	483	84
Mo	14	54	-302	33	10	71	78	31	61

[a] Corncob (CC). [b] Percentage reduction. [c] Oak Wood (OW). [d] Iron Wood (IW). [e] Saturated (S).

The ICP-MS results above help to explain a few of the questions previously posed. Corncob biomass appears to contain large amounts of easily removable potassium relative to oak wood and iron wood. This may be a direct result of mass transfer limitations present in the more dense wood feedstocks. Magnesium also appears to be a mineral which is more easily removed from corncob biomass during acid demineralization compared to the wooded species. Oak wood and iron wood biomass also seem to contain larger quantities of calcium relative to corncob biomass. The calcium present in wood also appears to be less easily removed during acid demineralization. Recall that calcium is associated with cell walls and can also be found as insoluble calcium oxalate and calcium phosphate in plant cell vacuoles. Perhaps oak wood and iron wood contain more deposits of insoluble calcium salts relative to corncob. In general it appears that ICP-MS results substantiate previous claims made is section 7.3 and 7.4 respectively, which is that mineral removal is more difficult for denser wood feedstocks compared to corncob biomass.

7.6 Ash migration

With reference to the literature survey in section 2.3, it is remarked that inorganic minerals are volatilized, oxidized and deposited, and removed from the point of heating as fly ash during biomass combustion and pyrolysis. It was observed from a range of lab-scale FC experiments that a lower amount of ash was retained in the charcoal compared with the initial amount of ash contained in the feedstock, i.e. the ash yield was significantly reduced. The percentage ash yield is calculated on a dry basis from the following equation:

$$y_{\text{ash}} = y_{\text{char}} \frac{\%\ \text{char ash}}{\%\ \text{feed ash}} \qquad \textbf{(9)}$$

Calculated percentage ash yields for a variety of biomass lab-scale reactor experiments ranged between 27.9 - 66.9% with the average being 46.3 ± 12.1%. These results however, were considered skewed towards lower percentage ash yields due to unrepresentative sampling. In addition, from the general FC experimental setup nominally employed by the R3 laboratory, qualitative information regarding

ash migration throughout the canister could not be determined. Earlier FC experiments however were performed with physically separated canister loaded biomass i.e. top, middle and bottom. Separation was achieved by use of two stainless steel screens having an aperture of 0.4 mm. Percentage ash yields were calculated from such runs and the statistical technique analysis of variance (ANOVA) was applied to test the null hypothesis; are all samples drawn from the same population or is there a statistical difference between the ash yield at the canisters top compared to the ash yield at the canisters bottom. Tabulated ANOVA results are illustrated in Table 7.16(a) and 7.16(b):

Table 7.16(a): Summary Data with respect to various Feedstock Charcoal 'Top', 'Middle', and 'Bottom' Ash Yields required for One-Way ANOVA

Groups	Count	Sum	Average	Variance
% Ash Yield - 'Top'	4	192.6	48.1	229.3
% Ash Yield - 'Middle'	4	213.6	53.4	333.2
% Ash Yield - 'Bottom'	4	200.7	50.2	280.4

Table 7.16(b): ANOVA Results with respect to various Feedstock Charcoal 'Top', 'Middle', and 'Bottom' Ash Yields

Source of Variation	SS	df	MS	F	P-value	F crit
Between Groups	56.1	2	28.1	0.1	0.9	4.3
Within Groups	2528.5	9	280.9			
Total	2584.6	11				

The calculated F value obtained from a one-sided F-test is less than the critical value of F therefore the null hypothesis is accepted; the sample means are not significantly different. The P-value is close to 1 providing additional support for the acceptance of the null hypothesis.

It is however remarked that the proximate analysis procedure employed (refer to section 4.2) to determine the percentage ash yields utilized in the above ANOVA calculation was considered unrepresentative. In order to learn more about the ash

migration phenomenon, a FC run was executed with special care. In this run, a bed of corncob feedstock was divided into three distinct sections, i.e. top, middle, and bottom, again by use of two stainless steel screens. In addition, 81.1 g of pistachio nutshell contained in a metal beaker was placed at the very top of the bed. After the run, all the charcoal products were ground and a representative sub-sample from each section was analyzed for ash content. Table 7.17 shows the proximate analysis results and the percentage ash recovery from this run.

Table 7.17: Proximate Analysis and Percentage Ash Yield Results for the FC Experiment Performed on 27-Jan-2005

Feedstock	Section[a]	Particle Size	Proximate Analysis (%)[c]			% Ash Yield
			Av. Moisture[d]	Av. VM	Av. Ash	
Corncob	Top	20-40[b]	8.9	3.1	3.7	
Corncob	Top	<425 µm	8.7	3.4	5.7	59.6
Corncob	Top	<425 µm				
Corncob	Middle	20-40	5.3	11.2	4.1	
Corncob	Middle	<425 µm	5.2	11.4	4.8	84.5
Corncob	Middle	<425 µm				
Corncob	Bottom	20-40	3.2	14.6	3.8	78.4
Corncob	Bottom	<425 µm	3.4	15.4	4.1	
Overall						76.7
Pistachio	Top	20-40	10.1	3.7	3.5	88.8
Pistachio	Top	20-40				
Pistachio	Top	<425 µm	10.9	4.3	7.5	
Pistachio	Top	<425 µm				

[a] Refers to the position of the charcoal within the lab-scale FC canister. [b] 20-40 particle size refers to a particle size of 425 - 850 µm. [c] Dry Basis - ASTM D1762-84 (Reapproved 1990). [d] Av. refers to mass weighted average.

From the proximate analysis results a difference in percentage ash content is observed between varying charcoal particle sizes. This phenomenon is most clearly seen in case of the pistachio nutshell charcoal, (20-40 = 3.5%, where as <425 µm = 7.5%). Because of this additional factor, percentage ash yields were calculated on a mass

basis with respect to different particle sizes. It is also important to note that percentage ash yields were calculated using average percentage ash values for raw biomass. The average percentage ash value for corncob is 1.63 ± 0.51%. The average percentage ash value for pistachio nutshell is 0.68 ± 0.05%. In addition it is also important to recognize that the percentage ash yield is a comparison between the ash in the initial feedstock and the ash in the resulting charcoal. Two distinct ASTM methods are used in determining ash in biomass and in charcoal. In order for a ratio to be established an assumption is made that the two ash determining methods are strictly comparable.

The ash recovery results illustrated in Table 7.17 are less than 100% indicating that ash has left the canister. Ash is likely to move within the FC system as fly ash, as part of the tarry pyrolytic byproducts, and as volatile ions and gases. Ash may also be deposited as oxides onto the sides and bottom of the canister. Combustion at the biomass surface results in inorganic minerals being oxidized and deposited on the surface of the charcoal, a phenomenon often observed in the top section. An observed distribution of ash recovery throughout the bed was also noted. The top charcoal portion showed the lowest ash recovery whereas the middle and bottom sections showed increased comparable ash recoveries, 59.6% compared to 84.5% and 78.4% respectively. It should be noted here that the top charcoal had the highest ash content due to pronounced carbonization; yet the ash recovery was low. A possible explanation of this distribution is the volatilization of ash[3]. As previously discussed the predominant air flow during FC is from top to bottom. It is therefore proposed that both volatilized ash and deposited ash is carried downward and captured by and/or condensed onto the charcoal at lower positions. The volatilization of ash was also implied by the behavior of pistachio nutshells. The percentage ash yield for pistachio nutshell biomass was 88.8%. The pistachio percentage VM content is similar to the 'top' portioned corncob charcoal indicating a similar degree of flash carbonization. Despite this similarity there is a significant difference in percentage ash yields between the 'top' portioned pistachio nutshell and the 'top' portioned corncob. Because the nutshells were contained in a beaker, the ash deposited on the charcoal surface was likely to be retained and thus a higher ash recovery should be

obtained relative to the corncobs. Proximate analysis results supplement this theory as the charcoal fines (<425 μm) portion contain the predominant amount of ash. However, the ash recovery was still less than unity and this suggests that the ash went through a gaseous phase to escape from the beaker. It is worth noting however that the two feedstocks are vastly different and are likely to contain varying ash compositions. The rate and amount of ash lost may be strongly dependent on the type of minerals present prior to FC. Moreover there are various inaccuracies associated with the ASTM ash analysis that may significantly affect the percentage ash yields. During ash analysis, inorganic minerals are retained as solid oxides. A discrepancy in ash analysis may result from an increase in ash mass caused by oxidation. This factor may not affect percentage ash yields providing that the two ash analysis procedures used are analogous in terms of oxidation. It is also important to note that average percentage ash contents of raw biomass were used to determine percentage ash yields and are likely to contribute the greatest amount of error. An estimate of <5% for the relative error in ash determination is offered[3].

To try and ascertain additional evidence supporting the ash migration theory elemental compositions of various biocarbon residues were analyzed via ICP-MS. Results are summarized in Table 7.18:

Table 7.18: Mineral Composition of Select Biocarbon Ash Residues Via ICP-MS (ppb)

Mineral	Demin. CC[a] 'Top'	Demin. CC 'Bot'	CC 'Mid[b]' 02-Jul-2004	BD[c] CC 03-Nov-2004	CC 'Bot' 03-Nov-2004
B	61	51	51	99079	15593
Na	390	206	4900	416	8040
Mg	5729	4031	15121	3160	28700
Al	3933	2716	3115	2003	78
Si	189	957	489	470	1675
P	11490	6779	53928	8180	31622
K	2320	2007	S[d]	1570	S
Ca	2042	4320	5670	5744	5102

Mineral	Demin. CC[a] 'Top'	Demin. CC 'Bot'	CC 'Mid[b]' 02-Jul-2004	BD[c] CC 03-Nov-2004	CC 'Bot' 03-Nov-2004
Fe	20317	9401	6745	21372	135
Mn	257	1273	570	555	664
Cu^{63}	647	1195	264	372	374
Cu^{65}	637	1175	246	348	351
Zn^{66}	2696	1408	1842	1484	4875
Zn^{68}	3673	1926	2525	2030	6646
Mo	177	63	61	47	4

[a] Corncob (CC). [b] 'Mid' refers to position within FC canister – Middle. [c] Boron-doped (BD). [d] Saturated (S).

Recall that the ash content of demineralized corncob charcoal increased from top (0.9%) to bottom (1.2%). The increase in ash content for the bottom section may be the result of ash migrating downwards via the predominant air flow. However associated ICP-MS results do not support this supposition; the concentrations of mineral species between the top and bottom sections are not distinct. The boron-doped corncob FC experiment (refer to section 7.7.1 and 7.7.2) does however support the theory of ash migration. The element boron is not typically found in biomass at very high concentrations (51 ppb in untreated cob charcoal). In the boron-doped corncob FC experiment, the canister was loaded bottom to top with 0.46 kg of untreated corncob followed by 0.15 kg of chopped boron-doped corncob and 0.31 kg of 5mm ø stainless steel caged boron-doped chopped corncob. The concentration of boron in the untreated whole bottom corncob charcoal (15593 ppb) is significantly greater than the amount of boron typical of corncob charcoal (51 ppb). This suggests that boron is migrating from top to bottom during FC.

7.7 Doping Charcoals

The term doping refers to the deliberate introduction of foreign atoms into a pure matrix, which in our case is carbon. Doping materials, in particular semiconductor materials such as silicon and graphite, has been extensively studied. The purpose of doping certain materials may include:

1. To change the distribution of electrons and hence electronic structure of a given material.
2. In the case of carbon, to affect the graphitization process.
3. To modify the chemical state of surface particles.
4. To alter the structural properties of given materials, i.e. certain carbon nitride compounds are found to be extremely strong.
5. To obtain a homogeneously housed catalyst.

Our interest in doping carbon materials is primarily to assess the possible influences specified dopants have on the electrical properties of various prepared carbonaceous materials. A detailed review on carbon conduction and the effect of doping on semiconductors is offered in section 2.4 of the literature study.

7.7.1 Boron Doping Corncob Biomass

Boron doping carbon materials to enhance both physical and electrical properties has been well documented. Substituting boron into a sp^2 hybridized hexagonal carbon arrangement as in graphite, results in an empty 2p orbital. This is more clearly illustrated in Fig. 7.6.

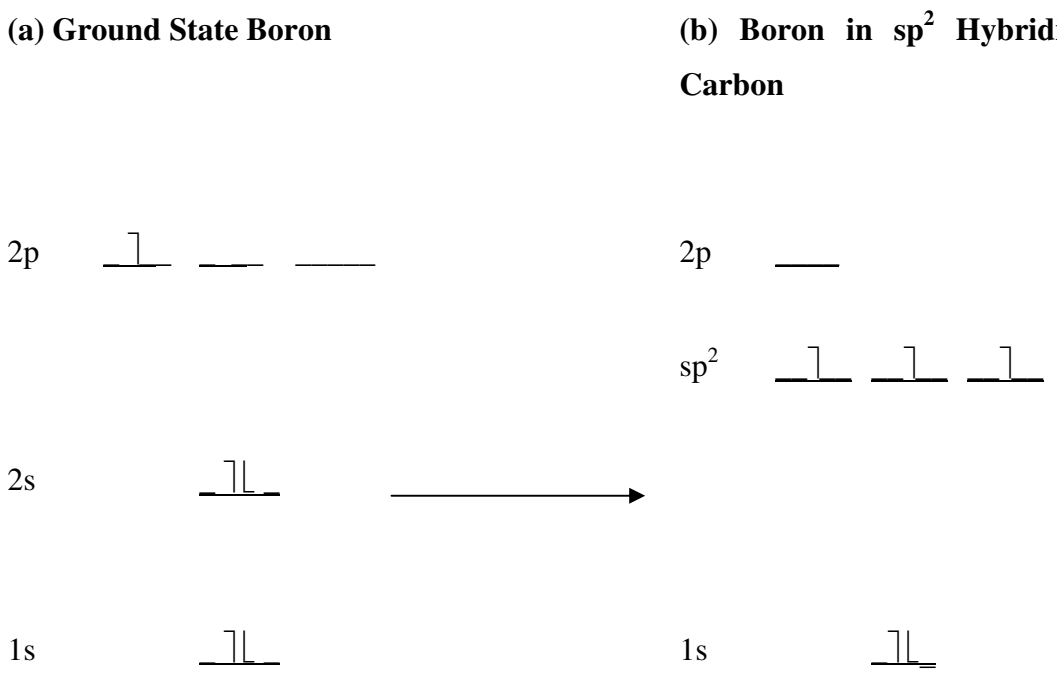

Figure 7.6: *Electron Configuration of (a) Ground State Boron going to (b) Boron in sp^2 Hybridized Carbon.*

With an empty 2p orbital, electrons in nearby carbon atoms can jump into the lower energetic state hole subsequently creating new holes. The positive hole moves to a new location with each electron jump enabling the solid to carry an electric current. In this specific case boron is acting as a p-type dopant. A recent paper produced by Y. Lee *et al*[11] examines the effects of boron doping in low and high surface area carbon powders. Boron-doped carbons were produced by placing elemental boron into porcelain crucibles containing various carbon materials. The carbon mixes were then subjected to extremely high temperatures (~2450 °C) under argon for repeated time periods of 15 minutes. X-ray diffraction was subsequently employed to examine crystallinity changes. The d-spacing of the boron-doped samples was lower than that of perfect graphite even though these were supposedly non-graphitizable carbon materials. Previous works substantiate these findings indicating that the incorporation of boron (~2.35 %) into a significantly condensed carbon lattice results in an increase in graphite crystalline height and width, and a decrease in interlayer spacing [12]. The mechanism for how this occurs is still not completely understood. Hagio *et al*[13] proposed that the inclusion of electron deficient boron into a carbon

lattice caused a decrease in the repulsive interaction between pi-electron clouds of adjacent graphene layers. The consequence of this was an observed reduction in d-spacing. It therefore appears that the inclusion of boron into a condensed carbon structure increases the conductivity of the material via two independent effects, by increasing the number of charge carrying holes and by reducing the interlayer spacing between graphene planes. It is important to note that difficulty in interpreting the true effect of dopants on heterogeneous carbons is frequently encountered[12]. Also of particular interest is the effect of substitutional boron on carbon oxidation. Oxidation protected carbons are utilized in the aerospace industry as strategic materials, in the ceramic industry, and in manufacture of carbon composites which are utilized as friction materials[14]. A detailed paper prepared by Radovic *et al*[14] concludes that substitutional boron reduces electron density at reactive carbon sites suppressing oxygen chemisorption. The formation of a thin film of boric oxide (B_2O_3) at the carbons surface is also implicated in inhibiting carbon oxidation. In low boron loadings however, substitutional boron was observed in having a catalytic effect in carbon oxidation. It was supposed that a complex balance exists between the influences of boron content and distribution, carbon nature and reaction conditions.

The industrial inclusion of boron based compounds into biomass, in particular wood, has been well developed in recent years due to the treated end product having desirable properties. Boron compounds are known flame retardants and reduce microbial attack upon inclusion into cellulosic materials[15-17]. Treatment of wood with boron is typically achieved by dipping freshly sawn lumber into a solution of concentrated (18%) boric acid and borax followed by storage in covered stacks. Figure 7.7 represents the reaction of boric acid with a polysaccharide. More recent developed processes which involve the vapor phase treatment of pine wood with trimethylborate grossly reduces the time required for boron to fully diffuse throughout the wood structure; 30 hours compared to 5 to 8 weeks respectively[15]. In addition biguanide derivatives of boric acid have been developed with the aim of fixing boron within the wood structure, whilst retaining the effective fungicide and insecticide properties; this is in an attempt to mitigate potential environmental hazards involving the leaching of boron from wood through exposure to rain[16]. Boric acid is recognized to catalyze dehydration and oxygen eliminating reactions at

relatively low temperatures (100-300 °C) and may also catalyze the isomerization of newly formed polymeric materials resulting in the formation of aromatic structures which ultimately promote charring[17]. It is also important to note that the inclusion of phosphorus compounds (guanylurea phosphate) in addition to boron compounds in wood, results in a synergistic effect with respect to fire retardation over a wide temperature range.

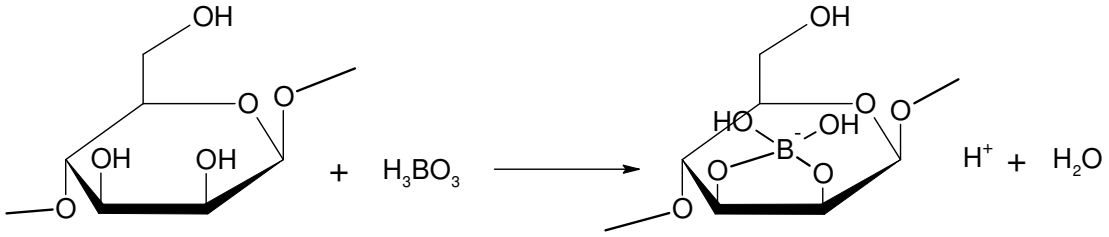

Figure 7.7: *Reaction of Boric Acid with a Polysaccharide – adapted from ref [17].*

With the industrial processes already available to treat a large amount of biomass with suitable boron compounds, an investigation was performed using boric acid and chopped corncob to establish ideal conditions for maximum boron loading.

A large portion (~570 g) of chopped corncob was demineralized according to the methodology outlined in section 7.2.6. A representative sample of dry demineralized chopped corncob was removed and its ash content determined in triplicate. The demineralized chopped corncob (200 g) was placed into a 4 L nalgene container followed by a weighted stainless steel Mesh screen and ambient temperature (0.08 $molL^{-1}$, 1500 mL) boric acid solution. An estimated 50 g portion of chopped corncob was subsequently removed at T = 30 min, T = 60 min, T = 120 min, and finally at T = 240 min. Using the experimental apparatus illustrated in Fig. 7.1, excess boric acid was removed from the distinct 50 g grab samples using two 1 L portions of ambient temperature DI water. Cob samples were then dried at 45 °C under hard vacuum for 48 hours. Each sample was then ground to a particle size of less than 1 mm before a 1 g ash analysis was performed in triplicate. The percentage ash results are illustrated in Table 7.19.

Table 7.19: Average Percentage Ash Content of Chopped Demineralized Corncob after Boric Acid Treatment

Soak time in 0.08 molL^{-1} boric acid solution (minutes)	Percentage ash content[a] (DWB)
0	0.54 ±[b] 0.00
30	0.74 ± 0.02
60	0.84 ± 0.02
120	0.91 ± 0.06
240	0.83 ± 0.09

[a] *Dry Basis – ASTM E 1755-95.* [b] *± value indicates sample standard deviation*

The percentage ash results indicate that as the soak time increases the percentage ash content increases. Boric acid appears to be successfully adsorbed by the porous corncob contributing to the corncob ash content as it decomposes to boric oxide upon thermal degradation. In addition the percentage ash results also indicate that the rate of boron adsorption into the cob structure is relatively fast with a maximum percentage ash content obtained after a soak time period of 60 minutes. The statistical techniques one-way ANOVA and the multiple range test were employed to test the null hypothesis; are all samples drawn from the same population. Tabulated ANOVA results are illustrated in Table 7.20(a-b):

Table 7.20(a): Summary Data with respect to 0.08 molL^{-1} Boric Acid Treatment of Citric Acid Demineralized Chopped Corncob required for One-Way ANOVA

Groups	Count	Sum	Average	Variance
% ash content of chopped demineralized corncob biomass	3	1.62	0.54	1.18E-05
% ash content of chopped demineralized corncob following a 30 minute soak in ambient temperature 0.08 molL^{-1} boric acid solution	3	2.23	0.74	2.80E-04
% ash content of chopped demineralized corncob following a 60 minute soak in ambient temperature 0.08 molL^{-1} boric acid solution	3	2.53	0.84	5.89E-04
% ash content of chopped demineralized corncob following a 120 minute soak in ambient temperature	3	2.72	0.91	3.06E-03

Groups	Count	Sum	Average	Variance
0.08 molL^{-1} boric acid solution % ash content of chopped demineralized corncob following a 240 minute soak in ambient temperature 0.08 molL^{-1} boric acid solution	3	2.49	0.83	7.63E-03

Table 7.20(b): ANOVA Results with respect to 0.08 molL^{-1} Boric Acid Treatment of Citric Acid Demineralized Chopped Corncob

Source of Variation	SS	df	MS	F	P-value	F crit
Between Groups	0.24	4.00	0.06	26.45	2.67E-05	3.48
Within Groups	0.02	10.00	2.31E-03			
Total	0.27	14.00				

The calculated F value obtained from a one-sided F-test is greater than the critical value of F therefore the null hypothesis is rejected: the sample means are significantly different. The calculated P-value is also very small providing an additional reason for the rejection of the null hypothesis. In order to determine whether soaking chopped corncob for varying lengths of time influences the inclusion of boric acid into the cob structure a multiple range test was performed. Tables 7.21(a) and 7.21(b) illustrate the calculated multiple range values ($Q x \sigma_d$) and their subsequent comparison to calculated differences between percentage ash content population means.

Table 7.21(a): Calculated Multiple Range Values with respect to 0.08 molL^{-1} Boric Acid Treatment of Citric Acid Demineralized Chopped Corncob

No. of treatments	Q value obtained from "The Studentized Range" table	Multiple range value ($Q x \sigma_d$)
5	4.66	0.18
4	4.33	0.17
3	3.88	0.15
2	3.15	0.12

Table 7.21(b): Calculated Differences between Corncob Percentage Ash Content Population Means with respect to the 0.08 molL^{-1} Boric Acid Treatment of Citric Acid Demineralized Chopped Corncob

Mean % ash content[a]					
0.91 (120)					
0.84 (60 min.)					0.07
0.83 (240 min.)				0.01	0.08
0.74 (30 min.)			0.09	0.10	0.17
0.54 (control)		0.20*	0.29*	0.30*	0.37*[b]
Mean % ash content	0.54 (control)	0.74 (30 min.)	0.83 (240 min.)	0.84 (60 min.)	0.91 (120 min.)

[a] *Dry Basis – ASTM E 1755-95.* [b] ** refers to a calculated significant difference.*

By comparing the appropriate multiple range value with calculated values in Table 7.21(b), a definite significant difference regarding the percentage ash content of demineralized chopped corncob and the percentage ash content of all boric acid treated chopped corncob samples is observed. This confirms that inorganic boron has been successfully included in the organic cob matrix. Furthermore the multiple range test indicates that there is no statistical difference between the ash contents of chopped corncob treated with boric acid for varying periods of time. Therefore a minimum time period of 30 minutes is all that is required to fully saturate chopped corncob with boric acid.

A second experiment was designed to investigate the effect of boric acid concentration on loading chopped corncob with boron. Three 50 g portions of citric acid demineralized chopped corncob were placed into separate 500 mL plastic beakers, followed by a weighted stainless steel Mesh screen, and varying concentrations of ambient temperature boric acid solution (375 mL). Concentrations of boric acid solutions employed in the above methodology included 0.008 molL^{-1}, 0.08 molL^{-1}, and 0.8 molL^{-1}. Chopped corncob samples were soaked for a time period of 120 minutes despite previous results indicating that a minimum of 30 minutes is all that is required to saturate 50 g of chopped corncob with boric acid.

After the boric acid soak all corncob portions were washed separately with two 1 L portions of ambient temperature DI water prior to being dried at 45 °C under hard vacuum for 96 hours. Each 50 g sample was then ground to a particle size of less than 1 mm before a 1 g ash analysis was performed in triplicate. The percentage ash results are illustrated in Table 7.22.

Table 7.22: Average Percentage Ash Content of Chopped Demineralized Corncob after Soaking in varying Concentrated Boric Acid Solutions for 120 Minutes

Concentration of boric acid solution ($molL^{-1}$)	Percentage ash content[a] (DWB)
0	0.54 ±[b] 0.00
0.008	0.67 ± 0.03
0.08	0.88 ± 0.05
0.8	2.61 ± 0.10

[a] Dry Basis – ASTM E 1755-95. [b] ± value indicates sample standard deviation

The percentage ash results illustrated in Table 7.22 indicate that as the concentration of boric acid increases more boron appears to be adsorbed by the chopped corncob. Adsorption of boric acid into the cob structure is likely to be occurring via two main processes, chemisorption (refer to Fig. 7.7) and physisorption. It is supposed that chemisorption of boric acid into corncob biomass is the minor process leaving the majority of boric acid being physisorbed throughout the porous corncob structure. Evidence of the dominant physisorption process was observed after samples of boric acid treated cob were dried; small clusters of white crystals were noted on the cob surface. The presence of solid boric acid on the cob surface also indicates that the DI water wash is not very effective in removing excess physisorbed boric acid. This phenomenon is largely attributed to the poor solubility of boric acid in water ~1 g in 18 mL of cold water[18]. The tabulated percentage ash results above also indicate that as the percentage ash content increases an increase in the percentage ash content standard deviation occurs. It was noted that great difficulty was experienced when trying to obtain stable crucible + ash residue weights after progressive furnace

heating periods at 575 °C. Pyrolysis of boric acid ultimately results in the formation of boric oxide (B_2O_3), which is highly refractory. Intermediates during boric acid pyrolysis include cyclotriboric acid ($B_3O_3(OH)_3$), and polymeric metaboric acid, $((HBO_2)_n)$[19]. One possible reason for the difficulty in obtaining stable crucible weights with respect to boron loaded biomass may be the continual volatilization of organoboranes upon progressive heat treatments. This effect is likely to be increased with heavily loaded boric acid doped biomass, which provides an explanation for the increase in percentage ash standard deviation with enhanced boron doping. The residue resulting from the ash analysis of boron-doped corncob was dark black compared to the light grey residue representative of untreated corncob ash, presumably due to residual borates. The statistical techniques one-way ANOVA and the multiple range test were subsequently employed to test the null hypothesis; are all samples drawn from the same population. Tabulated ANOVA results are illustrated in Table 7.23(a) and 7.23(b):

Table 7.23(a): Summary Data with respect to the varying Concentrated Boric Acid Treatment of Citric Acid Demineralized Chopped Corncob required for One-Way ANOVA

Groups	Count	Sum	Average	Variance
% ash content of chopped demineralized corncob biomass	3	1.62	0.54	1.18E-05
% ash content of chopped demineralized corncob following a 120 minute soak in ambient temperature 0.008 $molL^{-1}$ boric acid solution	3	2.02	0.67	8.47E-04
% ash content of chopped demineralized corncob following a 120 minute soak in ambient temperature 0.08 $molL^{-1}$ boric acid solution	3	2.65	0.88	2.06E-03
% ash content of chopped demineralized corncob following a 120 minute soak in ambient temperature 0.8 $molL^{-1}$ boric acid solution	3	7.84	2.61	9.34E-03

Table 7.23(b): ANOVA Results with respect to the varying Concentrated Boric Acid Treatment of Citric Acid Demineralized Chopped Corncob

Source of Variation	SS	df	MS	F	P-value	F crit
Between Groups	8.44	3	2.81	917.78	1.732E-10	4.0662
Within Groups	0.02	8	3.06E-03			
Total	8.46	11				

The calculated F value obtained from a one-sided F-test is far greater than the critical value of F therefore the null hypothesis is rejected: the sample means are significantly different. In order to identify which treatments are significantly different from each other a multiple range test was performed, the results of which are displayed in Table 7.24(a) and 7.24(b).

Table 7.24(a): Calculated Multiple Range Values with respect to the varying Concentrated Boric Acid Treatment of Citric Acid Demineralized Chopped Corncob

No. of treatments	Q value obtained from "The Studentized Range" table	Multiple range value ($Q x \sigma_d$)
4	4.53	0.14
3	4.04	0.13
2	3.26	0.10

Table 7.24(b): Calculated Differences between Corncob Percentage Ash Content Population Means with respect to the varying Concentrated Boric Acid Treatment of Citric Acid Demineralized Chopped Corncob

Mean % ash content[a]				
2.61 (0.8 $molL^{-1}$)				
0.88 (0.08 $molL^{-1}$)				1.73*[b]
0.67 (0.008 $molL^{-1}$)			0.21*	1.94*
0.54 (control)		0.13*	0.34*	2.07*
Mean % ash content	0.54 (control)	0.67 (0.008 $molL^{-1}$)	0.88 (0.08 $molL^{-1}$)	2.61 (0.8 $molL^{-1}$)

[a] *Dry Basis – ASTM E 1755-95.* [b] ** refers to a calculated significant difference.*

The results above indicate that all boric acid treatments are significantly different with respect to each other and with respect to the untreated demineralized corncob feedstock. Furthermore it appears that a concentration of 0.8 $molL^{-1}$ results in the highest amount of boric acid being included into chopped demineralized corncob biomass. As reported earlier the solubility of boric acid is relatively poor in ambient temperature water with a maximum concentration of approximately 0.9 $molL^{-1}$. Therefore the maximum loading of boron into biomass via ambient temperature aqueous means has been achieved.

7.7.2 Production and Properties of Boron-Doped Corncob Charcoal

Results from the two small scale boron doping experiments above led to the preparation of a large amount of boron-doped corncob. 500 g of room equilibrated chopped corncob previously demineralized with hot 0.1 $molL^{-1}$ citric acid was placed into a glass wash cylinder (refer to Fig. 7.1). Ambient temperature boric acid solution (4 L, 0.8 $molL^{-1}$) was added to the cob bed for a soak time period of 120 minutes. Following this, the boric acid was removed from the system and ambient temperature DI water (12 L) was percolated through the cob bed to remove excess physisorbed boric acid. The cob sample was subsequently removed and dried under laboratory conditions in a standard fume hood. Boron-doped corncob was then flash

carbonized at an elevated pressure of 1.14 MPa. The FC canister was loaded from bottom to top with 0.46 kg of untreated corncob followed by 0.15 kg of chopped boron-doped corncob and 0.31 kg boron-doped chopped corncob in a stainless steel cage. The boron-doped chopped corncob sample was contained within a cage at the top of the canister to enable easy identification after carbonization. The experiment was terminated after 1.27 kg of air was delivered at a flow rate of 0.03 kg/min. Biomass and associated charcoal percentage ash results are illustrated in Table 7.25.

Table 7.25: Mean Percentage Ash Content of Boron-Doped Corncob Feed and Proximate Analysis Results of Subsequent Flash Carbonized Charcoals

Feed	Mean % Ash Content[a] in Biomass	Section[b]	Proximate analysis (%)[c]		
			fC	VM	Ash
BD Corncob 031104[d]	1.93 ±[e] 0.06	Top	76.0	21.1	2.9
		Middle	69.0	28.3	2.7
Corncob 031104	1.69 ± 0.52	Bottom	79.8	18.4	2.6
		Overall[f]	76.5	21.2	2.7

[a] Dry Basis – ASTM E 1755-95. [b] Refers to the position of the charcoal within the lab-scale FC canister. [c] Dry Basis – ASTM D1762-84 (Reapproved 1990). [d] Number corresponds to date produced dd/mm/yy. [e] ± value indicates sample standard deviation. [f] Mass weighted average.

The mean percentage ash result for the boric acid treated cob is significantly greater compared to the mean percentage ash content of citric acid demineralized corncob, 1.93% and 0.54% respectively. Although the percentage ash value obtained from the scaled-up boron doping experiment is slightly lower than previous trial doping experiments, the ash result indicate successful inclusion of boron into chopped corncob. Ash contents of the boron-doped cob charcoal are also significantly higher than demineralized cob charcoal, 2.9-2.7% compared to 0.9%. This ash result again indicates that boron has been successfully retained in the cob structure after FC. As before (refer to section 4.3) a portion of 20-40 Mesh boron-doped cob charcoal was

carbonized within a closed Coors porcelain crucible at a HTT of 950 °C prior to an electrical resistivity measurement (refer to section 4.3.2). Proximate analysis, surface area, and electrical resistivity results associated with the boron-doped cob carbon can be observed in section 4.3, tables 4.4 and 4.7 respectively. The specific BET surface area (314 m^2/g) is comparable to untreated and demineralized cob carbons as is the electrical resistivity (0.20 Ω·cm) and density (0.54 g/cm^3). These results indicate that despite loading cob with boron the electrical and physical properties of the resulting carbon remain unchanged relative to untreated cob carbon. Three possible reasons for the unaffected electrical resistivity of the cob carbon subsequent to boron loading may be, (1) boron has not been substituted into the carbon sp^2 lattice but instead remains as an oxide or organically bound in the carbon matrix in a different manner, (2) the HTT was not great enough to enhance the graphitizability of the cob carbon whereby the presence of substitutional boron would have an effect, and (3) the concentration of substitutional boron within the carbon lattice is not great enough to cause a measurable effect.

7.7.3 Preparation and Properties of a Boron-Doped Sucrose Carbon

An alternate method of preparing doped carbons involves the dry mixing of feedstock and dopant chemical prior to FC. This procedure allows for greater flexibility in dopant concentration and in combination with a pure feedstock such as sucrose, results in a pure end product. Boric acid was utilized as the chemical dopant with sucrose being employed as the pure feedstock. Sucrose was selected on the basis that it is a readily available, relatively cheap, pure chemical, and has a similar decomposition temperature compared to boric acid, 160-186 °C and 171 °C respectively. 150 g of a 1:100 boron:sucrose powder was prepared and flash carbonized at an elevated pressure of 1.48 MPa in accordance to previous melt carbon preparations, i.e. composite powder was placed within a small metal beaker and situated at the canisters top during FC, (refer to section 1.2). The experiment was terminated after 1.06 kg of air was delivered at a flow rate of 0.02 kg/min. The entire charcoal sample was ground to a 20-40 Mesh particulate size prior to proximate analysis and carbonization at 950 °C. Proximate analysis results for boron-doped sucrose charcoal and boron-doped sucrose carbon are presented in Table 4.1 of

section 4.2, and Table 4.4 of section 4.3.1 respectively. The boron-doped sucrose charcoal has a high percentage ash content relative to untreated sucrose charcoal and boron-doped corncob charcoal, 9.7% compared to 0.0% and 2.9% respectively. As previously noted, difficulty was experienced when trying to obtain stable crucible + ash residue weights after progressive furnace heating periods at 750 °C. As before this was attributed to the continual volatilization of various organic boranes. The high ash percentage indicates the successful inclusion of boron into the sugar carbon. The percentage ash content of the boron-doped sucrose carbon is slightly higher than the respective charcoal, 10.2% compared to 9.7%, however the carbon has an expected lower VM content, 3.2% compared to 4.7%, which as discussed previously explains the slightly higher ash content via an inorganic concentrating effect. The electrical resistivity of boron-doped sucrose carbon at 0.14 Ω·cm was appreciably lower than untreated sucrose carbon of comparable VM content, 0.27 ± 0.03 Ω·cm. A possible explanation for the reduction in electrical resistance for boron-doped sucrose carbon compared to boron-doped corncob carbon may be an increase in impurity concentration as denoted by respective carbon percentage ash contents. An alternate explanation for the observed decrease in electrical resistivity obtained from boron-doped sucrose carbon may be associated with carbon oxidation. As stated previously oxygen chemisorption can increase the electrical resistivity of a carbon. It has been well documented that the inclusion of boron into carbonaceous materials at high concentrations suppresses oxidation. The specific BET surface area of the boron-doped sucrose carbon is also noticeable lower compared to the untreated sucrose carbon, 96 m^2/g and 172 m^2/g. The exact reason for this decrease is not clearly known, however it is recognized that boron-doping of carbon materials can enhance graphitization[11]. Graphite has a high density and low specific surface area[20, 21]. The reduced electrical resistivity results suggest that an increased concentration of boron is required in order to induce an effect on the electronic structure of carbohydrate based carbons. Due to the positive result obtained above, an additional sucrose doping experiment was performed utilizing an n-type dopant.

7.7.4 Preparation and Properties of a Phosphorus-Doped Sucrose Carbon

Monobasic ammonium phosphate ($(NH_4)H_2PO_4$) was the selected chemical employed to successfully dope sucrose with phosphorus. It was hypothesized that substituting phosphorus into a carbon lattice in a sp^3d type manner would result in two sp^3d electrons, one above the graphene plane and one below the graphene plane, free to roam the pi-conjugated system. This is more clearly illustrated in Figure 7.8 below:

(a) Ground state phosphorus

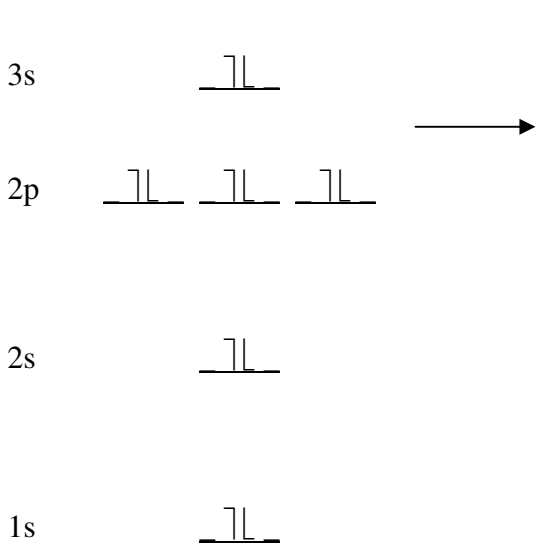

(b) sp^3d phosphorus (promotion of a 3s electron)

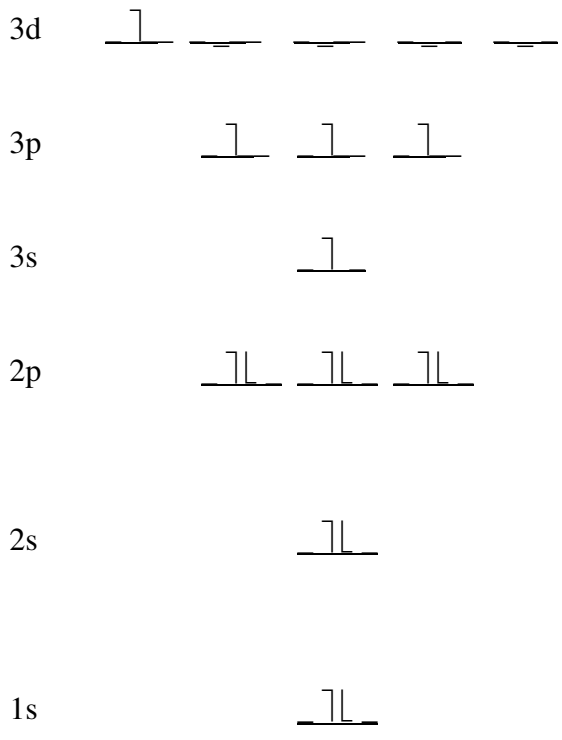

Mixing one 3s, three 3p and one 3d orbital generates five sp^3d orbitals (trigonal bipyramidal).

(c) sp^3d hybridized phosphorus

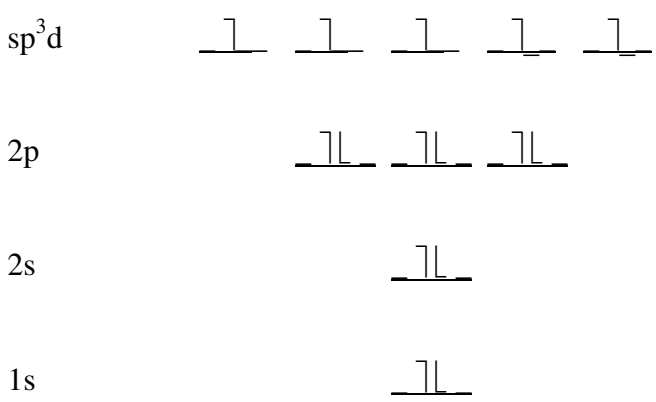

Figure 7.8: *Electron Configuration of (a) Ground State Phosphorus going to (b) sp^3d Phosphorus and (c) sp^3d Hybridized Phosphorus.*

With phosphorus substituted into the sp^2 carbon lattice, three sp^3d electrons out of the five are consequently involved in trigonal bonding with carbon leaving two free electrons. Phosphorus bonded in this manner acts as an n-type dopant, supplying additional electrons to the electronic structure of prepared biocarbons. In analogy to the boron doping experiment (7.7.3), 150 g of a 1:100 phosphorus:sucrose powder was prepared and flash carbonized at an elevated pressure of 1.48 MPa. The experiment was terminated after 1.4 kg of air was delivered at a flow rate of 0.03 kg/min. The resulting charcoal material was removed from the beaker and ground to a 20-40 Mesh particulate size prior to proximate analysis and carbonization at 950 °C. Proximate analysis results for phosphorus doped sucrose charcoal and phosphorus doped sucrose carbon can be viewed in Table 4.1 of section 4.2, and Table 4.4 of section 4.3.1 respectively. The percentage ash content of both the phosphorus doped charcoal and the respective carbon was significantly greater than the percentage ash content associated with untreated sucrose charcoal and untreated sucrose carbon, 5.2%, 5.2%, 0.0%, and 0.1% respectively. However despite the exact same ratio of dopant to sucrose being used with both sucrose doping experiments, the boron-doped

sucrose charcoal and carbon has a significantly greater percentage ash content compared to the phosphorus doped sucrose charcoal and carbon, 9.7% and 10.2%, compared to 5.2%, and 5.2%. This may indicate that phosphorus compounds resulting from thermal oxidation are more easily volatilized and removed from the heat treatment zone during FC and proximate analysis. It is also remarked that the color of the ash residue resulting from phosphorus doped sucrose carbon was markedly different from the ash residue resulting from boron-doped sucrose carbon, pale grey compared to jet black. The electrical resistivity of phosphorus doped sucrose was 0.19 Ω·cm which is lower than untreated sucrose carbon. Therefore the incorporation of phosphorus appears to have a small effect on the electrical resistivity of the sucrose derived carbon. Possible reasons for the lack of electronic effect include, (1) phosphorus not being substituted into the carbon lattice in an sp^3d manner, and (2) the concentration of phosphorus retained in the carbonaceous material is not great enough to exhibit an effect on the carbon matrix electronic structure. The specific BET surface area of phosphorus doped sucrose carbon is higher compared to untreated sucrose carbon, 235 m^2/g and 172 m^2/g respectively. This result indicates that the addition of phosphorus impurity has a positive effect on carbon surface area augmentation.

1. Miller, J. N.; Miller, J. C., *Statistics and Chemometrics for Analytical Chemistry*. Fourth ed.; Pearson Education Limited: 2000.

2. Piskorz, J.; Radlein, D.; Scott, D.; Czernik, S., Pretreatment of Wood and Cellulose for Production of Sugars by Fast Pyrolysis. *J. Anal. Appl. Pyrolysis* **1989,** 16, 127-142.

3. Nunoura, T.; Wade, S. R.; Bourke, J. P.; M. J. Antal, J., Studies of the Flash Carbonization Process. 1. Propagation of the Flaming Pyrolysis Reaction and Performance of a Catalytic Afterburner. *Ind. Eng. Chem. Res.* **2006,** 45, (2), 585-599.

4. Knudsen, J. N.; Jensen, P. A.; Dam-Johansen, K., Transformation and Release to the Gas Phase of Cl, K, and S during Combustion of Annual Biomass. *Energy & Fuels* **2004,** 18, 1385-1399.

5. Wigmans, T., *Fundamentals and Practical Implications of Activated Carbon Production by Partial Gasification of Carbonaceous Materials*. NORIT Activated Carbon.

6. Marsh, H.; Heintz, E. A.; Rodriguez-Reinoso, F., *Introduction to Carbon Technologies*. 1997.

7. Arenas, E.; chejne, F., The Effect of the Activating Agent and Temperature on the Porosity Development of Physically Activated Coal Chars. *Carbon* **2004,** 42, 2451-2455.

8. M. J. Antal, J.; Grønli, M., The Art, Science, and Technology of Charcoal Production. *Ind. Eng. Chem. Res.* **2003,** 42, 1619-1640.

9. Várhegyi, G.; Mészáros, E.; M. J. Antal, J.; Bourke, J.; Jakab, E., Combustion Kinetics of Corncob Charcoal and Partially Demineralized Corncob Charcoal in the Kinetic Regime. *Ind. Eng. Chem. Res.* **2006,** 45, 4962-4970.

10. M. J. Antal, J.; Allen, S. G.; Dai, X.; Shimizu, B.; Tam, M. S.; Gronli, M., Attainment of the Theoretical Yield of Carbon from Biomass. *Ind. Eng. Chem. Res* **2000,** 39, (11), 4024-4031.

11. Lee, Y.; Uchiyama, Y.; Radovic, L. R., Effects of Boron Doping in Low- and High-Surface-Area Carbon Powders. *Carbon* **2004,** 42, 2233-2244.

12. Marchand, A., Electronic Properties of Doped Carbons. *Chemistry and Physics of Carbon* **1971**, 155.

13. Hagio, T.; Nakamizo, M.; Kobayashi, K., Studies on X-ray Diffraction and Raman Spectra of B-doped Natural Graphite. *Carbon* **2001,** 39, 150-152.

14. Radovic, L. R.; Karra, M.; Skokova, K.; Thrower, P. A., The Role of Substitutional Boron in Carbon Oxidation. *Carbon* **1998,** 36, (12), 1841-1854.

15. Meder, R.; Franich, R. A.; Callaghan, P. T., ^{11}B Magnetic Resonance Imaging and MAS Spectroscopy of Trimethylborate-Treated Radiata Pine Wood. *Solid State Nuclear Magnetic Resonance* **1999,** 15, 69-72.

16. Anderson, K. B.; Franich, R. A.; Hedley, M. E.; Kroese, H. W.; Meder, R.; Waals, J. V. D., Synthesis, Charcaterisation and Effectiveness of Biguanide Derivatives of Boric Acid as Potential Fixed-Boron Wood Preservatives. *Material und Organismen* **1997,** 31, 63.

17. Wang, Q.; Li, J.; Winandy, J. E., Chemical Mechanism of Fire Retardance of Boric Acid Wood. *Wood Sci Technol* **2003,** 38, 375-389.

18. *The Merck Index - An Encyclopedia of Chemicals and Drugs*. Ninth ed.; Merck and Co., Inc.: 1976.

19. King, R. B., *Inorganic Chemistry of Main Group Elements*. VCH: 1995.

20. Torre, L. E. C. d.; Flores, E. S.; Llanos, J. L.; Bottani, E. J., Gas-Solid Potentials for N_2, O_2, and CO_2 Adsorbed on Graphite, Amorphous Carbons, Al_2O_3, and TiO_2. *Langmuir* **1995,** 11, 4742-4747.

21. CARBONS, A. Graphite and Carbon Grades For Conductive Plastic and Polymer Applications. http://www.asbury.com

8.0 Conclusions

1) All carbonized charcoals contain oxygen heteroatoms. Some carbonized charcoals also contain mineral matter, and small amounts of nitrogen and sulfur.

2) Charcoal retains the form and structure of its biomass precursor. However, charcoals derived from precursors, D-glucose, D-fructose, sucrose, inulin, and Kraft lignin retain none of their original crystalline structure as they proceed through a distinct liquid phase during pyrolysis. The visual appearance of each melt charcoal differed to some extent from each other.

3) Low VM corncob charcoal's have a larger specific surface area and total pore volume than high VM corncob charcoal's. Also, corncob charcoal that was located at a higher position in the carbonization canister possessed a higher porosity compared to corncob charcoal located at the bottom of the carbonization canister. Citric acid demineralized corncob charcoal had a greater porosity compared to untreated corncob charcoal, 58 m^2/g compared to 9 m^2/g.

4) Carbonized charcoals are microporous carbons having pore half-widths of 3 to 10 Å. Carbons derived from corncob have significantly greater surface areas than those of kukui nutshell and various sugar melt carbons, ca. 300-400 m^2/g and 172-261 m^2/g respectively. The BET specific surface area of demineralized cob carbon is comparable to the surface area obtained from untreated cob carbon, 403 m^2/g and 419 m^2/g respectively. Thus the influence of mineral matter upon surface area in carbonaceous materials is negligible after high heat treatment.

5) The electrical resistivity of a packed bed of carbon is affected by particle size and perhaps more precisely by the amount of conducting particle interfaces. Carbonized charcoals derived from diverse biomass feedstocks have high

electrical conductivities. Mineral matter present in the carbons at levels ranging from 2.4 to 6.1 wt% does not significantly affect their electrical resistivities.

6) Impurity minerals boron and phosphorus were successfully incorporated into manufactured biocarbons. The addition of boron to sucrose at a weight ratio of 1:100 produces a carbon of reduced surface area compared with untreated sucrose, ca. 96 m^2/g and 172 m^2/g respectively. Doping appears to have a small effect on the resistivity of the carbonized charcoals.

7) Volatile matter is a key metric that influences the chemical structure of charcoals and carbonized charcoals derived from different biomass substrates. Biocarbons with significantly different VM contents have different chemical structures.

8) All the carbonized charcoal samples evidenced very similar XRD spectra. The average graphitic crystallite size of the heat-treated biocarbons is significantly reduced compared to synthetic graphite, ca. 20 and 255 Å respectively. To put this finding in perspective, the size of a graphite crystallite in carbonized charcoal is similar to the size of the micropores that are responsible for most of the surface area of the carbon. The distance between graphitic planes in the (002) direction for carbonized charcoals does not vary much between carbon types. Doping did not enhance graphitization or reduce the distance between graphene planes. The average estimated aromaticity value associated with the carbonized charcoals equates to 71 ± 10%.

9) ESR signals indicated a carbon centered organic radical. Biocarbons contain two major free radical types: charcoals subjected to a lower HTT as indicated by their high VM content afford a narrow signal; whereas charcoals subjected to a high HTT as indicated by their low VM content afford a broad signal. The two types of radicals are not mutually exclusive.

10) NMR spectra of corncob charcoal are indicative of a highly conjugated aromatic material. Heat treatment intensifies the aromatic peak to the point where arcing and subsequent damage to the probe becomes a serious issue.

11) MALDI-TOF spectra of charcoals and carbonized charcoals significantly differed from those obtained from synthetic graphite. Biocarbons contain readily desorbed discrete ions, and at high laser powers low *m/z* carbon clusters are observed. No charcoals or carbonized charcoals contained stable fullerene structures.

12) In light of the structural information obtained using analytical techniques SEM, XRD, ESR, ^{13}C CPMAS NMR, and MALDI-TOF MS and acknowledgement of elemental analyses, a new biocarbon model has been proposed. The model successfully incorporates previously ignored properties associated with biocarbons including the presence of free radicals, oxygen heteroatoms, and porosity.

13) Out of the trialed demineralization experiments including a hot water extraction, a hot DI water extraction, an ambient tempered citric acid mineral extraction, and a hot citric acid mineral extraction, the most effective and consistent demineralization treatment for removing minerals from corncob biomass involved a hot 0.1 $molL^{-1}$ citric acid percolation treatment, ca. 67% of inorganic mineral matter was removed. No one treatment was able to successfully remove the entire mineral load from various biomass feedstocks.

14) Results from the numerous thermogravimetric experiments performed on various charcoals indicated that the level of grinding had considerable affect on combustion reactivity. It was however noted that the burn-off of the partially demineralized char was not affected by grinding at all.

15) In spite of the higher surface area, the partially demineralized cob charcoal evidenced much lower combustion reactivity; in linear heating rate experiments burn-off terminated ~130-160 °C higher relative to analogous

experiments with untreated cob chars. The difference in combustion was explained by the well-known catalytic effect exerted by acid-soluble inorganic minerals.

16) Removal of inorganic minerals from wood biomass feedstocks was found to be much more difficult compared to removing minerals from corncob biomass.

17) The recovery of ash subsequent to FC was always less than unity. During the FC runs, ash contained in the biomass feedstock migrated downward, probably in the form of fly ash and vapor, and some part of the ash was expelled from the canister.

8.1 Further Work

As illustrated in section 2.0 literature describing charcoal structure is vast with many authors developing their own unique char models. The oxygen functionality associated with charcoal evolves as the solid is exposed to increasing heat treatment temperatures. One char model in particular places emphasis on the presence of ether functionalities which are considered as the main form of bonding between graphitic crystallite units[1]. Ether functional groups at carbon surfaces are recorded as decomposing between temperatures 550-827 °C[2]. Therefore further work in this area can be carried out by investigating the possibility of hydrolyzing the hypothesized ether linkages to afford more manageable carbon fragments which could then be analyzed via various spectrometric techniques. Such work has been performed on diaryl ether model compounds, representative of thermally stable cross-links in coals[3, 4]. By producing a series of more manageable (soluble) carbon fragments it may also be possible to obtain information regarding the possible presence of furanones and pyranones.

More work can also be carried out in the area associated with doping biomass derived charcoals with different inorganic elements. For example it was shown recently that a promising high-quality carbon electrode material could be prepared by carbonization of nickel-loaded wood[5]. In addition MALDI work could be performed on doped charcoal's and carbon's.

One problem with multivariate data is that its large volume may make it difficult to see patterns and relationships. Principal component analysis (PCA) is a technique for reducing the amount of data when correlations are present. Throughout this study a significant amount of data was collected concerning the chemical and physical properties associated with charcoal's and carbon's prepared from different biomass feedstocks. Therefore a PCA analysis could be performed using the large volume of data collected in this work to try and establish additional correlations between prepared biocarbons.

1. Villegas, J. P.; Vallee, C. J. D.; Calahorro, C. V.; Serrano, V. G., Organic Chemical Structure and Structural Shrinkage of Chars Prepared from Rockrose. *Carbon* **1998,** 36, 1251-1256.

2. Szymański, G. S.; Karpiński, Z.; Biniak, S., The Effect of the Gradual Thermal Decomposition of Surface Oxygen Species on the Chemical and Catalytic Properties of Oxidized Activated Carbon. *Carbon* **2002,** 40, (14), 2627-2639.

3. Siskin, M.; Katritzky, A. R.; Balasubramanian, M., Aqueous Organic Chemistry: 5. Diaryl ethers: diphenyl ether, 1-phenoxynapthalene and 9-phenoxyphenanthrene. *Fuel* **1993,** 72, (10), 1435-1444.

4. Kamiya, Y.; Ogata, E.; Goto, K.; Nomi, T., Thermal Cracking of Coal Model Diaryl Ethers in Aromatic Solvents. *Fuel* **1986,** 65, (4), 586-590.

5. Suzuki, K.; Suzuki, T.; Takahashi, Y.; Okimoto, M.; Yamada, T.; Okazaki, N.; Shimizu, Y.; Fujiwara, M., Preparation of Crystallized and Mesoporous Carbon by Nickel-catalyzed Carbonization of Wood. *Chemistry Letters* **2005,** 34, (6), 870-871.

9.0 Appendices

9.1 Summary of Flash Carbonization Experiments Used in this Thesis.

Date of Run	Feedstock	Feed Weight (kg-wet)	Pressure (psig)	Air Flow (psig/min)	Avg. O_2 (%)	Ign. Time (min)	Run Time (min)	Air deltaP (psig)	Second. Air	Catalyst Preheat	Feed MC (%-wet bas.)	Feed ash (% dry bas.)	<<<<< Mass weighted average >>>>>				
													fC (%)	VM (%)	Ash (%)	Y_{char} (%)	$Y_{fC\ (\%)}$
29/10/03	corncob	1.13	150	47.5	4.81	23	46	2091	No	No	11.63	1.30	83.61	13.72	2.67	32.22	27.30
07/11/03	corncob	1.19	150	50.0	3.82	14	41	1949	No	No	11.40	1.30	83.29	14.89	1.83	32.19	27.16
12/11/03	corncob	1.17	150	64.0	4.36	14	39	2367	No	No	11.29	1.30	89.24	8.61	2.15	29.00	26.22
31/12/03	corncob	1.06	200	66.6	5.34	14	33	2066	No	No	11.74	1.30	84.64	13.60	1.76	30.31	25.99
07/01/04	corncob	1.12	200	71.1	4.38	14	33	2203	No	No	11.58	1.30	88.44	9.72	1.84	29.76	26.66
14/01/04	corncob	0.86	100	52.2	2.35	14	46	2298	No	No	11.05	1.30	92.68	5.15	2.17	31.50	29.58
03/02/04	corncob	1.17	150	49.0	-[c]	14	42	1958	Yes	Yes	11.85	1.30	83.35	14.75	1.89	34.61	29.23
10/02/04	corncob	1.15	150	49.1	-[c]	14	38	1766	Yes	Yes	12.02	1.30	80.82	17.16	2.02	34.71	28.42
18/03/04	macshell	2.88	150	51.7	-[c]	14	88	4448	Yes	Yes	10.26	0.41	90.89	8.32	0.79	35.02	31.96
13/04/04	corncob[a]	1.08	400	71.7	1.11	14	28.5	1900	No	Yes	11.23	1.30	74.88	22.83	2.28	36.04	27.35
04/05/04	corncob	1.06	300	65.1	-[c]	7	22	1302	Yes	Yes	11.99	1.30	74.22	22.97	2.82	35.88	26.98
02/07/04	corncob (oven-dry)	1.00	150	55.3	3.02	14	32	1660	-	-	7.97	1.30	84.61	12.97	2.43	32.36	27.74
09/07/04	oak wood (oven-dry)	2.12	150	52.4	5.68	14	44	1990	-	-	1.34	0.27	78.39	20.85	0.75	34.48	27.10
06/08/04	corncob + oak wood		200	50.5	4.21	20	42.5	1741	-	-							
	corncob (deashed)	0.54									7.29	1.30	85.35	13.71	0.94	22.52	19.48
	oak wood	1.06									6.49	0.27	-	-	-	-	-
02/09/04	corncob + kukui shell		150	52.3	4.62	14	67	3402	-	-			91.79	5.11	3.11	41.66	40.15
	corncob	0.51									17.25	1.69	91.37	5.41	3.22	26.47	24.60
	kukui nut shell	1.55									9.97	5.70	91.86	5.06	3.09	46.24	45.04
03/11/04	corncob[e]		150	45.4	5.05	14	49	2133	-	-			76.13	21.16	2.72	37.20	28.87
	usual corncob	0.46									10.96	1.69	79.01	18.38	2.61	35.22	28.30
	boron-doped corncob	0.46									11.04	2.15	73.52	23.66	2.82	39.18	29.44
13/12/04	cob+pineapple+sugar		300	61.8	1.80	7	27	1546	-	-			74.33	21.15	4.51		
	corncob (oven-dry)	0.50									0.51	1.69	75.27	22.18	2.56	36.47	27.92
	pineapple waste (Oven-dry)	0.31									1.63	7.60	66.27	25.16	8.57	41.64	29.87
	sugar cube	0.15									-	-	98.22	1.78	0.00	-	-
18/02/05	corncob+HMF+fructose		300	69.4	-[g]	7	25	1597	-	-							
	corncob (oven-dry)	0.75									1.48	1.69	-	-	-	-	-
	5-hydroxymethyl-2-furaldehyde	0.01											-	-	-	-	-
	fructose	0.15											93.05	6.83	0.12	-	-
22/03/05	corncob+lignin		300	64.4	1.71	7	29.5	1771	-	-			81.96	14.92	3.12		
	corncob	0.86									11.88	1.69	81.44	15.49	3.07	32.27	26.73
	Kraft lignin	0.05											90.44	5.66	3.91	-	-
12/04/05	corncob+inulin		300	60.7	4.05	7	31	1761	-	-			86.30	10.05	3.64		
	corncob (oven-dry)	0.82									3.12	1.69	85.87	10.37	3.76	28.35	24.76
	inulin	0.05											96.69	2.52	0.78	-	-
25/04/05	corncob+glucose		200	62.4	-[g]	14	32	1871	-	-			85.99	10.56	3.45		
	corncob (oven-dry)	0.75									0.95	1.69	85.60	10.81	3.59	24.46	21.30
	α-D-glucose	0.11											94.72	5.09	0.20	-	-
16/05/05	corncob+sucrose		200	59.1	-[g]	14	33	1832	-	-							
	corncob (oven-dry)	0.84									1.30	1.69	-	-	-	-	-
	boron-doped sucrose	0.15											-	-	-	-	-
18/05/05	corncob+sucrose		200	61.3	3.21	14	39	2269	-	-							
	corncob	0.82									11.93	1.69	-	-	-	-	-
	phosphorus-doped sucrose	0.15											-	-	-	-	-

9.2 ESR Spectra of Select Biocarbons.

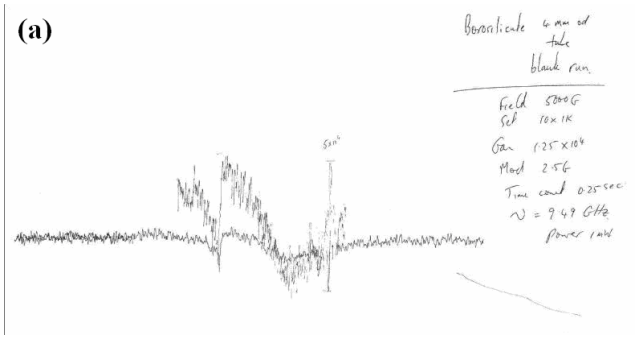

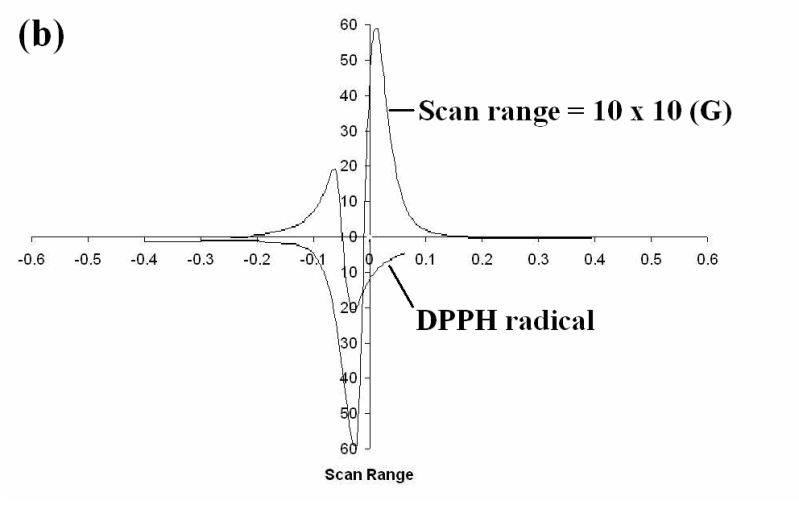

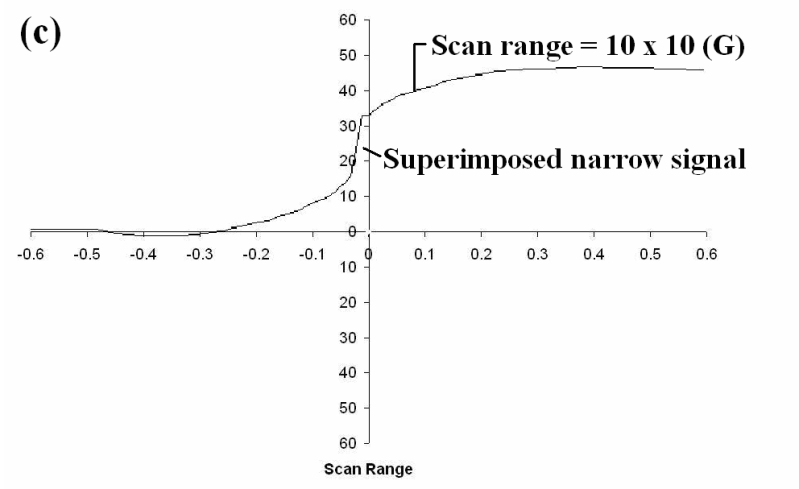

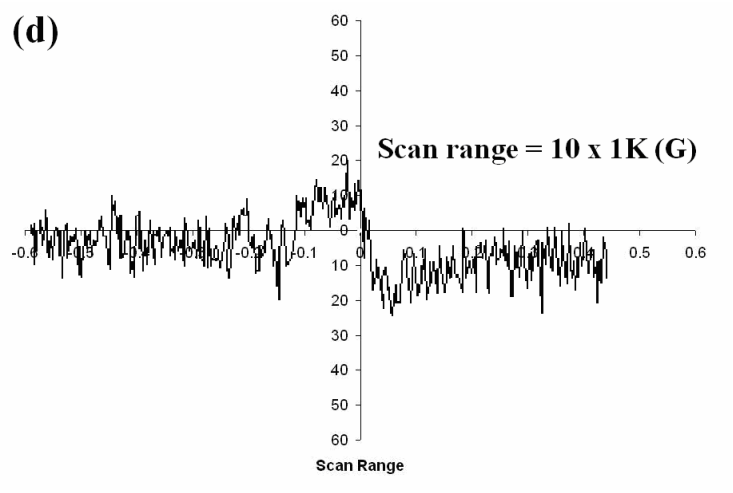
(d)
Scan range = 10 x 1K (G)
Scan Range

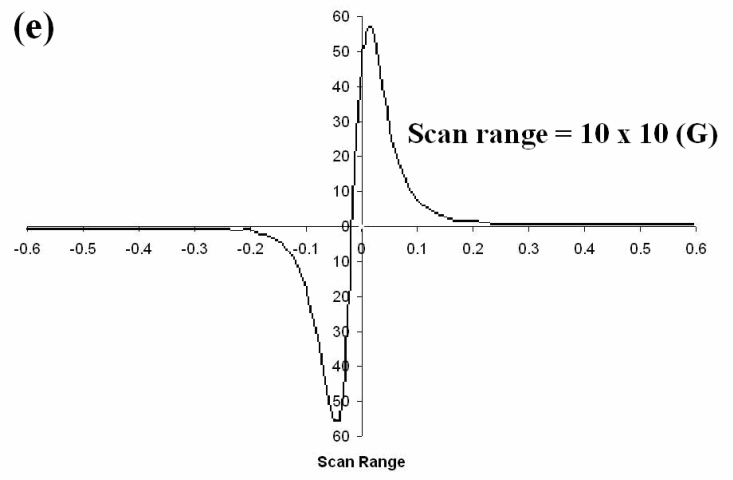
(e)
Scan range = 10 x 10 (G)
Scan Range

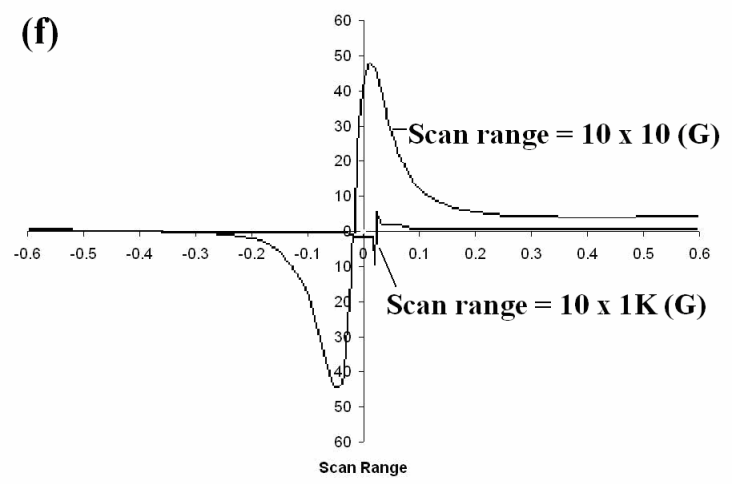
(f)
Scan range = 10 x 10 (G)
Scan range = 10 x 1K (G)
Scan Range

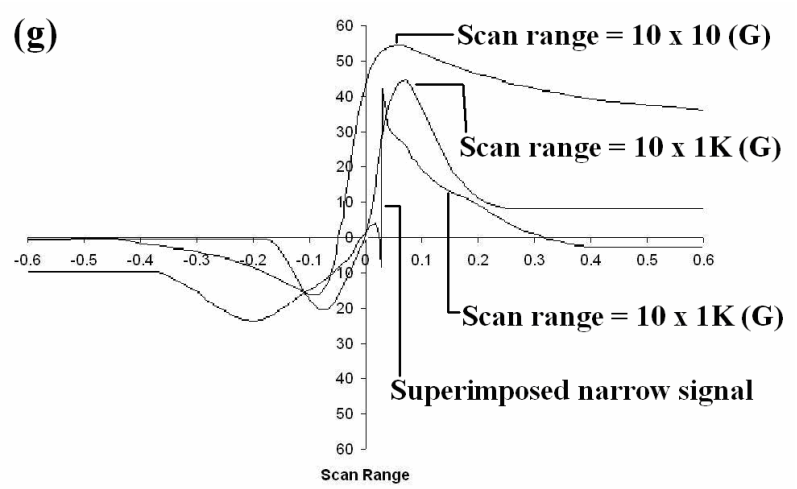
(g)
Scan range = 10 x 10 (G)
Scan range = 10 x 1K (G)
Scan range = 10 x 1K (G)
Superimposed narrow signal
Scan Range

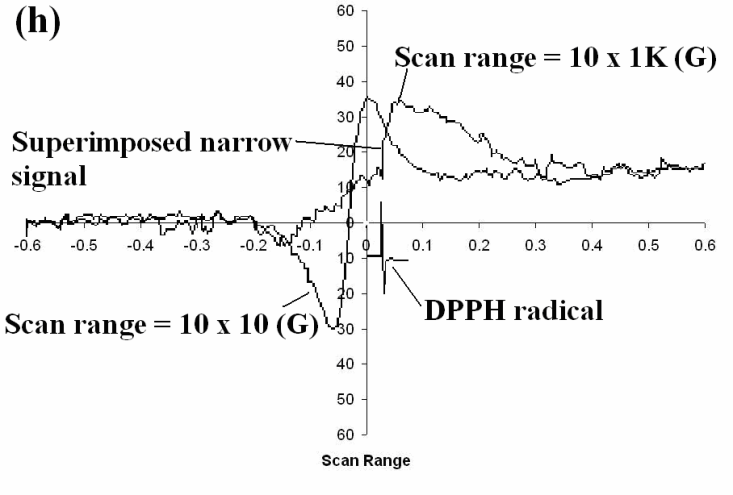
(h)
Scan range = 10 x 1K (G)
Superimposed narrow signal
DPPH radical
Scan range = 10 x 10 (G)
Scan Range

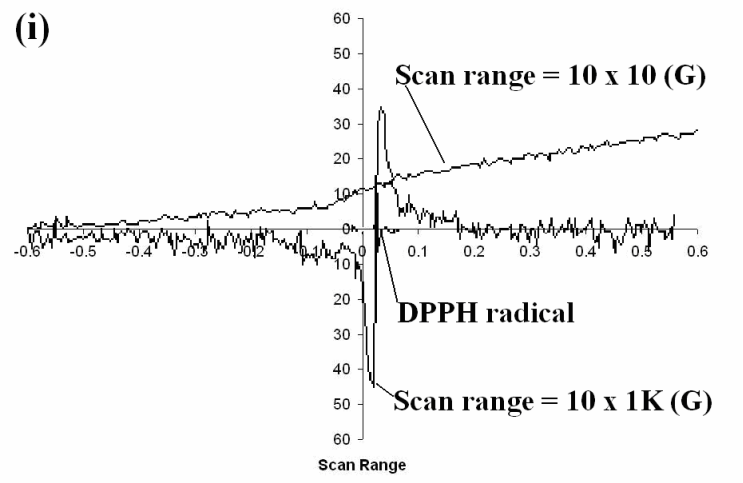
(i)
Scan range = 10 x 10 (G)
DPPH radical
Scan range = 10 x 1K (G)
Scan Range

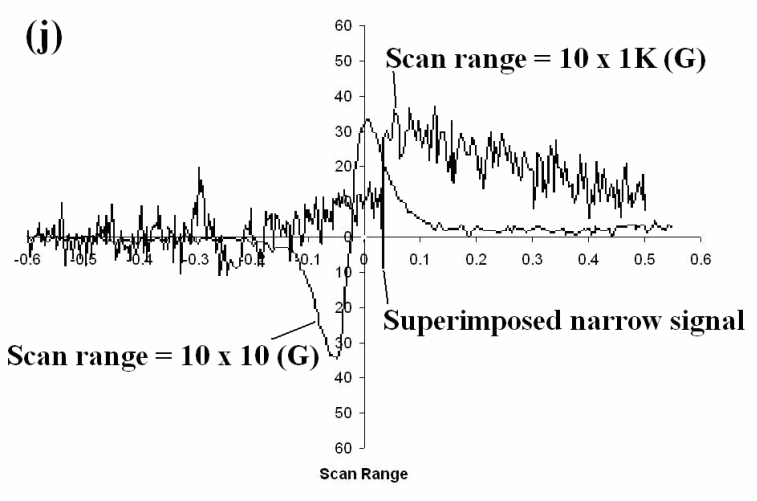
(j)
Scan range = 10 x 1K (G)
Superimposed narrow signal
Scan range = 10 x 10 (G)
Scan Range

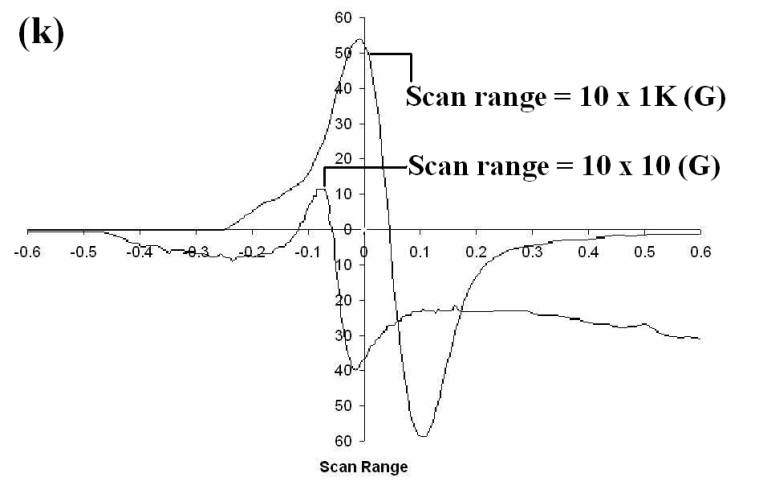
(k)
Scan range = 10 x 1K (G)
Scan range = 10 x 10 (G)
Scan Range

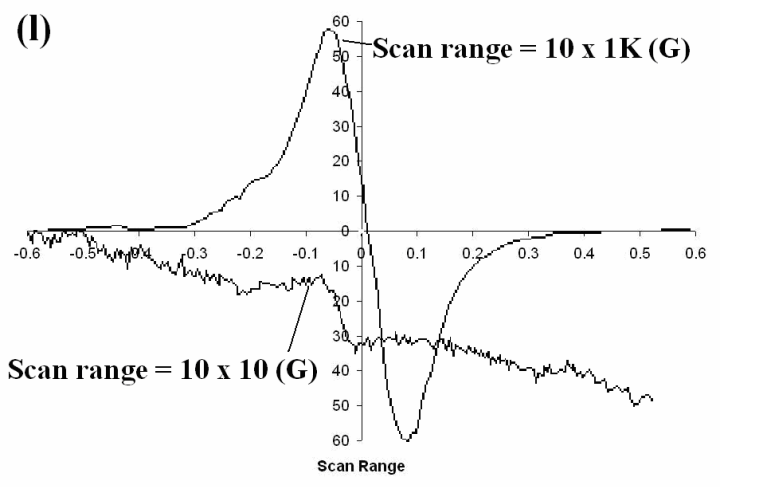
(l)
Scan range = 10 x 1K (G)
Scan range = 10 x 10 (G)
Scan Range

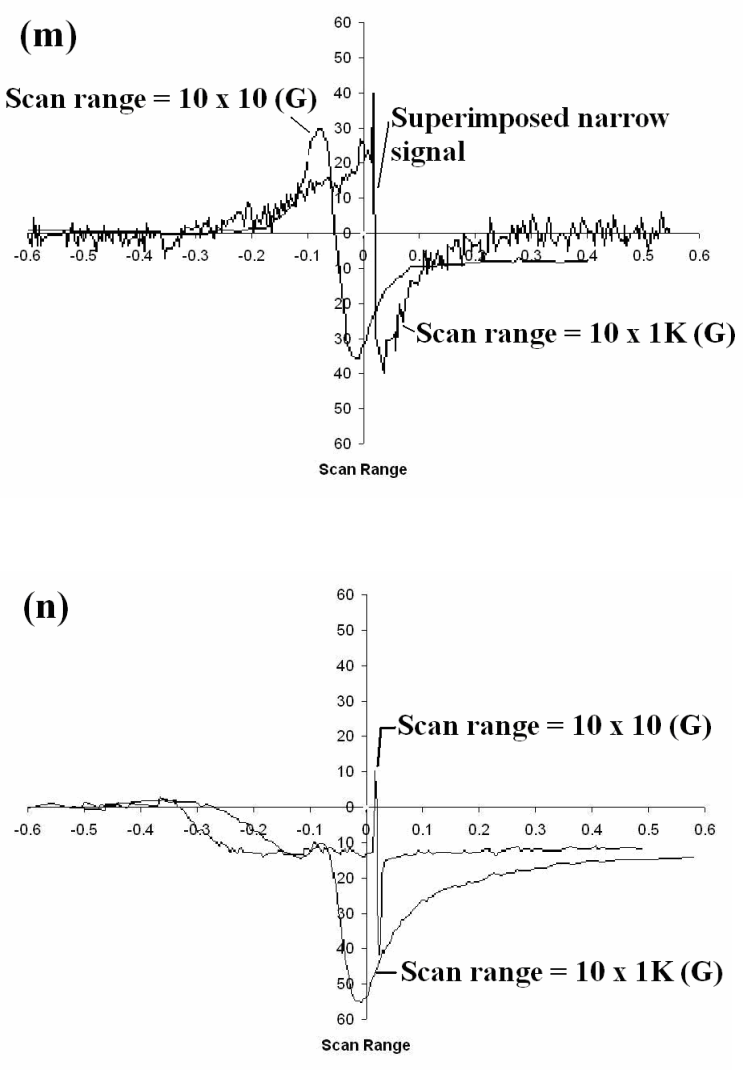

Figure 33: *ESR spectra of select biocarbons. (a) Empty borosilicate tube. (b) 'Middle' 020704 corncob charcoal. (c) Carbonized (750 °C) 'Middle' 020704 corncob charcoal. (d) Carbonized (950 °C) 'Middle' 020704 corncob carbon. (e) 'Middle' 090704 oak wood charcoal. (f) 'Middle' 180304 macadamia nutshell charcoal. (g) 'Top' 131204 sucrose charcoal. (h) Carbonized (950 °C) 'Top' 131204 sucrose Carbon. (i) Carbonized (950 °C) 'Top' 160505 boron-doped sucrose carbon. (j) Carbonized (950 °C) 'Top' 180505 phosphorus-doped sucrose carbon. (k) Carbonized (950 °C) 'Top' 180205 fructose carbon. (l) Carbonized (950 °C) 'Top' 120405 inulin carbon. (m) Carbonized (950 °C) 'Top' 220305 Kraft lignin carbon. (n) Synthetic graphite.*